UNIVERSITY OF
Southampton
School of Engineering Sciences

Influences on Nanocomposite Structural Performance: Experimental Study on Materials Processing and Bonding

Humphrey Alexander Copsey Carter

Engineering Doctorate Thesis

December 2008

Supervisory Team:

Prof. R. A. Shenoi
Dr. D. Jones
Dr. Y Didier Carter

UNIVERSITY OF SOUTHAMPTON
FACULTY OF ENGINEERING, SCIENCE & MATHEMATICS
SCHOOL OF ENGINEERING SCIENCES

Influences on Nanocomposite Structural Performance: Experimental Study on Materials Processing and Bonding

Humphrey Alexander Copsey Carter

Engineering Doctorate Thesis

December 2008

Abstract

Nanocomposites have been widely reported to enhance performance in polymers, in both mechanical and physical properties. An increasing amount of research has resulted in many nanocomposite polymers being applied to various consumer products from motorcars to golf balls. Yet, at this time, there are no structural applications despite a large number of reports claiming improved mechanical properties. Carbon nanotubes are renowned for their specific mechanical properties as well as their thermal and electrical properties. Researchers have put a considerable amount of effort in adopting these nano-materials to structurally enhance an epoxy composite matrix. Though considered very promising many issues such as the dispersion and the bonding interface have been identified and there remains still no guaranteed structural improvement.

The potential of epoxy/clay nanocomposite processing and application has been explored incorporating a study of composite processing methods and characterisation techniques. The key goals were to reliably achieve full dispersion and exfoliation of nanoclay without inducing air into the composite system. Two mechanical processes were used for comparison; a high shear rotary mixing and a laboratory bead mill. Microscopic observations of the resin before curing shows agglomerated nanoclay visible in the samples which decreases as the shearing time. Comparing the processing methods showed greater dispersion in the bead mill processed samples. TEM and X-ray diffraction were used to measure the exfoliation of the nanoclay. The analysis showed that the nanoclays had become intercalated, with the clay layer separation increasing from 2- 4 nm. Further testing looked at the mechanical and thermal properties of the nanoclay composites, comparing the nanoclay processing in amine hardener or solvent. The effect of changing the amount of nanoclay present in the epoxy was also recorded. Testing showed that a solvent processing

method gave best results, with a nanoclay loading of 2wt% processed with a solvent in a bead mill.

The performance of CNTs in epoxy composites was also assessed looking at different bonding mechanisms (covalent and Vander Waals) of the carbon nanotube to the resin. The rheological, mechanical and fracture toughness properties were tested in epoxy resin with different nanotube loadings. These properties were explored in a brittle and a flexible resin, achieved by using two amine curing agents. The covalently bonded tubes showed Newtonian rheological properties and the greatest enhancement in tensile compressive and flexural strength and modulus as well as K_{1c} fracture toughness. MWNT resins incorporating non-covalent bonds displayed shear thinning rheological behaviour and showed greatest improvement in Charpy impact toughness. Fibre reinforced composites laminates have also been investigated by enhancing a formulated pre-preg material. Compressive properties and interlaminar shear stress were tested in a woven carbon fibre composite and some increased properties have been seen which shows potential for further research.

Acknowledgement

I would like to thank my supervisor, Ajit Shenoi, and my Industrial supervisors, Yves Didier-Carter and Dan Jones, at my sponsoring company, Gurit, for their enthusiasm and support. I would like to thank them for accepting the risk and duty of taking on the supervisory role of the EngDoc during my time working at the university and the company, which they have done both professionally and amicably.

I would also like to thank Dr. Shuncai Wang for his help and patience working with me on the scanning and transmission electron microscope. Anton Page, at the Southampton general hospital, for his guidance in the microtome work. Mark Light, of the University of Southampton X-ray Diffraction centre, for his work on X-ray diffraction. Brian Thompson, in the mechanical test department at Gurit, for all his hard work and help with the material testing. The rest of the research and analytical team at Gurit whom I enjoyed working with and gained valuable experience.

I would like to thank Amroy, Nanoledge and Zyvex for their help and support with the supply of carbon nanotube resins. Nanocor and Elementis for their supply and support of nanoclay materials.

I would finally like to thank my wonderful mother, Patsy, for her kind support and valuable proof reading skills. Not only did she donate her valuable time but also on more than one occasion her well stocked fridge and delicious homemade cooking.

Contents

List of figures

List of tables

Declaration of authorship

Humphrey Carter

I, ……,
declare that the thesis entitled

……

Influences on Nanocomposite Structural Performance: Experimental Study on Materials Processing and Bonding

……

and the work presented in the thesis are both my own, and have been generated by me as the result of my own original research. I confirm that:

- this work was done wholly or mainly while in candidature for a research degree at this University;
- where any part of this thesis has previously been submitted for a degree or any other qualification at this University or any other institution, this has been clearly stated;
- where I have consulted the published work of others, this is always clearly attributed;
- where I have quoted from the work of others, the source is always given. With the exception of such quotations, this thesis is entirely my own work;
- I have acknowledged all main sources of help;
- where the thesis is based on work done by myself jointly with others, I have made clear exactly what was done by others and what I have contributed myself;
- none of this work has been published before submission, **or** [delete as appropriate] parts of this work have been published as: [please list references]

Signed: ……

Date:……

Abbreviations

CFRP	Carbon fibre reinforced plastic
CNF	Carbon Nanofibres
CNT	Carbon Nanotubes
DBDA	Dodecylbenzyldimethylammonium chloride
DGEBA	Diglycidyl ether of bisphenol A
DGEBF	Diglycidyl ether of bisphenol F
DMA	Dynamic mechanical analysis
DMP 30	2,4,6-tris-(dimethylaminomethyl) phenol
DSC	Differential Scanning Calorimeter
EtOH	Ethanol
FTIR	Fourier transform infrared spectroscopy
HEHM	highspeed emulsifying and homogenizing mixer
ILSS	Interlaminar shear strength
IPA	Isopropyl Alcohol
IPDT	Integral procedural decomposition temperature
IR	Infrared
MMT	Montmorillonite
MXD	M – xylylenediamine
MXDA	Meta-xylylenediamine
SAXS	Small angle scattering
SEM	Scanning Electron Microscope
TEM	Transmission Electron Microscope
Tg	Glass Transition temperature
TGA	Thermo gravimetric analysis
TGDDM	Tetraglycidyldiamino diphenylmethane
WAXS	wide angle X-ray scattering
XRD	X-ray diffraction

1 Introduction

Nanotechnology has been the focus of much research interest over recent years generating new and exciting developments across many areas of technology. Research in the development of nanocomposite material has quoted some incredible material properties (Coleman et al., 2006), but there have been some conflicting reports regarding the ability to harness these properties effectively as will be discussed in Chapter 2. To add to the confusion the term "nanocomposites" is used for a wide range of materials classifications with very different properties and purposes. Nanocomposites are usually split up into various types of nano-filler such as nanoclay (i.e. Montmorillonite and other layered silicates), carbon nanotubes, nanosilica and nano metal oxides, all of which are commonly used within a polymer to form a nanocomposite. Thus the generic term of nanocomposite can in itself create some confusion for their effective use and application.

The term nanotechnology can relate to a host of areas from medical to electrical and chemical engineering as well as materials technology. In fact the study of most nanotechnologies has often been referred to as a cross-over science using theories and techniques from physics, chemistry, biology and engineering sciences. For the wide range of technologies and applications associated with nanotechnology and the term "nano" has been become synonymous with an improved performance and marketing development where the use of nanomaterial may be added in some cases without any benefit to the application performance - for example of sporting equipment such as tennis rackets and ice hockey sticks. Demand for high-tech materials usually comes from the highest performance customers such as military, space exploration or other high-tech / high-cost applications.

The production and manufacture of nanocomposite structures is still in its infancy. However, there has been an abundance of materials science and chemistry research undertaken on these materials over the last few years. Nano-particles, by the nature of their size, provide a very large surface area for their relative weight/volume fraction which contributes to the mechanical bonding and toughness enhancing mechanisms (Fiedler et al., 2006). When combined with a polymer, some of the composite material properties are found to be significantly enhanced. These properties include mechanical strength, stiffness, fracture toughness, improved electrical properties, resistance to solvent and water absorption as well as gaseous barrier and improved thermal properties, as shown in Chapter 2. This makes them potentially desirable where applications require high performance at a low weight penalty.

1.1 Nanocomposite Risks

Nanotechnology has been described as disruptive technology (Avella et al., 2006,Gordon, 2003). This means that the development in manufacturing techniques in many industrial sectors will eventually phase out existing ones. It is billed as a revolution in technology that will make many positive changes in the way people live. However, nanotechnology runs the risk of being over hyped and losing credibility where it is deserved. This not only affects the commercial value but it also affects the money invested in research which can reduce the speed of development.

As often happens, with the development of a technology with a dramatic impact, getting to the stage of practical application can be obscured. Similar technologies, such as genomics, have promised as such ten years ago but have still to deliver the drugs and medical therapies partly due to public fears (Mnyusiwalla et al., 2003). This, along with production difficulties or even further disruptive technology that may deem even nanotechnology obselete, could cause delays before nano is a household name.

One major risk is the recent public fears, arising from the concern of the toxicity of these new nano materials and their effect to human health and the environment. New nano materials have been reported to be more toxic at the nanoscale, for example, there is the similarity between some nano materials and asbestos due to their long thin fibre like structure (Ryan, 2004). Some public health studies have found links between engineered nanoparticles and a wide range of health impacts including, for example, increased asthma hospitalizations, heart diseases, chronic bronchitis and even premature death (Nanoforum.Org, 2005).

In the UK the Royal Society and the Royal Academy of Engineering produced a joint paper on the opportunities and risks involved with nanotechnologies (Nanoscience and nanotechnologies: opportunities and uncertainties, 2004). Within this it highlighted possible adverse health, environmental and safety impacts. Based on some of its findings DEFRA commissioned two studies by the Health and Safety Laboratory and the Institute of Occupational Medicine to identify exposure and hazard data needs respectively for addressing the risks presented by nanoparticles and nanotubes. The Nanotechnology Research Coordination Group (NRCG) has recognised research objectives to fill the gaps in the understanding of risk in exposure to hazardous nano-material. Since publication of the report the NRCG has constituted task forces to look at possible exposure mechanisms, human health hazards, environmental hazards and social implications (N.R.C.G, 2006). At the moment, however, there is little regulation on the use of nano-materials and while legislation is being put together taking ethical lessons learned from the studies in genetics(Mnyusiwalla et al., 2003).

1.2 Opportunities and Applications

There are opportunities that can exploit the performance of these nanocomposite properties as described in Chapter 2. Mechanical enhancement is possible and there are some applications where nanocomposites can provide environmental and health benefits. Fire retardant materials are an example where traditional toxic polymeric fire retardant additives can be replaced by non-toxic nanoclay(Camino et al., 2005).

Most application of structural nanocomposites can be found in the sporting industry. Tennis rackets and other sporting goods seem to be the industry standard products for introducing novel materials in consumer applications. It can be argued that materials manufacturers try to generate as much positive "spin" as possible for their new material to create more demand and interest in further applications. The application of nanocomposite in bikes, tennis rackets, even fishing rods and other sporting equipment are good marketing tools. However, sometimes there is very little or only vague scientific data to back up their claims of how much benefit the nanoparticles add to the performance. This is a good example of why nanotechnology markets have been described as a hypercompetitive environment (Knol, 2004). The use of public relations to promote accomplishments, while accusing others of hyping theirs seems to be the strategy for claiming market territory in an area of nanotechnology.

There are many examples of this with nanocomposites, especially where the improvement in mechanical properties are concerned. The French company Babolat claims its NCT racket (Nano Carbon Technology) is twice as stiff as a normal racket because it incorporates carbon nanotubes into the structure. Wilson also says its own nCode racket is stronger because it uses nano-size silicon dioxide crystals. Easton Sports produce a range of sports equipment with carbon nanotube (EastonSports.com). Working with Zvyzex (zyvex.com), the manufacturers of Nanosolve, a carbon nanotube resin, companies produce sports equipment, such as ice hockey sticks, baseball bats and a bike frame with lighter, stiffer properties to increase performance. Amroy is another company marketing the use of carbon nanotube epoxy resin. Amroy, working with Montreal, Ice hockey stick manufacturers, have awards for their products at the 2006 World Nanotechnology Fair. Hybtonite®-nanoepoxies are also for use in marine, automotive, wind energy and in many industrial applications (Amroy.com). It is very difficult to find peer reviewed data to support any claims for improved properties. However, for other, non-structural, properties the difference is clearly visible. NanoZ, from Antaria ltd, an Australian company, is one that uses nano zinc oxide for dispersion in solvent-based paints. It is marketed as a UV protective additive and its performance is demonstrated well in simple environmental tests (www.Antaria.com).

Nanoclay enhanced epoxy is available from Pai Kong Nano Technology Co. Ltd. of Taiwan (www.itactrade.org). There is little information available about the product but it is claimed to show dimensional stability, heat resistance, low smoke with halogen free material and good mechanical performance.

Possibly the biggest user of nanocomposites is the automotive industry and in packaging applications. The Hummer H2 sport utility truck is an example with about seven pounds of nanocomposite used in the cargo bed for lighter and greater scratchproof qualities than previous plastics. Developed in conjunction with Southern Clay Products and Basell, besides the weight advantage the nanocomposite parts do not change shape when exposed to temperature changes and do not become brittle at lower temperatures (SCprod.com). However, the application is not used in structurally loaded parts. Other applications include the ability to statically charge manufactured parts for more environmentally friendly and economical finishing.

Typical adhesive, sealant, and coating applications of these products are found in barrier films to keep oxygen out of plastic beverage bottles, paper juice cartons, and thermoformed containers. One such product has even been used in the helium-filled plastic pouch in the heel cushion of Converse Helium sneakers that are sold in China and Japan (Petrie, 2003).

Nanoclays are becoming the preferred alternative fire retardant as they are non-toxic within the polymer. Traditional fire retardants reduce the resistance of the polymer to water resistance, high temperatures, sunlight, chemicals, etc. (www.flameretardants-online.com). Use of nanoclay can reduce the use of traditional flame retardant additives and also makes the products much less expensive and lighter (Camino et al., 2005). The tendency to develop a char layer and the decrease mass-loss rates is attributable to the barrier properties of layered nanoclay materials (Pandey et al., 2005). This could result in adhesives, coatings and structures with improved fire retarding properties thus reducing the smoke volume and toxicity and resistance to flame ignition of a product including adhesive materials. There is great potential for such products in eliminating current halogen-based flame retardants. Whilst having good thermal and combustion properties the nanoclays also enhance the mechanical properties, where traditional fire retardant additives have been detrimental (Petrie, 2003).

The US Missile Defence Agency has been interested in investigating carbon nanotubes as an alternative material to continuous carbon fibre composites for rocket motor casings. The major advantage is the ability to manufacture composite structures at a lower cost compared to other methods. During this program, Foster-Miller has developed a nanotube treatment

technology, and demonstrated 40% increase in flexure strength of a structural epoxy with the addition of 10 wt% of SWNT's (Foster-Miller).

Novel products such as NanoDynamics' patented golf ball have entered the market as well as other patented applications include applications in the optical polymers, microchip plastics and rubber applications. These are just a few examples of the wide variety of different commercial application and benefits of nanocomposites.

Most commercial applications identified here use nanoparticles in a thermoplastic polymer where property enhancements are easier to obtain due to the lower bulk properties and thermal properties. There are very few marketed epoxy nanocomposite products and even less nano-enhanced structural epoxy materials. Epoxies tend to become weaker with the addition of fillers or loose stiffness and with the addition of toughening agents (Ren et al., 2003). Yet this may not be the case with nano-fillers which may prove to be cheaper, lighter alternatives to some toughening additives as well as introducing additional benefits such as fire retarding properties which do not harm the environment and are not detrimental to the performance of the material.

1.3 Research aims and objectives

The aim of this project is to study the factors that affect nanocomposite manufacture and application, and measure their performance in relation to structural properties.

The following objectives have been identified to fulfil the project aim:

- Researching the processing factors that effect the dispersion of nanoparticles through characterisation techniques.
- Comparing the processing methods by measuring the property performance of the nanocomposite material.
- Comparing different nano materials and bonding methods of the nanocomposites by analysing the material property performance.

The project, in collaboration with Gurit Composite Technologies, has concentrated in the main on epoxy / nanoclay and epoxy / carbon nanotube composites. Gurit specialise in the design and manufacture of structural epoxy composite systems with focus on wind energy, automotive, marine, winter sports, aerospace, civil engineering and oil and gas markets.

The definition of performance in this case is gauged by the impact on composite structural design. The design is considered improved through reduction in weight, which the nanocomposites hope to achieve through increasing the material structural stiffness or strength. It also is considered improved through increases in structural working life and breaking strength and thus reducing costs.

The objectives set out a roadmap to investigate the main factors that influence the performance of nanocomposites. Once these are identified they can be researched in a study of the processing parameters. Characterisation will compare the dispersion of the processing methods and mechanical analysis will compare the performance factors in structural material properties.

The performance of the resins is not necessarily an indication of the nanocomposite's benefit to a structural application. It is therefore important to take into account the outstanding structural properties of fibre-reinforced composites.

2 Critical review of nanocomposite from process to properties

The motivation to investigate and apply nanocomposites in a structural capacity was initially fuelled by Toyota researchers, who successful demonstrated enhanced polymeric materials with nanoclays early in the 1990's. Since then many researchers have sought to enhance a variety of properties in different types of polymer with various different nano-sized fillers. Although this investigation concentrates on the use of nanoclay and carbon nanotube epoxy polymers, these different nano-fillers are introduced in the definition of the materials. Reviewing the literature of different processing techniques for modifying the nanoparticles, combining and applying them to epoxy resins have been critically assessed in terms of their success in enhancing the materials' properties. A range of characterisation techniques can determine the efficacy of the processing. These techniques are also reviewed. Finally, different material property enhancements that have been researched are examined and discussed. This will lay the foundation for the understanding and scope of the investigation into nanocomposites and create set parameters to take this concept from process to properties and eventually to applications.

2.1 Nanocomposites – definition and summary of materials

Nanocomposites form a class of material that has phase dimensions in the range of 1-100 nm (Messersmith and Giannelis, 1994). This new material is based on the nano-size particles, plates or tubes that yield extraordinary properties on their own and induce interesting properties in composites which has been much of the driving force for research in the attempt to harness these properties in a structural material. The second phase of the composite, the matrix, is used to disperse the nanoparticles. The matrix is usually a polymeric material which is combined with the nano-material in powder, molten or liquid form before polymerisation takes place. In homogeneous form this allows the nano-reinforcement to provide the maximum benefit to the material.

2.1.1 Types of nanocomposite

Nano materials can be categorised as carbon nanotubes, nano fibres or nano graphite plates, nanosilica, nano metal oxides and nanoclay. Carbon nanofibres are grown from the vapour phase with diameters of order of 100 nm and lengths between 20 and 100 μm. Carbon nanotubes can have diameters ranging from 1 to 100 nm and lengths of up to millimetres. Carbon nanotubes (CNT) were discovered in the early 1990's, after the discovery of fullerenes, by Iijima (1991) who observed and developed the first carbon nanotubes. They

are long slender fullerenes in the form of single and multi walled tubes composed of hexagonal carbon or graphite. Figure 2-1 shows how various carbon-based materials are formed with different carbon lattice structures. This includes a molecular diagram of CNT and how it looks under a transmission electron microscope. It is feasible to describe nanotubes as long slender fullerenes, which come in the form of single and multi walled tubes composed of hexagonal carbon or graphite.

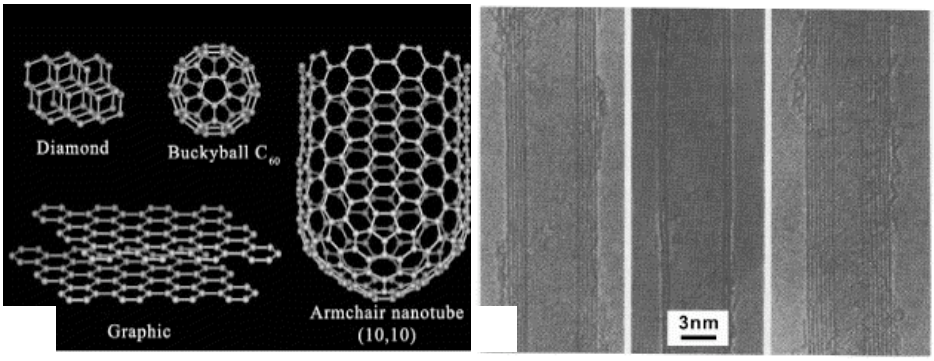

Figure 2-1 A) Different forms of carbon-based materials (Photo courtesy of Rice University) and (B) electron micrographs of nanotubes with different numbers of graphene layers. The out diameters of the nanotubes are 6.7 nm (left), 5.5 nm (middle) and 6.5 nm (right)

Nanoclays clays are layered smectite clay minerals. The most common smectite minerals come in the form of montmorillonite, taken from the ground in the form of Bentonite or Hectorite ore. Once refined and ground to size the clay are nano sized wafers, 1nm in thickness and up to 1000nm across and can be found in different forms of aspect ratio. They principally belong to a family of 2:1 layered silicates consisting of two fused silica tetrahedral sheets sandwiching an edge shared octahedral sheet of either aluminium (montmorillonite) or magnesium (hectorite) hydroxide, shown in Figure 2-2,The stacking of the layers leads to a regular Van der Waals gap or interlayer.

Isomorphous substitutions in the tetrahedral and octahedral sheets cause an excess of negative charges within the silicate layers. These charges are counterbalanced with cations situated between the silicate layers. The cations are inorganic so they are exchanged for organophilic cations to obtain an organosilicate, which can be effectively dispersed in organic media such as polymers.

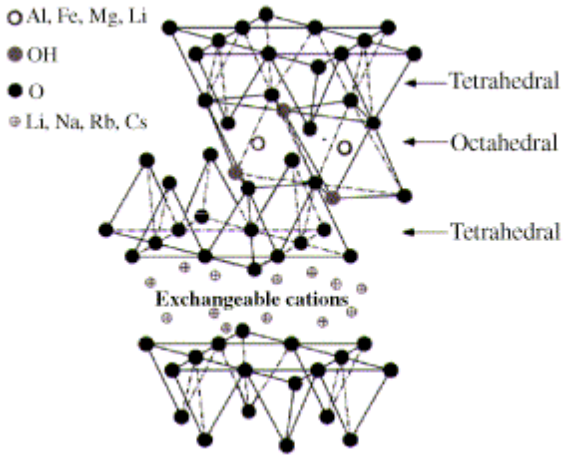

Figure 2-2 The structure of 2:1 layered silicate nanoclay, indicating the ratio of fused silica tetrahedral to octahedral sheets on the clay lamella.

2.1.2 Nanoparticle properties

The Young's Modulus of montmorillonite has been calculated to be between 10GPa, (Shah et al., 2004), 14 GPa , (Vanorio et al., 2003), and the elastic modulus of montmorillonite to be 51 GPa and hectorite to be 69GPa, found experimentally, (Wang et al., 2001). Theoretical calculations have put the in plane Young's modulus as high as 400 GPa (Manevitch and Rutledge), however, latest research shows that the value for montmorillonite to be between 178 GPa and 265 GPa, (Chen and Evans, 2006).

Carbon nanotubes have densities as low as 1.3 g/cm^3 (Hata et al., 2004). Their Young's Modulus is considered greater than 1000 GPa (Wong et al., 1997) and the strength for a carbon nanotube has been measured up to 63 GPa (Yu et al., 2000). Carbon nanofibres have Young's Modulus in the range 100–1000 GPa and strengths between 2.5 and 3.5 GPa (Tibbetts and Beetz, 1987). If this is compared this with existing Type I PAN based carbon fibre which has a modulus of 390GPa and a strength of 2.2GPa (Hull, 1981) it does not come as a surprise that the compressive buckling strength can be as much as two orders of magnitude higher than that of known fibre strengths (Lourie et al., 1998). Hence, the amazing individual performance of CNTs has motivated a great deal of research incorporating them for structural property enhancement in polymer composites and, due to their high specific area, these improved properties can be seen at low weight loading.

Research into thermosetting CNT composites has mainly been concentrated on epoxy resin. This is due, in part, to its use in the electronics industry and also in high performance structural applications such as sport, marine, automotive and aviation where an advantage in material properties is sought over its cost. The high cost of CNTs still restricts them for use in mainstream applications; however, with wide spread use the cost is expected to reduce.

2.2 Mechanisms of nanocomposite structural enhancement

Interactions between a composite matrix and nanoparticle inclusions are not fully understood. They show more complex mechanisms than their microscopic cousins traditionally used as composite fillers. The study and analysis of the mechanisms is also another order of magnitude, not only in terms of physical dimension but also in terms of the complexity involved with the intricate techniques used. In general, the strength and fracture properties of a conventional composite depend on the nature of the bonding at the interface and the interfacial mechanics governing the load transfer from the matrix to inclusion.

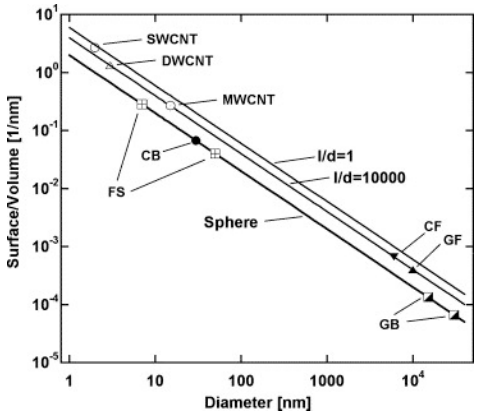

Figure 2-3 Ratio of particle surface and volume for spherical and fibrous particles as a function of the particle diameter (Fiedler et al., 2006).

At both nano and microscopic levels two types of stress develop at the particle – matrix interface in terms of micro mechanisms of composites. Elastic shear stress, in the region obtaining perfect bonding between the two phases, and surface forces: such as friction and adhesion. These are significant due to the large surface area to volume ratio of nanoparticles. In Figure 2-3 Fiedler et al. (2006) shows the comparison between fumed silica, carbon black and carbon nanotubes surface to volume ratios which decrease with increasing particle diameter. It can be seen that already a small volume content of nano-particles provides huge surface areas and can enhance the cross-linking density in thermo-sets, resulting in increased mechanical properties by changing the polymer morphology.

Nanoparticles can also have, specifically in the case of nanotube and nanoplate formed particles, an extremely high aspect ratio. This allows the composite to be compared to a fibre reinforced composite as well as a filled composite. Although on the macroscopic scale a polymer nanocomposite is defined as an isotropic material, some of the mechanisms of strength and fracture resistance can be looked at in terms of an orthotropic material on the nano-scale or the micro-scale, if the tubes / plates are aligned.

Take a comparison between conventional composite and a nanotube composite. Key mechanisms of energy dissipation in the fracture toughness of conventional fibre reinforced composites (without filler) include fibre fracture, fibre pull out, fibre matrix debonding,

crack bridging and matrix cracking. Strength and fracture properties of a composite depend on the nature of the bonding interface and the interfacial mechanics governing load transfer from the matrix to the reinforcing fibre. It is suggested that fracture mechanisms of nanotubes composites show similar micromechanical mechanisms: fibre bridging effect, particle / fibre debonding, crack deflection, crack pinning, fibre pull out, crack tip deformation localised inelastic matrix deformation and overall size of the plastic deformation zone (Norman and Robertson, 2003).

2.2.1 Nano - matrix interface

The interface between matrix and nanoparticles is responsible for providing effective load transfer by a number of methods. The particle can be directly covalently bonded to the polymer matrix, depending on the type of nanoparticles and surface treatment, to give a strong interaction. The polymer cannot always be directly bonded and often a surfactant or copolymer is used. In this case one end of the surfactant will directly bond to the polymer and one end will adhere to the particle with Van der Waals, electrostatic initiators or hydrogen bonding. The use of frictional force is also used with mechanical action of the polymer wrapping itself around the nanoparticle, and is often worked in conjunction with the other two bonding methods. With all methods they are most effective when the nanoparticles are homogeneously separated from each other.

2.2.2 Agglomeration of nanoparticles

Due to their size and polarity nanoparticles tend to agglomerate together. They can also be hydrophobic which makes them insoluble in polymers and reduces the ability to disperse effectively. Nanotubes often tangle themselves into bundles and nanoclay particles not only agglomerate together but are also made up of silicate layers, which can be separated further by efficient processing, for more available surface area and hence better nanocomposite properties. Efficient exploitation of their properties is often related to their homogeneous dispersion and break up of the agglomerations as well as good wetting by the polymer. To combat the agglomeration the particle surfaces are treated or functionalised to change their polarity, making them hydrophilic, and allows the matrix to bond to the nanofiller. In addition to this, mechanical shearing of the uncured Nanocomposite is used to disperse particles further.

2.2.3 Dispersion of nanocomposites

Processing applied for the fabrication of nanocomposite has the aim of dispersing the nano-filler evenly throughout the liquid phase of a polymer. (Kim et al., 2003,Kim et al., 2004)

investigated the relative time for mixing and showed that for their nanoclay in unsaturated polymer, a mixing time of 120 minutes was found to improve the material properties of the nanocomposite over 30 minutes. To disperse the nanoparticles and introduce the polymer between the lamella of the clay requires a high shear and / or chemical processes. In the case of the nanoclay filler, a high shear or chemical method is required to swell the galleries between the lamella and allow the polymer chain to penetrate between them. This will produce an exfoliated nanocomposite, required for most effective enhancement of the polymer . In the case of nanotubes the shearing actions is used to detangle the ropes formed by the tubes and separate them. This high shear action on the viscous uncured thermoset resin causes air bubbles to be generated, which also require removal from the solution.

Methods reported consist of, in the most part, a simple stirring or high shear mixing method as shown by Table 2-7 in the summary, section 2.56. Sonic agitation has also been used as a dispersal method as well as bead/ball milling techniques, a roll mill technique and high pressure mixing. The majority of nanoclay and carbon nanotube is directly processed with the liquid resin part of the polymer. However, some research has used the catalyst part or sometimes with a combination of acetone solution to chemically swell the nanocomposites, with varying success.

2.2.3.1 High shear mixing

Advantages	Disadvantages
Simple set up and use	Uncertain as to the exfoliation throughout sample
Easy to clean	Allows air to be mixed in
Adjustable speed	Often used with other methods, may not be effective enough by itself.
Adaptable head allows different mixing	
Relatively Cheaper	

Table 2-1 Advantages and disadvantages of the high shear mixing method.

High shear mixing consists of a high speed spinning disk, with an option of various toothed or barbed configurations to increase shear effect. This is the most common type of mixing method used.

Southern Clay, producer of the nanoclay Cloisite®, used in much research, recommends a Cowel dissolver (www.nanoclay.com), a round blade with teeth at about 1/3 the tank diameter, turning at high rpm with a tip speed of 20 m/s. For example this high shear mixing can be done using for 127mm blade; this is 1000-3000 rpm. A good vortex is desirable and baffles in the tank recommended.

2.2.3.2 *Bead milling*

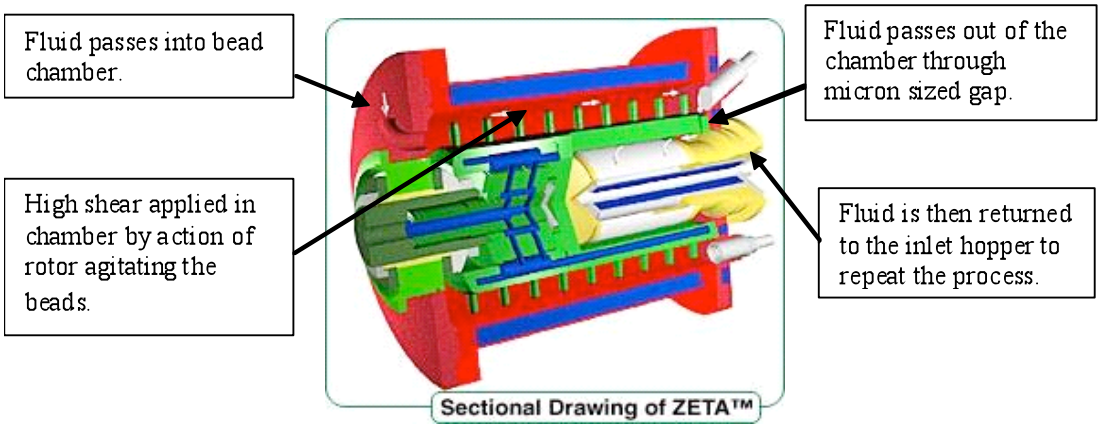

Figure 2-4 Diagram of bead mill chamber (www.netzsch-feinmahltechnik.de).

Milling is a common method of dispersal in the die and ink industry for its effectiveness on dispersing very small particulates throughout a liquid medium. A mini laboratory bead mill, a scaled down version used for making small samples for testing requirement. This method of mixing sucks the solution through a chamber with small beads, down to hundreds of microns in diameter. A rotating cylinder agitates the beads, causing the high shear effect required in the solution. This is shown in Figure 2-4 with a cut out diagram of a typical libratory bead mill.

Advantages	Disadvantages
Recommended for grinding to a sub micron level.	Requires a water and perhaps air supply.
Does not allow air to enter the solution, once in the chamber.	Limited sample size.
Unproven in comparison with cowel dissolver.	Very specialised – not as adaptable as other methods.
More homogeneous dispersion throughout sample.	Requires pre- mixing of sample.

Table 2-2 Advantages and disadvantages of the bead mill mixing method.

Ball milling of DGEBA epoxy nanocomposites has been investigated by (Lu et al., 2004). Their method was to mix into the epoxy first, then add ketone. This solution was then ball milled for 10 hours before allowing the ketone to be eliminated under vacuum and adding the hardener. The high shearing force of the bead mill was deemed necessary to further exfoliate the nanoclay to a separation greater than 8.8 nm. The best result of impact resistance was 50 % increase over the pristine epoxy value and an 8 % increase in flexural strength.

2.2.3.3 Ultrasonic agitation

Uses ultrasound to vibrate the nano-particles in turn causes shearing. This influences the dispersal and separation of the lamella. The university does have an ultrasonic bath used for cleaning of samples.

Advantages	Disadvantages
Heats up considerably allowing the sample to become less viscous. Applies the shearing force to the whole sample.	Causes sample to heat up excessively changing epoxy structure. Used in combination with other methods. May not cause exfoliation only dispersion.

Table 2-3 Advantages and disadvantages of the ultrasonic agitation mixing method

Lam et al. (2005) have looked at the effects of sonication. They claim that the best micro hardness of 4 wt% nanoclay / epoxy can be obtained at 10 min sonication time, however, exfoliation of the nanoclay platelets inside the nanoclay clusters cannot be done by simple ultrasound sonication.

2.2.3.4 High pressure impingement

This method was investigated in (Liu et al., 2005b), discussed in section 2.3.2, inserting acetone clay slurry into a high pressure mixer, where the mixture of clay and acetone was forced with more than 15,000 psi into a very small chamber and then impinged on the wall of the chamber many times.

The nanocomposites made with the high-pressure method showed dramatic improvement in fracture toughness at very low clay loading. K_{1C} and G_{1C} were increased by 1.89 and 3.25 times respectively, at 1wt% clay loading, over the pristine resin properties. Characterisation showed significant increase in layer separation. This high-pressure method did report problems, however, with a number of micro voids that increased as clay content increased.

2.2.3.5 Three roll mill

Yasmin et al. (2003) looked at a three roll mill as a method of applying shear to the composite in solution form. The method produced good dispersion of clay particles within a short period of time and also a inter-gallery spacing of over 7nm. Decreasing rate of elastic modulus improvement with higher clay content was attributed to the aggregation of clay particles. Lower or no improvement in tensile strength of the nanocomposites over pure epoxy can be attributed to the clustering of nanoparticles and / or to the occasional occurrence of nano to micro-size voids in the microstructure. Higher tensile strength with better degassing confirms the importance of degassing in reducing the number of nano- to

micro-size voids. Seyhan et al. (2007) looked at the three roll mill with dispersing CNTs and found it more effective than a sonication technique.

2.2.4 Removing entrapped air

The addition of nanocomposites has been often been linked to an increase in air within the polymer matrix. This is not encouraged from a structural point of view as it decreases the bulk properties and also the entrapped air reduced the wetted surface decreasing the interface strength between a reinforcing fibre and the matrix. The degassing process has been shown to be an important but difficult process, using a combination of vacuum, heat, kinetic energy and sometimes solvent to reduce viscosity and remove the entrapped air. The importance of removing air was shown by Mohan et al. (2005) showing the tensile strength of a nanocomposite improving with increased degassing time.

2.3 The state of clay

The state of the morphology between the polymer matrix and the clay sheets or lamella can be defined by the interaction between the two parts and the regularity of the silicate lamella. Lan and Pinnavaia (1994) described the layered silicate polymer nanocomposite as primarily divided into three categories; conventional composites intercalated nanocomposite and exfoliated nanocomposite. Where conventional composites involve nanoclay in their original aggregate state, a few molecular layers of the polymer matrix have penetrated intercalated nanoclay, separating the lamella sheets, but they remain in regular fashion. Exfoliated nanoclay leaves the individual clay layers separated by a continuous polymer matrix to much greater average distances depending on the loading of clay. This is demonstrated schematically in Figure 2-5.

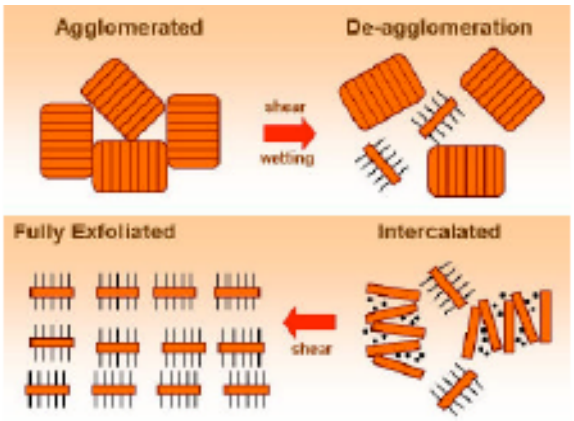

Figure 2-5 Schematic diagram of different clay states, as described by Elemantis Inc.

Chen and Tolle (2004) agree with this in principle but goes further to introduce two states of exfoliation; ordered and disordered. In ordered exfoliation large amounts of polymer penetrate between the clay lamella, however, the ordered structure of the nanosilicate still

remains. This differs from intercalated by the larger average distance between nanoclay sheets. The ordered exfoliated nanocomposite has therefore a more homogeneous dispersion throughout. Disordered exfoliation is also homogeneous but randomly dispersed.

2.3.1 Influencing the state of clay

Kornmann. also investigated the polarity of the surface modifier on nanoclay morphology, (Kornmann et al., 2001b). Lan et al., (1994) showed that varying the chain lengths of the alkylammonium ions was found to be the key to facilitating the diffusion of diglycidyl ether of bisphenol A (DGEBA) epoxy resin and curing agent molecules between the silicate layers because it reduces the electrostatic interactions present between them.

There are four main processing techniques for nanoclay composites described by Alexandre and Dubois (2000). These can be categorised as:

- Exfoliation absorption
- In-situ polymerisation
- Melt Intercalation
- Template Synthesis

2.3.1.1 Exfoliation absorption

Clay is separated into single silicate layers using a solvent in which the polymer is soluble. Pinnavaia et al. (2002) took 6 wt% clay and Shell Epon 826 epoxy and premixed them in the presence 25%wt of acetone, ethanol (EtOH) or isopropyl alcohol (IPA). It was found that pre-intercalation of the epoxy monomers prior to curing results in a higher degree of clay nanolayer exfoliation. Pre-swelling the clay galleries was more pronounced for glassy epoxy resins than for rubbery epoxy systems. EtOH and IPA were more effective swelling agents than the acetone, leading to more effective exfoliation.

In Lui et al. (2005b) created an acetone-clay slurry by inserting the solvent and clay into a high pressure mixer, creating a pasty mixture containing about 10 wt% clay. The desired amount of paste was added to tetraglycidyldiamino diphenylmethane (TGDDM) epoxy resin and mixture was mixed by hand at room temperature. The mixture was then mechanically stirred at 1000 rpm in a fume hood at room temperature for 30 minutes. However, a dry mixing method with no acetone showed a higher toughness and modulus than normal filler composites. Acetone was also used, combined with an ultrasonic processing technique (Miyagawa et al., 2004). Alternatively, Lu et al.,(2004) combined ketone with an epoxy / nanoclay mixture in a bead mill to aid the dispersion.

2.3.1.2 *In-situ polymerisation*

This is a technique where clay is swollen in liquid monomer, allowing polymer formation to occur between the intercalated sheets. Polymerization is initiated by heat or by organic initiator or by catalyst fixed through cationic exchange inside layer before swelling. The insertion of catalyst or organic initiator is made in the modification process of the clay before it is dried out and then milled down to the nanoscale. Na^+ montmorillite clay (PGW Nanocor Inc) can be modified to produce H+ and Li+ forms of the montmorillite clay (Pinnavaia et al., 2002). This was then dried and ground down to 50 nm. (Potschke et al., 2004) used M – xylylenediamine (MXD), a commonly used hardener, dissolved in water and a small of quantity hydrochloric acid. This was blended with a nanoclay water solution. The suspension was then washed and condensed before combining with the bisphenol A epoxy at a raised temperature to vaporise any remaining water. This method produced disordered exfoliated nanocomposite.

This modification method allows epoxy curing to take place throughout the resin once the hardener is added, including inside the galleries. More epoxy is pulled into the galleries during curing, further expanded galleries and greater exfoliation. (Chen et al., 2004). The extra catalyst can accelerate epoxy curing within the galleries, leading to further exfoliation of the clay. Kornmann et al. (2001b) and Salahuddin (2004) investigated the swelling of the silicate layers in different types of polyoxyalkylene amines. The intention was to graft the clay to the polymer by ionic bond through the exchange of the Na cation. When Jeffamine T-500 or octadecyl substituents are introduced, to lower surface energy, the largest separation of clay layers was achieved.

2.3.1.3 *Melt intercalation*

Layers are mixed with polymer matrix in molten state under certain conditions. If the layer surfaces are compatible with the chosen polymer the polymer is drawn in space between silicate layers and forces either intercalation or exfoliation without the use of solvent. This method usually requires more shear work to infuse the nanoclay layer with the epoxy resin and temperature has also played a key roll as it is significant to reduce the viscosity of the resin. Yasmin et al. (2003) used this method by utilising a three roll mill as described in 2.2.3.5. Lam et al. (2005) used different sonication times to test dispersions of a commercial nanoclay into Araldite GY 251. It was found that different sonication times affect the size of the nanoclay clusters however the interlamellar distance was not affected

2.3.1.4 *Template synthesis*

Silicates are formed in situ in an aqueous solution containing the polymer and the silicate building blocks. Based on self-assembly forces, the polymer aids the nucleation and growth of the inorganic host crystals and gets trapped within the layers as they grow.

2.4 *Property enhancement in nanoclay composites*

2.4.1 Mechanical properties

The clay nanolayers are more effective in improving mechanical properties when the polymer is in its rubbery state rather than glassy. For instance, 7.5 vol.% of the exfoliated 10 Å-thick silicate layers improves the strength of elastomeric polymer matrix by more than 10-fold according to Lan and Pinnavaia (1994) using flexible amine cured epoxy resins. Work has also shown that clay nanolayers reinforce glassy epoxy matrices under compressive strain, graphically shown in Figure 2-6.

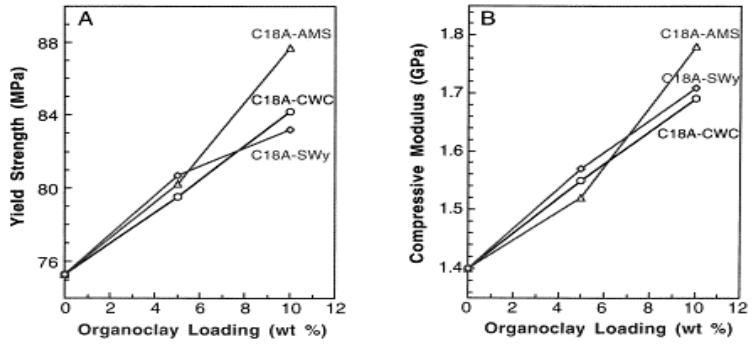

Figure 2-6 Yield strength and compressive modulus against organic clay loading, (Massam and Pinnavaia, 1998)

Nanoclays have shown improvements in epoxy systems with low *Tg*, of 10 times the tensile strength at 15 wt% nanoclay. Improvements of nearly six times fracture toughness of pristine epoxy resin at 3wt% of nanofillers have also been reported (Liu et al. 2005). Kornmann (2001b) found that exfoliated nanocomposites showed an increase in tensile modulus which exhibited an increase with clay content; however, the tensile strength decreased with addition of exfoliated nanoclay. Fracture toughness was also tested showing an improvement in K_{ic} and G_{ic} for both exfoliated and intercalated particles suggesting that the exfoliated nanoclay, which still had some structure, were dispersed in the epoxy as swollen micro-aggregates. Conventional filler was found to have better performance possibly because it was a smaller aggregate. Nanocomposites made with the high pressure method also showed improvement in fracture toughness at very low clay loading. K_{1C} and G_{1C} were increased by 2.2 and 5.8 times respectively at 3wt% organoclay loading over the pristine resin properties (Liu et al., 2005a).

Yasmin (2003) made tensile tests which showed that the strain to failure decreased as the clay wt% went up but elastic modulus increased. This was attributed to the exfoliation and homogenous dispersion of the nanoclay restricting the mobility of the polymer chain under loading as well as good interfacial bonding between particles and matrix and the appearance of tiny voids reducing the failure stress. Degassing a sample for a longer time increased the strength to 58 MPa very close to the 63 MPa of pristine epoxy. With improved interfacial adhesion, using long chain alkyl and alkylene groups added to the resin and anhydride hardener (Zilg et al., 2000) showed significant increase in tensile strength whilst only minor decrease in Young's Modulus.

Miyagawa and Drzal (2004a) show that fracture toughness improves with clay content, also concluding that the fracture toughness is governed by the morphology of the nanoclay. However, there is evidence that the exfoliation of nanoclay is not necessary for the improvement in fracture toughness and the larger size of nanoclay is important to stop the crack tip opening. Exfoliated nanoclay was found to be shorter due to the breakage in the shearing process and hence had a lower energy for crack propagation. Good bonding at the clay-epoxy interface due to modification also contributed to improved fracture toughness.

Other improvements include increase in wear resistance (Zhang et al., 2006,Xing and Li, 2004,Jawahar et al., 2006) and reduction in coefficient of friction (Q. M. Jia, 2006). Water and solvent uptake has also been investigated (Kim et al., 2005,Becker et al., 2004,Chen et al., 2003). Research has shown that nanoclay present a barrier or tortuous path that stops the ingress of liquid (Liu et al., 2005a) which would lead to degradation of properties impact properties (Berketis and Hogg, 2007). Flame retardance has seen an increase (Chen et al., 2003) and improvement in thermal degradation has been shown due to good insulating properties and the formation of a char layer on the surface of the epoxy(Gu and Liang, 2003,Guo et al., 2004).

2.4.2 Characterisation of structural enhancement in nanoclay composites

2.4.2.1 Optical and electro optical

To judge the compatibility, dispersion and exfoliation certain techniques are used to make images or for qualitative comparison and show the structure and formation of the clay. Some circumstances allow the comparison of agglomerated material, which can be viewed through a microscope. This is done before the epoxy is polymerised, observing the processed epoxy-nano solution between two glass slides. The microscopic image in Figure

2-7 can clearly show agglomerations of nanoclay up to 100µm across. This clay is phase separated and in an agglomerated state.

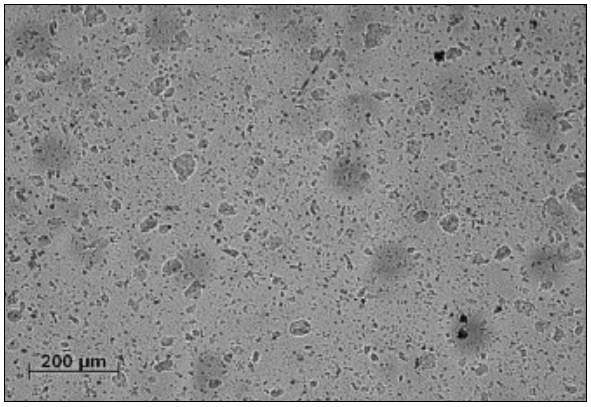

Figure 2-7 Microscopic image of low shear dispersion, (Hackman and Hollaway, 2006)

For higher resolution images of the nanoclay a Scanning Electron Microscope (SEM) can show surface details. With micrograph resolution of a few microns the fracture surface will exhibit concentrations of nanoclay and give details on how the composite failed. The Transmission Electron Microscope (TEM) will give even higher resolution images down to the nanometre scale. Images taken through an ultramicrotomed section, up to 100nm thick, these will show the configuration and separation of the individual nanoclay whilst also having the ability to image the clay at lower resolution, showing the dispersion as demonstrated in Figure 2-8. This shows the TEM images of the different states of nanoclay. In Figure 2-13A, the micro-sized black areas are nanoclay aggregates. B and C intercalated and ordered intercalated nanoclay and D shows the clearly separated clay lamella indicating they are exfoliated.

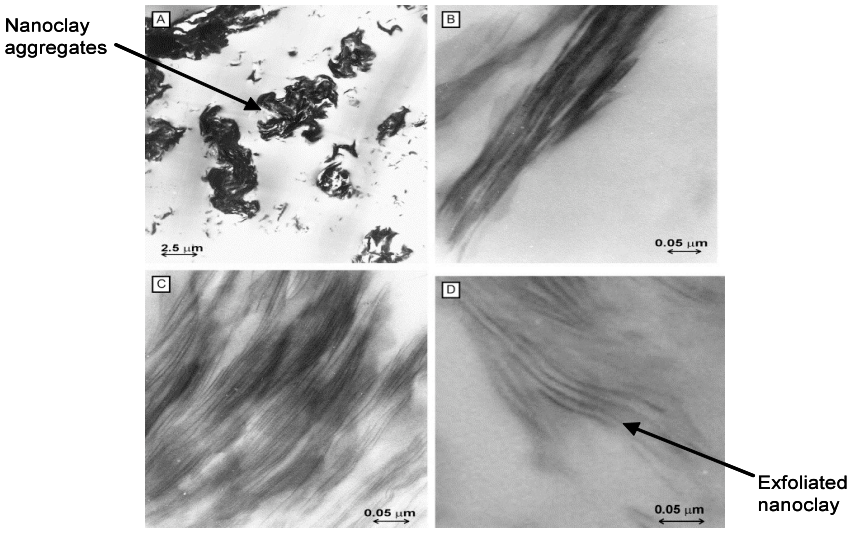

Figure 2-8 TEM images of cured epoxy resin composites: (A) microcomposite (aggregates); (B) intercalated nanocomposite; (C) ordered intercalated/exfoliated nanocomposite; (D) intercalated/exfoliated nanocomposite (Camino et al., 2005).

2.4.2.2 X-ray diffraction

X-ray diffraction (XRD) can be used to measure the average distance between the silicate layers. When X-rays are fired at the nanoclay the electromagnetic waves will diffract through the gaps between the layers and cause a line of intensity at the detector where the diffracted frequencies become in phase. This can be represented by a peak on an Intensity graph in which, using Braggs Law, equation 2-1, the position of a peak in the intensity - 2θ graph can be translated into a separation distance.

$$n\lambda = 2d \sin\theta \qquad \textbf{Equation 2-1}$$

Where n, an integer, λ, the wavelength (1.54Å), θ, the angle of incidence of the scattered X-ray and d, the interplanar spacing of the clay layers.

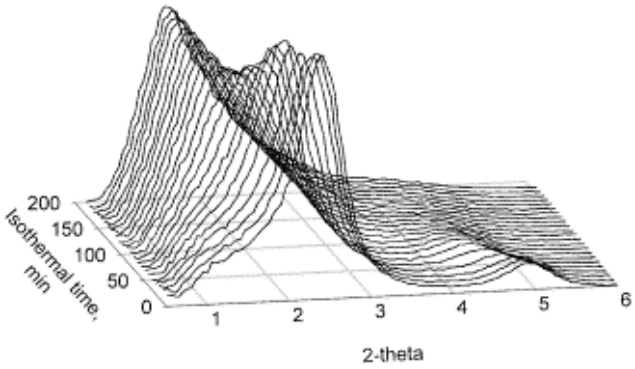

Figure 2-9 Intensity / 2θ graph showing the change in peak over different curing temperatures (Chen et al., 2002).

Figure 2-9 shows the peak decreasing along the 2θ axis as the cure temperature increases. This actually represents an increase in the separation of the clay layers. The broadness of the peak is also thought to represent the relative deviation of the layer distance. When the clay separates to a point lower than 2θ (corresponding to about 4nm or greater) the wide angle X-ray scattering (WAXS) is not able detect accurately the lamella spacing the below this. For a more accurate measure of the separation of exfoliated nanoclay small angle scattering (SAXS) is required.

2.4.2.3 Other characterisation methods

Nanoclays have been used as rheological or thixotropic agents in liquid adhesives for some time and therefore has been characterised by their rheological footprint, which is very much dependent on the polymer system used and the amount of nanoclay. The rate of increase in viscosity against filler content for resin filled with organo-modified clay particles has been found to be higher than that of the unmodified clay filled resin, (Mohan et al., 2005). This is due to the homo-polymerization of the epoxy and also the increase in effective clay particle size due to increased separation of clay layers. This method could be a useful characterisation tool, specifically for production quality. However, if exfoliation occurs

through curing then it would be difficult to assess this unless a curing shear rate test can show a significant trend for exfoliated nanoclay.

Thermo gravimetric analysis (TGA) has also be a useful tool for showing the morphology of the nanocomposite. Measuring the thermal stability of a material by precisely measuring its weight across a constant increase of temperature, the energy of activation for decomposition and another characterisation of thermal stability, integral procedural decomposition temperature (IPDT) can be calculated. These values increase with the number of exfoliated structures within the epoxy (Guo et al., 2004).

Dynamic mechanical analysis (DMA) measures the loss and storage modulus of a sample and which and can be used to find the glass transition temperature when the sample is heated due to the change on visco-elasticity. For cross-linked polymers both E' and T_g generally increase with crosslink density (Bellenger et al., 1988). Changes of glass transition temperature, due to clay content, has been shown to depend on the type of amine treatment and clay dispersion techniques used. With the addition of nanoclay the tan δ peak has shown a slight shift to a higher temperature, indicating a higher T_g over pristine epoxy (Messersmith and Giannelis, 1994). The anhydride-cured epoxy nanocomposites exhibited few changes or marginal reductions in T_g depending on the type of amine treatment of clay.

2.5 *Influences on carbon nanotube enhancement*

As discussed previously, in section 2.2, the extremely high specific mechanical properties of CNT's have created a lot of interest for the purpose of structural enhancement of composite materials. CNTs have a high aspect ratio in the region of several thousand, which allows certain micromechanical strengthening and fracture resistant mechanisms. To get the maximum benefit to the composite the influences on the enhancement have to be understood. CNTs come in many forms with slightly different structures: Chirality, number of walls, length of nanotube, the purity of the nanotubes, all effect the micromechanics of the load transferred between the two phases. .

Surface treatment is also important, effecting how the nanotubes are dispersed within the matrix and how the nanotubes can be bonded to the matrix. Equally the chemical make up and the curing of the matrix can affect the interface.

2.5.1 Carbon nanotube surface treatment

Carbon nanotubes have an anatomically smooth and non-reactive surface making it very difficult to attach them to anything. Treating the surface of the nanotubes allows better dispersion and bonding of the nanotube with the polymer. Liu and Wagner (2005) agree with most evidence that the functionality of the CNTs improves the overall composite

material properties. To improve the interfacial interaction of the nanotubes the surface polarity needs to be increased, more sites for possible Van der Waals, hydrogen or covalent bonding need to be created and the possibility of mechanical locking between the CNT and matrix needs improvement. Various surface treatments can be applied to achieve this such as, oxidation in acid solution, dry oxidation in oxygen, anodic oxidation, plasma treatments and oxy fluorination.

2.5.2 Nano-matrix bonding methods

Carbon nanotubes can be attached to the epoxy matrix by non-covalent and covalent bonding. Non-covalent attachment uses mechanical bonding mechanisms such as polymer wrapping of the nanotube and utilise frictional stresses to bind the two phases (Yang et al., 2007). Covalent bonding mechanisms use the strongest of chemical bonds, grafting the two together.

According to Park et al. (2004) oxyfluorination can condition the surface to effectively change the polarity and activity. The resulting increases in interfacial adhesion forces between CNT and epoxy matrix increase the K_{1c} and impact fracture properties. The author claims that hydrogen bonding interrupts fracture behaviour in impact conditions by hindering the formation of crack growth paths.

Covalent bonding often involves the oxidation of the open ends of nanotubes or defects in the side wall that produce functional groups such as amino-, carboxyl- or glycidyl- groups that can bond with amine to become part of the polymer. Zhu et al. (2003,, 2004) reported a 30% improvement in Young's Modulus and 18% increase in tensile strength of epoxy with 1.0 wt% loading of nanotubes when the nanotubes are functionalized with amino groups or a combination of carboxyl and fluoride groups prior to nanocomposite fabrication Fluorination has been reported to chemically manipulate the CNT side walls through a process of derivatization, taking fluorination as a precursor (Wang et al., 2006b). Ma et al. (2007) argue that better dispersion and interface bonding within the matrix occurs when silane, with epoxy end groups, is grafted, covalently, on to the CNT. This results in better wetting of the CNT and enhances thermal stability, flexural modulus and strength. According to Frankland (2002) if only 1% of the CNT surfaces is bonded to the matrix covalently then the interfacial shear strength would be improved by over an order of magnitude without decreasing the Young's Modulus significantly (Frankland and Harik, 2003).

2.5.3 Property enhancement in CNT nanocomposites

2.5.3.1 Mechanical properties

With homogenous dispersion CNTs can provide a high performance lightweight structural network within a composite matrix. Schadler et al. (1998) gained a 20% increase in tensile modulus with 5wt% MWNTs and Breton (2004) also showed an improvement in modulus by 32% at 6wt% MWNT but yield strength and strain to break decreased when ultrasonically dispersed in epoxy. Alloui et al. (2002) found that the Young's modulus and the yield strength of a 1 wt.% CNT composite have been increased by 100% and 200% respectively when the CNTs were agglomerated in a low modulus matrix. Liu and Wagner (2005) show improvements in tensile strength and modulus as well as improvements in tensile impact properties. An increase of 29% was seen in pristine MWNT and 50% with 1wt% terminal amino functionalised MWNTs nanocomposite. This is attributed to the higher flexibility and deformability under load of the CNT in the matrix. Carbon nanotubes are able to elastically deform under relatively large stresses, both in tension and compression leading to highly energy absorbing processes. The increase in properties of functionalised MWNT is recognised to be an effect of the enhanced interfacial adhesion. Dispersion also accounts for this behaviour as it allows more surfaces to be made available for bonding as well as preventing the filler acting as a filler concentration slippage of nanotube during loading.

Ganguli et al. (2006) compared ball milling and nitric sulphuric acid treatment on the multiwalled nanotubes. A 10% increase in onset of thermal degradation and CTE decrease of 40-70% as well as a 20°C increase in *Tg* was observed. The increase in *Tg* is a result of the restriction in molecular motion and due to the decrease in free volume of the nanocomposite. Better dispersion had been achieved with acid treatment compared with the ball milled resin, though both the 0.1wt% ball milled and acid-treated MWCNT composites performed better than the neat resin sample. At 0.25wt% some tensile properties dropped. Fracture toughness went up 40% with ball milled samples and 80% with acid-treated MWCNT. SEM observations showed topological differences were observed between the different samples. Striation ridges where observed in both samples with acid treated showing more curved and tortuous ridges as well as an increased number of fracture surface features.

2.5.3.2 Fracture toughness properties

Fracture behaviour of nanocomposites is likely to be characteristic in a similar way to fibre-reinforced composites. This is a combination of complex micro damage events such as fibre

break out, interface decohesion and matrix failure. The performance and fracture mechanism can be analysed through microscopy techniques as described in sections 2.3.5 and 2.3.6.

2.5.4 Characterising failure mechanisms in CNT nanocomposites

To determine the cause of failure or, indeed, property enhancement within a CNT material it is once again important to characterise the micro or nano structure. This means observing the dispersion of the nanotubes as well as collecting information on the tube structure, functionalisation, charge transfer between the polymer and tubes and alignment of the tubes within the matrix.

Microscopy on the micro (optical) and the nano (SEM, TEM and AFM) scale are used to determine the dispersion and agglomeration of the nanotubes. Table 2-4 shows an example of differing microscopic dispersions under different mix conditions. In this case it is useful for determining poor dispersion in a short time frame.

Sample	Mixing Conditions	Optical Microscopy	
Sample 1 1% SWNT CP2	Direct Mix	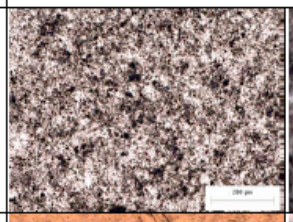	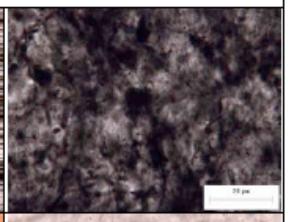
Sample 2 1% SWNT CP2	*In-situ* polymerization under sonication	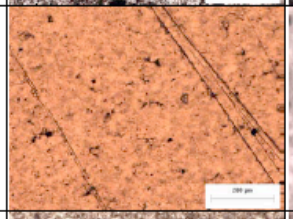	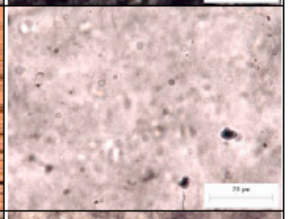
Sample 3 0.5% SWNT β-CN	*In-situ* polymerization with HiPco SWNT	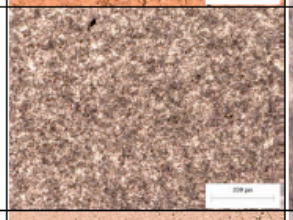	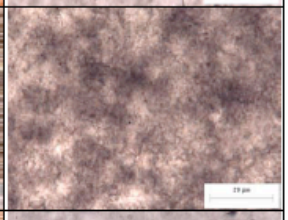
Sample 4 0.5% SWNT β-CN	*In-situ* polymerization with laser ablation SWNT	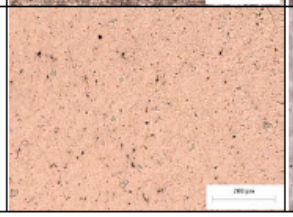	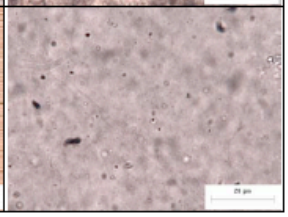

Table 2-4 Table of mixing techniques and dispersion characterisation (Lillehei, 2001).

There are two main reasons for using a scanning electron microscope on samples of carbon nanotubes. First of all it can be used to observe the amount of agglomeration of the CNT. SEM on uncoated samples and with the right detector is able to cover nearly all lengths and

scales from TEM to light microscopy and simultaneously allows shallow insight into the sample. It not always possible to achieve the techniques and resolution for SEM to detect an individual nanotube within the epoxy matrix, however, the surface of the resin or fracture surface should reveal agglomeration in the hundreds of nanometres to micron dimension. SEM images of fracture surfaces can give an indication of failure mode. Very often the difference between brittle failure in pristine resin fracture surface and ductile failure in CNT composites can characterise the difference in the micromechanical behaviour of the nanocomposite. Kovacs et al. (2007) observed SEM topological differences occured between the different samples. Striation ridges were observed in all samples except the neat resin, with acid treated showing more curved and tortuous ridges as well as an increased number of fracture surface features.

A TEM of CNT polymer composite shows individual dispersion of composites. The increased intensity (200 – 300KeV) over the SEM allows the electron beam to pass through the microtomed sample giving images of all CNT in the section. The nanotubes or nanotube bundles beneath the matrix surface can be imaged for characterisation. Researchers have also managed to characterise the crack bridging and crack pinning mechanism by observing images of the CNT pull. Figure 2-11 is an example of the TEM being used to characterise failure mechanisms showing how CNTs tend to aligned perpendicular to the crack path as they are pulled out. Tube A shows a telescopic failure where the middle tubes are pulled out as the outside tubes break. A few of the aligned nanotubes,, such as tube B in Figure 2-11b, have broken and subsequently pulled out of the matrix. The MWNTs that are aligned more parallel to the crack propagation direction tend to break between the crack faces rather than in the matrix (see tube D in Figure 2~11b) and some tubes have broken at obvious defects, such as tube C (Qian et al., 2000).

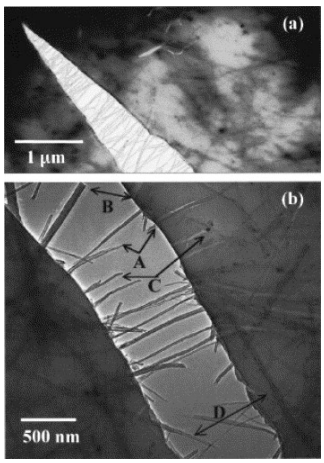

Figure 2-10 In situ observation of MWNT (a) across the crack path and (b) the failure of MWNT across the crack nucleation and propagation in MWNT-PS thin films as induced by thermal stresses (Qian et al., 2000).

DMA testing is, once again, useful for characterising the nanocomposites thermo mechanical properties. This can also be a way of assessing the relative fracture toughness of samples. The value of the loss modulus, *E″*, is a measure of viscoelasticity of the polymer. It implies how much energy the specimen can absorb and the larger the area under the loss modulus curve, the higher the toughness of the material (Suhr and Koratkar, 2008).

2.6 Performance of nanocomposites with fibre reinforcement

Traditional fibre reinforced composites have excellent strength and modulus properties in the direction of the fibre. These fibre dominated properties are only influenced a small fraction by the resin matrix properties. Other influences include volume fraction, fibre alignment and fibre interface. Of which the later can be effected by use of nanocomposites, increasing the bond between the resin and the fibre.

Translated through rule of mixtures, the enhancement, by nanocomposites, on the bulk property performance in resin cast is likely to increase the properties of a laminate. This is especially true in the case of the transverse direction and to a lesser extent the in-plane (in the direction of the fibre) properties. However, the mechanisms that have been demonstrated in the previous sections may provide enhancement in the critical failure modes of fibre-reinforced laminates. Crack retardation, as one such example, has been proven to improve by nanocomposites in a resin without the reduction in modulus seen with other fillers. Improve the resin in this area could reduce the likelihood of failure in delamination or interlaminar shear stress and increase the performance of the composite after impact damage. This would also reduce the onset of microcracking or crazing in compression, a composite is also very much driven by the quality of a laminate. This failure method has many contributing mechanisms which are not all fibre dominated. The nanoparticle reinforcement mechanism may support the fibre in a way that prevents it from buckling by preventing microcracking in the resin in an area where the buckling occurs.

2.6.1 Applying nanocomposites with fibre reinforcement

The application of nanocomposites in composite structures has not lived up to the hype of the reported epoxy materials performance (Veedu et al., 2006). Despite the potential, issues such as dispersion, alignment and interfacial strength have hindered the success.

The method of composite manufacture and the materials chosen play a significant part in the effectiveness of the three-phase composite. The fibre reinforcement has to be wetted by the epoxy resin before a force is applied to remove air. This also ensures a good interface between fibre and matrix as well as consolidating the layers of laminates to fit whatever form it is being moulded to before it is heated to a temperature it initiates the best curing

process. There are many methods of doing this, which include: vacuum resin infusion, pre-impregnating the fibre and then moulding it, as well as wetting the fibre by hand. Depending in the application and fibre lay-up and cost requirements will determine which method of manufacture is chosen. The first two methods are generally regarded by industry to bring out the best performance of the composites due to the good wetting and alignment of the fibre. Infusion, however, requires a low viscosity resin to wet out the fibres, which may restrict the use of nanocomposites. Pre-preg uses a different chemistry which becomes semi solid when laid against the fibre and usability requires a criteria of tack and drape.

2.6.2 Structural enhancement of fibre reinforced composites

Subramaniyan et al., (2003) studied the effects of nanoclay on the compressive strength of fibre composites and to develop a method for processing this type of composite material. The resin was reinforced with modified montmorillonite clay and testing showed the 5% clay samples gave the best improvement in the compressive strengths. Siddiqui et al.(2007) showed that with CFRP (carbon fibre reinforced plastic) / nanoclay / epoxy composite there was an improvement in flexural modulus at the expense of a gradual drop in flexural strength with clay content. Static fracture toughness increased with clay content; the best result was found at 3wt% clay content. Impact fracture toughness decreased by 45% at 1wt% clay content. Initiation and propagation of interlaminar fracture is increased and is almost doubled at 7wt% nanoclay, as shown in Figure 2-11.

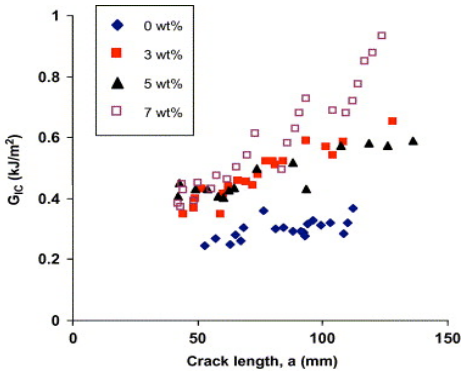

Figure 2-11 Mode I interlaminar fracture toughness, G_{IC}, as a function of crack length, a, for CFRP composites containing different clay contents(Siddiqui et al., 2007).

Timmerman et al. (2002) was interested in a specific application of nanocomposites. Traditional composite cryogenic liquid storage, which incurs thermal cyclic induced stresses, suffers from micro cracking and hence a good application for clay/ epoxy pre-preg laminates. Thermal expansion and microcracking (50 % decrease on pristine resin at 5wt%) properties were improved over the pristine laminate. Transverse flexural yield strength, however, was lower for 2 and 5wt% nanoclay but similar values for 8wt% were found to the pristine epoxy pre-preg.

Haque et al. (2003) looked at 1 and 2wt% Southern Clay, SC15, nanoclay. At 1%wt clay content flexural strength increased by 24% over the pristine resin lay-up, increasing to 2wt% nanoclay would only show an 11% increase. 1–2 wt% of clay loading also improved fracture toughness by 23% and 20% respectively. This is due to the enhancement of matrix from the silicate lamella structure, the synergistic interaction between the matrix, clay and fibres and enhanced matrix-fibre adhesion promoted by the clay. However, at higher loadings it is thought that the degradation of properties was due to the phase-separated agglomeration of clay structures and defects in the cross-linking of the polymer.

Cho and Daniel (2008) created a fibre reinforced nanocomposite using CNT enhanced five-harness satin weave carbon fibre. Nanotubes were dispersed with Disperbyk – 2150, a commercially available block copolymer, pigment affinic groups and a bisphenol –A epoxy using rotary mixing and followed by ultrasonication. Carbon fabric was impregnated with the solution to create a pre-preg layup. The glass transition temperature was increased by 39°C, Interlaminar shear strength by 15% and compressive strength by 39%. Gojny et al. (2005) studied the addition of amino-functionalised double walled nanotubes (DWCNT-NH_2) to a glass fibre composite. The laminates infused by resin transfer moulding (RTM) successfully allowed the nanotubes throughout the mould without any significant filtering effect of the nanophase. At higher loading of nanotubes the processing caused problems due to increased viscosity, hence tensile strength and Young's Modulus were not increased.

Instead of using the conventional method of dispersing nanoparticles in the resin, Zhu et al. (2007) used woven glass fabric was sprayed with a nanotube solution coating the fibres with the nanotubes. Two nano-enhanced laminates were placed in the midplane of a 12 ply laminate and infused with vinyl ester resin. Under 0.2wt% CNT of the fibre weight would improve the laminate properties, the nanotubes acting as coupling agents for the interphase between the polymer and fibre. Over 0.2wt% content would adversely affect the fibre wetting ability. Bekyarova et al. (2007) utilised electrophoresis to deposit multi- and single-walled carbon nanotubes (CNTs) on to woven carbon fabric. The CNT-coated carbon fabric panels were subsequently infiltrated with epoxy resin using vacuum-assisted resin transfer moulding (VARTM) to fabricate CNT fibre hybrid composites. This process increased the interlaminar shear strength by 30% compared to the traditional carbon fibre/epoxy composites without carbon nanotubes and demonstrates significantly improved out-of-plane electrical conductivity. Zhou et al. (2008a) took various levels carbon nanofibre loadings combined with a satin weave carbon fabric to produce a CNF epoxy laminate by a VARTM process. 2wt% loading was found to give the all round greatest enhancement with 17% tensile strength increase in the resin and 11% tensile strength increase in the laminate. A stress controlled tension-tension fatigue test showed that the fatigue life of the CNF epoxy is

significantly higher than that of neat epoxy. Figure 2-24 shows at the lowest stress of 35MPa the number of cycles to failure for the 2wt% CNF epoxy is an order of magnitude higher than the neat epoxy and this increases even more for higher stresses tested. Fracture toughness was also measured using single edge notch tensile test and increased 30%.

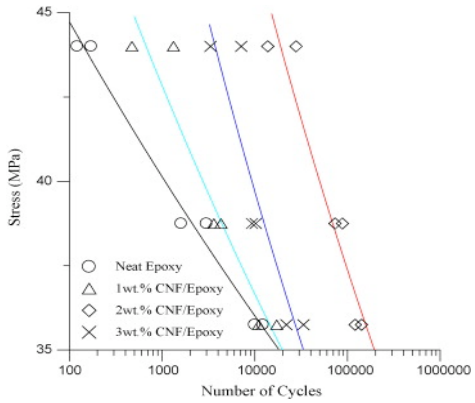

Figure 2-12. S–N curves of epoxy and nanocomposite (Zhou et al., 2008a).

In the laminate the 2%wt CNF epoxy produced an increase in flexural strength of 22.3% and tensile strength of 11%. S-N curves for the CNF laminate also show an increase in fatigue strength. Zhou et al. (2008a) also tested MWCNT in a bisphenol-f epoxy system and infused a carbon laminate with the nanocomposite. The epoxy system had a higher tensile strength but lower modulus than the pristine SC-15 system used. With 0.3wt% MWCNT the neat resin increased 30% in tensile strength and maximum of 12% increase in modulus at 0.4wt% MWCNT. K_{1c} fracture toughness was also improved by 32% at 0.3wt% loading. Laminate testing showed a flexural strength and modulus increase of 3% and 6% respectively. Re-agglomeration of the MWCNT also occurred during the degassing stage of the process due to a lack of stabilization treatment on the nanotubes.

2.6.3 Discussion

Table 2-5 summarises the results from a range of nanoparticle enhanced laminates. It compares the change in compressive strength and interlaminar shear strength as well as some flexural properties where indicated. These are related to the different fibre types, fibre weaves and fibre volume fraction, as well as the type of matrix used and nanoparticles and loading. With this variability it does make it difficult to compare the properties but it does highlight the great effect manufacturing process can have on the composite structure.

Author(s) / year	Nanoparticle / modifier	wt%	Resin	Hardener	Fibre	Process	Compressive strength MPa	Enhanced strength MPa	% Increase	Interlaminar strength MPa	Enhanced strength MPa	% Increase
Cho, Chen, Daniel 2007	Graphite nanoplatelets	5	GY 6010	Aradur 917/DY070	1.8g/cm^3 Carbon UD		551	638	16%	374	416	11%
Cho, Daniel 2007	MWNT/Disperbyk2150	0.5	GY6010	4,4-DDS	AGP370-5H carbon fabric		565	785	39%	57	65.5	15%
Gojny 2005	MWNT/amino	0.3	Bakelite L135i	H137i	Non crimp glass fabric	RTM				31.8	38.1	20%
Zhou 2008	CNF	2	SC-15	cycloaliphatic amine	10oz and Carbon satin weave		488	597	22%	556	617	11%
Imahori 2004	CSNF	10	Epikote 827	Epikure W (aromatic amine)	T300 plain woven 0/90 carbon Vf 56%		447	511	14%	667	790	18%
Yokozeki 2007	CSCNT	10	EP827	dicyandiamide	UD T700SC 12K		488	539	10%	875	912	4%
Klosterman 2007	VGCF oxidised	8	Epon 862	DETDA	UD 290g/m^2	Pre-pregnated	486	603	24%	143	184	29%
Zhu 2006	SWNT coating fibre		Derakane 510A-40 Bis A epoxy based	Vinyl ester	24oz E-glass woven roving					27	39	44%
Fan 2008	MWNT oxidized	2	SC-15		Woven glass 800g/^2 Vf50-55%	INVARTM				25	34	33%
Veedu						CNT grown on fibre						
Haque 2003	nanoclay	1	sc-15	cycloaliphatic amine	S2 glass plain weeve	VARTM	299	370	24%	23	33	44%
Timmerman 2002	nanoclay	2			150g carbon UD T300	Prepreg	56	49	-13%	64	71	11%
Quaresimin 2008	nanoclay		DER331 + epoxy novolac	anhydride	ud carbon	prepreg	640	640	0%	43	42	-2%
resimin 2009	VGCF		DER331 + epoxy novolac	anhydride	ud carbon	prepreg	640	590	-8%	43	50	16%

Table 2-5 Table of fibre reinforced composites compared with the nano-enhanced fibre composites.

2.7 *Summary of Nanocomposite Performance*

A study of the various published nanocomposite process, characterisation techniques bonding and properties of nanoclay and carbon nanotube or nanofibre composites has been made and summarised in tabular form below. The compatibility problem has been reviewed by looking at a number of published papers, as shown in Table 2-6, comparing epoxy functionality to different categories of clay modification. The processing method and material used is examined in Table 2-7 and different characterisation techniques and properties measured are shown in Table 2-8. The aim is to identify the materials and methods that are most commonly published to give trends in the gaps in existing research. Each paper is indicated by a number in a square bracket, which corresponds to a reference with that number in Appendix A.

2.7.1 Types of nanocomposite

The size, chemistry and structure of the nanoparticle influence not only its specific properties but those of the composite that it constitutes as well. With nanoclays the type of clay and its shape affect the dispersion as it does with nanotubes. A smaller particle or higher aspect ratio increases the SSA and attraction between particles causes tighter agglomeration, which is harder to disperse. The larger the particle the more material, in terms of % or the total weight, is used to get the greatest enhancement. This is because smaller particles such as SWCNT have a lower percolation threshold than larger ones such as CNF or even micro-fillers. The chemistry and structure of the carbon nanotubes lend themselves well to a structural enhancement, the carbon-carbon lattice being one of the strongest bond mechanisms known. This gives the CNT not only the incredible strength properties reported but renders it capable of withstanding large strains as well as having an impressive modulus. However, as discussed this chemical make up is not ideal for good bonding interface and it has shown drawbacks because of this.

2.7.2 Dispersion effect on properties

The combining of nanomaterials, especially inorganic nanoclays, with polymers shows much more potential when they are modified on the surface with organic surfactants. Exfoliation absorption, in-situ polymerisation and melt intercalation are most commonly used processes with epoxy nanocomposites. Melt intercalation is similar to the standard epoxy composite fabrication with little added, once the clay is modified, to the processing and composition of a two part epoxy or wet system. In-situ polymerisation requires a process before the nanoclay is added to the epoxy; however, it often only requires heat to start the epoxy curing, similar to the one part epoxy or dry systems found in pre-pregnated

composite systems. The in-situ polymerisation often favours the exfoliation of nanoclay over other methods. This suggests that the modification of the nanoclay has to be compatible with the epoxy system used and therefore is a much more important factor in the fabrication process.

Compatability		Epoxy				
		Epoxy monomer	DGEBA	DGEBF	Tri-functional	Tetra-functional
Clay modification	Quarternary Alkylamine		[1],[2],			[2]
	Quarternary Ammonium/ Alkyammonium	[3] (7.5nm)	[4](3.8nm), [5] (3.5nm), [1], [6], [7](8nm), [8], [9](10nm), [10](3.5nm), [11]			[11]
	Primary Ammonium (e.g.Octadecyl)		[12],(8nm) [8, 13](3.5nm) [14]>4nm		[12](4.5-5nm)	[12](4.5-5nm)
	Primary Amine n-decylamine hexadecylamine dodecylamine		[15](4-5nm),[16][I], [17, 18](>20nm), [1], [19], [20](>8.8nm), [21]	[17, 18](25nm) [22](>4nm)		[23]
	Epoxy accelerator		[24][ii] (1.9nm), [25][iii](3.9nm) [26][iv](<8.8nm), [27][v]			
	Other		[28][vi]			

Table 2-6 Table of the different types of epoxy and surfactant types used.

Table 2-6 breaks down the different epoxy types into their functional groups, splitting the bifunctional into diglycidyl ether of bisphenol A (DGEBA) and diglycidyl ether of bisphenol F (DGEBF) categories. The clay modification is categorised as quarternary alkylamine and alkyammonium, primary ammonium and amine surfactants. Other surfactants that were referred to in the reports as epoxy catalysts or accelerators are placed in their own category as this implies an in-situ process. These catalysts are identified in the footnote. Those that do not apply to any of the above description, but were used in a process to modify the nanoclay were categorised as other, also identified in the footnote. Where possible the maximum interlamella spacing has been identified in nanometres. This should give an indication of which combination of epoxy and modifier has had best success.

[I] Worked with different length alkylamine (c4-c18)
[ii] Jeffamine
[iii] M-xylylenediamine (MXD)
[iv] Meta-xylylenediamine (MXDA) with Dodecylbenzyldimethylammonium chloride (DBDA)
[v] 2,4,6-tris-(dimenthylaminomethyl) phenol (DMP-30)
[vi] Acified Cocamidopropyl Betaine (CAB)

Table 2-6 also shows that the majority of research in epoxy has been with DGEBA and much of it has produced an exfoliated nanocomposite. The clay modification used has been manly with quarternary alkylammonium or primary amine surfactants. The greatest measured lamella separation is with a primary amine surfactant combined with a bifunctional epoxy, both DGEBA and DGEBF. There does not seem to be a direct trend in the degree of exfoliation this would suggest that the mixing process is as important to the exfoliation process.

With the polarity and chemical compatibility permitting, the process of dispersing and exfoliating the nanoclay is crucial to creating a fully homogeneous enhanced polymer. Different methods of high-shear milling, high pressure mixing and sonication processing have shown improvement in dispersion, exfoliation and material properties. With this high shear processing the problem of keeping the composite air free has shown to be greater with an increased viscosity entrapping air and also making the degassing process difficult.

Processing	Stirring Unspecified	Stirred at specific temperature	High shear stirring	Ultrasonic mixing	Ball/bead/ three roll milling
Solvent mixing	[6],	[27],[23]	[23]	[6],[8]	[26]
Catalyst/ Hardener mixing		[25],[24]	[3]		
Resin mixing	[15],[6],[23],[8], [4],[17], [13]	[18],[5],[20],[28], [12],[16],[14], [9],[10],[10],[11]	[2],[23]	[15],[1],[29],[4], [9],[10], [21]	[7],[26]

Table 2-7 Table of processing methods.

Table 2-7 categorises processing as stirring; indicating low speed mechanical or hand mixing; high shear, which is a high speed mechanical mixing; ultrasonic, a sonic or vibration agitation and milling, which includes other types of mechanical dispersion processes. The table quite clearly indicates that most research used the resin to process with the nanoclay. The most common process used was stirring at a specified temperature. However, it also shows that much of the processing is at an unspecified temperature. Dispersion of the product has been accomplished at low shear rates when the materials are compatible and enough time has been allowed. More time gives greater energy, and allows the clay can be dispersed homogeneously. If not compatible, only excessive grinding (high impact with the clay particle) will disperse the particle. However, there appears to be a shortfall of research in high shear processing and no comparison between high shear methods.

The critical review has highlighted some contradictions found in material performance, most significantly in the bulk properties, such as tensile modulus and strength. There are some unknown factors that could influence this, such as void content in the cured sample or in some cases the dispersion of nanoclay has not been quantified and this may have affected properties.

Characterisation	Optical Visual/ infra red	Micro-scopic	SEM	TEM	WAXS	SAXS
No physical properties measured				[25]	[25]	
Thermo mechanical	[19],[6]	[11]	[2],[19]	[18],[2],[20],[1], [6],[8],[12],[10]	[5],[3],[18],[19] ,[20],[1],[6],[12], [10],[11]	[18]
Mechanical Bulk properties		[14]	[2],[7],[4]	[2],[20],[7], [16],[10]	[20],[16],[4],[14], [10]	[7]
Mechanical Impact/fracture	[19],[24]	[11]	[2],[19], [26],[23], [29],[24], [4],[21]	[2],[26],[23],[29], [8],[16],[24], [10],[21]	[19],[26],[23], [16],[24],[4],[10],[11]	
Thermal analysis	[24],[13] ,[9]	[14], [11]	[2],[23], [28],[24], [4]	[2],[15], [27],[23],[8],[12], [24],[17],[9],[10]	[15],[27],[23], [28],[12],[24], [4],[17],[9],[14], [10],[11],	[17]
Rheology	[13]		[23]	[23]	[18],[23]	[18]
Barrier			[23]	[20],[1],[23],[12], [17]	[20],[1],[23], [12],[17]	[17]
Fire						
Electromechanical				[17]	[17]	[17]

Table 2-8 Table of the Characterisation techniques employed and the physical properties analysed.

Table 2-8 shows observational characterisation along the top row and physical measurements in the left hand column. The table shows wide-angle X-ray diffraction WAXS as the most commonly used characterisation tool along with TEM. The thermal and mechanical properties are also frequently analysed for change in the material properties. This includes cone calorimeter testing, which gives a measure of the mass lost during combustion or at high temperatures, some of criteria for a fire retarding material testing.

The table can be used to highlight where there may be a gap in knowledge. There has been a fair proportion of research in fracture toughness. The results, on the whole, agree that greater fracture toughness properties occur with increasing clay content. The fatigue performance of nanoclay/epoxy composite, unlike their CNT composite cousins, is not reported on thus far.

Research in this area of nanocomposites has tended to concentrate more on the state of exfoliation and as a result the overall dispersion throughout the composite has been left off the agenda. Several papers demonstrated the ability to exfoliate nanoclay by inserting the polymer molecule between the silicate sheets. This has been done, with varying success, using a range of chemical modifications on the clay and applying kinetic energy to help break the sheets apart and disperse the nanoclay. However, less attention has been paid to the overall dispersion of the nanoclay and the removal of air in the liquid epoxy before it is hardened and the measurement of these processes. The critical review has identified some key points in the processing of nanocomposites; the homogeneity of dispersal, the exfoliation of the clay layers and the degassing of the epoxy / Nanoclay solution.

2.7.3 Bonding effect on Properties

Research into nanoclays has indicated that enhanced material properties correlate with exfoliation. This effect causes greater surface area to be available but due to the chemical nature of clay the dispersion issue has lent heavily on the use of surfactants to aid break up and prevention of agglomeration. In this case Van der Waals bonding is nearly always used. Bonding method has been critical to enhancement for properties of CNT nanocomposites. Surface treatment or functionalisation of the nanotubes is used for dispersing and increasing the interface strength for the benefit of increasing composite mechanical properties. Table 2-9 summarises the modulus and fracture properties of the CNT nanoresins relative to the CNT type, surface modification and processing. In general it shows that a low percentage loading of nanotubes can improve the composite properties. The most desirable loading is at around 0.5wt%. Covalent bonding methods are most widely tested and tend to show the biggest percentage increase. However, the oxyfluorinated hydrogen bonding shows that the non-covalent methods can provide significant increase in fracture toughness.

Pristine CNT nanocomposites also show some property increase as with Zhou et al. (2007b), Sun et al (2008) and Ci and Bai (2006). Between them they show from 0% change to up to 18% increase in modulus,16% increase in tensile strength and nearly 30% increase in flexural strength. This may not be as great an increase as the covalently bonded nanocomposites but still shows significance.

Author(s) / year	Nanoparticle / modifier	wt%	Resin	Hardener	Process	Modulus GPa	Enhanced modulus GPa	% increase	Fracture Toughness MPa m^1/2	Enhanced Toughness Mpa m^1/2	% Increase	Strength MPa	Enhanced strength MPa	% Increase
Tseng 2007	plasma treatment; , maleic anhydride (MA) MWNTs	0.1	Bis-A		sonication shear mixing	0.6	1.2	100%				45	61	36%
Zheng 2006	MWNT/NH2	0.6	Epoxy	amine		1.55 Flexural	2.45	58%	8.5 Izod Impact	15.5	82%	33 Flexural	66	100%
Moniruzzaman 2006	SWNT esterification	0.05	Bis-F	PACM	sonication + shear mixing	1.1 Flexural	1.28	16%				158 Flexural	173	9%
Wang 2006	SWNT / amino	0.5	Bis-F			2.44 DMA storage modulus	3.04	25%						
Miyagawa 2005	flourinated-SWNT	0.2	Bis-F	anhydride	sonication	3.2 DMA storage modulus	4	25%	0.523	0.78	49%			
Park 2004	F-SWNT (oxyfluorinated)	0.5	Bis-A	DDM amine	sonication				K1c 2.45 Impact 21.34	3.05 24.04	24% 13%			
Subramanian 2005	SWNT PVP	0.5	Bis-F		impingement mixer	1.13	1.57	39%				80.12	84.67	6%
Gojny 2005	DWCNT-NH2	0.5	DGEBA	amine	3 -roll calendar	2.6	2.98	15%	0.65	0.82	26%	63.8	69.13	8%
Zhu 2004	SWNT-R-NH2		Bis-F	diamine	sonicatoion	2.03	3.4	67%				83	102	23%
Zhou 2007	pristine MWNT	0.3	Bis-F	agent W	sonication	2.46 Flexural	2.65	8%				93.5 Flexural	121	29%
Sun 2008	PAMAM-O grafted SWCNT	1	Bis-F	agent W	rotary stirring	2.76	3.49	26%	0.56	0.76	36%	64.1	74.7	17%
Sun 2008	pristine SWCNT	1	Bis-F	agent W	rotary stirring	2.76	3.27	18%	0.56	0.58	4%	64.1	74.1	16%
Ci, Bai 2006	pristine	0.5	Bis-A	triethylenete tramine	mechanical shearing	2.44	2.45	0%				45.4	47.7	5%
Ganguli 2006	acid treated	0.15	Bis -A		Ball milling				5.6	10	79%			

Table 2-9 Summary of CNT resin performance and surface treatment

When the value of the pristine epoxy properties and the processing is taken into account then certain influences stand out. Modulus, specifically, has been shown to affect the property enhancement. A low modulus resin usually enhances its stiffness with CNT more than a high modulus resin. Consequently the accompanying high fracture toughness of a low modulus resin shows little improvement compared to a brittle, high modulus resin, as shown by Quaresimin and Varley (2008) and Zhou et al.(2007a). They also show that in a soft ductile composite carbon nanotubes display significant stiffness reinforcement. This is due, however, to a possible accelerated curing process and better interface. In a brittle resin the interface interaction is poor due to complete cross-linking of the polymer molecules surrounding carbon nanotubes.

2.7.4 Concluding remarks

Throughout nearly all research published the experimental data indicate that homogeneous dispersion functionalised interfacial bonding increases mechanical properties. This is proved by analysis of the fracture surface and comparison of dispersion to be a result of the bonding and processing method. There is no clear comparison between many of these techniques employed. As Table 2-9, demonstrates a straight comparison between the research data is not simple due to the many inconsistencies that occur. From an industrial point of view the relationship between materials, process and bonding is of great interest if developing a material. To get maximum benefit from a nanocomposite system will, no doubt, depend on the type of system and the application for the composite. This requires a form of design process to tailor the type of nanoparticles, the type of interface and the process of manufacture.

3 Motivation and Method

The ultimate goal of the project is to gain structural enhancement of composite materials using nanoparticles. This motivation is based on the structural improvements reported in literature and industry. On a higher level, motivation for this work is aimed at gaining improvement for high performance composite structural design. This fundamentally attempts to improve performance, which nearly always translates to reduction in weight. Improving the structural working life and breaking strength and thus reducing costs are also considered motivation to research nanocomposite for structural applications.

3.1 Criteria of investigation

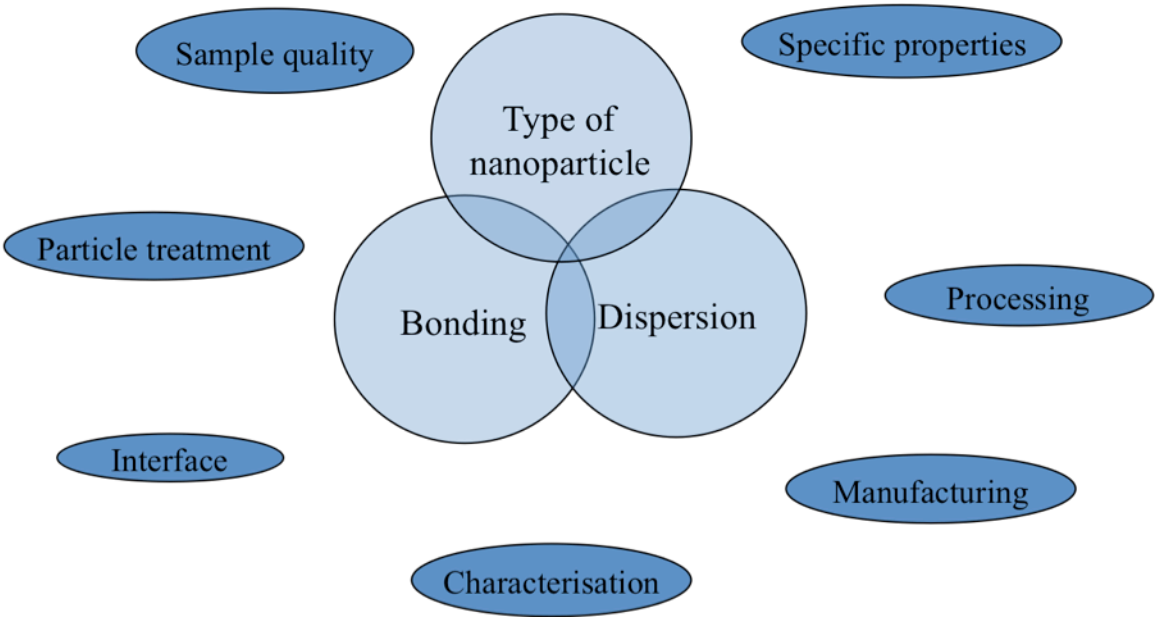

Figure 3-1 Criteria and influencing factors on the achieving structural performance in nanocomposites.

Looking at the inner circle of the Venn diagram in Figure 3-1 essentially there are questions regarding the type nanoparticles used, the bonding mechanism and the dispersion. A common theme can be concluded from the literature in cases where the nano-enhanced resin systems have not performed as well as the pristine resin. When failure mechanisms are assessed, usually by electron microscopy, it is found that that the weakness is often in the interfacial bonding. The cause of this is either the dispersion or the actual bond mechanism. The characteristic topology often shows this and with signature fracture surfaces or identifiable conglomerates of nanoparticle identified in post testing assessment.

Guaranteeing the dispersion and good bonding, on an industrial scale, is very difficult to attain. This is one reason why there are, after over 10 years research into nanocomposites, very few examples of structurally enhanced applications.

The type of nanoparticles also plays a role in the assessment of performance. As discussed in chapter 2 sections 2.2 and 2.6.1 the physical way the particle interacts with the polymer can be affected by its structure and its properties. This not only refers to the type of particle classification but also the type of particle within the classification.

The specific properties of a particle affect the nanocomposite in the same way the specific fibre properties effect traditional composites and can be simply calculated by the rule of mixtures for simplistic values. With nanocomposites the prediction is not so simple, as the Venn diagram in Figure 3-1 shows, the properties rely on the range of criteria in the outer circle, which affect the criteria in the inner circle. The most effective use of the three main criteria; material, dispersion and bonding, as explained in sections 2.2 and 2.6, are influenced by a number of other factors also highlighted around the main criteria.

The sample quality or the purity of the nanoparticles is driven by the production process and filtering which, if includes impurities or deformed particles, would introduce weakness in the nanomaterial. This would cause defects in the bonding mechanism and may hinder the dispersion, all contributing to reducing the nanocomposite effectiveness. This also can apply to the quality of the processed nanocomposite or indeed the laminate quality.

Manufacturing of the resin composite or laminates is, as discussed in 2.2.4 and 2.5, not only is important for the material property with reduction of air, alignment of fibres as well as dispersion of nanoparticles but also important from a fibre interface perspective, with different manufacturing techniques being adopted to overcome dispersion difficulties with varying success.

Particle treatment, reviewed in section 2.2.1, 2.4 and 2.4.1, is critical to the bonding of the nanoparticles as well as the dispersion. Processing of the nanoparticles resin, which is important to the dispersion and thus influential on the structural enhancement, can be dependent on the type of nanoparticles as shown in section 2.2.3 and 2.3.1.

The interface, investigated in sections 2.2.1, 2.3 and 2.4 and 2.5, is determined by the bond mechanism. This influences the whole behaviour of the composite similar to the way it does with structural fibre composites. The phase interface determines the how the composite reacts to out of plane forces and deflections.

Finally characterisation considers assessment techniques discussed in 2.3.6 and 2.4.4 and 2.6.2. It is essential to the production of good quality nanocomposites and, as seen in Figure 3-2, is part of the production process.

3.2 Method of investigation

The aim of this work is to explore these areas, looking at the structural properties of epoxy nanocomposites and comparing their effectiveness in a fibre-reinforced composite. The study will research the importance of dispersion methods in nanoclay composites to determine the best dispersion according to the characterisation tools available.

The characterisation criteria will initially make an assessment with optical microscopy on the wet resin. More detailed analysis can be made with SEM and TEM and x-ray spectroscopy. Finally a study of the material properties can build comparison between the dispersion methods. Figure 3-2 shows the approach to the work on the left hand side and the analytical methods that can be used on the right. Starting the analysis on the wet resin through to the cured sample and mechanical testing, there are analytical techniques at all stages to assess the effectiveness of processing used, the interface and nanoparticle for how they behave.

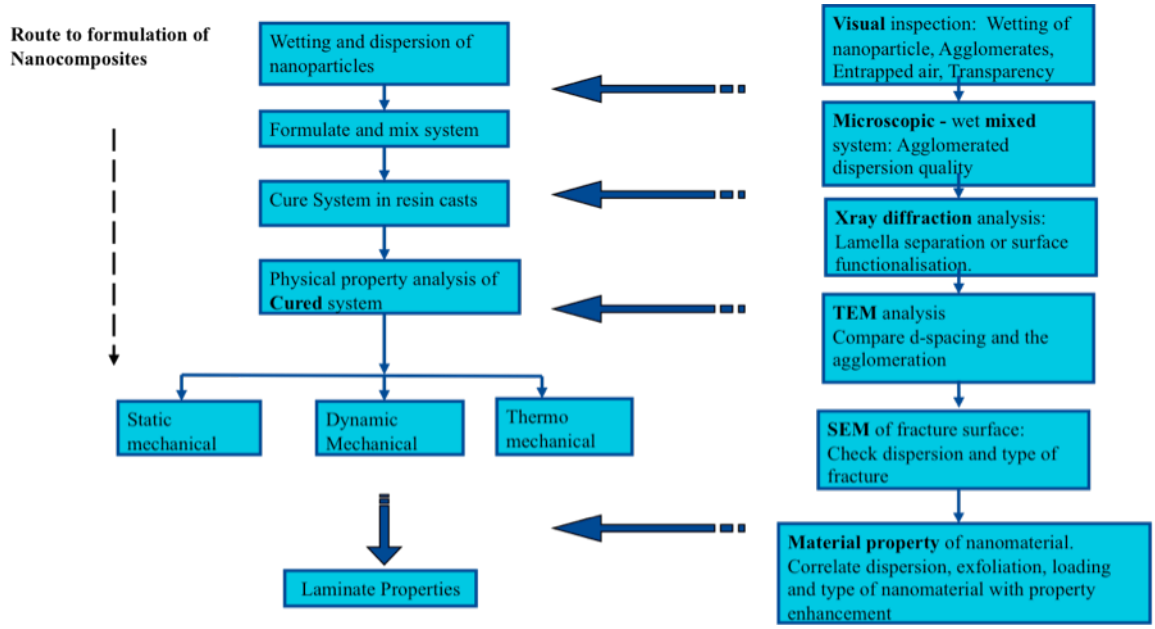

Figure 3-2 Flow diagram of nanocomposite dispersion and structural criteria analysis.

A comparison of bonding mechanisms will also explore the behaviour of CNT nanocomposites with respect to the CNT loading. Structural property analysis of the nanocomposite will be made on the nano-matrix interface. This will incorporate different commercially available CNT dispersions. Mechanical properties of each nanocomposite system will be tested and compared to gain understanding of performance and processing behaviour. The next step is to investigate nanocomposite/fibre interface. This will incorporate the assessment of the performance of fibre reinforced nanocomposites and analysis of the fibre/matrix fracture mechanism.

4 Investigation of the nanoclay dispersion process

This investigation into processing is a detailed look at the factors that affect the way in which nanoclay is dispersed and exfoliated in epoxy resin. Nanoclay has been chosen in this study because it is cheap and easy to obtain in dry, modified form and represents less of an unknown health risk than other dry forms of nanoparticles due to the larger size of the particle relative to other nanoparticles. Due to these dimensions of the clay, characterisation is also relatively easier in visualisation terms and as a function of measuring the separation of the layered structure. Chapter 2 identified that dispersion and hence measurement of dispersion is a key issue in the use of nanocomposites for structural use. The mechanical dispersal methods discussed in 2.2 identified three main dispersion routes: high shear mixing, milling and ultrasonic dispersion. The effectiveness of two of these routes, milling and high shear mixing are compared here according to the method set out in Chapter 3. In the first stages of Figure 3-2 the dispersion is checked optically and after curing, SEM, as well as X-ray diffraction, can be compared with TEM to show the clay dispersion, exfoliation or agglomeration.

4.1 Materials

The nanofiller Bentone2010, from Elementis Inc., organically modified montmorillonite nanoclay, was recommended for its polarity to be used with epoxy. This is bentonite clay which has been modified with quaternary ammonium surfactants to increase the polarity of the clay and make it an organophilic compound to help combine with the epoxy. The shape of clay particles are irregular and the particle size can vary with different deposits, but their approximate dimensions are 800 x 800 x 1 nm and can be seen in agglomerated form in Figure 4.1.

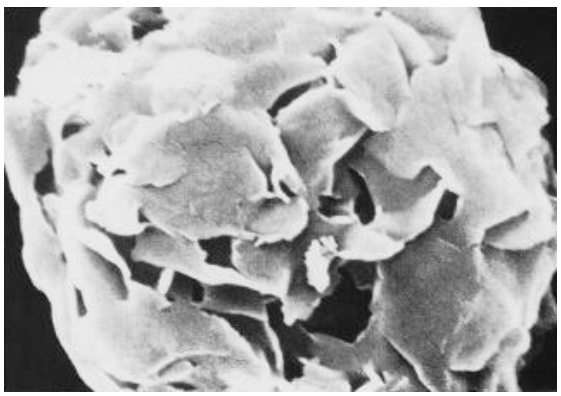

Figure 4-1 Clay particle magnified 10,000X showing platelet stacks prior to full dispersion (from Elementis).

The nanoclay was mixed with the two separate epoxy resin systems: Araldite DY-T, a low viscosity tri-functional (Triglycidylether of trimethyolpropane) epoxy and Dow DER330, diglycidyl ether of bisphenol A (DGEBA), a comparatively higher viscosity epoxy resin used in a wide range of applications. Jeffamine D230 was the curing agent added to the epoxy at the stoichiometric ratio for curing, calculated by the molecular weight of each epoxy, 100:48 for DY-T and 100:33 for DER330, by weight of the pristine resin to hardener. Each sample batch of epoxy was mixed with the equivalent of 2wt% bentone 2010 nanoclay of the final cured nanocomposite. For a typical batch the amounts were as in Table 4-1:

Component properties	DY-T	DER330
Epoxy Viscosity at 25°C(mPas)	100-300	7000-10000
Epoxy(g)	200	200
Jeffamine D230(g)	96	66
Bentone 2010(g)	5.92	5.32

Table 4-1 Epoxy properties from Huntsman (www.Huntsman.com) and Dow (epoxy.dow.com/) showing typical sample component weights for DY-T and DER330 batches.

4.2 Processing

To initially transport and disperse the Bentone into the liquid epoxy a centrifugal (DAC) mixer was employed. Each sample batch of resin was mixed for 5 minutes at the maximum speed of 2500rpm, to wet-out any traces of dry nanoclay and disperse all large clusters. The resin and the nanofillers were then mechanically processed using two separate methods. Firstly, a pneumatic powered high shear mixer was used. This rotated a 60mm cowel dissolver (a toothed disc) at the maximum revolutions of 3000rpm. Secondly, a Netzsch mini zeta horizontal bead mill (see Figure 4-2) was run at 4400Hz. This was found to be the maximum speed at which the returning stream of fluid into the hopper did not cause extra air to be induced into the solution. Each process was run for 15, 30 and 60 minutes. The temperature of the epoxy in each process was monitored by thermocouple.

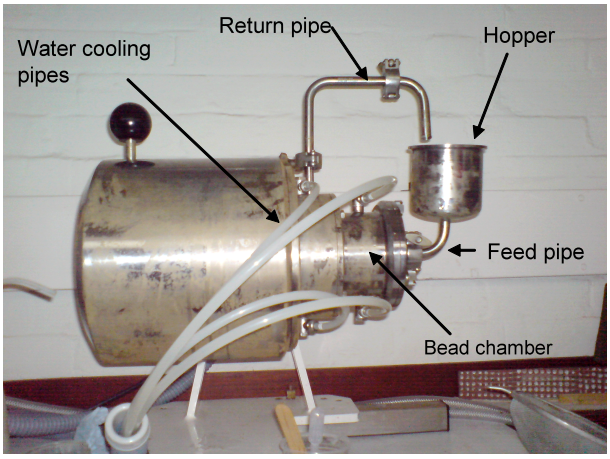

Figure 4-2 Netzsch Mini Zeta bead mill.

The mixed batches were then degassed. The DAC mixer was also used to remove larger bubbles; however, the best method was found to be at -1bar in a heated degas tank from West Systems Technology. The degas tank temperature could be increased to 50□C and monitored by thermostat to decrease the viscosity of the epoxy. A mixing paddle, sealed in the lid of the degas tank, was used to help break down the expanding bubbles and prevent the mixture from foaming up and overflowing the container.

The hardener was then added to the resin by either DAC or hand stirring, trying to add as little air as possible to the solution. The samples were then set to cure in simple disk sample moulds or pellet type microtome moulds for 24hrs at room temperature then post-cured at 50□C for 16hrs. One set of samples was cured at 50□C for 40hrs for a comparison of the curing temperature effect on the exfoliation.

Table 4-2 details the sample numbers and the parameters changed in each batch. The mixing methods are denoted as:

None: The initial centrifugal DAC mixing only.

High shear (HS): A cowel dissolver, run at 3000 rpm, in a metallic container of nanoclay/epoxy mixture to apply high shear to the solution.

Bead mill (BM): A hopper of the epoxy/nanoclay feeds a horizontal chamber that full of ceramic beads 3mm diameter. The solution is then sucked through a 100micron gap and pumped back to hopper in a continuous process. Each process was run for 15, 30 or 60 minutes.

A set of control samples for each type of epoxy was also made to compare curing temperatures and processing of nanoclay in the curing agent, D230. Sample Nano015 was an attempt to look at anhydride cured nanocomposite but the sample could not be cured properly without the use of a catalyst.

Sample No.	Nanofiller	%wt	Epoxy	Hardener	method/time (min)	time (min)
Nano001	Bentone 2010	2.00%	DY-t	D230	none	0
Nano002	Bentone 2010	5.00%	DY-t	D230	none	0
Nano003	Bentone 2010	2.00%	DY-t	D230	High shear–15min	15
Nano004	Bentone 2010	2.00%	DER330	D230	High shear-15	15
Nano005	Bentone 2010	2.00%	DY-t	D230	High shear-30	30
Nano006	Bentone 2010	2.00%	DER330	D230	High shear-30	30
Nano007	Bentone 2010	2.00%	DY-t	D230	High shear-60	60
Nano008	Bentone 2010	2.00%	DER330	D230	High shear-60	60
Nano009	Bentone 2010	2.00%	DY-t	D230	bead mill	Trial
Nano010	Bentone 2010	2.00%	DY-t	D230	bead mill-15	15
Nano011	Bentone 2010	2.00%	DY-t	D230	bead mill-30	30
Nano012	Bentone 2010	2.00%	DY-t	D230	bead mill-60	60
Nano013	Bentone 2010	2.00%	DY-t	D230 cured at 20˚C	bead mill-60	60
Nano014	Bentone 2010	2.00%	DY-t	D230 cured at 50˚C	bead mill-60	60
Nano015	Bentone 2010	2.00%	DY-t	Anhydride	High Shear-60	60
Nano016	Bentone 2010	2.00%	DER330	D230	bead mill-15	15
Nano017	Bentone 2010	2.00%	DER330	D230	bead mill-30	30
Nano018	Bentone 2010	2.00%	DER330	D230	bead mill-60	60
Nano019	Bentone 2010	2.00%	DER330	D230	Highshear in D230	60
Nano020	Bentone 2010	2.00%	DY-T	D230	Highshear in D230	60

Table 4-2 Different process parameters and their relevant sample numbers.

4.3 Characterisation

A variety of analytical methods were used to characterise the nanocomposites and compare the effectiveness of the processing methods and the separation of the nanoclay. As described in Chapter 3, the pre-cured processed wet nanoclay / epoxy was observed visually under a microscope between two slides at 50x, 100x and 200x magnification. Once the nano composites were cured the samples were prepared for examination under TEM and X-ray diffraction (XRD).

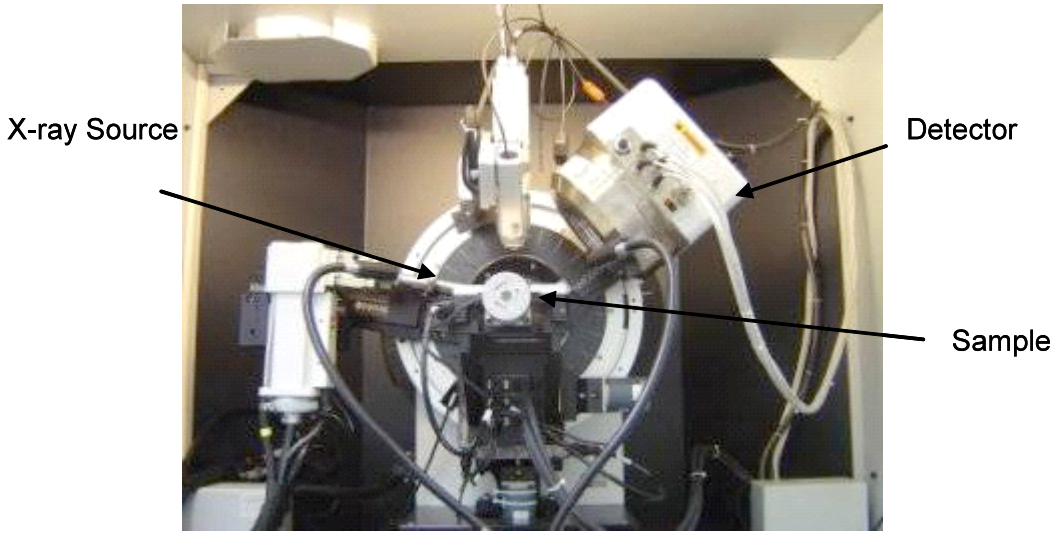

Figure 4-3 Bruker C2 with a Highstar Area Detector.

XRD of the cured nanocomposite used a Bruker C2 with a Highstar Area Detector (see Figure 4-3) which used an X-ray of wavelength of $\lambda = 1.541$ Å to measure the distance between the clay lamellae and compare this distance with process method and time. The sample, which required no preparation, could be placed directly in to the apparatus. The X-rays focused on a point on the sample and the detector arranged to pick up the lowest angle possible. X-rays penetrate below the surface and thus most of the signal will be from the bulk rather than the surface set. The peaks in the XRD graphs can be translated into spacing between the clay lamella using Bragg's law as in equation 2.1.

TEM images were used to compare the spacing of the clay lamella and at lower resolution to observe any agglomeration on a Joel fasTEM. The TEM Samples were prepared by ultramicrotomy which slices samples at 60-100nm thickness using a glass blade. The microtome samples were placed on a carbon coated grid. Good images allowed a contrast graph to be made along a line perpendicular to the clay lamella. The peaks in the line, if clear enough, gave a measured indication as to the distance between the lamella.

4.4 Observations, results and discussion

Due to the unknown nature of the material many observation tests were carried out to make judgement on the processing behaviour. These observations led to the initial testing matrix (table 4-2) and formed the basis of the processing study.

4.4.1 Pre-dispersion

The DAC mixer 'wets out' the nanoclay and disperses it very effectively with little or no air induced into the mixture, producing a solution with the consistency and colour of milky tea.

It is argued that air is brought into the resin and trapped by the nanoclay becoming visible in the form of opaque colouring. If the solution was left to stand at room temperature the nanoparticles would settle to the bottom of the container. Allowing the mixture to stand for a day caused the clay to settle to the bottom and left a clear layer on the top. The different viscosity resins required different wetting times. The Araldite only required 5 min mixing while the higher viscosity Dow needed 10 min. Similarly if a greater percentage of clay was mixed more wetting time was required, for example for 5wt% Bentone 2010 in Araldite DY-T, 10 min mixing time was required.

4.4.2 High shear and milling dispersion

Applying shearing to the resin caused the temperature to increase to 35 - 40°C for the high shear and up to 50°C for the bead mill process with the water cooled jacket off. Both shearing methods entrapped a lot of air into the mixture. The high viscosity Dow resin became very foamy and hence the shear energy is not dispersed throughout the mixture unlike the low viscosity Araldite resin which remained in a more fluid state.

The bead mill showed a level of impurity in the form of discolouration and darkening of the resin, which was observed visually caused by grinding of the stainless chamber surface. The discolouring did decrease after initial cleaning and as testing progressed, the chamber became more polished, but the discolouration was still noticeable in the resin. The bead mill also required the Dow resin/ nanoclay mixture to be heated to 50˚C before the chamber could start rotating as the mixture was too viscous and the motor would not turn.

4.4.3 Degassing

Shorter shear times allowed degassing at room temperature. For longer shear times the temperature was raised to 50°C and a mixing paddle added with a laboratory degassing tank to reduce the viscosity and to interfere with the forming of the bubbles expanding in the vacuum. This proved successful but due to the expansion of the trapped air only small amounts could be degassed at a time. It also required a technique of releasing the pressure in the tank before the bubbles over-flowed the beaker. Once the bubbles had initially been broken down and the viscosity had reduced significantly the degassing could be kept on -1bar without supervision. Figure 4-4A shows a cream, cloudy mixture, before degassing, and Figure 4-4B after, with more transparent resin. Adding the curing agent D230 with the epoxy further decreased the viscosity and the action of further degassing also incurred good mixing of the hardener.

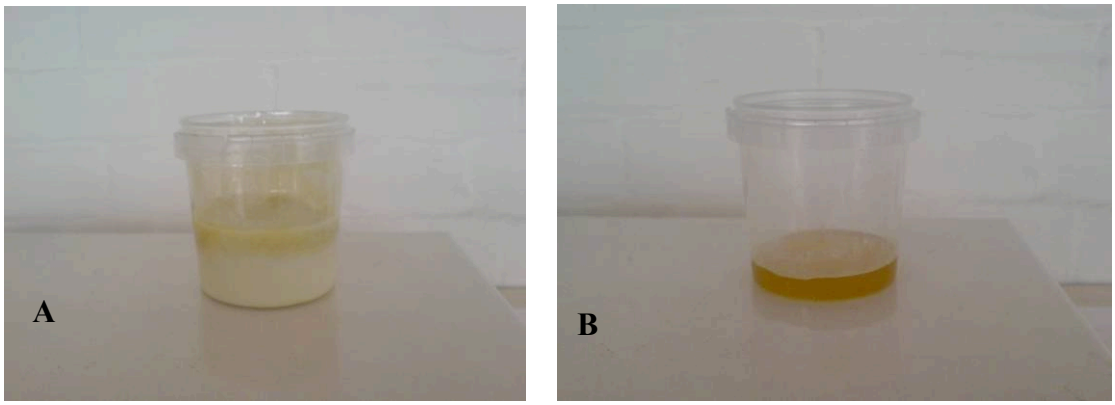

Figure 4-4 Bead milled DER330 resin after 60 min. process time A) before degassing, and B) after degassing.

4.4.4 Curing observations

Once the curing agent, D230, was added the solution became very fluid and appeared transparent with little or no trapped air. When hardened a few bubbles reappeared in the resin at an array of depths in the mould. Shallow sample moulds showed no visible voids. When mixed by hand air could be entrapped into the resin and stayed there in an open mould.

4.5 Characterisation

4.5.1 Visual inspection

Visually the difference between the processed epoxies was observed in their viscous behaviour when stirred, the bead milled epoxy showing higher viscosity. The longer the process time the more visibly viscous the epoxy appeared, though all showed similar tone of colour. The centrifugal dispersed sample, which had a very fluid motion and returned very quickly to its original shape, was compared with the 60 min high sheared sample, which on degassing was the same tone of colour but showed much more thixotropic behaviour taking some time to relax back to its original form. On curing the non-sheared sample (nano001) showed very obvious colour variations observed in a network of lines where the nanoclay agglomerated back together and the surface of the open cast sample shows a mottled relief effect (see Figure 4-5). It was also observed in sample nano020 and nano019 when the nanoclay was high shear mixed with the curing agent Jeffamine D230 and cured at room temperature. This, however, did not occur when the curing temperature was increased to 50°C. All other high shear or bead milled processed samples showed only homogenous monotone transparent beige colour. This interesting effect to the consistency and surface of the open cast sample is thought to be caused by an effect on the cure kinetics of the nanocomposite causing surface tension.

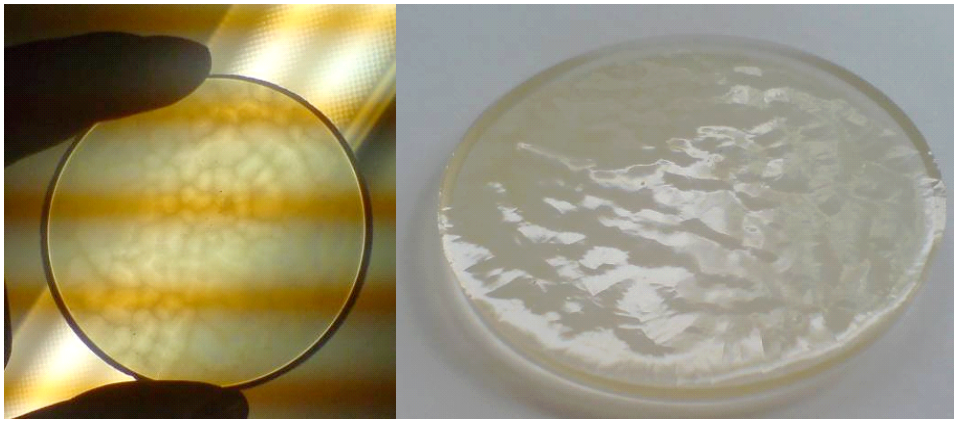

Figure 4-5 Visual inspection of sample nano001 showing the mottled relief, tortoise shell effect.

Another observation was the difference in the opacity between the two types of epoxy nanocomposite. Both were transparent, however, the DER330 gave a sharper, clearer image than the DY-T. This did not change with the amount or type of processing as long as the sample was properly degassed.

4.5.2 Microscopic

A visible difference was also observed through the microscope. Figure4.6 *A* to *D,* below, show the processed epoxies at *200*x optical zoom. Particles, that were clearly part of the epoxy liquid, due to their visible flow with the solution as the wet epoxy spread between the glass slides, are present in all figures. These particles appeared smaller, decreased in number and became less evident as the process time was increased. The large white circles are air bubbles and clay agglomerations can be seen on their edge. The centrifugal dispersion showed large agglomerated particles that had not been broken up to tens of microns in size.

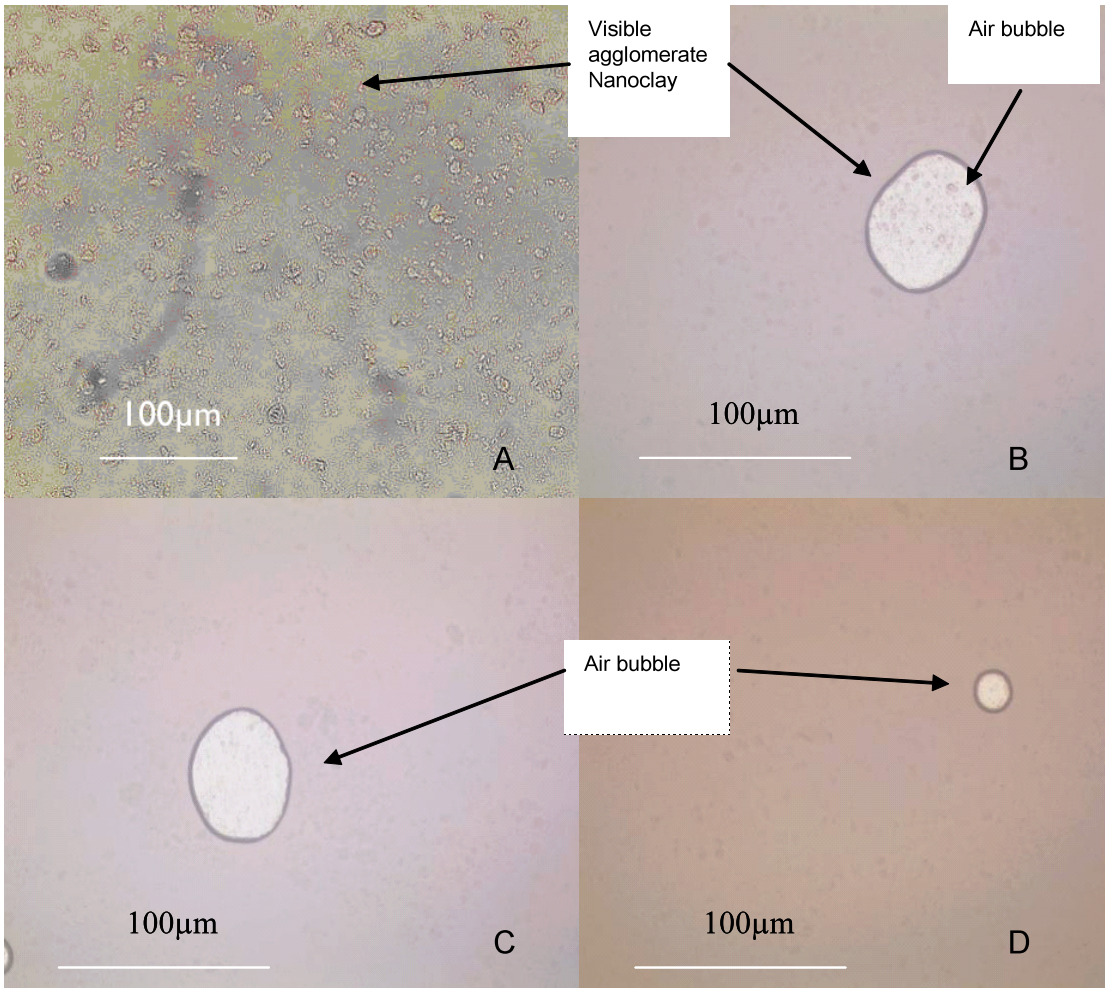

Figure 4-6 Microscopic images of unhardened DY-T / Bentone 2010. a) Centrifugal dispersion of Bentone 2010 100x, b) 15 min High Shear 200x c) 30 min High Shear, d) 60 min High Shear 200x.

The images of the bead milled nanocomposite had to be viewed by changing the aperture of the microscope light source. By doing this, some of the much finer particulates present in the epoxy were visible. In visual comparison, the 60 min high shear process (see Figure 4-6D) shows similar dispersion to the 15min bead mill process (see Figure 4-7A).

Figure 4-7 B and C show 30 min bead milled epoxy and a close up of the indicated area at 100 and 200 times magnification respectively. There is a concentration of particles around the elliptical bubble. There are also a lot of darker particulates which are likely to be impurities from the bead mill. Figure 4-7D shows 60 min bead milled DY-T and even finer dispersion than the previous figures.

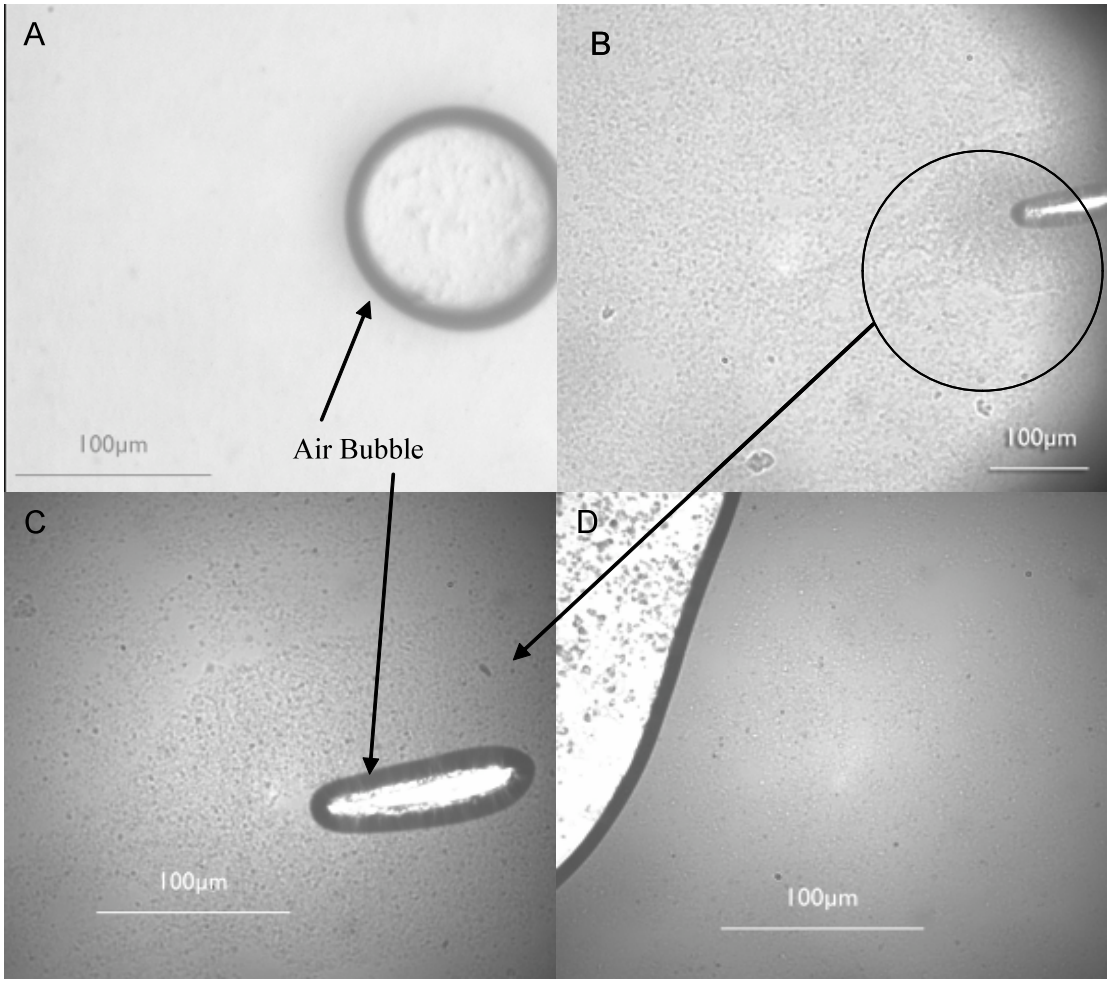

Figure 4-7 Microscopic analysis of bead milled Araldite DY-T / Bentone 2010 A) bead milled DY-T 15min 200x B) bead milled DY-T 30min 100x C) bead milled DY-T 30min 200x D) bead milled DY-T 60min 200x.

The Dow DER330 nanocomposite was much more viscous and more opaque than the DY-T resin and showed many more air bubbles trapped in the processed resin, even after being placed between two glass slides. Figure 4-8 *A* and *B* show the increase of air induced into the system from 15 to 30 minutes. They also show the darker, "opaque", tone of the background reducing the ability to identify agglomerations. After degassing, the morphology of the high sheared mixture could be seen more easily. However, Figure 4-8 *C* and *D* show very similar dispersal, perhaps even more localised agglomeration in the 60 min high sheared sample.

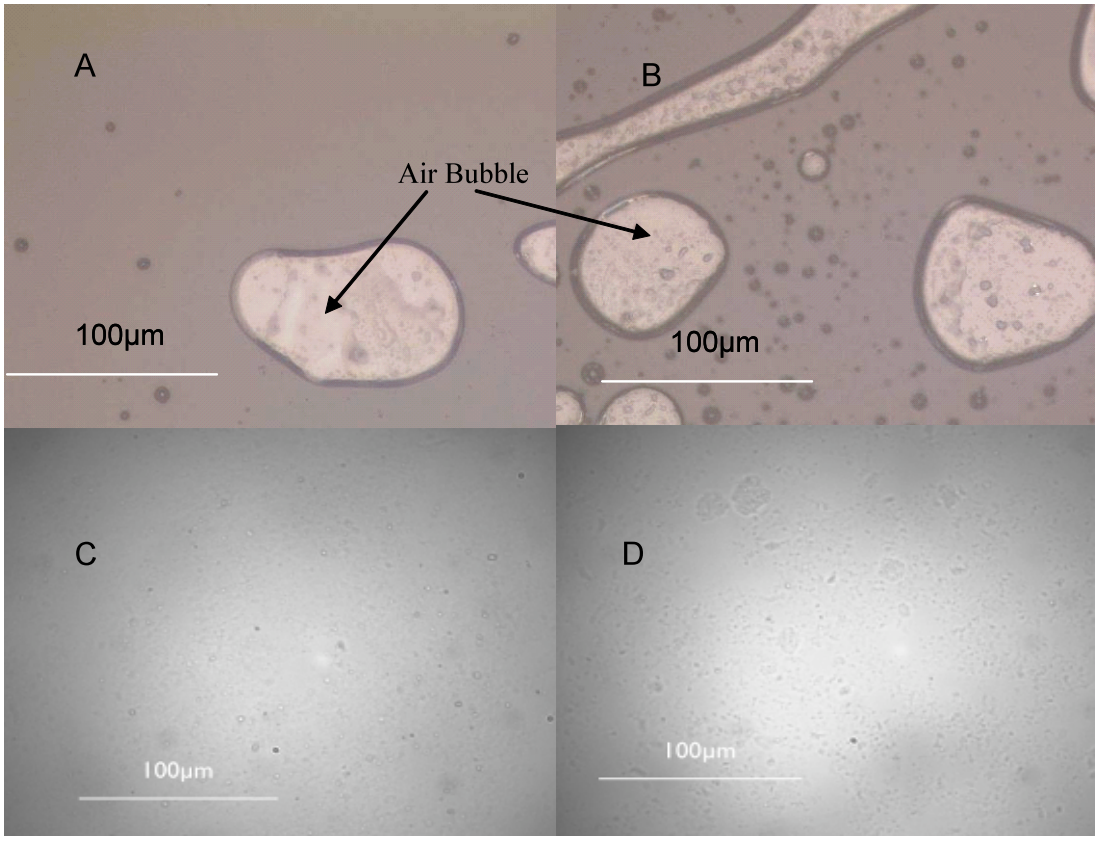

Figure 4-8 High Shear processed Dow DER330 / Bentone 2010 microscopic analysis A) DER330 High shear 15min 200x B) DER330 High shear 30min 200x C) DER330 High Shear 30min degassed 200x D) DER330 High Shear 60min degassed 200x.

The Bead milled DER330 nano filler showed a good dispersion. Figure 4-9 A and B show the fine dispersion achieved, however, the 60 min bead mill sample shows a lot of dark particulates. These are either impurities from the bead mill chamber or they could be very fine bubbles left in to the system due to improper degassing.

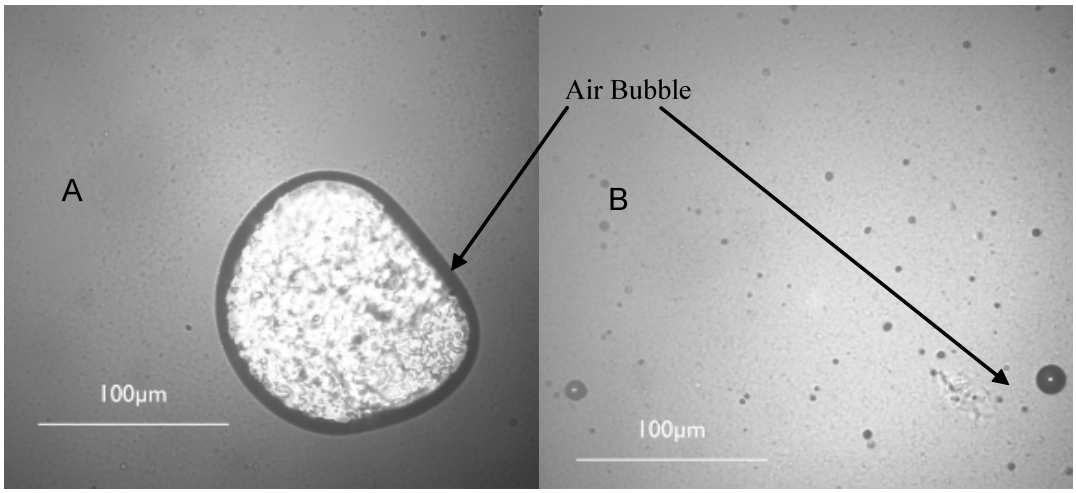

Figure 4-9 Microscopic analysis of Bead milled Dow DER330 / Bentone 2010 a) 15min Bead milled DER330 200x b) 60min Bead milled DER330 200x.

4.5.3 X-ray diffraction

The X-ray diffraction results show intensities given by the diffraction between the nanoclay layers and the intensity curve given by the amorphous epoxy. Figure 4-10 shows the pristine examples of the nanoclay and cured DY-T epoxy separately, as well as the cured centrifugally mixed sample of these materials. The Bentone 2010 graph has a peak in intensity (001 reflection) at 3.8 2θ, which corresponds to a layer separation, d, of 2.32 nm for the modified clay. This is an increase over unmodified nanoclay due to the surfactants used in the modification process expanding the interlamella gap. A smaller peak at 19.5 2θ represents the crystallographic planes (110) and (020) of the layered silicate, (Kornmann *et al.*, 2005), which is independent of the interlamella spacing. The Araldite DY-T shows an amorphous intensity curve peaking between 17 and 18 2θ.

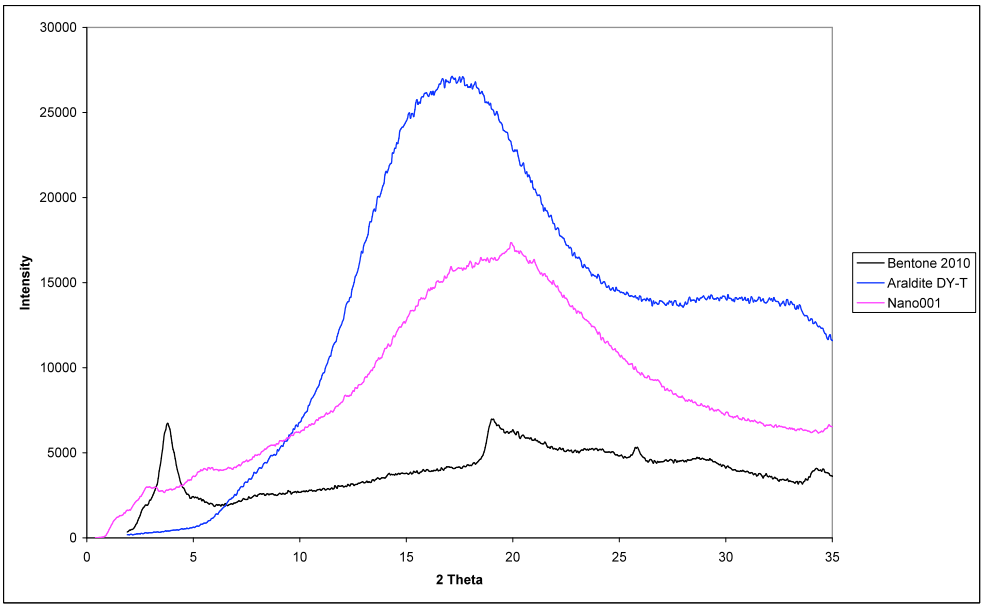

Figure 4-10 X-ray diffraction intensities for pristine cured epoxy and dry nanoclay and sample Nano001, DY-T nanocomposites processed with centrifugal mixing only.

The cured nanocomposite sample, Nano001, has two smaller primary and secondary broader peaks (001 and 002 reflections) at 2θ = 3 and 6. The $d_{(001)}$ corresponds to the primary 001 reflection layer separation of 2.94 nm and $d_{(002)}$ corresponds to the secondary 002 reflection layer separation of 1.47 nm. The 001 reflection gives an expansion of up to 0.6nm due to intercalation of the polymer into the clay galleries. Additionally, on the graph for sample Nano001 is the combination of the epoxy amorphous curve and the (110)(020) peak, which shows that diffraction from the silicate layers has been detected.

In figures 4-11 to 4-15 the XRD results are organised, so that the different lines relate to the different process times for the different resin samples and process methods. Each figure

shows the wide angle X-ray diffraction sweep in full, showing that a large background peak at approximately 18 - 20 *2θ* was found for all samples. A close up of the smaller angle section also shows smaller peaks relating to the *d* spacing separation of the clay layers.

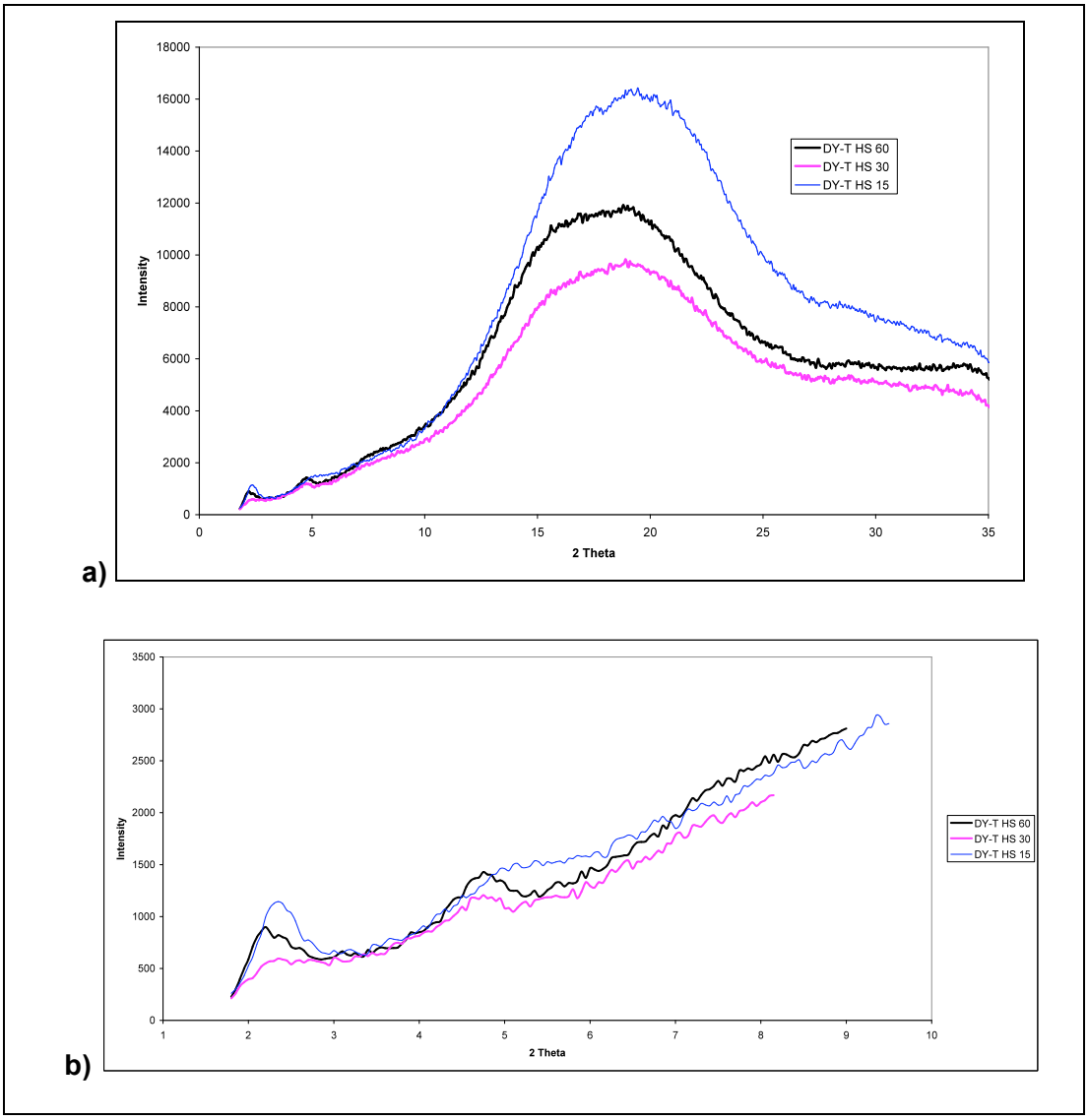

Figure 4-11 High sheared DY-T nanocomposite XRD intensity data found over a) the total swept angle. b) Low angle close up of 2θ for the same samples.

Figure 4-11 shows the results for high sheared processing on DY-T resin. The XRD peaks occur when *2θ* is equal to 2.25 for 60 min processing and 2.4 for the 15 and 30 min. The 30 min sample is not so well defined. These peaks correspond to 3.9nm and 3.7nm interlamella *d* spacing respectively. Secondary peaks are observed at 4.8 *2θ,* which corresponds to a *d* spacing of 1.84 nm. This gives an increase of 1.4nm over the pristine Bentone 2010. The polymer curves, in Figure 4-11a, show that all samples have graphs of very similar shape with some indication of a (110)(020) peak at around 19 *2θ,* the 30 min sample giving a relatively lower intensity.

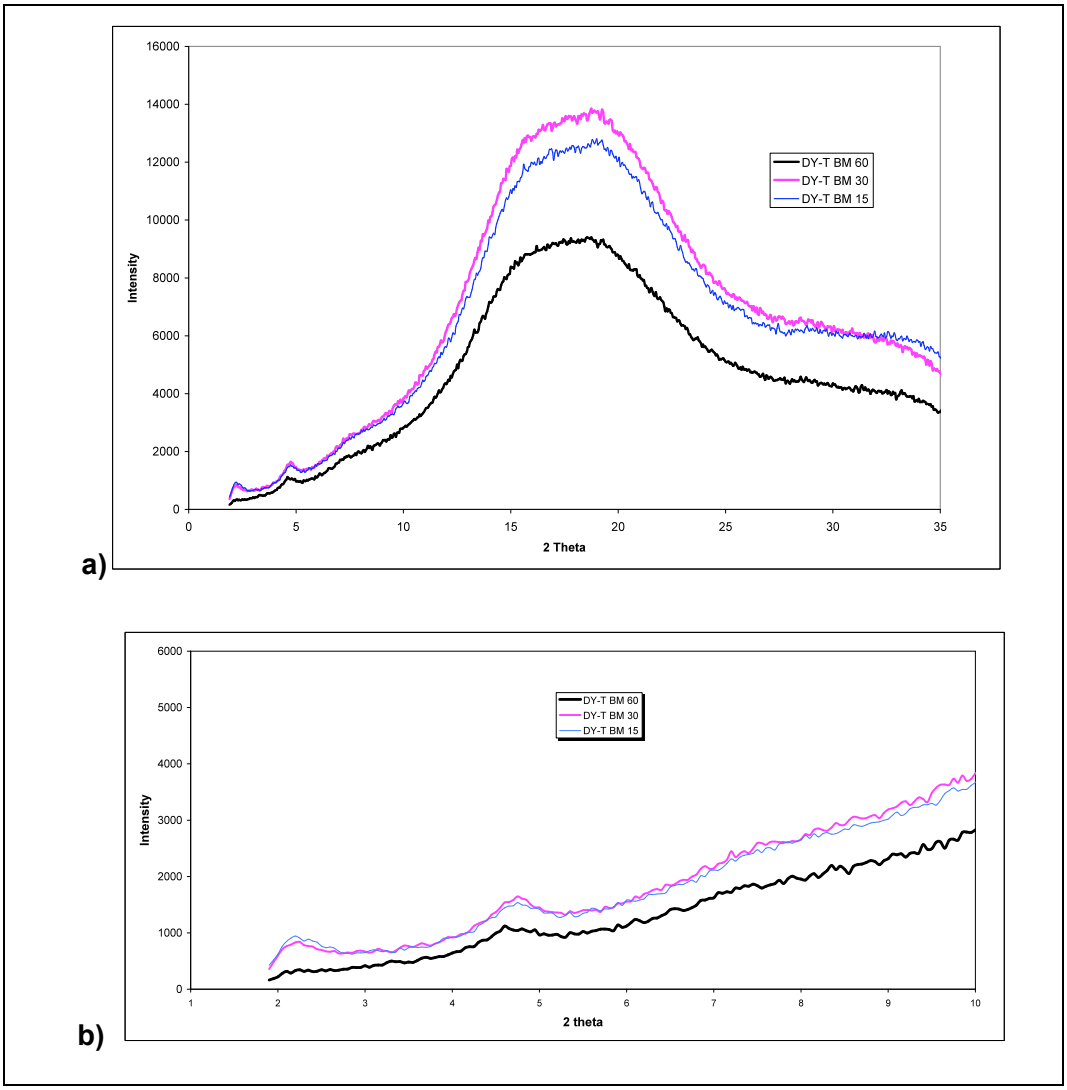

Figure 4-12 Comparison mixing time of bead milled DY-t nanocomposite.

Peaks, in Figure 4-12a and b, indicated on the 15 and 30 min curve at 2.2 *2θ* correspond to an interlamella *d* spacing of 4nm. On the 60 min curve there is no defined peak, however, a small and very broad peak can be made out where *2θ* =2.1. This broad curve may indicate that the silicate layers were not detected or that there is a large variation in interlamella spacing. All processing times show similar definition of the (110)(020) crystallographic planes at approximately 19 *2θ*. This would suggest that the 60 min sample has a *d* separation of 4.2 nm detectable by the WAXS equipment. . 15 and 30 min graphs show a secondary peak at 4.75 *2θ,* whilst the 60 min has a slightly smaller angle at 4.7 *2θ*.

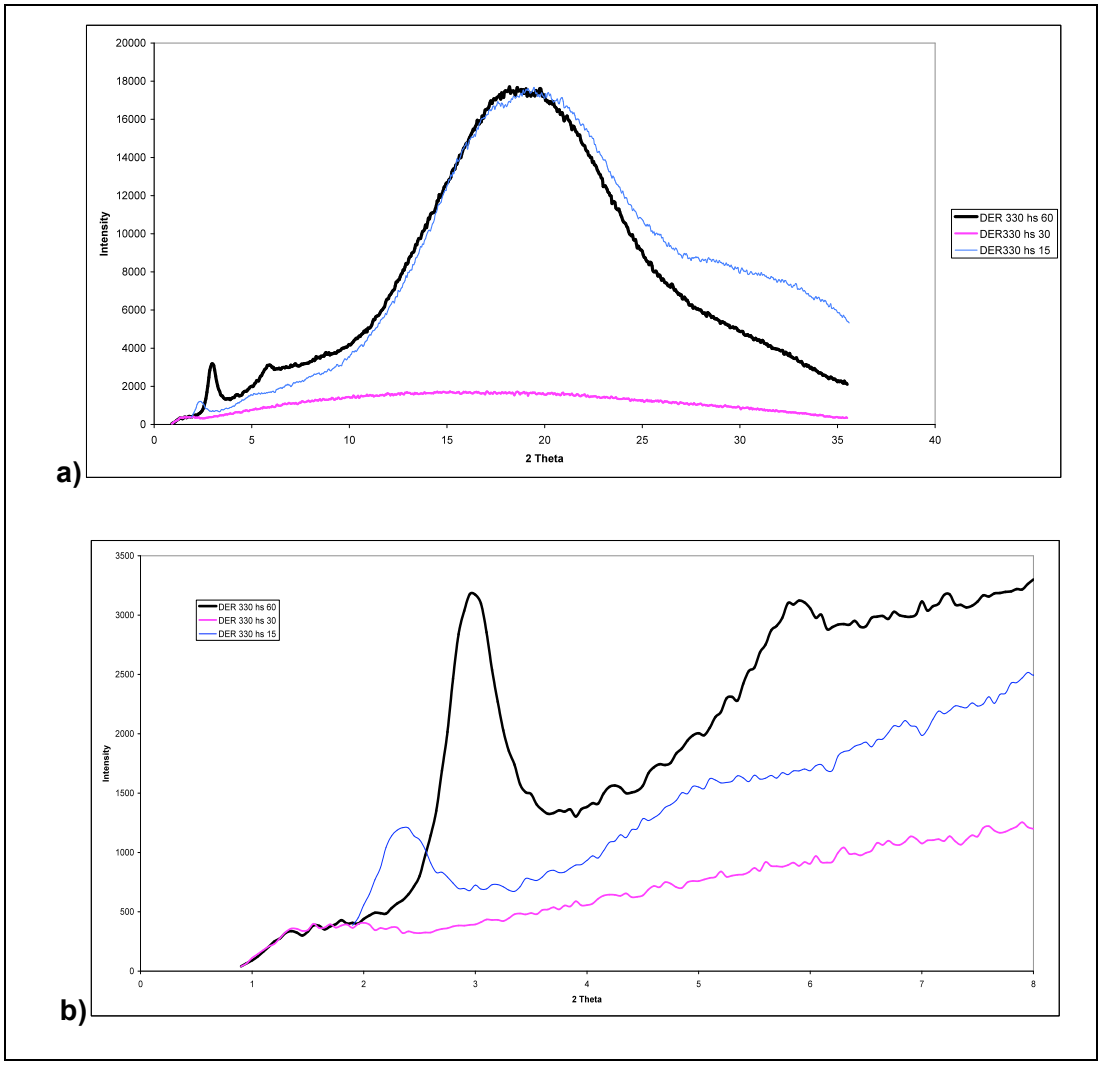

Figure 4-13 Comparison of High shear proceesing times of DER 330.

Figure 4-13 shows Dow DER330, high shear processed epoxy nanocomposite samples processed for 15, 30 and 60 minutes. The figure shows a well-defined intensity peak at 3 *2θ* for the 60 min processing indicating a 2.94nm interlayer spacing. The 30 min sample shows no peak and from the large angle sweep it can be seen that there is not a good definition of the epoxy curve. This may indicate an unsuccessful detection of the sample. The 15 min sample shows a peak at 2.4 *2θ*, which indicated a larger separation of 3.68nm.

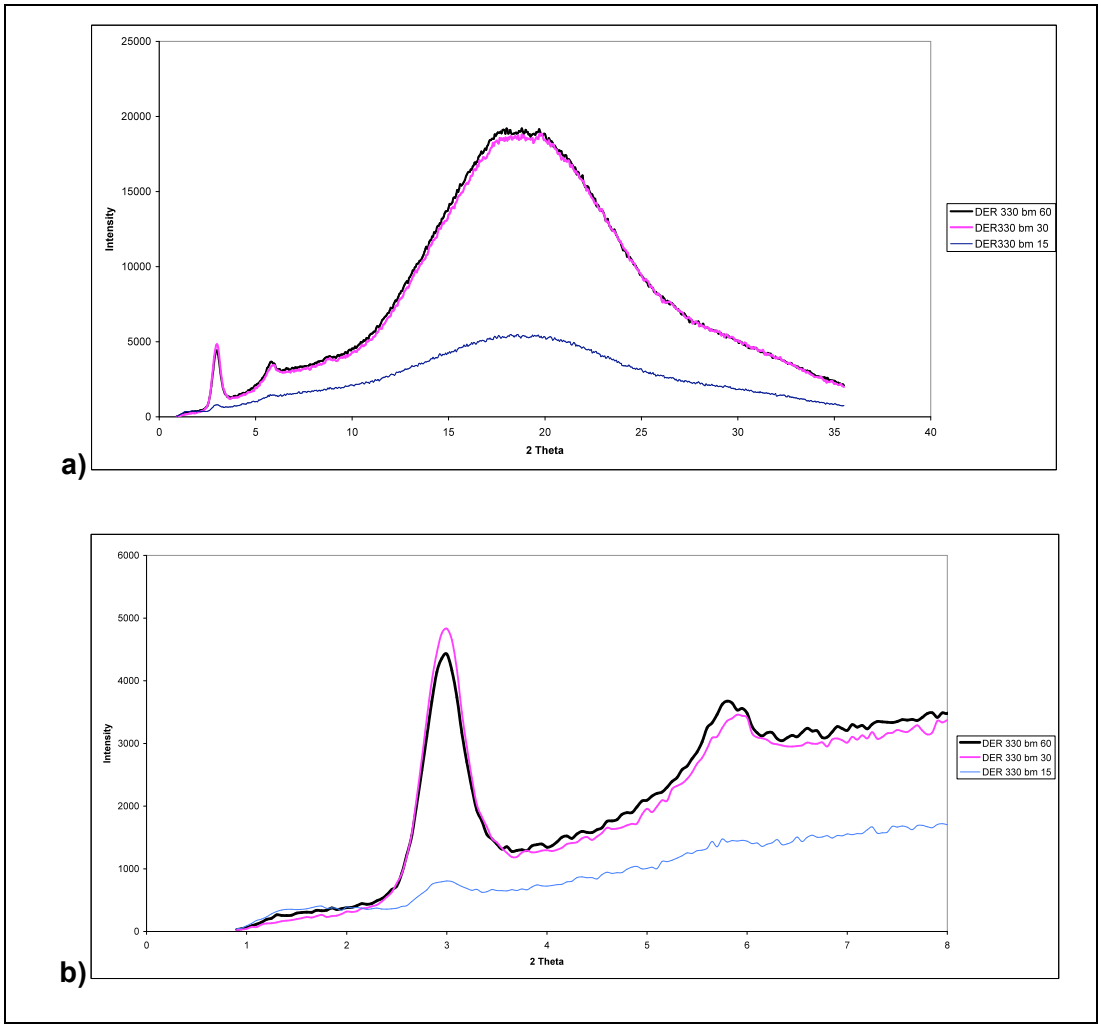

Figure 4-14 Bead mill processed Dow DER epoxy nanocomposite samples.

In Figure 4-14, the X-ray diffraction graph shows peaks from all three samples at 15, 30 and 60 minute bead mill processed DY-T Nanocomposites at 3 2θ giving an interlamella d spacing of 2.94nm. Both 30 and 60 minute samples show a defined peak and a smaller secondary peak at 5.9 and 5.8 2θ respectively. The 15 min sample has a much less defined peak at both points. It also demonstrates a much lower intensity polymer curve, shown in Figure 4-14a and gives very less definition to the (110)(020) corresponding peak and therefore may have not detected the silicate layers.

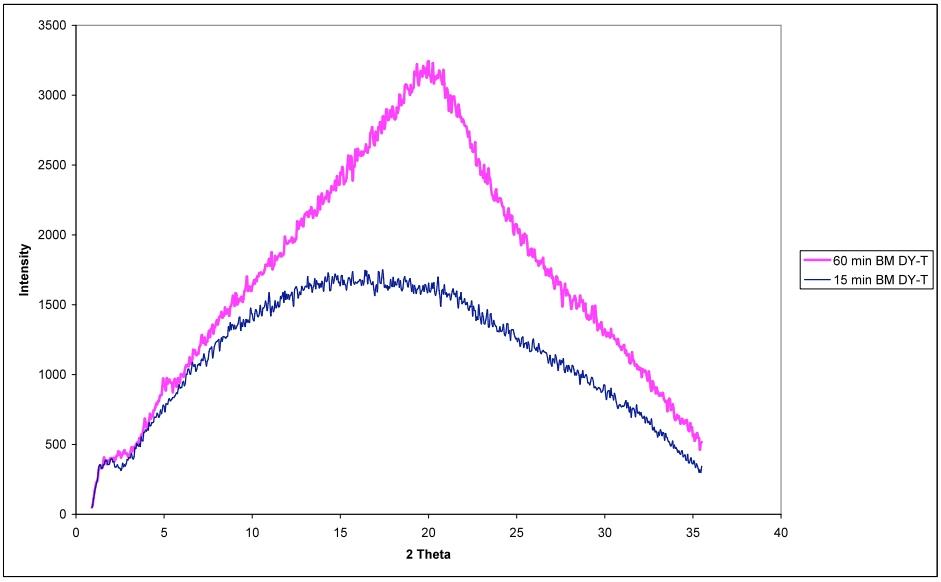

Figure 4-15 XRD graph of Uncured, Bead milled DY-T nanocomposite resin.

Figure 4-15 shows X-ray scattering intensities for two uncured samples after bead mill processing. The aim of these tests was to show how the curing effects the separation. These graphs both show very low angle peaks, at around 2 *2θ*, which may have been caused by some interference. There is also an irregular shape to the intensity sweep of the 60 min sample. Although the peak is in approximately the same place, it is not the same bell shape curve as in other samples but a peak in itself. Both samples have not produced smooth curves and they are relatively low intensity compared with other curves.

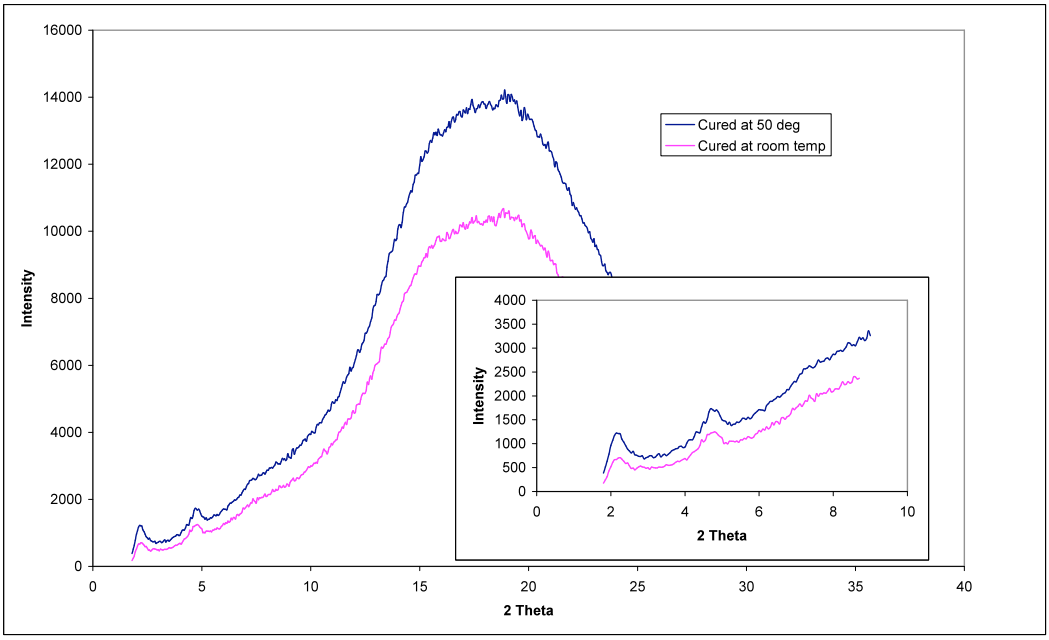

Figure 4-16 XRD graphs comparing DY-T, 60min bead mill processed samples cured at room temp and 50°C.

Figure 4-16 compares the how the different curing temperature effects the silicate layer expansion. There is little difference in the peaks with the 001 reflections both occurring when 2θ= 2.2 and the secondary peak 002 reflections at 4.8 2θ. This corresponds to a *d*-spacing of 4nm. There is increased relative peak intensity in the 50°C cured sample being more well-defined than the room temperature cured sample.

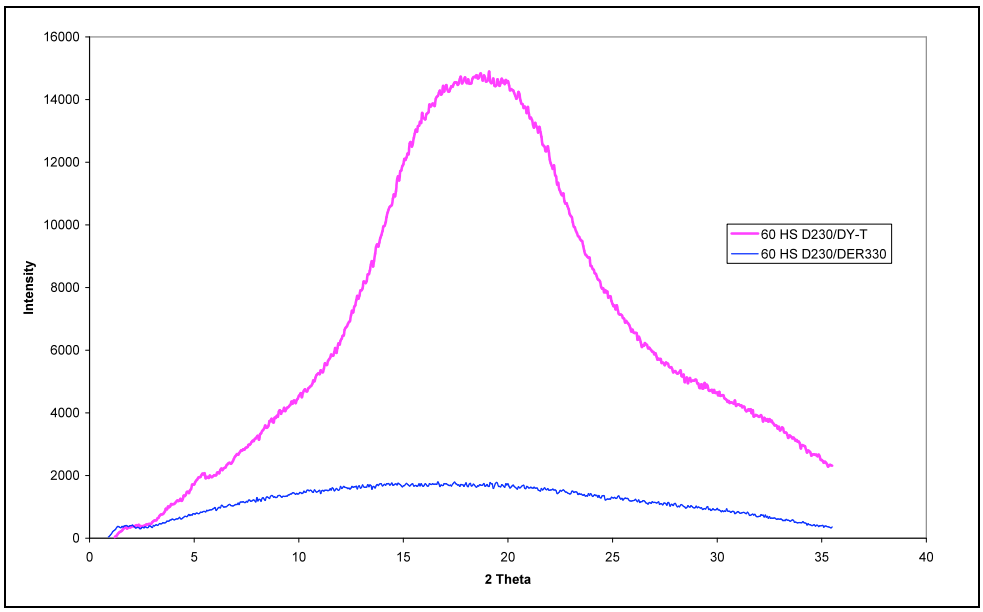

Figure 4-17 X-ray scattering of cured Nanocomposite samples Nano019 and 020, High shear processed in Jeffamine D230

The Jeffamine processed samples, Figure 4-17, show no defined low angle peaks. The DY-T sample shows a small peak at 5 2θ. This peak, which may be a secondary peak, corresponds giving an interlamella *d* spacing of 1.77nm. It is very difficult to say whether any scattering due to the silicate layers has occurred or if the separation is increased so it is undetectable with the WAXS instrument. There are some very small rough peaks at between 19 and 20 2θ, these may represent (110)(020) peaks, which are not present in the DER330 sample.

4.5.4 TEM

The clay plates were observed using a TEM as shown in Figures 4-18 –4-25 where groups of agglomerated and intercalated clay and can be seen. The enhanced pictures in each figure show the individual nanoclay edges. At higher resolution the clay lamella can be seen and the distance can be measured by looking at the intensity peaks along a defined line, X~X. The spacing does show a degree of variation so it is difficult to say what the true spacing of the lamella is. Therefore it is very difficult to qualify between the different materials and process methods by looking at single clays.

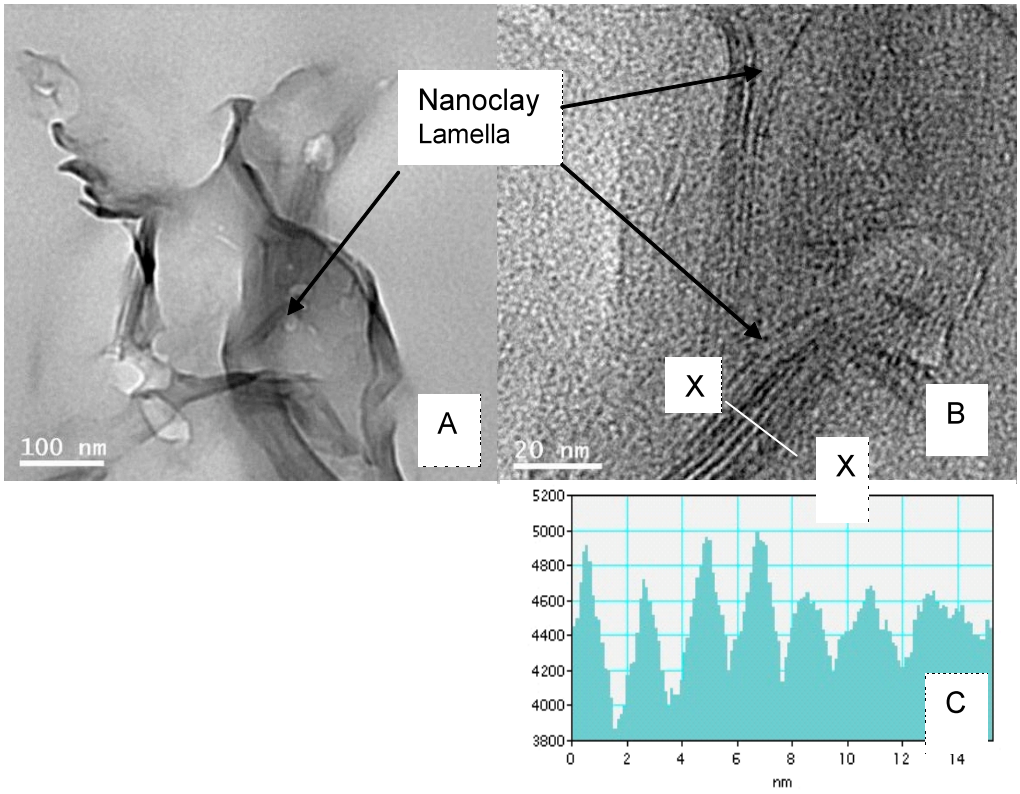

Figure 4-18 TEM of 15 min High sheared DY-T Epoxy/ Bentone 2010. Image A) shows a number of nanoclay agglomerated together. B) Shows the high resolution close-up of the nanoclay lamella with line XX representing the source of the graph C) which shows the contrast intensity taken across line XX in B indicting the lamella, allowing the separation to be measured.

The images Figure 4-18A and 4-18B shows a selected area where some of the nanoclays are agglomerated together. Figure 4-18B shows darkened lines representing the clay layers or lamella. The distance between the lines can be measured and the line XX is represented in Figure 4-18C, where the peaks are 2 – 3 nm apart.

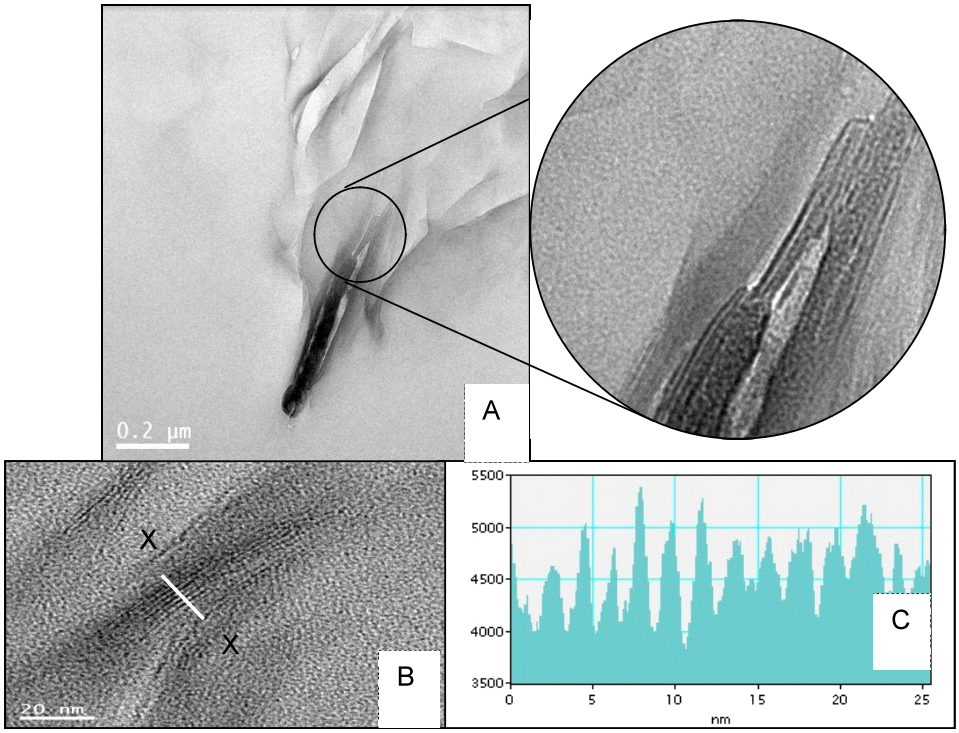

Figure 4-19 TEM of 30 min high shear epoxy/ Bentone 2010. Image A) shows the agglomerated nanoclay with a close up of the section indicated. B) Shows the high resolution close-up of the nanoclay lamella with line XX representing the source of the graph C) which shows the intensity graph taken across line XX in B indicting the lamella allowing the separation to be measured.

Figure 4-19 shows a similar scenario is observed; however, at 50nm resolution in the excerpt of image A there is seen to be a several lamella close together. These appear not to be separated. It could also represent several clays close together and in parallel due to the high number of lines present. Compared with image B, taken from the same sample, this appears to be much more separated with fewer lamellae present in each nanoclay particle. It is estimated that each clay platelet has between 6 and 12 layers. The graph in image C, although taken at a lower resolution, shows much more defined peaks than in Figure 4-18C, with a slightly larger separation in the range of 2.5 to 4nm.

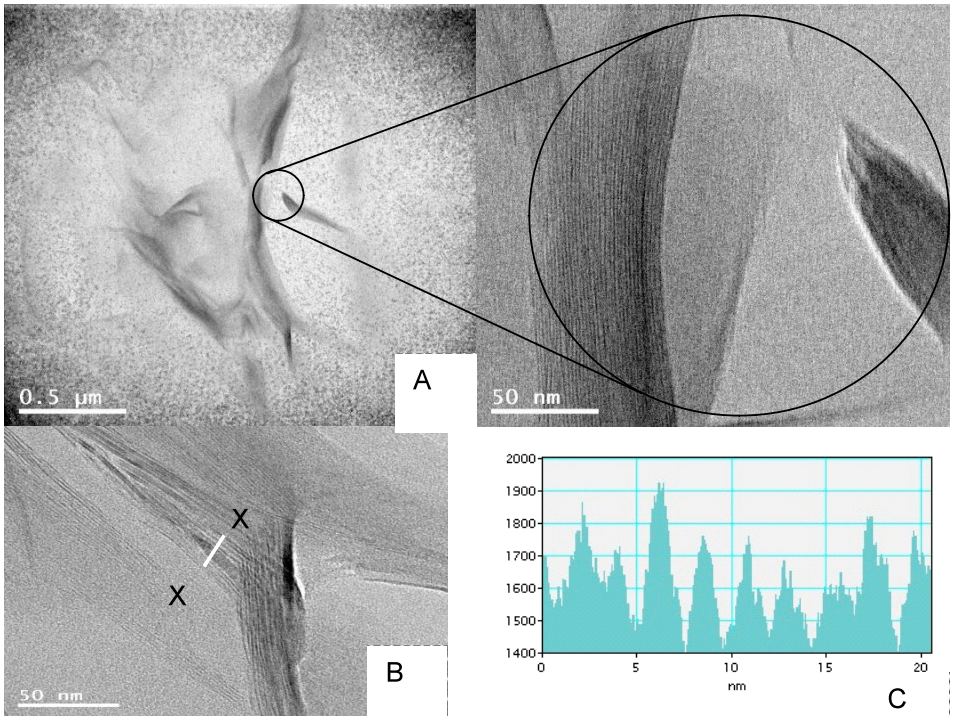

Figure 4-20 TEM of 60 min High shear Epoxy/Bentone 2010. A) shows the agglomerated nanoclay with a close up of the the section indicated. B) Shows the high resolution close-up of the nanoclay lamella C) which shows the intensity graph taken across line XX in B.

Figure 4-20 shows a quite different picture for 60 minute high shear processing. Image A shows perhaps 2 or 3 nanoclay close together with other clays, in separated form and more dispersed, surrounding them. The quality of the scan is not so good due to the difficulty in focusing the TEM image. However, image B shows a pattern of lines which give the separation of the lamella to be slightly lower than that found for the 30 and 15 minute processing.

This highlights the problem of using TEM for analysis of the dispersion and exfoliation. It can show the separation and agglomeration of a particular group of nanoclays, which may not be representational of the nanocomposite sample and processing method as a whole. It is also sometimes difficult to get quality images as demonstrated in Figure 4-21 where it was not possible to focus the image to make a comparison on the morphology of the clay.

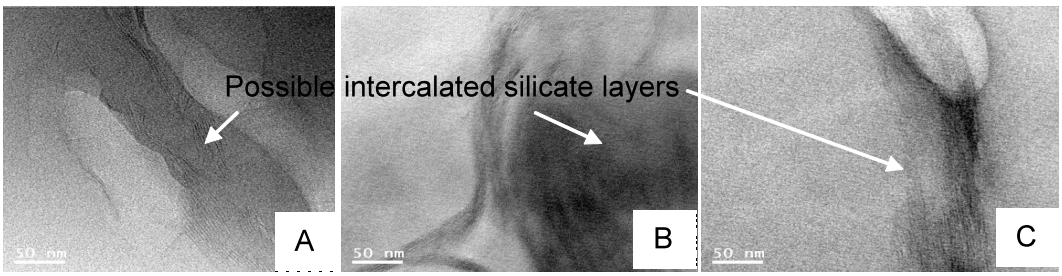

Figure 4-21 Examples of TEM pictures of the High shear processed DER330 nanocomposite. a) shows 15 min processing, b) 30 min processing and c) 60 min processing.

The nanoclays shown in Figure 4-22 show signs of some delamination where the silicate layers appear to have been damaged by some force, breaking from the rest of the clay. The high shear force applied by the beads in the bead mill chamber can explain this. The graph in Figure 4-22*A* is of the line XX in Figure 4-22*B* giving a spacing of up to 4nm between peaks. However it is also clear to see the irregularity of the gaps and Figure 6.18*A* apart from the few delaminated layers on the edge the clay looks like it is phase separated.

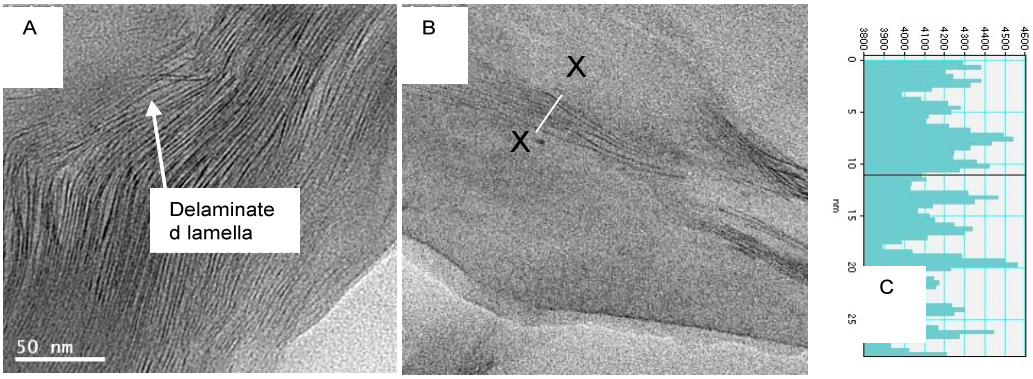

Figure 4-22. TEM images of Bead milled DY-T nanocomposite samples processed for 60 min.

Figure 4-23 shows an excellent example of intercalated or even ordered exfoliated nanoclay. The fine clay layers can be seen evenly and equally separated as in Figure 4.24 and Figure 4-25. It is also significant that there is no agglomeration of nanoclay within the area scanned.

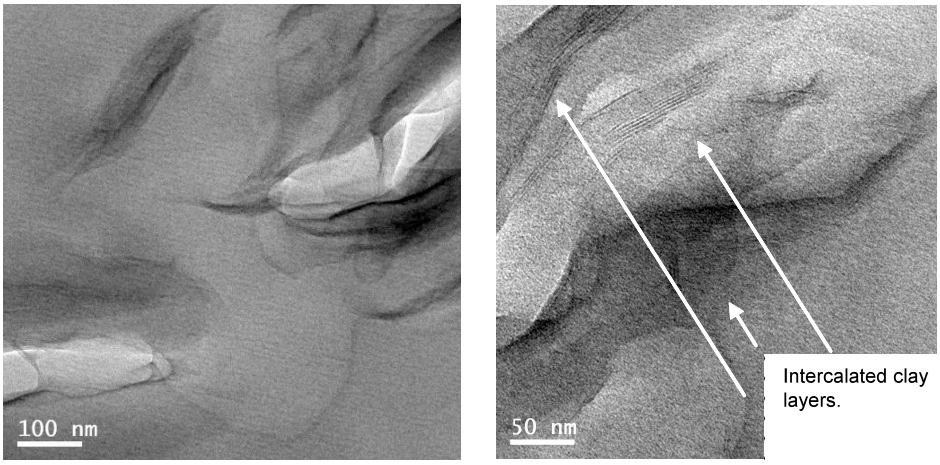

Figure 4-23 TEM images of Bead milled DER330 nanocomposite processed for 60 min showing intercalated clay lamellae at two resolutions.

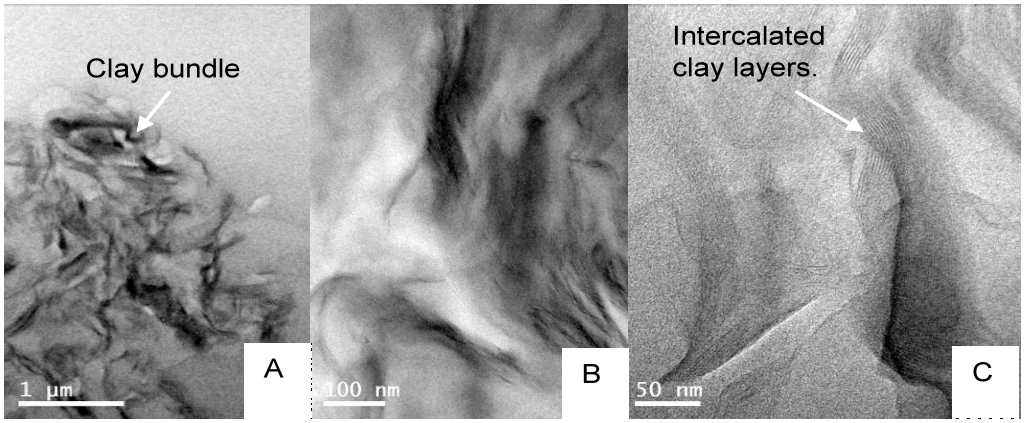

Figure 4-24 TEM images of DY-T nanocomposites processed for 60 minutes by high shear mixing in Jeffamine D230.

Figure 4-24 and Figure 4-25 show images of the nanoclay after high shear processing in Jeffamine D230, the curing agent used. With these samples it was possible to get lower resolution pictures showing clearly an area where nanoclays have agglomerated. Within these areas it is possible to see the network of clay layers, even individual layers.

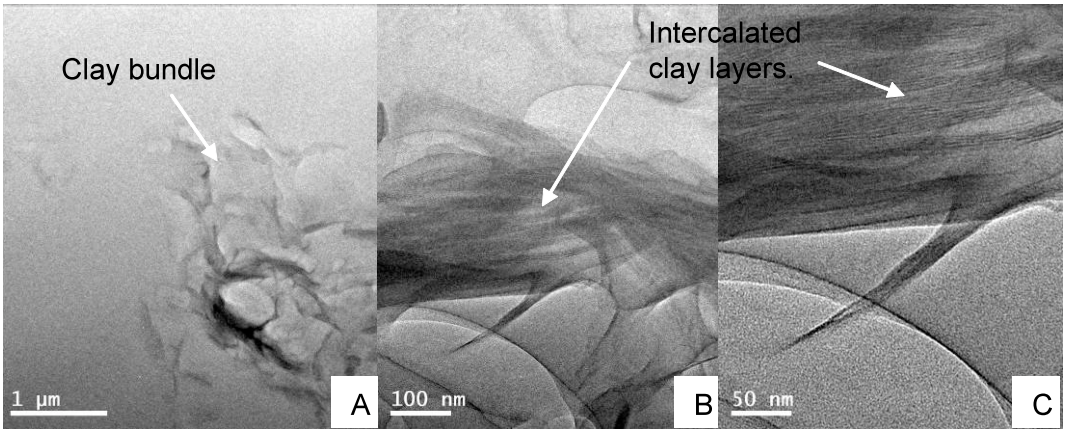

Figure 4-25 TEM images of DER330 nanocomposites processed for 60 minutes by high shear mixing in Jeffamine D230. Images A, B and C show different resolutions of the same clay agglomeration.

4.5.5 Discussion of characterisation results

Microscopic observations of the resin before curing have shown agglomerated nanoclay visible in the samples. The amount of nanoclay visible decreases as the shearing time increases and there are still some particles visible even after an hour of high shear processing indicating that not all the nanoclay is fully dispersed and unlikely to be exfoliated. This cannot be quantified but comparison of the texture of the images can be made and it can be used as evidence to back up other observations. Possible impurities in the resin were also identified with the bead mill processing which would affect any mechanical properties of the material. This can be solved by extensive cleaning of the beads and chamber and with the

use of a harder, ceramic chamber to prevent the chamber wall being eroded by the action of the beads. Utilising this method proved to be a very quick and useful tool for identifying and comparing the agglomeration of the nanoparticles and dispersion of different processing methods. Hackman and Hollaway (2006) recognised the presence of agglomeration using optical microscopy in their study of nanoclay processing. The addition of glass beads to the shearing process acted similar to the bead mill, and showed a visual improvement under the microscope. Microscopy comparison of the processed materials showed similar change in appearance in dispersion. In Figure 4-8 and 4-9 the DOW DER330 shows dark, agglomerated areas in the high –shear dispersed system, which is not visible with the bead milling.

Table 4-3 summarises XRD data gathered for primary peaks and their corresponding lamella *d* spacing as well as he secondary peak data. The secondary reflection data is calculated with consideration for the first multiple (n=1) and second multiple (n=2) Bragg's law. The primary data shows that there is an increase in the *d* spacing of the clay which is normally 1nm for unmodified clay but expanded to 2.32nm when modified with a surfactant in agreement with literature on other commercial clays such as Cloisite 20A (Southern Clay Products), (Ryu *et al.*, 2004), and Nanomer I.30E (Nanocor), (Liu et al., 2005b).

A secondary peak is observed in most of the samples analysed. By calculating as a second multiple, using n=2, the results show a good comparison with the primary peak data. However, when the primary peak is below 3 2θ a discrepancy between the *d* values is seen even though similar trends are observed; where the sample with the greatest $d_{(001)}$ spacing also has the greatest $d_{(002)}$ spacing. Dong et al., (2008) explained the secondary peak as a reduction in interlamella spacing by the surfactant degradation. A significant portion of surfactant loss, through the processing could make clay galleries collapse shown as the decrease of *d* spacing for the second peaks. By calculating the peak with integer n=1, *d* is found to be smaller than the pristine dry modified clay. Both data in Table 4-3 for the secondary reflection agree with the primary reflection indicating there is a trend with the lamella spacing increasing as shear time increases.

Description	Sample	*2θ*	*d* nm	2nd *2θ*	2nd *d* nm	
Dry Nanoclay	Pristine	3.8	2.3		n = 1	n = 2
	DY-T					
centrifugal	Nano001	3.0	2.94	6	1.47	2.94
HS 15	Nano003	2.4	3.7	5.1	1.75	3.5
HS 30	Nano005	2.4	3.7	4.8	1.84	3.68
HS 60	Nano007	2.25	3.9	4.8	1.84	3.68
BM 15	Nano010	2.2	4.0	4.75	1.86	3.71
BM 30	Nano011	2.2	4.0	4.75	1.86	3.71
BM 60	Nano012	2.1	4.2	4.7	1.88	3.86
D230 HS processed	Nano020	-	-	5	1.71	3.5
Cured at room temp	Nano013	2.2	4.0	4.8	1.84	3.7
Cured at 50°C	Nano014	2.2	4.0	4.8	1.84	3.7
	DER330					
HS 15	Nano004	2.4	3.7	-		-
HS 30	Nano006	-	-	-		-
HS 60	Nano008	3	2.9	5.9	1.50	2.99
BM 15	Nano016	3	2.9	-		-
BM 30	Nano017	3	2.9	5.95	1.48	2.96
BM 60	Nano018	3	2.9	5.8	1.52	3.04
D230 HS processed	Nano019	-	-	-		-

Table 4-3 Values of *2θ* and corresponding *d* spacing between the clay lamella for primary and secondary reflection peak data. Secondary reflections show equivalent *d* spacing for n= 1 and n=2 for comparison.

The relative intensity and sharpness of the peak can be an indicator of the accuracy and the overall average exfoliation. A broader peak suggests that there is large variance in the *d* spacing and the sharper peak a more consistent spacing that would give a more apparent, intense peak at a certain angle. The presence of secondary peak broadening is a sign of disorder in the nanocomposite layer structure. Higher order peaks in a XRD curve are more susceptible to broadening due to layer structure faults secondary peak broadening means it is likely that the process has caused considerable disorder among the outermost silicate layers in each clay platelet (Pavlidou and Papaspyrides, 2008).

Taking this into account the DER330 nanocomposites in general show much more pronounced peaks. Chen et al. (2004) and Wang (2005), suggest that the XRD peak becomes broader and flatter, becoming almost invisible with complete exfoliation. The peak shifts to a smaller angle before broadening and disappearing due to the separation of the peaks becoming so large that it is no longer detectable with the WAXS instrument. The data obtained shows no correlation between the increased process time and peak broadness. The fact that DER330 nanocomposites show a more defined, intense, X-ray peak than the DY-T

samples, suggests that the lamella separation is more uniform and a high proportion of the *d* spacing is concentrated around a specific distance.

This indicates a particular synergy about the physical make up of the specific epoxy and interaction with the nanoclay. The XRD data suggests that more of the DER330 epoxy produces a more consistent separation of a greater proportion of the clay. In contrast, the DY-T is penetrating the clay galleries and intercalating a lower proportion but separating them by greater, but more varied amounts.

Some layered silicates do not exhibit well-defined basal reflections. For example in sample nano012 and nano019 there is a less obvious primary peak from which to obtain data, however there is a secondary peak. There are a number of explanations for this. The absence of the first peak for the bead milled sample (nano012) is likely to be due to a large *d* spacing which would have caused a peak in the graph at such a low angle that it was not detected as the equipment used; which was not designed to effectively pick up readings where $2\theta<2.0$. Thus it would show that some clay has become intercalated or exfoliated while other layers have only swelled slightly. It could also mean the first peak is caused by interference due to the low angle. Thus, peak broadening and intensity decreases are very difficult to study systematically. Therefore, concrete conclusions cannot be made concerning the mechanism of nanocomposite formation and structure based solely on XRD patterns.

In comparison with TEM, which was used to observe the state of individual clays and their lamella, the XRD results agree in principle. Variable separation was observed of between 2 and 4 nm. None of the images indicate a fully exfoliated nanocomposite. The TEM images show very effectively the delamination of the silicate layers for confirmation with other techniques and analysis. However, in terms of comparing processing methods, one has to make a general assumption on the effectiveness of each process based on a group of images taken in a small area. However combined with the previous techniques evaluations of the state of the nanoparticles can be made.

4.6 Comparing processing methods

This chapter has looked at the dispersion parameters of nanoclay / epoxy composites. It has compared mechanical processing and how the dispersion quality varies with time and the materials used in the processing medium. A comparison of the methods of dispersal and exfoliation, however, is difficult to quantify. The TEM images do not give an overall picture of the dispersion and XRD also only shows the average lamella separation through the scanned section. From observations and honing techniques with experience, the different processing methods can be compared qualitatively. The behaviour of the resin during the

processing gives subtle indications of the invisible structure of the nanoclay. Most notably, the ease of degassing entrapped air from the resin depends on the time spent processing. However, it is difficult to compare how different methods affect the clay filler because they entrap different amounts of air in the processing. Viscosity plays a key role here in two respects. A low viscosity resin will behave differently to a high viscosity resin under shearing and both may or may not have shear thinning properties. Higher viscosity liquids will normally entrap more air due to cavitations of the liquid and they will normally be more difficult to degas due to surface tension properties.

Table 4-3 compares XRD data for the process parameters and their effect on the clay layer separation. This gives an indication of the requirements for efficient exfoliation of nanoclay to produce good quality nanocomposites. An XRD comparison of high-shear processing and bead mill processing indicates that both methods have increased the lamella spacing of the clay in epoxy over the dry clay. The DY-T epoxy nanocomposite data indicates that both process methods produce intercalated nanocomposites with a *d* spacing greater than the centrifugally mixed composites. The bead mill is more efficient at intercalation, showing similar separation to the 60 min high shear processed sample with only 15 min process time. The largest separation detected is at 4.2nm, produced from 60 min bead mill processing. Contrary to this the bead mill shows no improvement in intercalation of the Dow DER330 nanocomposites where the best result occurred at 15 min high shear processing, however, TEM can not confirm this.

In summary, none of the processing methods examined have shown evidence of exfoliation, however, intercalation has been achieved. Interestingly, the processing in Jeffamine D230 produces some good intercalation but agglomeration of the nanoclay was also obvious in observation and TEM images but not shown so well on the XRD. The insertion of the amine between the lamella would increase the speed of reaction through intragallery curing. This allows the migration of epoxy resin from outside the gallery to inside the gallery (Chen and Curliss, 2003b).

DY-T resin showed greater separation of clay lamella than the DER330. The tri-functional epoxy molecule being, smaller in dimension than the bisphenol-A, would have an increased rate of diffusion. Kornmann et al., (2001a) suggested that with increased diffusion rate by increased mobility of the curing agent the greater the exfoliation. This demonstrates that it is also true for the diffusivity of the epoxy molecules.

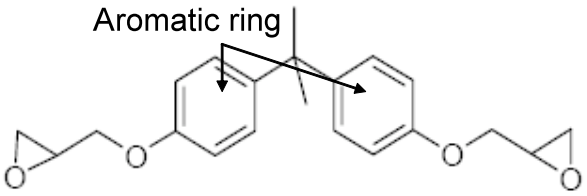

Figure 4-26 Chemical structure of DOW DER330, Diglydyl ether of bisphenol A (DGEBA) epoxy molecule.

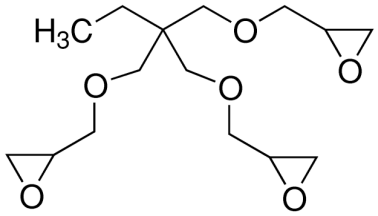

Figure 4-27 Chemical make up of Araldite DY-T trifunctional epoxy molecule.

Figures 4-26 and 4-27 show the chemical make up of the two types of epoxy used. The diagrams show how the trifunctional epoxy is relatively smaller than the bisphenol A epoxy. This has been measured on Chem3D Draw program and the difference in molecule length is approximately 5Å. The DY-T is also a much more flexible molecule due to the lack of the stiff aromatic ring structure in the DER330. The combination of both factors as well as changes in compatibility such as polarity would aid the migration of the DY-T between the silicate layers.

Other characterising evidence shows that after an hour in the high shear mixer the particles were still visible in the micrographs. This shows a degree of agglomeration. The bead mill shows better overall dispersion in both epoxies used. The TEM images show individual clay layer and straight measurements give the distances between them. The images show evidence of both intercalated and unintercalated nanoclay in most samples, which correspond to the broad peaks in the XRD graphs. Nanoclay samples that were high shear processed in Jeffamine D230 and samples which were bead mill processed in Dow DER330 epoxy gave the best examples of visible intercalation, not due to the separation distance but for the evenly intercalated silicate layers throughout each image. However, this did not necessarily correspond to the XRD graphs, which had no obvious diffraction peaks.

Changing the curing temperature made no difference with the clay separation as shown by samples nano14 and nano15. Although, according to Chen et al. (2002), the rate of cure is a major influence on the exfoliation process. Separation of the silicate layers requires the rate of the intragallery reaction to be faster, relative to the speed of the extra gallery curing. Curing at high temperature generally increases the reaction rate which would suggest at lower temperatures greater exfoliation would occur. However, increasing the temperature

would increase the mobility of the molecules and hence the diffusivity. It is suggested that the rate of epoxy and curing agent diffusion between the silicate layers can effect the clay exfoliation.

4.7 Concluding remarks

The aim of this chapter was to examine possible processing methods of epoxy / clay nanocomposites that will ultimately give the best structural performance. Figure 4-26 highlights those areas that, having been suggested in Chapter 3 as key issues for the structural success of nanocomposite, are covered in this chapter. The motivation for this work came from claims proposed in reported literature that nanocomposites can improve the material properties of various types of polymer.

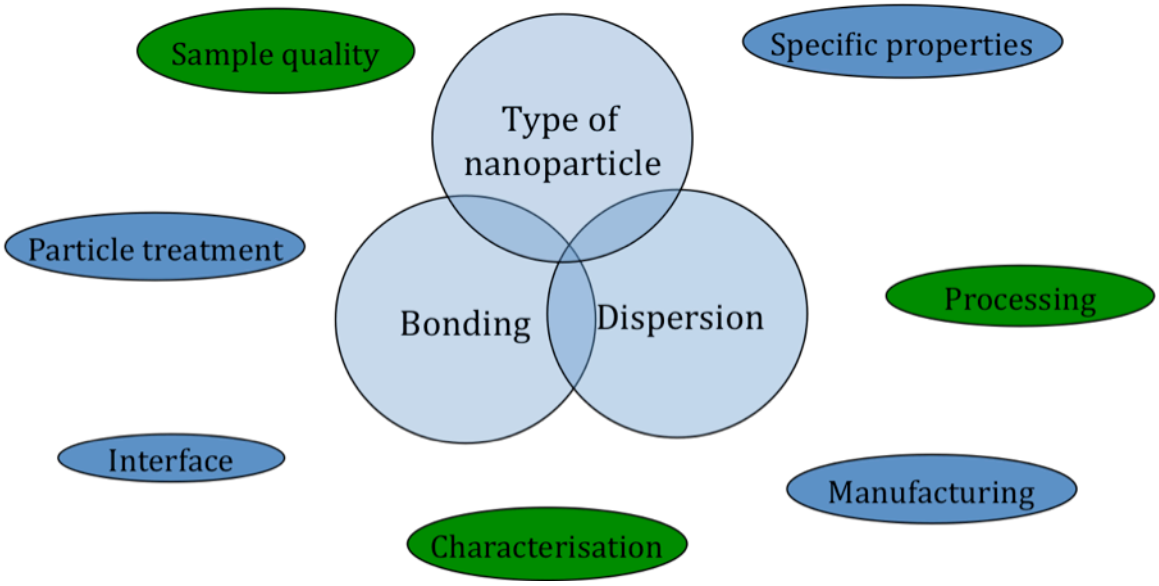

Figure 4-28 The key issues regarding structural nanocomposites with areas that have been investigated in chapter 4 highlighted in red

High shear mixing and bead milling processes were selected for comparison of dispersion of the nanoclay epoxy nanocomposites. The criteria was to create a homogenous dispersion, breaking up the aggregate phases of the nanoclay, and to exfoliate the silicate layers that make up the clay by introducing the polymer chain between them. To examine the processing a trifunctional epoxy and a bifunctional epoxy resins were compared for dispersal and exfoliation. The aim was also to produce a void free nanocomposite i.e. a minimum of air entering the system during processing and the removal of air after processing. This would ensure the quality of composite to be manufactured. It was also important during this first processing activity to take into account environmental and health hazards due to the release of nanoclay. To compare the processing methods and air entrapment visual, microscopic, X-ray diffraction and transmission electron microscope analysis techniques were utilised to

characterise the processed mixture, its homogeneity and measure the distance between the clay lamella.

The review of processing methods concluded that a high shear mixing and bead mill method could improve nanoclay morphology while introduction to the epoxy in a safe and contained manner was achieved with initial processing in a DAC centrifugal mixer. This work can agrees with referenced literature on the insitu polymerisation, claiming the mobility of the curing agent is directly related to exfoliation, and melt intercalation methods, inserting the polymer between the clay lamella, showing that that the type and mobility of the epoxy resin has an effect on the exfoliation.

From the processing experiments it was also found that all shearing methods required a degassing stage in manufacture due to air entrapment. Initially it had been thought that a bead milling method would remove the issue of entrapped air as the mixing occurred within an enclosed chamber. Regardless of the bead mill manufacturing claims, the air was still entrapped and required a further degassing stage. The degassing technique was successful, using a heated degassing tank with a stirring paddle, heating the mixture to 50°C. Introducing a step; adding the curing agent and applying the vacuum again improved the amount of air entrapped. This reduced the viscosity and allowed trapped air to escape with less stirring.

Intercalation of the nanoclay was achieved with a maximum *d* spacing of 4.2 nm for the trifunctional epoxy processed for 60 minutes in the bead mill measured with XRD. The bifunctional resin showed a smaller *d* spacing but TEM images showed good dispersion and even spacing of the intercalated layers. This is comparable with published reports claiming intercalated clay morphology. In conclusion the bead mill provided a better processing method for dispersal. The different epoxy types cause different clay morphology, identified with XRD, which is a factor of the epoxy molecule mobility and compatibility with the clay. The viscosity of the resin did not pose significant air entrapment problems with the processing and degassing equipment used.

Further work is needed to obtain greater separation of the clay layers to achieve exfoliation, as indicated in the review of the literature. The next phase of research will test variables such as the concentration of nanofillers and thermal parameters to find the optimum setting for production of exfoliated nanoclays. Further characterisation using DMTA and mechanical properties of the nanocomposite can be analysed for trends with the clay morphology. This will provide the basis to explore further the use of nanocomposites with fibre reinforcement for tests on structural performance.

5 Mechanical behaviour of different nanoclay processing

The work carried out in chapter 4 raises issues regarding the dispersion and characterisation process such as the dispersion medium and the dispersion time as well as suggesting issues on the concentration of the nanofillers. This work can be continued, taking the lessons learnt from the processing, to the next stage as described in chapter 3, figure 3-2. This describes the dispersion and curing of samples for physical testing. In assessing the effect of dispersion on the nanocomposite properties, the weight percentage of nanoclay is an important variable in the effectiveness of the mechanical and thermal performance. This is central to improving structural performance and reducing weight, one of the key objectives in composite design as stated in chapter 3. Manufacturing of good quality samples for testing is also important in assessing the performance. Characterisation of the nanocomposites can be made through analysis of the fracture surface, to determine the materials' failure mechanism and behaviour, as well as previously used dispersion analysis.

One of the key issues to test is to find best weighting% of nanoclay and therefore each processed batch consists of 0, 1, 2, 3, 4 wt% loading of nanoclay in the mixed system. The work also compares dispersal effects with curing agent as well as with the cure temperature. To this end the work compares dispersion in two different amine hardeners, as well as dispersion in an ethanol solution.

The purpose of these experiments is to determine the best conditions required to maximise flexural modulus and strength as well as impact toughness. The glass transition temperature of the samples, measured on the DMTA, is a gauge of how the nanomaterial affects the polymer mobility and cross-linking. Another key question that will be asked is whether the optimum performance can be achieved with the ability to maximise exfoliation and dispersion and minimise air inclusion.

5.1 Experimental work

The materials used are Nanocor I.30e nanoclay, commercially available montmorillonite clay treated with a primary ammonium surfactant. This is obtained from a different manufacturer than used the previous chapter but is essentially the same type of nanoclay and recommended polarity and surface treatment for use with epoxy.

The resin used was DOW DER330, a bisphenol-A epoxy resin and two hardeners were compared: Isophoronediamine (IPD), a cycloaliphatic amine, which produces a rigid, brittle,

highly cross-linked epoxy network and Jeffamine D230, an aliphatic amine, which produces a flexible, tough epoxy system with lower cross-linking. All resins were all mixed at ratios based on DER330:

IPD - 100:22.8
D230 - 100:33

The process incorporated centrifugal mixing of the clay in ethanol (EToH) epoxy or the amine hardener and a bead mill (BM) for 1 hour to provide the shear. As shown in Chapter 4 the bead mill process for 60 minutes gave the greatest lamella separation. For amine processing a standard rotary cowel high shearer (HS) was used as the bead mill was not designed to be resistant to an amine hardener and any epoxy residue left in the mill after cleaning may induce a cross-linking reaction that, although unlikely, could result in exothermic damage to the bead mill and contamination of the sample.

Material/ Batch	Material / Process Description	Clay Content %
D230 control -	24 hrs at ambient - 12hrs @ 50deg	0 wt%
D230 control -	24 hrs at ambient - 10hrs@70deg	0 wt%
IPD control -	24 hrs at ambient 12hrs @ 50deg	0 wt%
Batch 1	I.30.e high shear processed in D230	1 wt%
(D230 HS70)		2 wt%
	Cured 24 hrs ambient and 10hrs@70deg	3 wt%
		4 wt%
Batch 2	I.30E high shear processed in IPD 60 mins.	1 wt%
(IPDHS)		2 wt%
	Cured 24 hrs ambient and 12hrs @ 50deg	3 wt%
		4 wt%
Batch 3	I.30E processed in ethanol high shear and then DER 330	1 wt%
(EtOHHS)		2 wt%
	Cured 24 hrs ambient and 12hrs @ 50deg	3 wt%
		4 wt%
Batch 4	I.30E high shear processed in D230 60 mins,	1 wt%
(D230HS)	Vacuum mixed with resin.	2 wt%
	Cured 24 hrs ambient and 12hrs @ 50deg	3 wt%
		4 wt%
Batch 5	I.30E high shear processed in IPD 60 mins, vacuum mixed	Not made
(IPDHS)	with resin.	
Batch 6	I.30E processed in ethanol and then high shear with DER 330	1 wt%
(EtOHHSvac)	vacuum mixed with resin	2 wt%
		3 wt%
	12hrs @ 50deg	4 wt%
Batch 7	I.30E processed in ethanol and then bead milled with DER 330,	1 wt%
(EtOHBMvac)	Vacuum mixed with resin and hardener	2 wt%
		3 wt%
		4 wt%

Table 5-1 Batch number with the corresponding description of processing method, cure temperature and clay content.

Table 5-1 shows the different batches and the materials and processes used. This describes test matrix of the process used and curing m

Processing in the amine hardener was shown in chapter 4 showed to give an evenly intercalated dispersion of nanoclay. This was said to be due to the ease in which the amine molecules enter between the nanoclay lamella allowing the epoxy molecules to follow. The same mechanism has been described for the use of solvent slurry, which constitutes an exfoliation absorption method as discussed in section

Table 5-2 and Table 5-3 show the weights of material used for each type of processing. For the hardener mixing the total amount of nanoclay was weighed out and added the hardener to create a hardener master-batch solution. This was then DAC-mixed to wet the nanoclay and high shear mixed for 1hr. This masterbatch was then diluted with extra hardener to create the desired loading for the total nanocomposite loading. This was then added to the stoichiometric amount of resin.

resin	hardener	wt	Nanoclay I.30E wt(g)	%wt	% in Hardener	added hardener (g)	equivalent added epoxy (g)
Dow	**D230**	198	31.92	4.00%	16.12%	0	600
DER 330	**ratio**	148.5	23.94	3.00%	12.09%	49.5	600
	33:100	99	15.96	2.00%	8.06%	99	600
		49.5	7.98	1.00%	4.03%	148.5	600
Total (g)		495	79.8			297	2400

Table 5-2 Manufacture of D230 hardener processed batch.

resin	wt (g)	hardener	wt(g)	Nanoclay I.30E wt (g)	Total wt(g)	%wt	% in resin	added resin (g)
Dow	180	**D230**	41.0	8.8	188.8	4%	5%	0
DER 330	135	**ratio**	41.0	6.6	141.6	3%	4%	45
	90	**33:100**	41.0	4.7	94.7	2%	3%	90
	45		41.0	2.4	47.4	1%	1%	135
total	450		164.2	22.1	472.1			270

Table 5-3 Manufacture of solvent/resin processing batch with D230 hardener.

The same master-batch method was used for the resin mixing as described for the amine mixing method, however, the epoxy / nanoclay concentrate was diluted with added resin before curing with the hardener. The solvent slurry processing was essentially the same as the resin mixing method. The total weight of clay used was added to the required amount solvent to make a 10wt% paste, which was then DAC mixed for 5 mins to wet the clay. This was then added to the required amount of resin and processed in the bead mill for 1 hr and left in the vacuum chamber at a heat of 50 degrees to evaporate the solvent.

The mixed samples, after degassing, were then poured through a funnel into a cast. This consisted of two release coated glass plates. The plates were coated with a solvent based release coat which was applied with a paper cloth and left for 15 min, before polishing with a clean dry cloth. The glass plate edges were separated and sealed by a 5mm diameter rubber

o-ring chord and clamped together. These were then left to cure vertically at room temperature for 24 hours. The cured resins were then post cured at 50°C or 70°C for 16 hours before being released from the glass plates and cut into test coupons.

5.1.1 Testing

Testing on the IPD samples could not be undertaken due to the very high brittle nature of the cured resins. This meant that nearly all IPD samples fractured when the small amount of force to remove them from the mould was applied.

All D230 cured batches were tested for thermo mechanical properties and flexural properties. Thermo mechanical properties were assessed using a DMA to measure the glass transition temperature. The DMA samples were cut to 10mmx35mm specimen sizes and tested on a double cantilever apparatus and set to oscillate at a constant frequency and set displacement over a temperature range of 25 - 200°C at a temperature ramp of 3°C/min.

Flexural properties were tested on a Zwick test machine with double cantilever apparatus, as shown in Figure 5-, used to measure force and displacement. Five coupons of 10mmx100mm were cut for flexural strength testing. The testing was displacement controlled and carried out at a rate of 5mm/min using a span of 80mm and data recorded using a 5KN load cell according to test standard ISO 178.

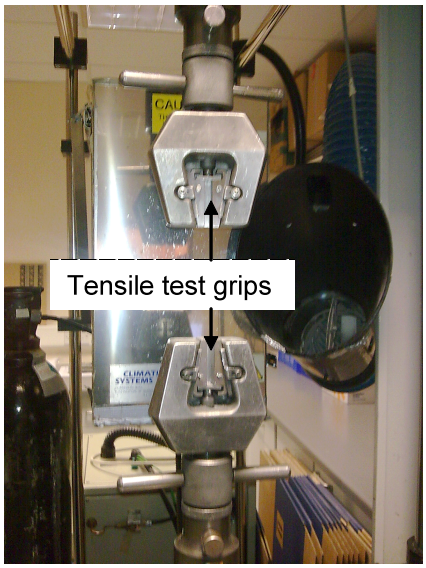

Figure 5-1 Material testing apparatus set up for tensile testing

The best performing batch in flexural properties was submitted to further testing in tensile strength and modulus as well as Charpy impact toughness. Tensile dog bone specimens were cut on a computer controlled router and sanded and polished to remove and burs or chips that may cause stress concentrations. These were then tested on a Zwick testing apparatus as

shown in Figure 5-1 using 30KN wedge grips at a rate of 1mm/min using a 5KN load cell according to ISO 527-2:1996.

Charpy impact toughness was tested on batch 7 to give an indication of the dynamic fracture properties of the nanoclay. Samples were cut to 80mm x 10mm and a v-shaped notch cut into it using a bespoke notch saw. The specimen was then placed in a Zwick impact test machine. A 7-joule hammer was then released to collide with the specimen, connecting with the opposite side to the notch. The distance the hammer travelled after impact was converted into the energy absorbed by the specimen.

5.2 *Nanoclay results and discussion*

5.2.1 Characterisation of Nanoclay composites

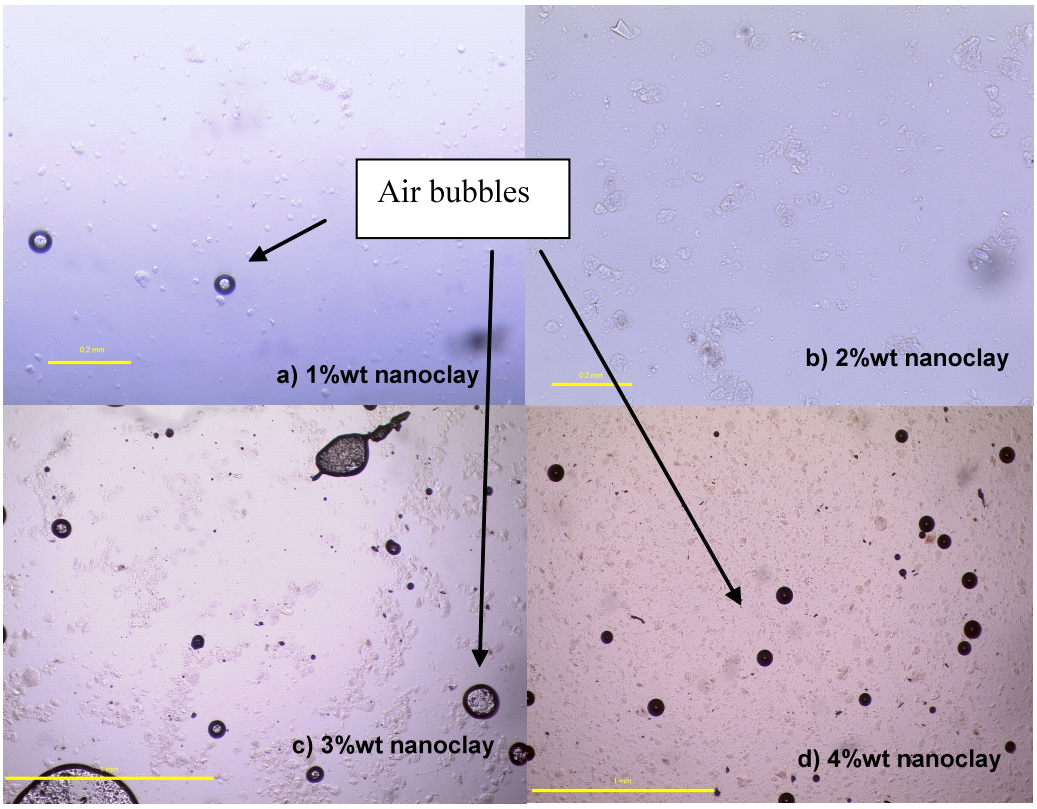

Figure 5-2 Micrographs of different nanoclay loading, using a solvent dispersion method. a) 1wt% nanoclay b) 2wt% nanoclay, c) 3wt% nanoclay and d)4wt% nanoclay. The increasing amount of entrapped air and agglomeration can be visible with the increasing amount of nanoclay loading.

Both agglomeration and air bubbles were observed in the manufacture of the nanoclay resins. Observation of processing of nanoclay in the hardener showed that both D230 and IPD absorbed into the nanoclay at a greater speed than the resin. In particular IPD, gave the appearance that the nanoclay was more effectively dissolved in the hardener when initially mixed together. However, the IPD samples cured very quickly and became exothermic

before the resin could be fully degassed. The Control DER330 + IPD shattered on de-mould with a cure of 24 hrs ambient and 16 hrs at 50°C. This is a more brittle, highly cross-linked system but this behaviour is unexpected. A possible explanation is that an incomplete cure causes the brittle nature and shattering due to thermal shock. Similar problems were observed with DER330 + IPD with nanoclay sheared into IPD. However, there appears to be less agglomeration with clearer mixed solution observed. This does changes to an opaque cream colour after the cure. When the nanoclay is sheared into D230, voids and agglomeration are also visible after curing. It is proposed that the clay and any microscopic voids re-agglomerate during the curing. 10wt% nanoclay in ethanol became solid paste on DAC mixing. Subsequent processing into the resin gives a better dispersion as shown in Figure 5-2, however, air bubbles are also visible. Least agglomeration appears, with microscopic analysis, to be obtained with the solvent slurry route.

Figure 5-2 is an example of how the increasing clay wt% content shows up under the microscope. Not only is it easy to see areas of concentrated nanoclay increasing as the loading increases but also, apart from the 2wt% micrograph, an increase in what appears to be air bubbles. This may explain some of the following property traits observed.

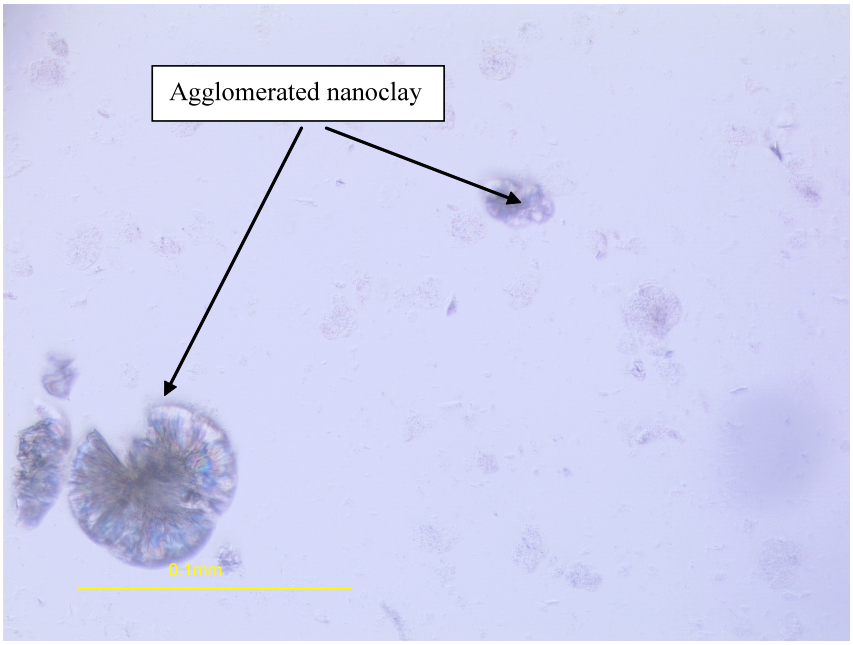

Figure 5-3. 3% I.30E 200x. showing expanded nanoclay agglomeration.

At higher resolution in Figure 5-3, the nanoclay appears to be expanded relative to the previous analysis in Chapter 4. Previous tests with nanoclay sheared in resin shows less agglomeration but on a smaller scale and in tighter formation. This could suggest that the nanoclay has either been dispersed and exfoliated but re-agglomerated or the lower viscosity

has reduced the shearing action of the system and not provided enough energy to separate the clay lamellae.

A JOEL 6500 SEM was used to take micrograph images of high sheared nanoclay / epoxy composite surface. This was used to for analysis of how the nanoclay disperses and the morphology with different loading the cured sample.

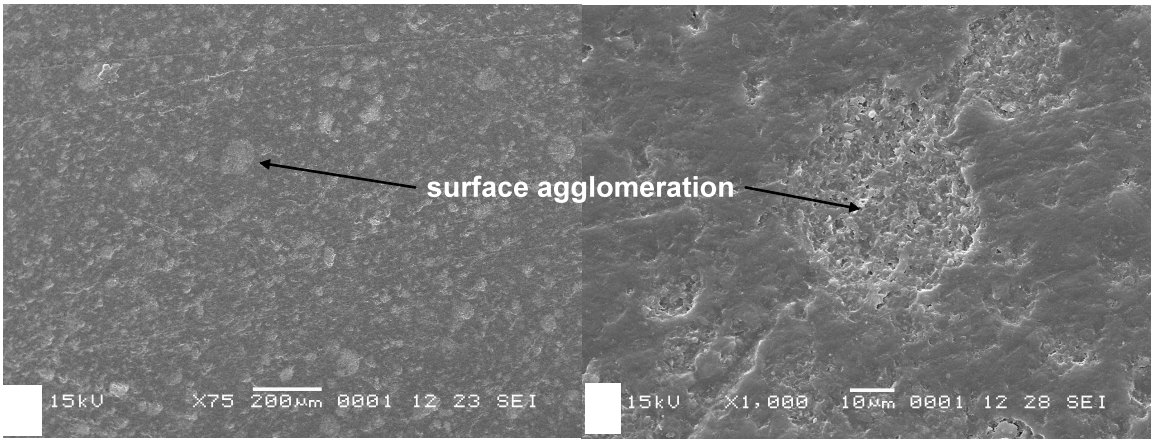

Figure 5-4 SEM micrograph of the unprepared 2wt% nanoclay resin cast surface showing the agglomerated clay visible on the surface at A) 75x magnification and B) 1000x magnification.

Figure 5-4 and 5-5 show the surfaces of a 2wt% and 4wt% high sheared nanoclay epoxy resin sample. They both show agglomerated nanoclay on the surface of the resin cast. The agglomerations are visible where they break smooth the surface of the polymer and create relief topography with small crevasses between the nanoclay particles. The 4wt% sample shows more disturbances on the surface and also more pronounced agglomerations.

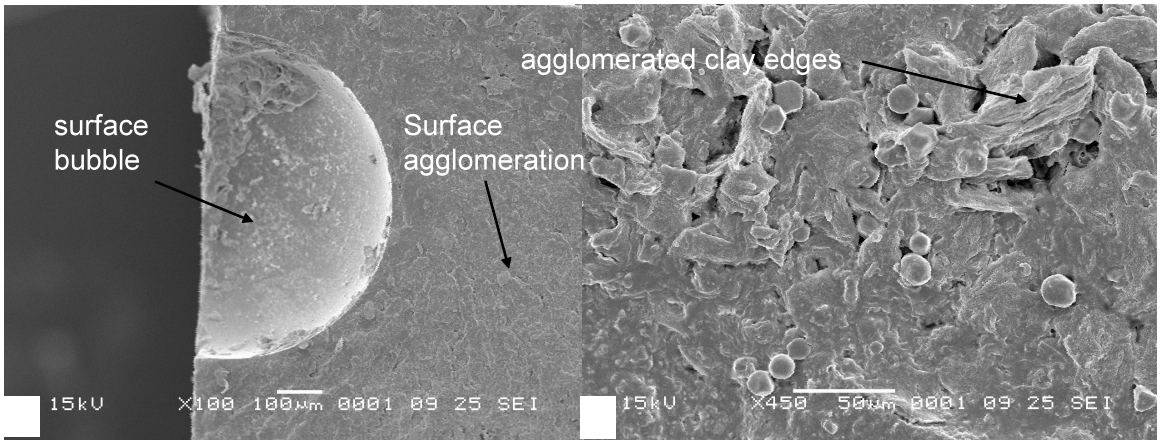

Figure 5-5 SEM micrograph of unprepared 4wt% nanoclay resin cast surface showing the clay visible on the surface at A) 100x and B) 450x magnification.

Figure 5-6 and Figure 5-7 show the X-ray diffraction results from the D230 processed batch 4 and the ethanol processed batch 5. The results clearly show the amorphous curve and the peaks that correspond to the *d*-spacing between the clay lamella. In each case the higher the wt% of nanoclay the more prominent the diffraction peaks. However, the peaks occur at the

same value 2θ irrespective of the nanoclay loading indicating that the amount of nano does not effect the separation. The nanoclay batches were all processed as a master-batch before being separated and diluted into the various clay loadings. It confirms that the different clay loading did not effect the exfoliation during the dilution, addition of hardener and curing. Batch 4 shows a value of $5 2\theta$ corresponding to 1.77nm which is lower than the batch 6 value of $4 2\theta$ corresponding to 2.21nm. These results imply that processing in a solvent allows greater separation of the clay lamella.

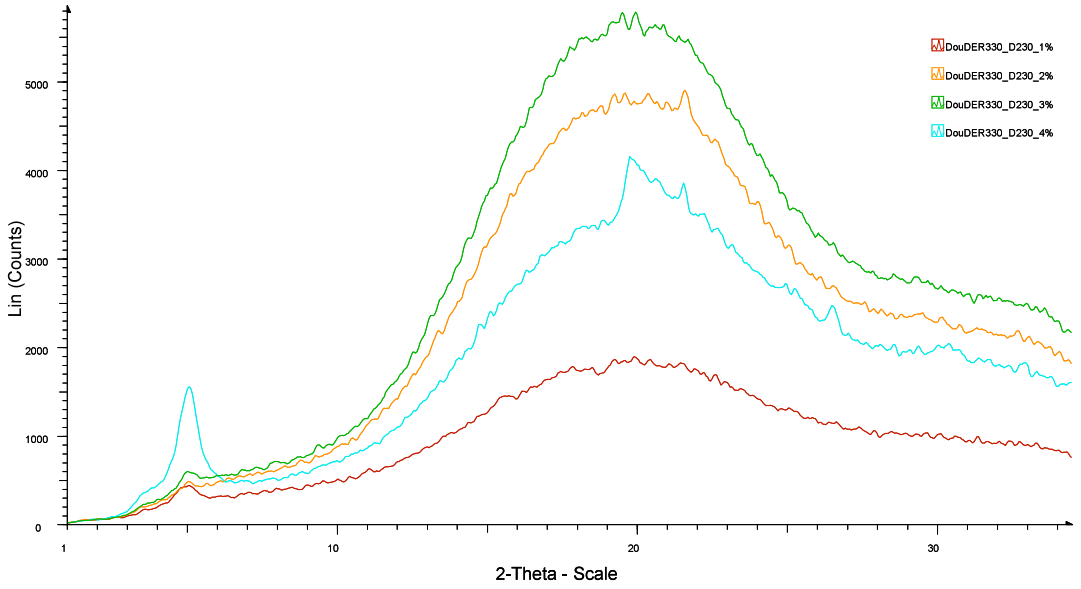

Figure 5-6 X-ray diffraction of D230 processed batch 4 samples.

The *d* spacing in Figures 5-6 and 5-7 are relatively small compared to the previous Chapter 4 analysis. The nanoclay material being from a different manufacturer may show different exfoliation behaviour. Figure 5-6 shows a shoulder in the XRD intensity peak at $2.5 2\theta$. There is a possibility that the prominent peaks represent the secondary peak while the primary peak is not measureable on the XRD due to the d-spacing being greater than the XRD diffraction. In this case the spacing would be twice as large and comparable with the previous work. This would give a *d* spacing of 3.54nm and 4.42nm.

The Nanocor I.30e clay tested showed the *d*- spacing of 2.37nm for the pristine ammonium modified clay (Liu et al., 2005a). In the same work, processing with acetone increased the *d* spacing to 3.22nm. High pressure mixing the clay/acetone slurry in epoxy increased the spacing even further to above 4nm suggested by the disappearance of the prominent peak in the diffraction pattern. This makes it difficult to compare the X-ray results presented here with previous work or current knowledge. The prominent peaks, if taken as the primary clay diffraction does not give a *d*- spacing great enough according to measurements of the the

pristine clay. This would imply that they are a secondary peak, which produces *d*-spacing similar to that seen in previous work but this theory is not generally recognised and may be misleading.

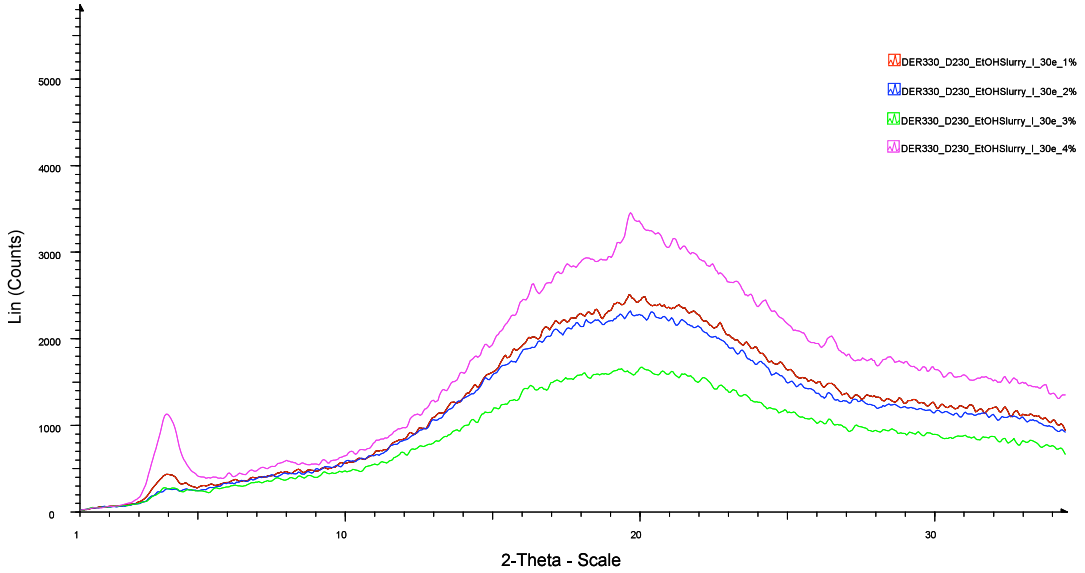

Figure 5-7 X-ray diffraction peaks of the solvent processed nanoclay batch 6 samples.

5.2.2 Dynamic mechanical analysis results

DMA was carried out in a Texas Instruments Q800 Dynamic Mechanical Analyser (DMA) according to ISO 6721-1, Plastics- Determination of Dynamic Mechanical Properties. The Q800 is a force-controlled instrument applying a force (the control parameter) until it measures the required amplitude.

Dynamic mechanical analysis (DMA) involves applying an oscillatory strain to a sample while monitoring the resultant stress, consisting of in-phase and out-of-phase components. These stresses can be used to calculate the in-phase modulus (E') and the out of phase modulus (E''). The ratio of $E''/E' = \tan\delta$ is a measurement of the ratio of energy lost to energy stored per cycle of strain. This ratio usually has a maximum peak, along with a step down in E', as temperature of the experiment increases corresponding to the glass transition temperature (Tg). For resin cast Tg measurement, the single cantilever beam apparatus is used to apply designated bending amplitude to the sample. Data on the width and breadth of the sample is supplied into the instrument and once the sample is camped in place the amplitude is set so that the force applied is between 0.1N and 1N. The sample is then oscillated under a controlled temperature ramp of 2°C per minute from 25°C to 200°C.

The instrument takes raw data of the force, the amplitude of deformation and phase angle to calculate the complex stiffness *K**. This is then used to work out the storage and the loss modulus using the raw stiffness data K' and *K"* calculated with the phase angle and multiplied by the geometric factor, GF. Tan delta is calculated as the ratio of *K"* to *K'*. *Tg* is measured from dissection of tangents of the straight line of the storage curve at the points either side of the initial transition phase. Figure 5-8 shows an example of the storage and delta tan curves used to calculate the *Tg* value of the batch 7 sample.

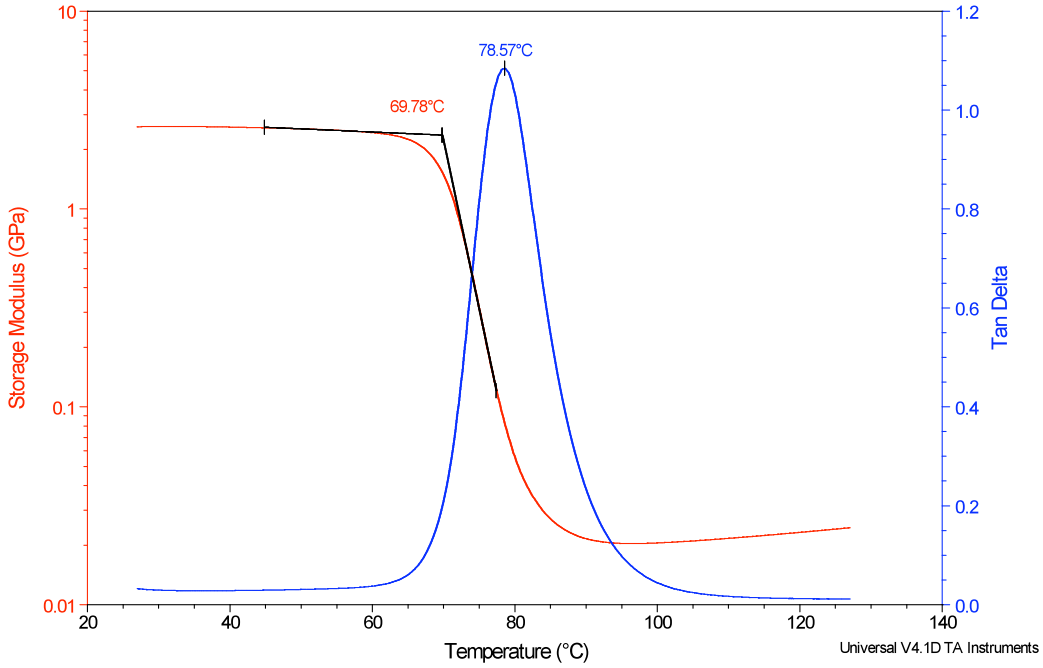

Figure 5-8 Storage modulus and tan Delta results for Batch 7, 3% nanoclay.

Table 5-4 gives the glass transition (*Tg*) temperature data of the different processing methods at different clay loadings measured on the Dynamic Mechanical Analyser (DMA). Figure 5-9 shows data in graphical form.

Batches 3, 4 and 5 show decreasing value with clay content,. Temperatures, however, only drop by a maximum of 5°C in Batch 4. Batch 1, being cured at 70°C, shows a slightly higher *Tg* with 1 and 2wt% clay loading. Batch 7 also shows some increase at 1and 2wt%.nanoclay. Many reports show a significant decrease in the *Tg* with the addition of nanoclay (Yasmin et al., 2006) and also with the increase in clay lamella separation (Chen et al., 2002). This is demonstrated in all samples above 2wt%.

Batch	Nanoclay wt%	Average *Tg* (°C)
D230 / DER330	0	70.2
D230 / DER330 (70 deg)	0	79.0
1	1wt%	82.6
	2 wt%	82.1
	3 wt%	80.3
	4 wt%	77.8
3	1 wt%	63.1
	2 wt%	61.6
	3 wt%	60.3
	4 wt %	60.7
4	1 wt%	65.2
	2 wt%	63.4
	3 wt%	64.4
	4 wt%	63.0
6	1 wt%	66.0
	2 wt%	64.5
	3 wt%	65.0
	4 wt%	64.0
7	1 wt%	71.2
	2 wt%	71.4
	3 wt%	69.8
	4 wt%	65.0

Table 5-4 Glass transition results from the DMA.

Increasing the cure temperature showed a slightly different trend with the *Tg* increasing at low loadings of clay, which has also been observed in literature (Messersmith and Giannelis, 1994,Agag et al., 2001). Increased *Tg* is attributed to good adhesion between the polymer and the nanoparticles, which restrict the segmental motion of cross-links near the interface.

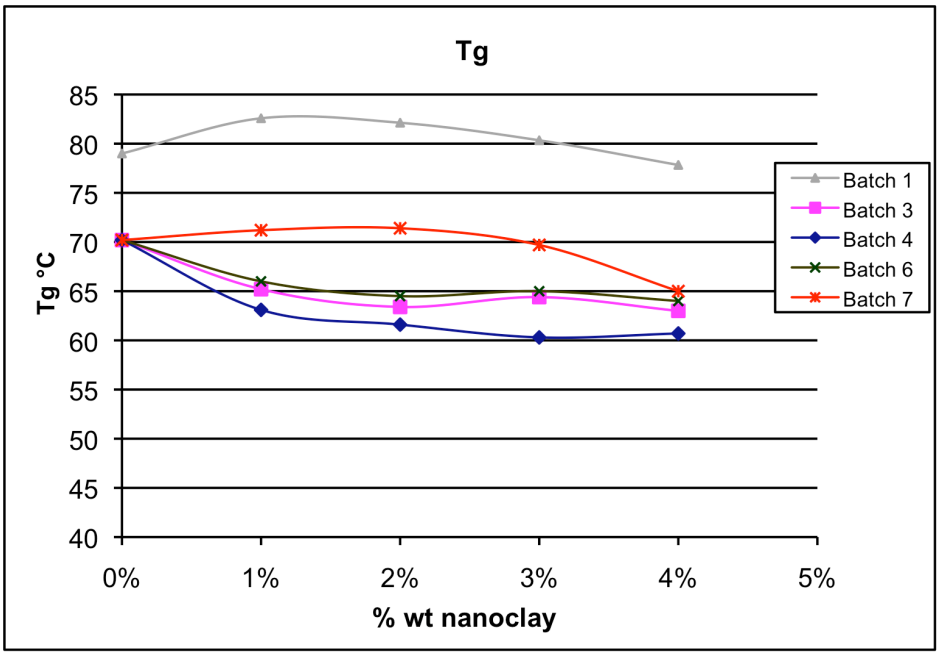

Figure 5-9 *Tg* of samples related to Nanoclay wt%.

Batch 1 and 7 in Figure 5-9 demonstrate these opposing effects, increasing the *Tg* at low clay content and then a detrimental effects becoming dominant as the content increases. At low filler content the restriction of the segmental motion, combined with some insulation thermal properties provided by the nanoclay, takes precedence. At higher loadings the interaction of the polymers chain with the surface of the particles can drastically alter the chain kinetics in the region surrounding them and lead to lower cross-link density. The plasticisation of the interphase region surrounding the nanoclay, caused by surfactant chains, can also lower the *Tg*. There are many factors that affect the *Tg* such as cure temperature, cure speed.

5.2.3 Flexural results

The resin samples were tested according to the flexural ISO standard 178:2003 Plastics-Determination of flexural properties.

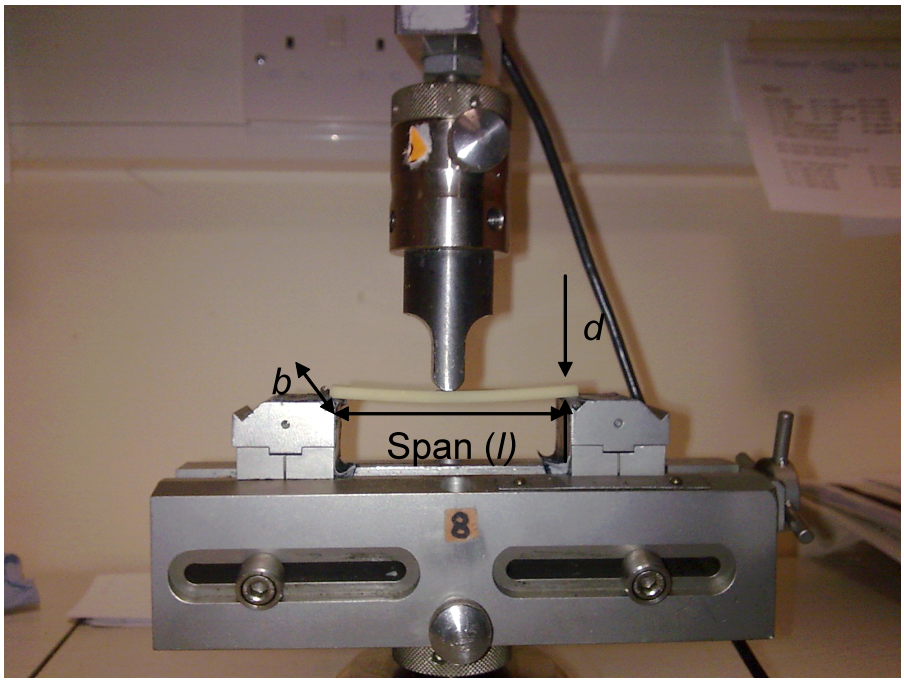

Figure 5-10 Arrangement of the flexural testing apparatus.

Flexural mechanical tests were carried out on Zwick hydraulic test apparatus shown in Figure 5-10 which shows the 3-point bend testing jig with a support span of 80mm. The actuator test speed was 3mm/min and the load measured with a 5KN Load cell. The modulus and strength were calculated using:

$$E = \frac{L^3 m}{4bd^3}$$ **Equation 5-1**

$$\sigma = \frac{3PL}{2bd^2}$$ **Equation 5-2**

Where:

L is the support span

m is the slope of the tangent to the initial linear portion of the load deflection curve

b is the width of the test specimen.

d is the depth of the test specimen.

P is the load given on the load deflection curve

Average results of the flexural modulus and the flexural strength with the standard deviation are given in Table 5-5 and the. This will give a comparison of the strength and stiffness of the different clay processing methods over increasing clay content, which is displayed graphically in Figure 5-11 and 5-12.

Material Description	Flexural modulus GPa)	Modulus standard deviation (Gpa)	Breaking stress(MPa)	Stress standard deviation (MPa)
50°C Control	3.07	0.058	105.80	1.072
70°C Control	3.13	0.114	108.95	1.583
Batch 1 1%wt	3.08	0.026	105.57	0.585
Batch 1 2%wt	3.05	0.044	87.01	8.815
Batch 1 3%wt	3.14	0.022	83.27	6.379
Batch 1 4%wt	3.19	0.109	79.84	10.062
Batch 3 1%wt	3.08	0.107	91.85	6.911
Batch 3 2%wt	3.30	0.019	89.58	3.544
Batch 3 3%wt	3.31	0.038	82.02	3.972
Batch 3 4%wt	3.33	0.033	73.95	5.678
Batch 4 1%wt	3.30	0.027	109.62	1.181
Batch 4 2%wt	3.30	0.019	98.30	10.305
Batch 4 3%wt	3.32	0.027	86.04	12.557
Batch 4 4%wt	3.41	0.033	87.53	7.862
Batch 6 1wt%	3.41	0.061	106.74	4.159
Batch 6 2wt%	3.45	0.036	95.33	4.685
Batch 6 3wt%	3.40	0.223	92.66	1.409
Batch 6 4wt%	3.50	0.250	107.31	0.878
Batch 7 1%wt	3.25	0.035	109.51	6.974
Batch 7 2%wt	3.30	0.059	111.30	1.213
Batch 7 3%wt	3.42	0.044	110.87	1.303
Batch 7 4%wt	3.45	0.061	106.22	8.473

Table 5-5 Flexural test results.

Table 5-5 and Figure 5-11 gives the behaviour of the flexural strength with increasing clay content. The horizontal line represents the control pristine resin, post cured at 50°C, flexural strength of 110.2MPa. The 70°C control had a flexural strength of 109MPa. All batches show a decline in strength with nanoclay content except the values of batch 7, which increased at 2 and 3wt% before dropping at 4wt%.

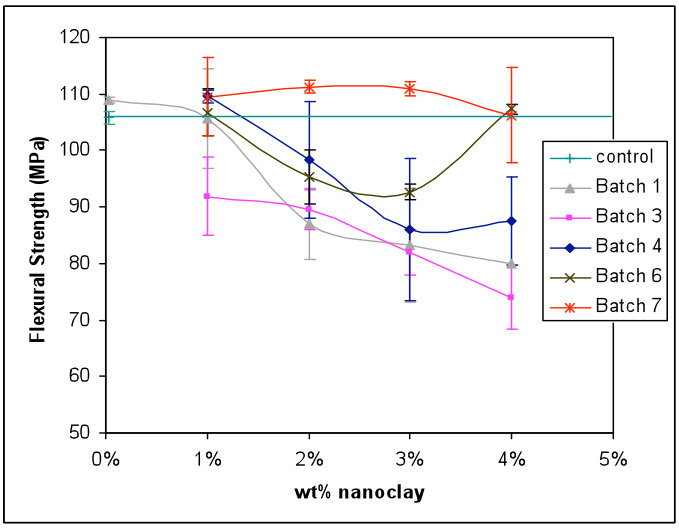

Figure 5-11 Flexural strength of samples related to nanoclay wt%.

Lu et al.(2004) showed a similar trend with an increase in flexural strength under 3wt% nanoclay by about 8 % with the high shear milled processed nanoclay /polyamide. The normal stirring processing showed no increase over the pristine epoxy. Sinha Ray and Okamoto (2003) showed an increase in nanoclay composite flexural strength and modulus up to a loading of 5wt% nanoclay.

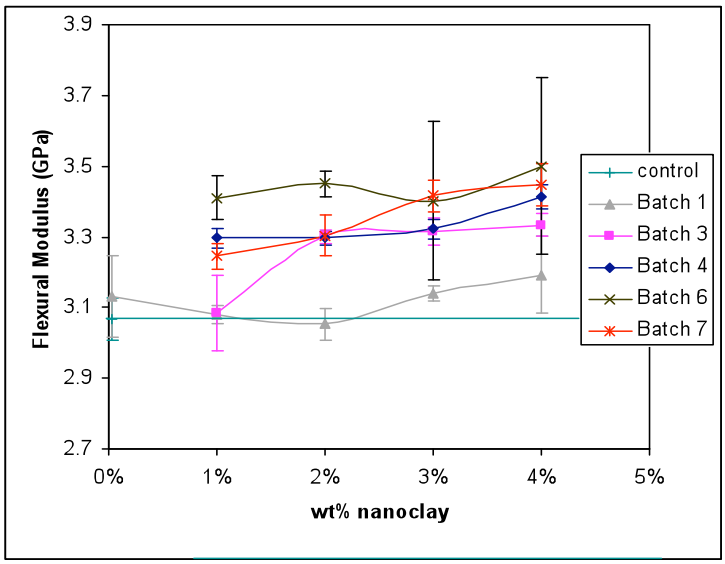

Figure 5-12 Flexural Modulus of samples related to nanoclay wt%.

Figure 5-12, shows some increase in flexural modulus depending on the processing. Batch 6 and 7 show the biggest increase with a modulus of 3.5 and 3.45GPa respectively at 4wt% nanoclay. Batch 6, however, has a very large standard deviation, which may be due to the quality of sample or the process method. This reduces the confidence modulus results of this batch. The lowest modulus is given by the 70°C post-cured batch which actually decreases to 3.05 at 2wt% before increasing again at 3 and 4wt%.

The interesting observation for these results is that, although there is a net tendency to increase in modulus, the performance does not translate to an increase in the *Tg* results. The increase in the Batch 1 *Tg* would normally indicate an increase in modulus; instead a reduction in modulus performance is seen. The opposite is true for the other batches, which increase in modulus when the decrease in *Tg* performance would normally dictate a lower modulus due to the reduction in the polymer cross-linking.

5.2.4 Further testing on Batch 7

Due to the overall increased performance batch 7's in the *Tg* and flexural testing this work was specifically interested in the effect of the clay loading on the impact toughness.

5.2.4.1 Tensile testing

Tensile testing was made according to ASTM D 638M-89 / ISO 527 - 2 : 1996 test standard. The test occurred at a displacement rate of 1mm/min on five specimens from each sample. From these the average strength and modulus results are given in Table 5-6 and graphically given in Figure 5-13 relative to their clay loading.

Clay content wt%	0wt%	1wt%	2wt%	3wt%	4wt%
Tensile Strength (MPa)	68.48	67.70	64.85	58.77	61.15
Change in strength		-1%	-5%	-14%	-11%
Standard deviation(MPa)	0.517	1.874	2.639	4.571	2.254
Young's Modulus (GPa)	3.29	3.52	3.55	3.51	3.52
Change in modulus		7%	8%	7%	7%
Standard deviation (GPa)	0.048	0.051	0.058	0.075	0.052

Table 5-6 Tensile strength and modulus of the solvented bead milled, batch 7, nanoclay/epoxy

Tensile results in Table 5-6 and Figure 5-13 show the strength reducing in value while the modulus increases with the addition of nanoclay to the composite. The strength decreases by a maximum of 14% at 3wt% nanoclay where the standard deviation is also the maximum of 7%. This may be due to an excess of entrapped air creating more variable results. The modulus also has the greatest variability for this sample with 2% standard deviation. The greatest increase of modulus is 8% at 2% nanoclay.

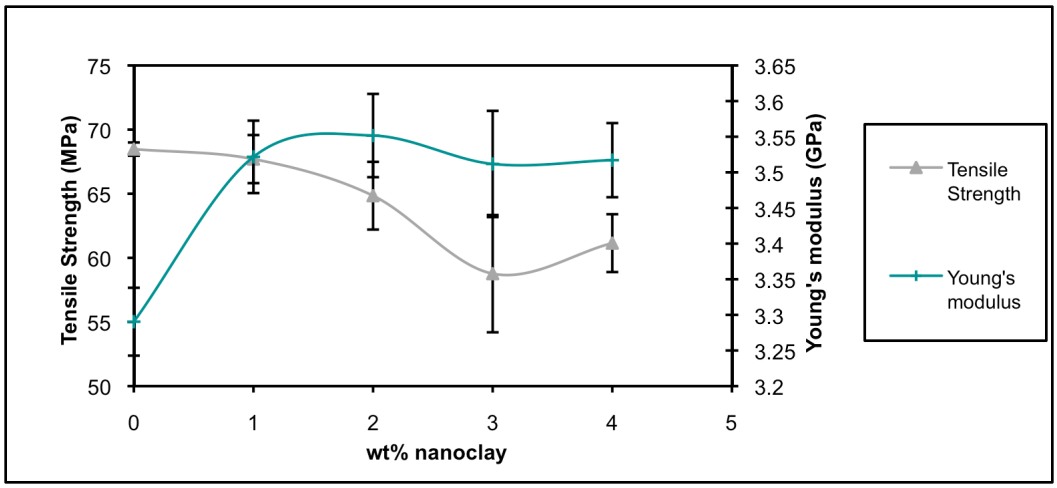

Figure 5-13 Tensile strength and modulus of the solvented bead milled batch 7 nanoclay/epoxy

5.2.4.2 Charpy impact toughness

The aim of the work on the Charpy Impact toughness was to progress from the quasi static flexural strength and look at the dynamic high strain impact strength. There are many claims that nanomaterials may show an increased performance in impact situations due to their ability to retard crack propagation as described in Chapter 2. Different clay loaded samples of batch 7 where prepared and tested according to ISO 179 / EA, Plastics – Determination of Charpy impact strength which specified 10 specimens of each sample should be testes. The average values and standard deviation are given Table 5-7 and graphically in Figure 5-14.

Clay loading	**0wt%**	**1wt%**	**2wt%**	**3wt%**	**4wt%**
Charpy impact strength (KJ/m^2)	6.79	2.66	1.82	1.61	1.39
Standard Deviation (KJ/m^2)	2.627	0.143	0.270	0.105	0.068

Table 5-7 Charpy impact fracture results for solvented bead milled epoxy nanoclay, batch 7.

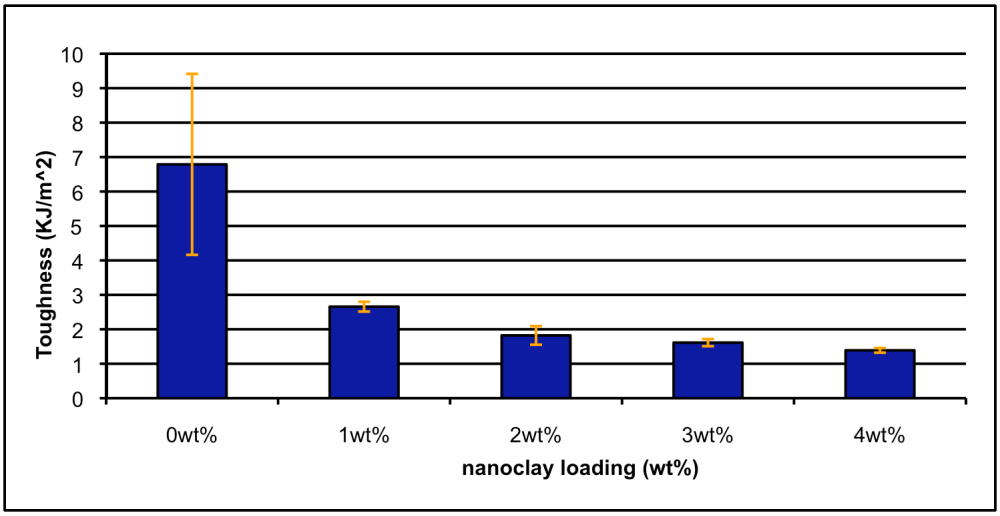

Figure 5-14 Charpy impact toughness of solvented bead milled epoxy nanoclay, batch 7.

Figure 5-14 shows Charpy impact toughness testing was only conducted on batch 7 against the weight fraction of nanoclay. A significant drop in the energy absorbed by the specimen was observed. Even though there is a large standard deviation of 39% the change in the Charpy impact toughness has enough confidence to show a decreasing trend from 5.2KJm^{-2} in the pristine resin to 1.4KJm^{-2} with 4wt% nanoclay. Data from Lu et al.(2004) disagrees with this and shows that the impact strength can be increased up to 50 % higher than that of pristine matrix. In this case the pulverisation and dispersion of nanoclay in a ball milling process was increasing dispersion and exfoliation causing the mechanical properties to increase. Comparing these epoxy system the tested in Lu et al., was cured with anhydride rather than amine hardener which makes our system a lot less brittle and may make the epoxy and less sensitive to entrapped air or agglomerations which can be detrimental to the impact toughness.

5.3 Discussion Summary

From the DMA results very little increase is seen in the *Tg* as the loading of nanoclay is increased. Two processing parameters; higher cure temperature and bead milling with a solvent, show that at low nanoclay weighting, between 1 and 2wt%, the *Tg* can increase slightly where as other processing methods produced a decrease in *Tg*. The trend with all processing batches is for the *Tg* to decrease at higher loading of nanoclay. Many reports have also observed a decrease in *Tg* with increased nanoclay content (Yasmin et al., 2006) and increased interlamella separation (Chen et al., 2002). However there are cases where epoxy-based nanocomposites, containing octadecylamine-modified nanoclay, exhibited a lower *Tg* than the pure resin. This reduction was more pronounced when the clay was dispersed in acetone using a high-pressure mixing technique (Liu et al., 2005b) than mixing without solvent. It is suggested that these processing conditions effectively changed the clay–polymer interfacial interactions, modifying the constraint of the polymer chain mobility near the reinforcements, which is responsible for the variation of *Tg* (Kim et al., 2005) and that there is a plasticization effect of the organoclay (Chen and Curliss, 2003a).

The most significant change is caused by a change in post-cure temperature. The *Tg* is an indication of the cross-linking of the polymer and results with the higher temperature cure, batch 1, show that the post-curing greatly effects the cross-linking. With increased post-cure temperature, as suggested in Chapter 4, there is an increase in the thermal properties. The higher post cure temperature increasing the interphase cross-linking and reducing the mobility of the polymer chain relative to the lower temperature post-curing may cause this. This also can be the reason that the IPD-cured samples failed in such a brittle manner and it suggested that this particular system required a higher temperature post-cure.

The XRD data shows that the solvent dispersion method gives better lamella separation than the amine dispersion method. Both the vacuum mixed and non-vacuum mixed solvent batches 3 and 6 have similar *Tg* values at all nanoclay loadings. In each case both had higher *Tg* values than the amine mixed batch 4. The assessment can deduce that the solvent processing produced the largest clay separation and this represented also by the *Tg* value, The bead-milled solvent processing, batch 7 showing even greater *Tg* value.

The flexural results show that vacuum mixing does translate to improved properties. The flexural test results batch 1, with the 70°C, does not show any improvement in strength or modulus, where the opposite effect might be expected from an increase in *Tg*. Batch 1 and 3, not receiving any vacuum; show consistently the lowest mechanical properties. The high shear, solvent-dispersed, batch 6, only shows greater flexural modulus than the high shear amine dispersion and at higher clay content the same is true or the flexural strength. This suggests that the increased clay exfoliation is responsible for the increased performance. The largest improvement is seen with batch 7. This suggests that high shear milled processing, with the aid of a solvent to help exfoliation, is most suitable for structural application of nanoclay. The results reiterate the findings in Chapter 4, which hypothesised that bead milling and solvent slurry attain the most effective dispersion and exfoliation. This also agrees with many researchers and earlier comments that the structural performance of the composite is closely linked to the dispersion and also exfoliation (Lu et al., 2004).

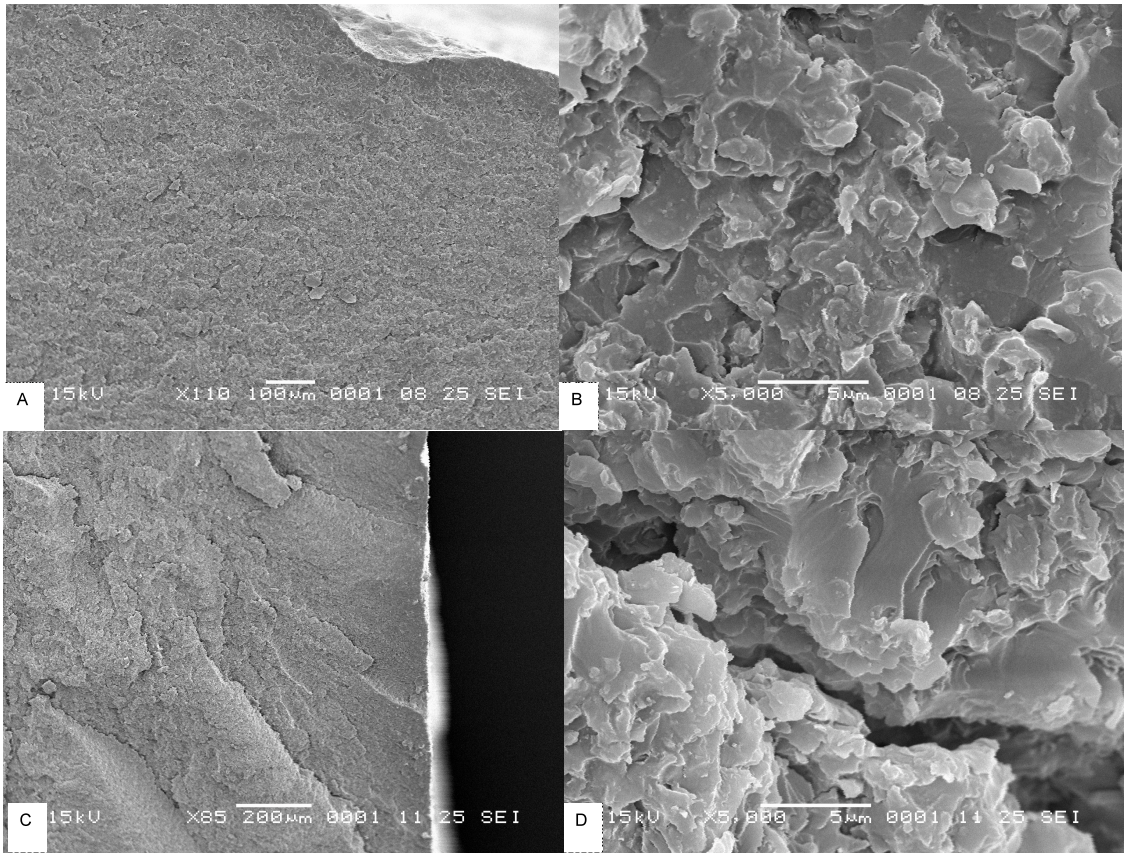

Figure 5-15 SEM micrographs of the A) 2% nanoclay at the 100μm scale and B) 2% nanoclay at 5μm scale. Image C) 4% nanoclay at 100μm scale and D) 4% nanoclay at 5μm scale.

Figure 5-15 shows the SEM micrograph of the two samples of differing nanoclay loading. The images show the topography of the flexural test fracture surface of the different clay loadings. The appearance is very similar showing the rough fracture surface and jagged clay platelets on the epoxy surface. Even though the two samples have different magnifications it is possible to identify the differences in the number platelets visible. At 4% nanoclay there appears to be a greater number of rough, jagged edges than in the 2% nanoclay sample. The rough surface would also be indicative of some void content, or crazing caused by low nanoclay interfacial strength.

Tensile strength and Charpy impact toughness appears to decrease with the introduction of nanoclay, however, the tensile modulus showed an increase in value. Any crack pinning or deflection effect seems to be insufficient to counter the detrimental effects of the nanoclay and the effects observed with the SEM analysis. The cause may be an effect of the curing mechanism decreasing the performance of the interphase bonding mechanism between the epoxy resin and nanoclay due to the restriction imposed by the nanoclay on the polymer while in gelation. This would result in the epoxy becoming mechanically deficient by allowing an easier path for cracks to propagate. There was no improvement in tensile strength and a decrease in impact strength but also an increase in tensile modulus with added nanoclay

reported by Isik et al (2003). Cloisite 30b from Southern Clay was sonicated in Bisphenol A resin with varying amounts of polyether polyol, an impact modifier. The resultant nanocomposite was only partially intercalated with a *d* spacing of 3.8nm similar to the amount reported here. This will have affected the mechanical properties, as would the dispersion of nanoclay. The reason why many systems do not exhibit significant improvement may be due to the different cure speeds. Within the bulk epoxy and the clay interface variations in cure speeds may occur. This would provide conditions for internal stresses to occur go someway to account for the loss of mechanical properties along with the interfacial properties between the epoxy and nanoclay (Zilg et al., 2000).

When assessing the clay wt% the best overall performance is given by approximately 2wt% nanoclay. With the Batch 7 processing it gives an increase of 2% in *Tg* and 5.2% flexural strength and 7.5% flexural modulus.

5.4 Concluding remarks

Previous work in Chapter 4 gave some understanding of the processing and characterising of silicate layered nanocomposites. In this chapter the processing has been assessed in terms of thermal and mechanical characterisation as stated in Chapter 3, Figure 3-2. Figure 5-16 shows the key areas for the use of nanocomposites in structural application; highlighted in green are the areas covered in this chapter.

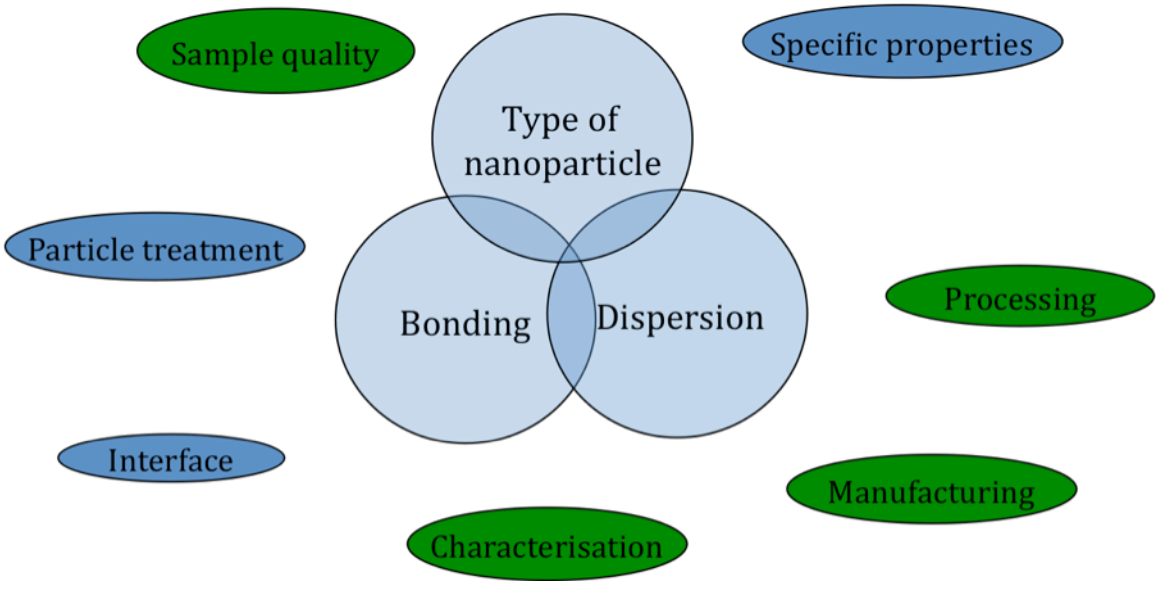

Figure 5-16 The key factors regarding structural nanocomposites with areas that have been investigated in Chapter 5 highlighted in green

Analysis of the different dispersion processing of the epoxy system was made to gauge the effect of the nanoparticles on the mechanical properties. This involved the development of a mixing and manufacturing process and that would create good quality resin casts for testing.

The result gives tangible evidence as a comparison between the effects of processing and the morphology of the nanoclay. The work has also looked at the effect of the nanoclay loading and how this affects the mechanical and thermal behaviour, giving a clear indication on the amount that should be used in structural application. This can be combined with the characterisation of the state of the nanoclay and the assessment of dispersion. Through Chapter 4 and continued in Chapter 5 the process of manufacturing nanocomposites has been refined taking advantage of milling and the degassing equipment. The assessment has been specific to structural enhancement, working with materials that are the basis of the composite structural matrix.

There are still many other properties that could be tested to make further conclusion on the effect of nanoclay in a structural composite. Repeating these tests would also gain further confidence in the results. The overriding question, though, is that can a significantly better performance than the results produced in this chapter be gained by using nanoclay. When looking at the field of nanocomposites there are other materials that will in theory perform better. This work with nanoclay can aid the study and use of other nanomaterials with the dispersion process, the manufacturing and even testing procedures, having been refined here.

6 Properties and behavioural trends of different CNT dispersion routes

The type of nanoparticle in a composite matrix can influence the material properties significantly. This is due to the dimensions and specific properties of the nanoparticles that can affect the way the cross-linking of the polymer or propagation of cracks through it. Carbon nanotubes are well renowned for their extremely high specific strengths and stiffness. This chapter examines the structural changes in performance when CNTs are added to enhance an epoxy matrix. The study also looks at the effects of the bonding mechanism of the nanocomposite and how different interface mechanisms affect the mechanical properties of the material. Characterisation of the dispersion and mechanical properties as seen in Chapter 3, Figure 3-2, compares the two bonding methods and looks at the behaviour over a range of nanotube loadings. The performance of the nanofillers will be analysed in two different cured systems. Both systems are commonly used in structural resin formulations; they differ by their brittleness and flexibility.

6.1 Introduction

The use of carbon nanotubes is expected to enhance the mechanical properties of epoxy composites. The degree of enhancement and the best method of bonding the polymer and nanotubes, as discussed in Chapter 2, are wide-ranging. Various improvements in material properties have been seen across a range of epoxy systems and when compared in Chapter 2, table 2-9, the degree to which these improvements differ can be seen. For structural properties the aim is to assess the bulk properties across the range of CNT loading as well as the fracture toughness and impact properties. A comparison of a covalent bonding mechanism and a Van der Waals bonding mechanism between the nanoparticles and epoxy is made to assess the composite materials' structural performance. Many studies have chosen one or other type of bonding mechanism but the work here directly compares the two types mentioned.

6.2 Experimental work

This experimental work compares the mechanical and physical properties of different loading of Amroy's Hybtonite® carbon nanotube enhanced resin, Nanoledges Nano-in® resin system and Zyvex Kentera™ system. Three commercially available pre-dispersed resins were tested; Amroy resins used covalently bonded nanoparticles and Nanoledge and Zyvex both use Van der Walls forces to bind to the epoxy polymer. The exact composition of the resins is secret due to the commercial sensitivity of the materials.

6.2.1 Materials

The carbon nanotubes dispersed in all three resins are in multiwalled form, based on a fullerene molecule structure or similar to the molecular structure of graphite sheets rolled up.

The dimensions of the nanotubes are:

- Number of walls 3-15
- Outer mean diameter 13-16 nm
- Outer diameter distribution 5-20 nm
- Inner mean diameter 4 nm
- Inner diameter distribution 2-6 nm
- Length 1 - >10μm

The manufacturer, Bayer, claims that the properties of the tubes are:

- Tensile strength > 10 GPa
- E-modulus > 1 TPa
- Thermal conductivity > 2000 W/mK
- Electrical conductivity > 104 S/cm.

(source: Baytubes® C150 P material data sheet)

All CNT systems came pre-dispersed in Epikote 828 and for the purposes of testing two hardeners were used: Isophoronediamine (IPD), a cycloaliphatic amine, which produces a rigid, brittle, highly cross-linked epoxy network and Jeffamine D-230, an aliphatic amine, which produces a flexible, tougher epoxy system with lower cross-linking. Resins were all mixed at ratios based on Epikote 828. For IPD - 100:22.7 and D230 - 100:32.0.

6.2.1.1 Amroy Hybtonite

Amroy uses an ultrasonic technique to disperse and covalently bond the Nanotubes to the epoxy resin, in this case epikote 828, to produce the Hybtonite® enhanced epoxy resin. Hybtonite is covalently bonded using ultra high sonication to initiate breaks in the carbon structure and allow oxygen bonding with carbon atoms to produce carboxylic functional groups. These in turn react with the epoxy ring becoming part of the cross-linking configuration of the epoxy.

Pre-dispersed carbon nanotubes from Bayer were formulated by Amroy in Epikote 828 to produce three loadings of Hybtonite® G4 Resin C is supplied at 1.4wt% (G4 ++), 0.7wt% (G4), and 0.35wt% (G4.E) master batch levels and is a golden / translucent green appearance.

6.2.1.2 Nanoledge

Nanoledge, a French company, specialise in the dispersion of carbon nanotubes. They claim increases in fracture toughness and modulus of the resin at low nanotube content (around 0.3wt% CNT). The resin is highly viscous and black, similar in appearance to tar.

Nanoledge also use Bayer MWCNT in their formulations, however, the nanotubes are adhered to a surfactant using Van der Waals bonding and pre-dispersed carbon nanotubes were formulated by Nanoledge in Epikote 828 to produce a masterbatch of 3%wt enhanced epoxy. This was then diluted with pristine Epikote 828 in batches with amounts described in Table 6-1.

Nanoledge: Epikote ratio	*Nanotube loading wt%*	*IPD-CNT Loading wt%*	*D230 –CNT loading wt%*
0 : 100	0	0	0
5.75 : 94.25	0.17	0.14	0.13
11.5 : 88.5	0.35	0.28	0.26
23 : 77	0.69	0.56	0.52
46 : 54	1.38	1.12	1.05

Table 6-1 Formulation ratios and CNT loading of Nanoledge material.

6.2.1.3 Zyvex Nanosolve

Zyvex, based in North America, specialise in performance materials in thermosets and thermoplastics. They produce a carbon nanotube epoxy called Nanosolve, which incorporates MWCNTs from Arkema and their patented Kentera™ technology. The technology is used for structural and electrical enhancement of epoxy polymers. Although limited information is available, it is known the Kentera / nanotube interaction is Van der Waals while the Kentera/matrix interaction is a covalent bond. The use of solvent, specified in the MSDS, is often used to help the dispersion of the CNTs.

Pre-dispersed CNT was formulated by Zyvex in Epikote 828 to produce a masterbatch of Nanosolve enhanced epoxy at a loading of 0.5wt% and 3wt% CNT. This was then diluted with pristine Epikote 828 to produce a range of resins with loadings of carbon nanotubes as indicated in Table 6-2.

Nanosolve: Epikote ratio	*Resin Loading wt%*	*IPD - CNT loading (wt%)*	*D230 - CNT Loading (wt%)*
100:0	3.00%	(not made)	2.27%
46.0:54.0	1.38%	1.12%	1.05%
100:0(0.5wt%CNTresin)	0.50%	0.41%	0.38%
11.5:88.5	0.35%	0.28%	0.26%
5.7:94.3	0.17%	0.14%	0.13%
0 : 100	0	0	0

Table 6-2 formulation ratios CNT loading of Nanosolve material.

6.2.2 Mixing process

The epoxy and hardeners were first mixed in the DAC centrifugal mixer and then vacuum mixed at –1bar till fully degassed. IPD formulations were not degassed for more than one hour to prevent early curing and an exotherm of the resin. Resins samples were moulded by pouring the mixed system using a funnel between two sealed and released glass plates

separated by 5mm diameter rubber O-ring tube. All samples were prepared at room temperature and left to cure for 24hrs at room temperature then post-cured for 1hr at 120°C with a ramp of 2°C per minute.

6.3 Results and discussion

6.3.1 Viscosity

The viscosity of the Amroy Hybtonite samples was measured on a Brookfield CAP 2000 viscometer. A small amount of resin was placed between the viscometer cone and plate, filling the 1000μm, covering the surface of the cone without flowing out on to the plate. The CAP 2000 viscosity data is shown in Figure 6-1. Due to the shear thinning properties of Nanoledge and Nanosolve resins the viscosity could not be measured through this method.

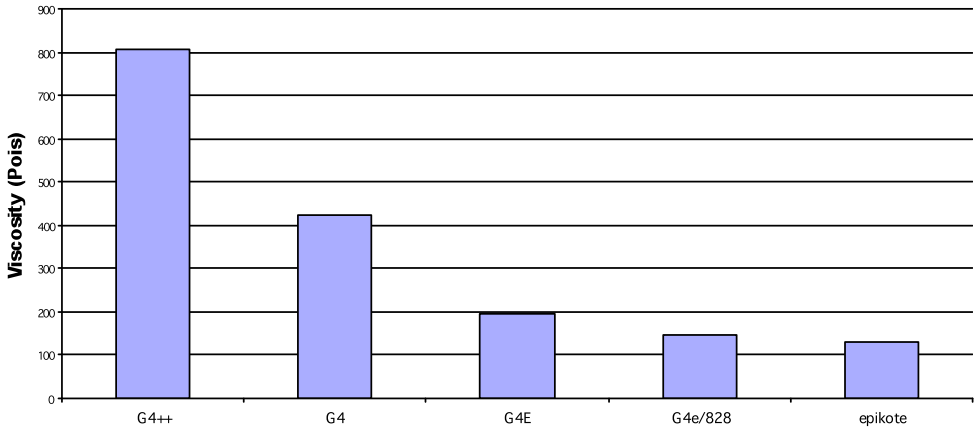

Figure 6-1 Viscosity of the neat Hybtonite epoxy/CNTsystem at 25°C run on a Brookfield Cap 2000 viscometer at a speed of 50 rpm with spindle size of 4 –6.

Rheology of all samples was tested using a TA Instruments AR2000 rheometer with a 20mm diameter steel plate and the Peltier cooling system. Coarse shear rate sweeps were performed on each sample from 0.01 to 1500s^{-1} at a temperature of 10°C with a gap setting of 1000μm. The shear profiles for all resins are given in Figures 6-2 to 6-4.

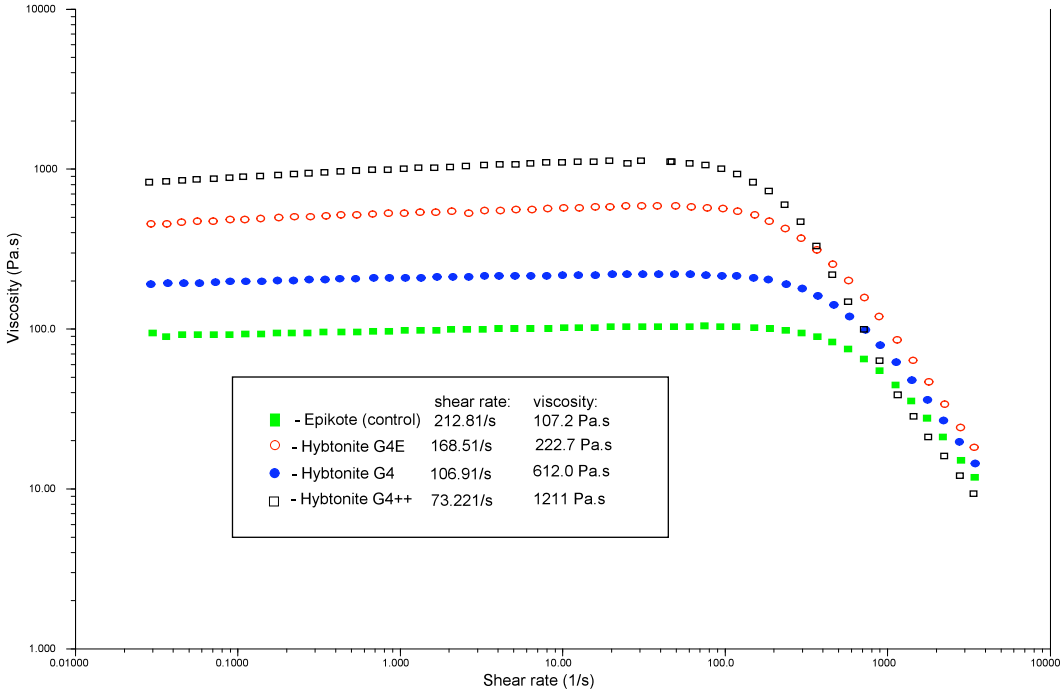

Figure 6-2 Shear rate viscosity profile of Epikote 828 and Hybtonite samples.

Commercial and patent reasons prevented the actual values CNT wt% of the Hybtonite resins to be released by Amroy. From the spot viscosities and the shear sweep data the viscosity reduces by approximately half with the different CNT samples it is assumed that the respective loading of nanotubes reduces by half for each level. It was made known that the maximum loading of the Amroy resin was at percolation point, which for the Hybtonite G4++ sample is 1.38wt% CNT, allowing calculated sample loadings to be made, as shown in Table 6-3.

Sample	Nanotube loading wt%	IPD system Loading wt%	D230 system loading wt%
Epikote 828	0		
G4e / 828	0.17	0.14	0.13
G4e	0.35	0.28	0.26
G4	0.69	0.56	0.52
G4++	1.38	1.12	1.05

Table 6-3 Calculated Hybtonite nanotube sample loading.

Due to the different cure ratios the IPD and D230 cured CNT wt% loadings are slightly different in each system. For the Nanosolve and Nanoledge resins equal loadings were matched and mixed from the supplied master-batch of 3wt% (and 0.5wt% in the case of Nanosolve) as described in Tables 6-1 and 6-2.

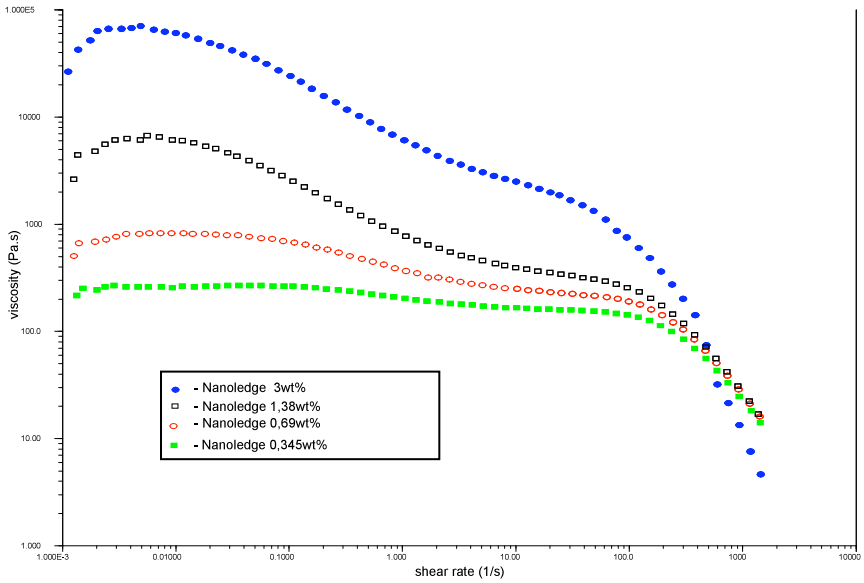

Figure 6-3 Viscosity of the Nanoledge epoxy CNT systems at 10°C.

The rheology of the Nanosolve and Nanoledge resins (Figure 6-3 and Figure 6-4) show shear thinning properties, however, pure epoxy and the Hybtonite resin (Figure 6-2) display Newtonian behaviour, as the viscosity is almost constant as the shear rate increases.

The comparison between the Nansolve and Nanoledge materials shows an almost parallel shear thinning behaviour, though the latter has a much higher viscosity, almost two magnitudes greater. The highest loaded, 3%wt, Nanosolve resin has a maximum viscosity of approximately 500 Pa.s which is lower than both the 1.4wt% CNT loaded Nanoledge resin and the Newtonian Hybtonite resin. This viscosity drops even further due to the shear thinning. In this case the propriety solvents or other additive present in either system used in the dispersion process may be responsible for the significantly lower viscosity. The difference may also be related to the level of nanotube agglomeration, indicating that shear thinning is due to shear-induced deflocculation of the tubes where the bundles of CNT separate and in doing so allow laminar flow of the resin.

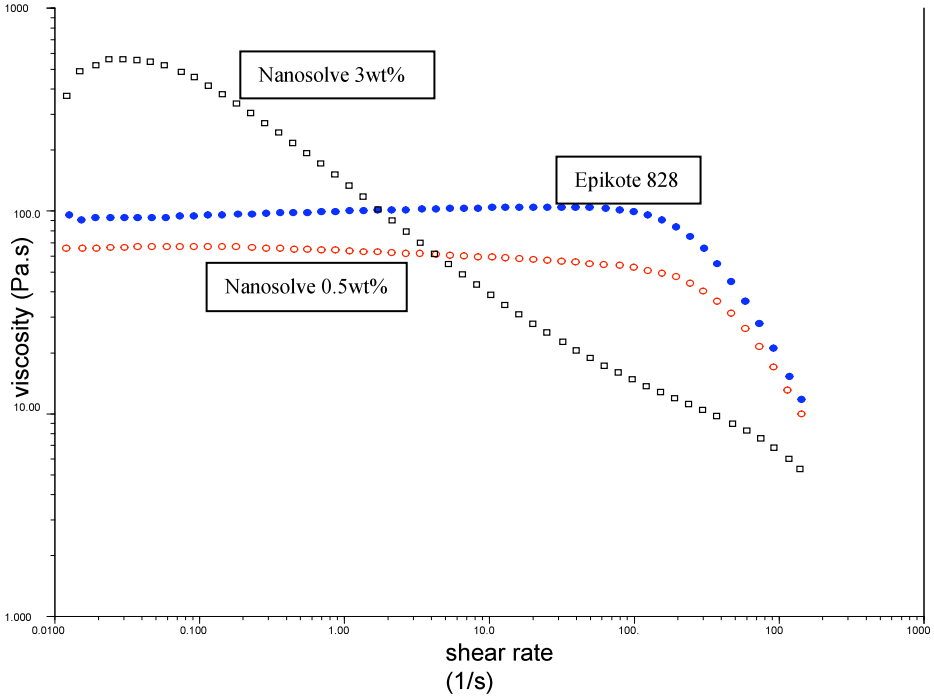

Figure 6-4 Viscosity shear sweep of Epikote 828 and 0.5wt% and 3wt% Nanosolve epoxy CNT system at 10°C.

The thixotropy behaviour of the Nanoledge resin was also assessed at two different CNT loadings. The test was made using a TA instruments rheometer by holding the samples at 25°C for 10 minutes. A low shear rate ($5x10^{-3}s^{-1}$) was applied for 3 minutes followed by a high shear rate ($50s^{-1}$) for 3 minutes. The sheer rate was then reduced to $5x10^{-3}s^{-1}$ and the viscosity was recorded whilst the sample recovered. Table 6-4 shows the recovery times for resin C at 0.75 and 1.4wt% CNT. The results show that the recovery time was longer for the lower percentage CNT resin and after 3 minutes the sample had only recovered by 76%.

Sample	Recovery Onset (mins)	Viscosity Recovered at onset (%)
Nanoledge 1.4 wt%	3.3	76
Nanoledge 3 wt%	2.1	102

Table 6-4 – Nanoledge viscosity recovery results.

6.3.2 Glass transition temperatures

The glass transition temperature, *Tg*, was evaluated using Differential Scanning Calorimetry, (Mettler Toledo DSC821E). The instrument heated the cured sample using a programmed temperature range from 25°C to 250°C at a rate of 10°C/min. A dynamic mechanical thermal analysis (DMA) was also used to measure *Tg* values of the nano-enhanced epoxy. This applied an oscillating force to the cured sample, cut to 50mm x 10mm, over a controlled temperature ramp of 2°C per minute from 25°C to 200°C.

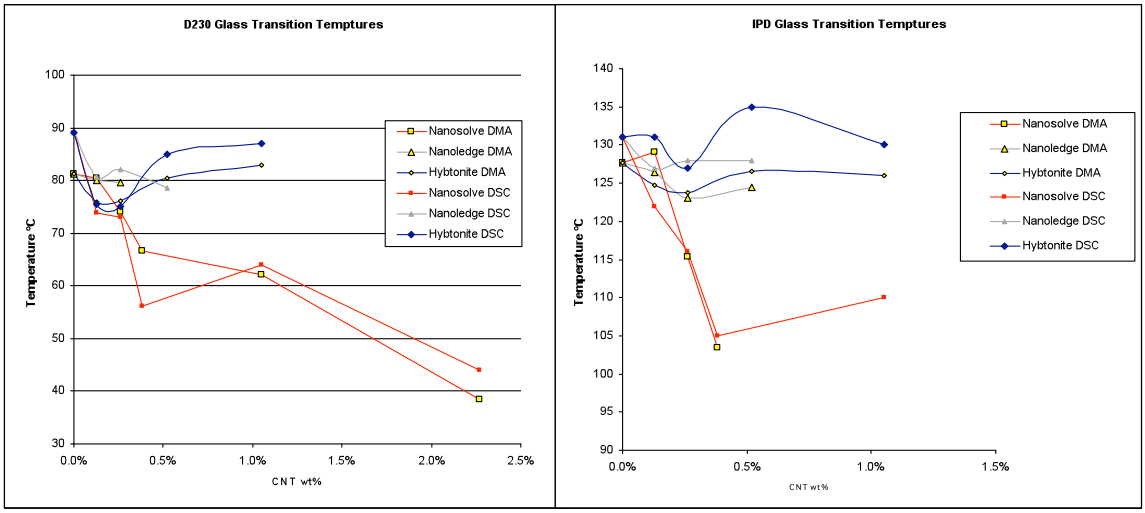

Figure 6-5 *Tg* of the D230 and IPD systems with the different CNT resins measured by DSC and DMA.

The results in Figure 6-5 compare the effect of the CNTs loading on the thermo-mechanical properties of the nanocomposite in a brittle, highly cross-linked, epoxy system and a more flexible system with a greater degree of freedom in the cross-linked polymer. By comparing results from the DSC and the DMA some discrepancy can be seen. The general difference is that often the DSC gives greater values than the DMA. Despite this, however, the two sets of data show very similar trends for the different test methods. Each resin system showed similar trends for the IPD and D230 cured systems. Nanosolve shows a significant reduction in its *Tg* with the addition of CNT. Nanoledge data also indicates a slight drop in *Tg* but in comparison to Nanosolve the change is not as significant. Hybtonite resin shows a drop in resin properties followed a rise, suggesting that the *Tg* does not decline with the addition of CNT.

6.3.3 Tensile test

All tensile tests were carried out on a Zwick mechanical test machine for tensile according to ISO 527 - 2 : 1996 test standard. Tensile dog-bone samples were routed on a CNC machine. The parallel straight edges were sanded and polished to remove defects that could cause stress concentrations. At least five specimens of each sample were tested at a rate of 1mm/min. The results are given in graphical form for examples of the stress-strain taken from the TestXpert software used to drive the Zwick equipment. The software was set to calculate the modulus between 0.05% and 0.25% strain. Tables of the average tensile data and standard deviation values and the percentage value change from the pristine resin are given in the appendix B in Table B-1 and Table B-2. The results are also presented graphically in Figures 6-7 to 6-9.

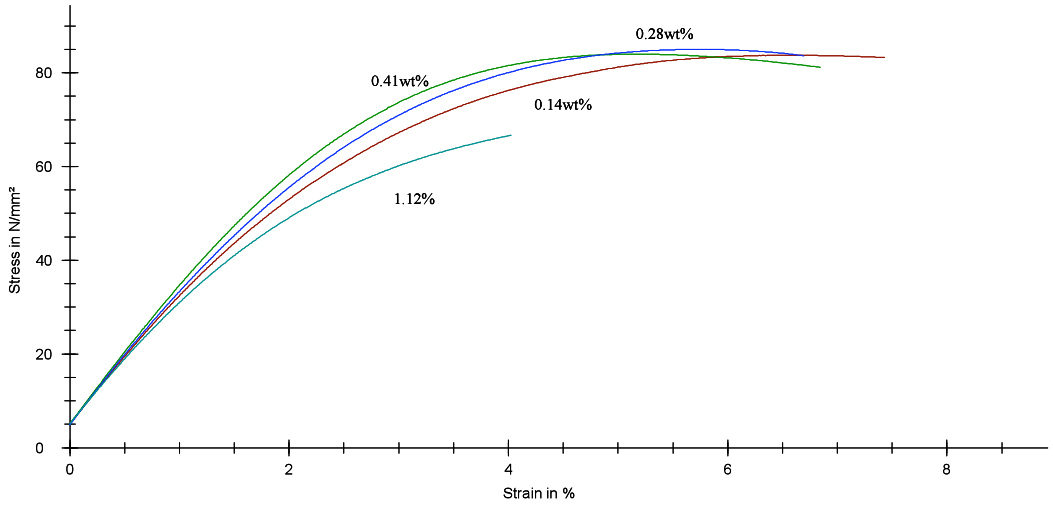

Figure 6-6 Nanosolve IPD cured tensile test curves for differing CNT loading.

Figure 6-6 shows examples of the stress strain curves seen for the different CNT loadings of Nanosolve resin nanocomposite. It shows that the modulus and breaking stress is greatest in the 0.41wt% and 0.28wt% sample with the reduction in properties at higher and lower loadings. The greatest strain-to-break value is observed in the 0.14wt% sample.

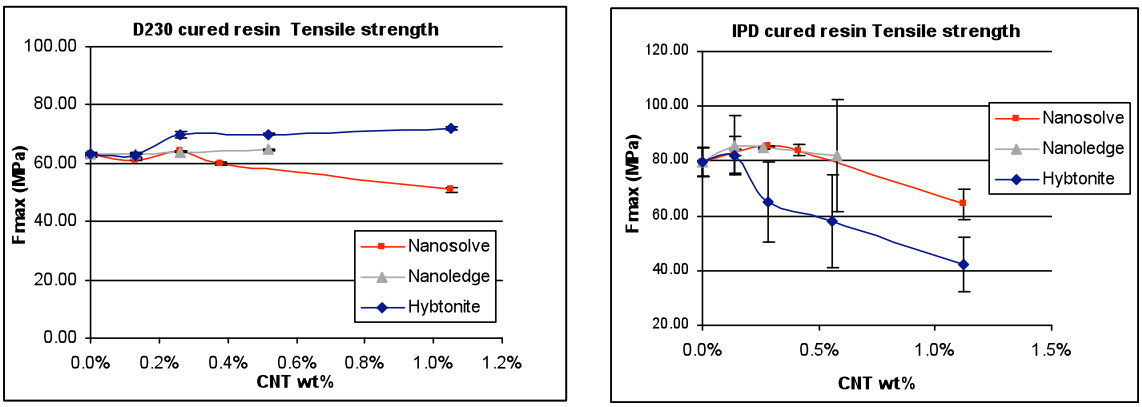

Figure 6-7 Tensile strength, at different loadings of CNT, for the Hybtonite, Nanosolve and Nanoledge resins.

Hybtonite increased the properties of the D230 resin by up to 14.2% at 1.05wt%, however, the Nanosolve and Nanoledge resins show no significant improvement. In the IPD system the reverse effect is observed; Hybtonite reduced the properties significantly and Nanosolve and Nanoledge resins increased the tensile strength by 7.2% at 0.14wt% and 7.6 at 0.26wt% respectively. At higher CNT levels all resins show reduced properties apart from the Hybtonite D230 system.

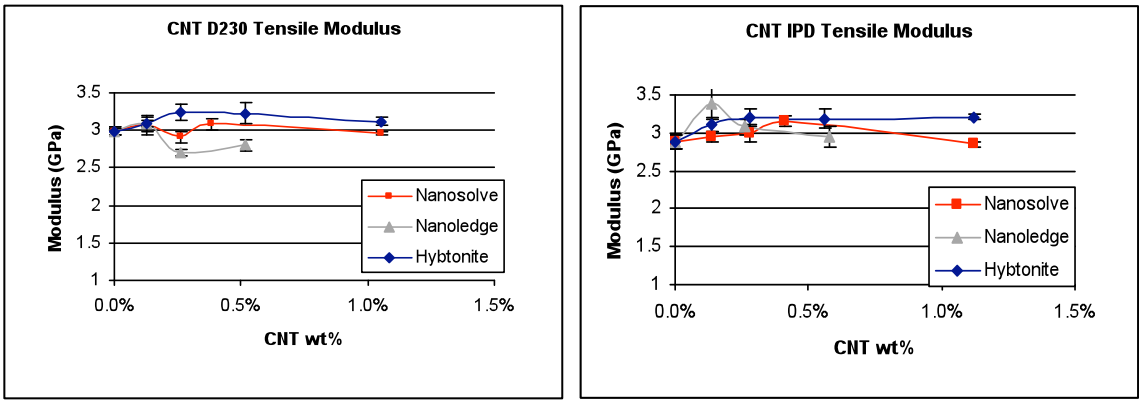

Figure 6-8 Young's modulus at different loadings of CNT, for the Hybtonite, Nanosolve and Nanoledge resins.

The trend for the Young's modulus, shown in Figure 6-8, of Hybtonite resins in both IPD and D230 systems is to increase in value up to a loading of approximately 0.3wt% CNT. Above this loading the modulus remains at an almost constant level or decreasing slightly in the D230 system. Again, Nanosolve and Nanoledge resins show less significant increase in the D230 system but in the IPD system increases of 9.5% and 17.5% are observed before the drop at higher wt% loadings.

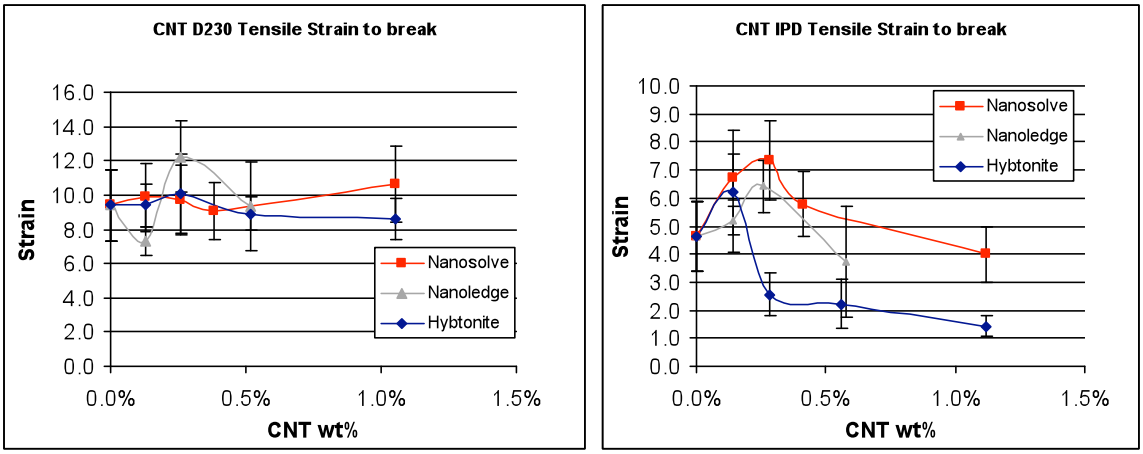

Figure 6-9 Strain-to-break at different loadings of CNT, for the Hybtonite, Nanosolve and Nanoledge resins.

Figure 6-9 shows the average values of strain that the samples experienced at the point at which they failed. The strain was measured by an extensometer up to the yield point but for calculating the strain to failure the position of the test jaws were used which reduces the accuracy and does not take into account any slipping of the specimen in the jaws that may occur. The standard deviation values of the strain-to-failure data are very high, reducing the confidence in these results. From these results it can be seen the less flexible IPD system has a lower strain-to-break value than the D230 system, as expected. This can account for the significant increase in the IPD system, increasing 38% at 0.14wt% for the Hybtonite

system before losing performance at higher loading, a trend which is also seen in the Nanosolve and Nanolodge material.

6.3.4 Flexural test

Flexural properties were measured according to test standard ASTM D 790M-86 and ISO 178. Sample coupons of dimension 100x10mm were tested with a 3-point flexure test with a support separation of 80mm and the actuator test speed of 3mm/min. The load measured with a 5KN Load cell. Average results of the flexural strength and the flexural modulus measurements with the standard deviation are shown in Figures 6-10 and 6-11 and this data, along with percentage changes, is given in Appendix B, Table B-3 and Table B-4.

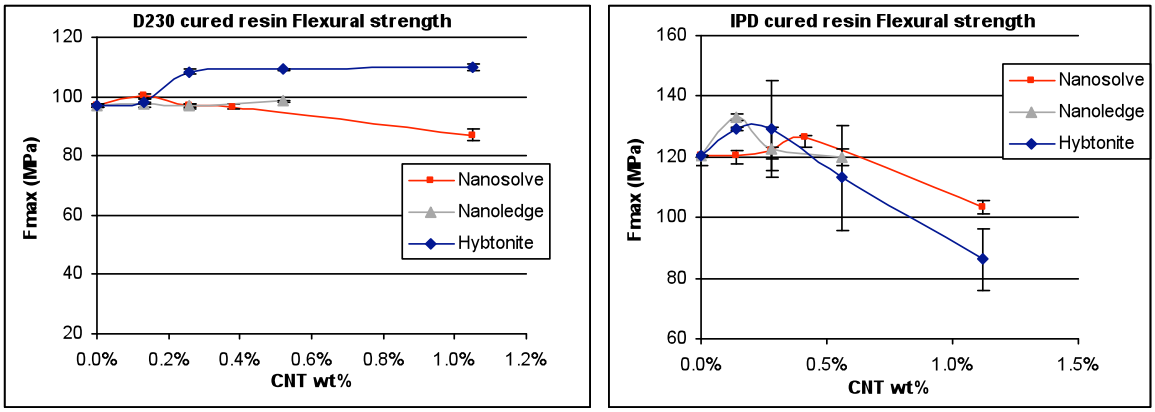

Figure 6-10 Flexural strength of D230 and IPD cured CNT epoxy systems.

Flexural strengths, given in Figure 6-10, show an increase in performance with both D230 and IPD systems for the Hybtonite resin. The Nanoledge resin, however, shows most improvement of 10.6% seen at 0.14wt% loading for the IPD system; above this CNT loading the flexural strength decreases to approximately the same value as the pristine resin. All resins with IPD show a similar trend, with Nanosolve and Hybtonite resins decreasing to 13% and 28% lower than the normal epoxy respectively at CNT loadings over 1wt%. The Hybtonite-D230 system, however, maintains its enhancement at an increased flexural strength of 13% over the pristine Epikote 828. The CNT loading in the Nanoledge and Nanosolve D230 resins show no significant increase.

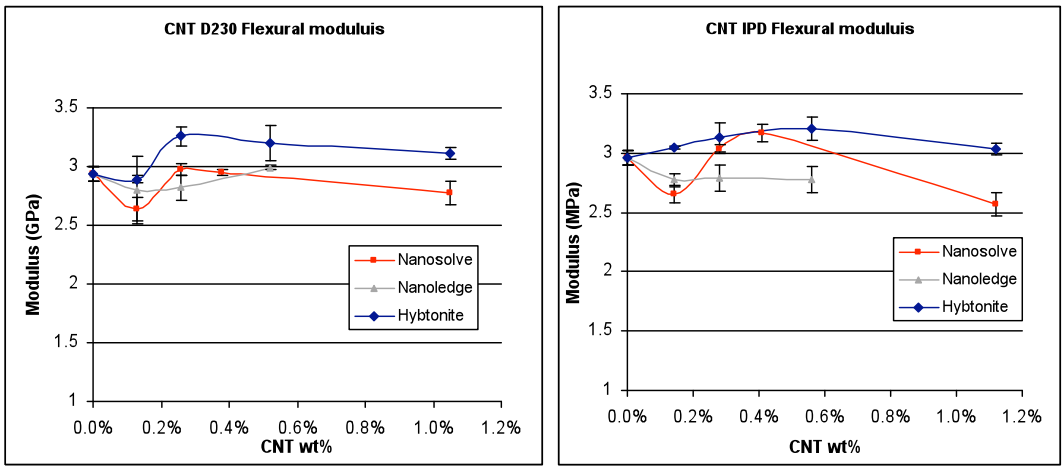

Figure 6-11 Flexural modulus of D230 and IPD cured CNT epoxy systems.

In Figure 6-11 the flexural modulus of the D230 resin system is increased most significantly with the Hybtonite resin, increasing 11% at 0.26wt% CNT loading. Nanosolve and Nanoledge, cured with D230 improve by up to 1.7%. With IPD curing the flexural modulus is improved in the Nanoledge and Hybtonite resins up to 8% at 0.41wt% and 0.56wt% respectively. The Nanoledge resin shows no increase in flexural stiffness with IPD curing.

6.3.5 Compression test

Compression data was measured on a Zwick testing rig with specimen grips modified for ASTM D 695M-89. The compressive strength was measured using 10x10mm sample coupons and compressed at a rate of 2mm/min according to ISO 604. The Compressive modulus was measured using a 80x13mm sample coupon tested at a rate of 1mm/min according to ISO 14126:1999. Both were tested using a 250KN load cell. Average results of both strength and modulus of the D230 and IPD systems are shown graphically in Figures 6-12 and 6-13 for each material type at each CNT wt% with the standard deviation represented by the error bars. This data is also given in Appendix B with the relative percentage change in Table B-5 and Table B-6.

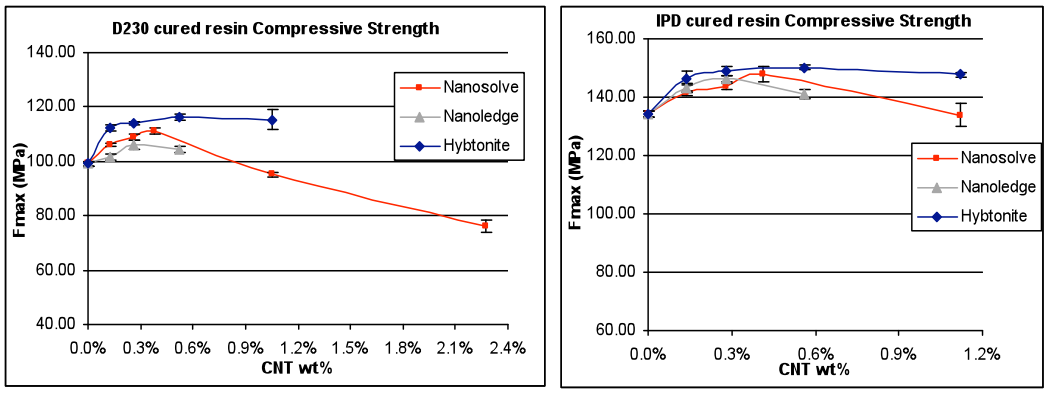

Figure 6-12 Compressive strength of D230 and IPD CNT epoxy systems.

Figure 6-12 shows that the Hybtonite resin exhibits the greatest improvement in compressive strength with a 17.2% increase with D230 curing and 16.1% increase with IPD. Both Nanosolve and Nanoledge resins also demonstrate improvements in compressive strength of 12% and 7% in D230 and 10.2% and 8.5% IPD respectively. All resins appear to have a maximum improvement between 0.3wt% and 0.5wt% CNT content. Above this CNT weight fraction the compressive strength properties decrease. However, the Hybtonite resin appears to have a relatively greater strength at higher CNT levels compared to Nanosolve and Nanoledge.

Figure 6-13 shows the compressive modulus values for each material CNT loading in D230 and IPD cured systems. The highest compressive modulus is seen in the Hybtonite resin at 0.14 wt% loading, increasing by for both D230 and IPD systems. Nanosolve also shows some increase in compressive modulus at 0.41wt%. The Nanoledge shows no significant increase or decrease.

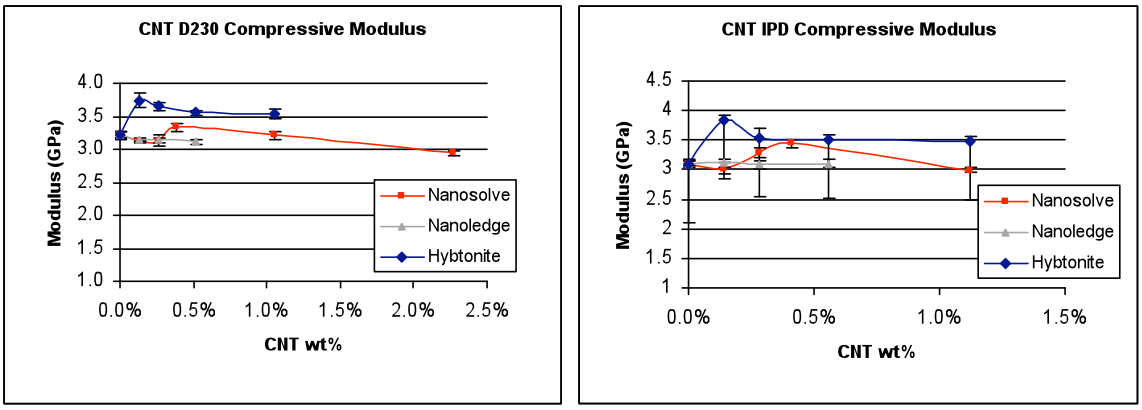

Figure 6-13 Compressive modulus of D230 and IPD CNT epoxy systems.

6.4 *Discussion and analysis*

The rheology work showed a difference in thixotropic behaviour between the bonding mechanisms used for the MWNT-epoxies. The CNT in Nanosolve and Nanoledge resins is not bonded to the epoxy but is bonded by Van der Waals adhesion to the dispersal functional surfactants or copolymers. These are described as non-covalently bonded CNT. The difference in rheological properties may be described in terms of the bonding energy. The Van der Waals adhesion requires less shear energy to break apart than the equivalent amount of covalent bonding and thus gives a similar physical interaction to that of traditional filler once this has occurred. The resin then displays shear thinning properties initially through freedom of movement, being separated from the copolymer chains and then also due to induced lamellar flow in the filled epoxy.

Another explanation is the analogy with fumed silica and coated fumed silica. Standard fumed silica is hydrophilic and bonds to the silica by hydrogen bonding of the O-H groups

on the silica surface to the epoxy backbone. Coated silica is treated with polydimethyl siloxane and it does not function via hydrogen bonding, as the untreated grades, but via Van der Waals bonding with the epoxy. The result is a greater thixotropic performance in the coated silica. In these circumstances the thickening effect is caused by the extension of the silicone chains from the surface of the silica by the dimethyl coating. This allows the particles to interact and build structure due to mechanical entanglement of and physical attraction between the silicone polymer chains. These interactions are easily broken by shear forces and give rise to shear thinning and thixotropic behaviour, to greater effect than the untreated grades (Cabot). The same process can be applied to the treatment of the Van der Waals bonded CNT. The proprietary dispersant would require a surfactant to act as a branch between the CNT and epoxy. This may create a gel structure network, which is not present in the covalently bonded CNT. The mechanical tangling of the CNT copolymer chains creates the structural network. These would also break down with the onset of shear forces as represented by the shear thinning observed.

Shear thinning behaviour related to CNT filler has also been observed in polyester in (Seyhan et al., 2007), and in epoxy (Song and Youn, 2005,Rahatekar et al., 2006). There is thought to be some disentanglement between the CNT and the shear thinning is due to shear-induced deflocculation of the tubes. This leads to the reduction in viscosity and the return to the Newtonian behaviour at higher rates. The neat polyester, like the epoxy displays Newtonian behaviour. With addition of CNT the viscosity of the polyester becomes greater as does the gradient of shear thinning. The Nanoledge viscosity-shear curve in Figure 6-3 is an example of a decrease in the gradient of the viscosity- shear rate curve; however, it does not reach a Newtonian constant plateau before shear heating takes over at a shear rate between 10^2-$10^3 s^{-1}$. The rheology data for the covalently bonded CNT, Hybtonite resin, is not consistant with this argument. The viscosity is increased with addition of CNT but no shear thinning is observed.

The *Tg* results appears to show that the covalently bonded Hybtonite resin can maintain the same performance with the addition of nanotubes while the non-covalently bonded resins show a reduction in *Tg* as CNT content increases. This can be explained by the bonding mechanism, which in the covalent bonded system, would allow the CNTs to be bonded with the cross-linking matrix. Nanoledge resin tends to decrease less than the Nanosolve resin that may be due to proprietary dispersants and the surfactants used in the formulation of the CNT resin. This is reinforced by the fact that a much lower viscosity is measured in the Nanosolve resin. Some non-covalent mechanisms have shown surfactant-induced plasticisation in epoxies with the *Tg* falling below the value for the neat epoxy (Vaisman et

al., 2006). It also seems that increasing the interface area with good anchoring can increase the *Tg* in competition with the plasticizer effect (Cui et al., 2003).

From the mechanical test results it can be seen that covalently bonded MWNTs in the Hybtonite resin showed most improvement in tensile, compressive and flexural strength and modulus in the D230 system. IPD cured epoxy showed differing results as the tensile and flexural tests showed that Nanoledge had the largest increase. Nanoledge also had the largest Young's modulus, increasing by 23%, yet it did not improve on the flexural or compression modulus. In compression, Hybtonite resin improves strength by 16% in IPD and 17% in D230 cured systems. In tensile and flexural strength the Hybtonite resin resulted in greater enhancement in the D230 system by 14% and 13% respectively compared to a 3% and 8% enhancement in the IPD system. This would suggest that the CNTs interact differently with the microstructure and chemistry of these different systems.

Comparing all the resin systems the change in strength was smaller with IPD curing than the D230 curing. Ci and Bai (2006) compared the effectiveness of CNTs relative to the epoxy modulus by adjusting the epoxy hardener levels and the cure time. They found that a flexible and ductile composite showed a better interface interaction with the CNTs and suggested that the poor interaction in a stiff composite was due to complete cross-linking of the molecules surrounding the CNT and volumetric shrinkage during the curing process. Other improvements in modulus and strength have been shown in a flexible or rubbery epoxy (Liu and Wagner, 2005). Overall, the greatest enhancement usually occurs at a lower wt % nanotube loading in the IPD matrix compared with D230, with a large reduction of strength properties at higher loading. The IPD system also shows a greater standard deviation represented by the error bars in the graphs. These points indicate that there may be some curing induced effect on the IPD resin system by the CNT, specifically with the covalently bonded Hybtonite resin. A separate study into the off-ratio curing properties was undertaken and described in Appendix C. Results from the pristine Epikote 828 and Hybtonite G4.E tested at -2 to +4 parts of the IPD stoichiometric ratio are given respectively in Table C-1 and Table C-2. A difference in the property values was seen in each resin and while the Epikote 828 showed greater cross-linking, indicated by higher *Tg* at the stoichiometric ratio the Hybtonite showed higher *Tg* and increased mechanical properties at +2 parts ratio.

The effect of diluting the pre-dispersed master-batches may also be a causing a change in material properties. It has been observed that where the "as supplied" master-batch has been diluted the material properties seem to have decreased in value. At the lowest nanotube loading for the Hybtonite resin, a lower tensile strength value is observed

compared to increased CNT content. This could be caused by mixing the CNT master-batch with pure Epikote 828 to achieve this level of CNT in the overall resin.

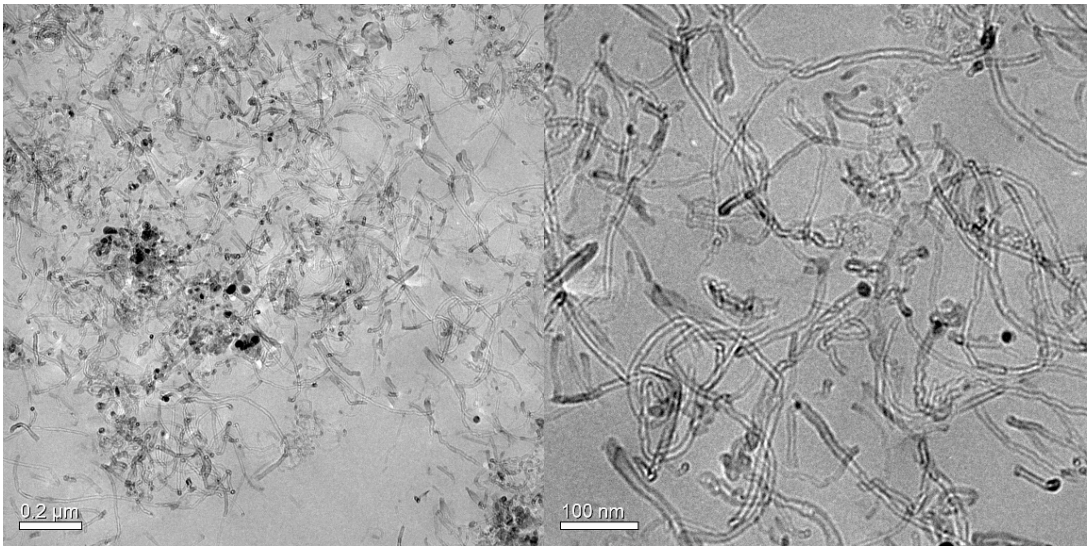

Figure 6-14 Hybtonite 0.13wt% TEM micrographs at two different magnifications.

The TEM micrograph images in Figure 6-14 and Figure 6-15 show the individual nanotubes dispersed within the matrix at two different magnifications in the Hybtonite and Nanosolve system respectively. They indicate that there is some agglomeration observed in the Nanosolve 2.3wt% sample, which is less obvious in the 0.13wt% Hybtonite sample where the nanotubes appear to be more homogeneously dispersed. Even though the amount of CNT loading is much greater in the 2.3wt% sample, the dilution process is not designed to disperse any agglomerations that occur, relying on the manufacturer's modification and patented dispersion of the CNT to separate the agglomerates. The dilution process may have not increased the dispersion of the nanotubes enough and thus resulted in MWNT-rich zones and pristine resin zones.

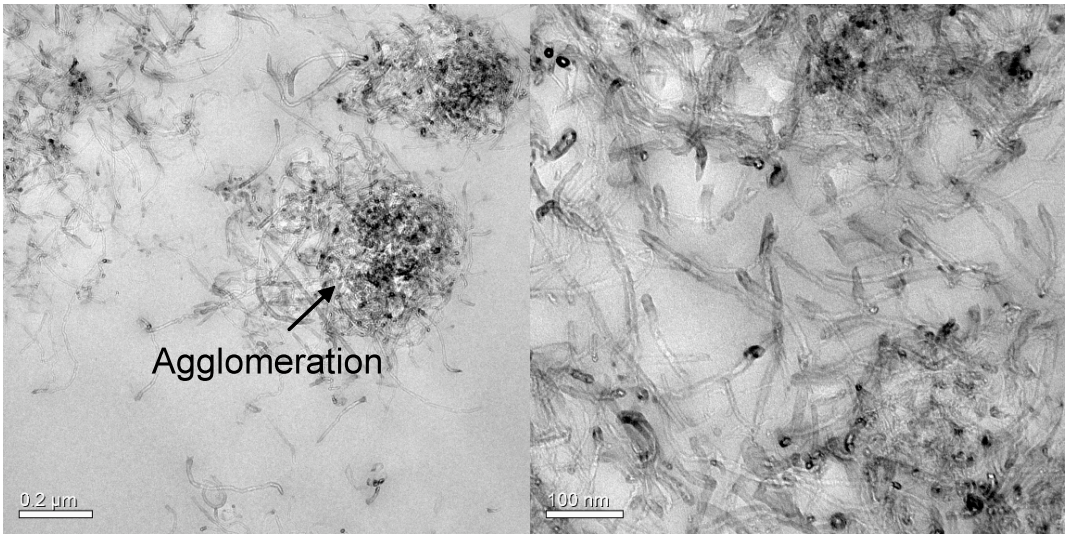

Figure 6-15 Nanosolve, 2.3wt% CNT TEM micrographs at two different magnifications.

The Nanosolve resin, shown in Figure 6-15, was supplied in two master-batch levels; 3wt% and 0.5wt%. Only the 0.4wt% cured samples were made from the 0.5wt% master-batch, the rest being made from a mixed ratio of the 3wt% master-batch and Epikote 828. The Nanoledge resin samples were all from a diluted mixture from a 3wt% master-batch and the lowest loading (greatest dilution of master-batch) in tensile and flexural shows a significant reduction in property values.

Figure 6-16 shows the microscopic images for the 0.13wt% CNT, D230 cured resin B. The highly viscous nature of Nanoledge master-batch resin made it hard to produce good air-free casts. For this reason only low CNT loaded samples were made. The colour of the resin reduced the ability to observe and measure the amount of air in the resin.

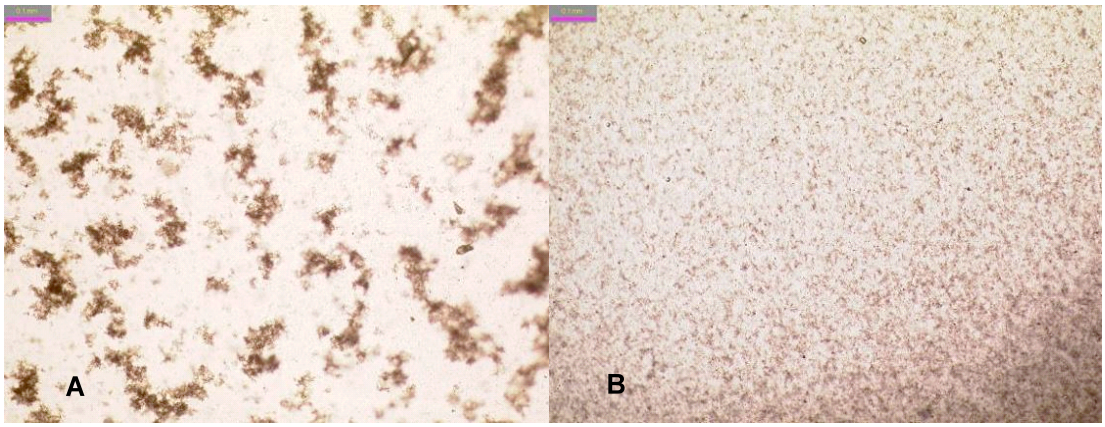

Figure 6-16 Micrograph of cured 0.13wt% CNT resin residue for A) mixing pot and B) post cured casting plate, at the same magnification

The micrographs in Figure 6-16A and 6-16B are taken from the cured thin excess residue left in the mixing pot and on the glass plate when the sample was cast. They clearly show two different amounts of agglomeration, which are visible with the naked eye. This effect was not observed at any other loading of Nanoledge. The reason may be due to the amount of dilution that occurs in the sample. The energy required to separate and disperse the 3wt% master-batch down to a homogenous 0.175wt% CNT resin may be more than required in higher concentrations. The difference in the two agglomerations also suggests that there is a different amount of CNT re-agglomerated depending on the cure. Alternatively, this may have been affected by the different surface properties of the glass plate and the plastic mixing cup.

6.5 *Fracture toughness of carbon nanotube composites*

The previous section concentrated on the effect of the carbon nanotubes on the bulk properties of an epoxy nanocomposite. In this chapter the fracture toughening properties are explored. Chapter 2 explained the many ways that CNTs can improve the fracture toughening properties including crack bridging / pinning crack deflection. Here the fracture

toughness behaviour is explored in the same two-epoxy systems previously tested, which incorporated a Jefamine D230 and a IPD hardener. The different CNT bonding interfaces are compared for their effectiveness in improving both the quasi-static crack resistance and also the dynamic impact toughness. The tests measure the fracture toughness of the resin samples in a three point bend configuration with a crack pre-cut into the sample.

6.6 K_{1C} fracture toughness

Fracture toughness, K_{1C}, was calculated using a single-edge-notch bend (SENB) test, (ASTM D 5045 -99 and BS ISO 13586:2000 Plastics – Determination of fracture toughness). The samples are tested in a three point bend configuration that is described in Figure 6-17 with a 5KN load cell. The dimensions requirements for the fracture toughness sample are described below the schematic in the key. This gives the overall length, thickness and crack length relative to the sample width.

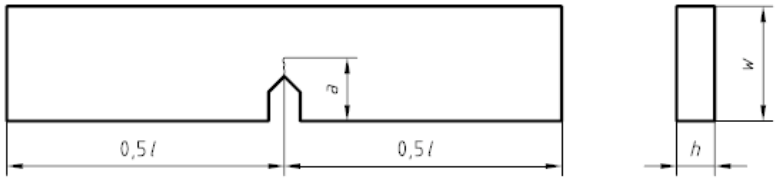

Key

w	Width	
l	Overall length	$l > 4{,}2w$
h	Thickness	$w/4 < h < w/2$
a	Crack length	$0{,}45w \leqslant a \leqslant 0{,}55w$

Figure 6-17 Diagram of the SENB fracture coupon and the relative size criteria.

The basis of the test standard for fracture toughness testing in plastics has been taken from the earlier work on fracture toughness in metals where it is thought that plain strain fracture toughness occurs in thick section and thin sections behave with plane stress conditions. It is known that fracture toughness in plastics is dependant on the specimen size. The size requirement for metallic K_{1c} test coupons had been incorporated into the ASTM K_{1c} standard for plastics regarding the relative size of the plastic zone, claiming that the plastic zone should be small compared to in-plane dimensions to ensure the presence of an elastic singularity zone ahead of the crack tip. It also assumes the plastic zone should be small compared to the thickness to ensure predominantly plain strain conditions. This results as a thickness dependence of fracture toughness in metals due to the mixture of flat fracture and shear fracture morphologies. However, it has also been claimed that plane strain conditions can exist near the crack tip even in the fully plastic regime; the plastic zone need not be small relative to thickness to ensure high triaxility near the crack tip increases (Anderson, 2004).

6.6.1 Methodology

Materials and quantities used for the nanocomposite resin batches are described in section 6.2. From the cured resin samples a coupon was cut to the required dimension on a wet circular saw. A notch was then sawn along the centre line of the coupon to so that it met the $0.55<h<0.45$ criteria. A sharp dissection blade was placed in the notch and tapped with a hammer to create a sharp notch. Special care was taken at this point to make the notch as deep as possible without causing the crack to propagate the width of the sample. The standard specifies that the crack length should not differ by more than 10% over the crack front. This was measured after the test using images from a microscope or a magnifying glass. Three measurements across the crack face are made and the average is taken. The samples are tested under a three point bend with a span of 50mm. The yield stress is measured on a 5KN load transducer. For each material batch five coupons were tested. For these specimens the epoxy displayed brittle elastic behaviour. They showed a linear load–displacement behaviour till a total failure at maximum load. The tests and corresponding data reduction were done according to the ASTM standard D 5045–99 and in all cases $F_{max} = F_Q$.

The critical strain energy release K_{1c} was calculated from Equation 6-1

$$K_{IC} = f\left(a/w\right)\frac{F_Q}{h\sqrt{w}} \qquad \textbf{Equation 6-1}$$

where F_Q is the breaking load and the dimensions are indicated in the key of Figure 6-17 are measured in cm.

To calculate the function of (a/w) for a SENB Equation 6-2 is used when α satisfies $0< \alpha <1$

$$\alpha = \left(a/w\right)$$

Where:

$$f(\alpha) = 6\alpha^{1/2}\frac{1.99 - \alpha(1-\alpha)(2.15 - 3.93\alpha + 2.7\alpha^2)}{(1+2\alpha)(1-\alpha)^{3/2}} \qquad \textbf{Equation 6-2}$$

6.6.2 Dimension analysis

Due to the fact that the method of sample manufacture used has limited variability in thickness (h) a fracture coupon size test was carried out. It was designed to check the fracture toughness dimensional analysis for preparation of fracture toughness of nanocomposite samples and confirm the point at which width (w) does not affect the K_{1c} value. Samples were made from 5mm thick (h) notched 3 point bend resin fracture toughness samples with width (w) and length (l) dimension at:

Sample size: (w x l cm) 3.0 x 12.0cm, 2.5 x 10.0cm, 2.0 x 8.0cm, 1.5 x 6.0cm, 1.0 x 4.0cm, 0.5 x 2.0cm.

Samples were made from Dow DER330 epoxy resin and cured with Jeffamine D230 at the stoichiometric ratio of 100:33. Details of the sample manufacture are described in section 6.5.3. Five samples were made of each size. The manufacturing process proved difficult with many of the samples fracturing before the testing was complete.

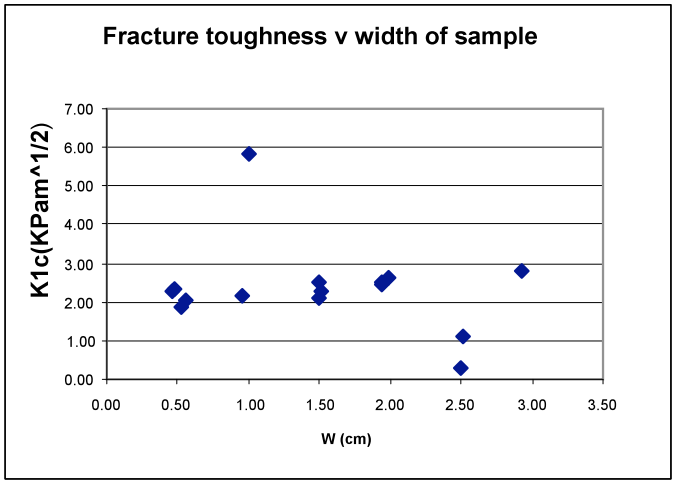

Figure 6-18 K1c fracture toughness of different width test coupons.

Figure 6-18 is a scatter graph of the critical stress intensity factor of different sized samples. Each individual result shows the extent of the scatter and how the fracture toughness varies with sample width. Apart from a few outlying results there is a consistent trend. Comparison with the work in Anderson(2004), which shows a steep rise in K_{1c} before becoming constant, it can be argued that this data represents the horizontal plateau being constant fracture toughness. The purpose of this graph is to indicate a suitable size of sample for the nanocomposite comparative testing and with consideration for the manufacturing a sample size of 1.25 x 6.0cm was chosen. This is slightly larger than the 2*h* constraint in the standard however it allows easier manufacturing of the notch.

6.6.3 Carbon nanotubes composite fracture toughness results

Fracture toughness of the D230 cured CNT resins is given in Figure 6-19 in a graphical form of K_{1c} critical strain energy release rate against the percentage weight of nanotube in the cured system. Each point depicts the average value and standard deviation values as error bars. The value of each point and the standard deviation is also given in Table 6-5 along with the percentage change. The data for IPD cured systems fracture toughness is given in the same format in Figure 6-20 and Table 6-6.

D230	Average K_{1c} (MPam^1/2)	% change	Standard Deviation
Nanosolve			
0	2.75		0.23
0.13	2.58	-6%	0.07
0.26	2.23	-19%	0.30
0.38	2.27	-21%	0.46
1.05	2.40	-14%	0.12
2.14	2.06	-34%	0.06
Nanoledge			
0	2.75		0.23
0.13	2.70	-2%	0.14
0.26	2.66	-3%	0.19
0.52	2.82	2%	0.14
Hybtonite			
0	2.75	0%	0.23
0.13	1.82	-34%	0.25
0.26	2.85	4%	0.43
0.52	3.05	11%	0.30
1.05	2.70	-2%	0.28

Table 6-5 K_{1c} for D230 cured epoxy systems.

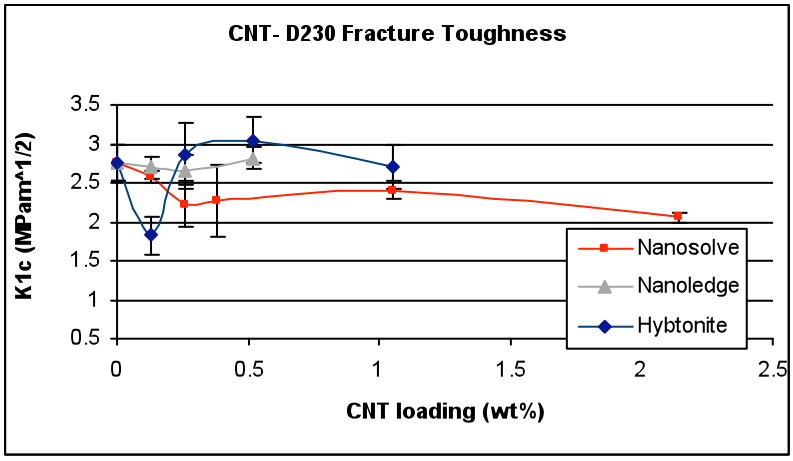

Figure 6-19 K_{1c} Fracture toughness of D230 cured resin systems epoxy systems.

The results for the pristine resin fracture toughness for the Jeffamine D230 cured system, shown in Figure 6-19 and Table 6-5, give a relatively high K_{1c} value for an epoxy resin system. The D230 system has a value 2.75 $MPam^{1/2}$ that is over twice the fracture toughness of the pristine IPD value. To put this into context bisphenol F epoxy resin with a K1c fracture toughness of 1.11MPam1/2 has been described as a high cross-linking epoxy that exhibits brittle failure (Zunjarrao and Singh, 2006) .

IPD	K_{1c} ($MPam^{1/2}$)	% change	Standard deviation
Nanosolve			
0	1.07	0%	0.43
0.13	1.10	3%	0.50
0.26	0.70	-35%	0.17
0.38	1.50	39%	0.45
1.05	1.28	19%	0.41
Nanoledge			
0	1.07		0.36
0.13	1.57	46%	0.15
0.26	1.38	28%	0.65
0.52	1.08	0%	0.65
Hybtonite			
0	1.07	0%	0.43
0.13	1.98	84%	0.50
0.26	2.08	94%	0.45
0.52	2.33	117%	0.45
1.05	2.01	87%	0.57

Table 6-6 K_{1c} rate for IPD cured epoxy systems.

Table 6-6 shows that fracture toughness is improved by up to 117% in the 0.52wt% Hybtonite IPD. Nanosolve and Nanoledge systems improve by 39% and 46% at 0.38wt% and 0.13wt% respectively.

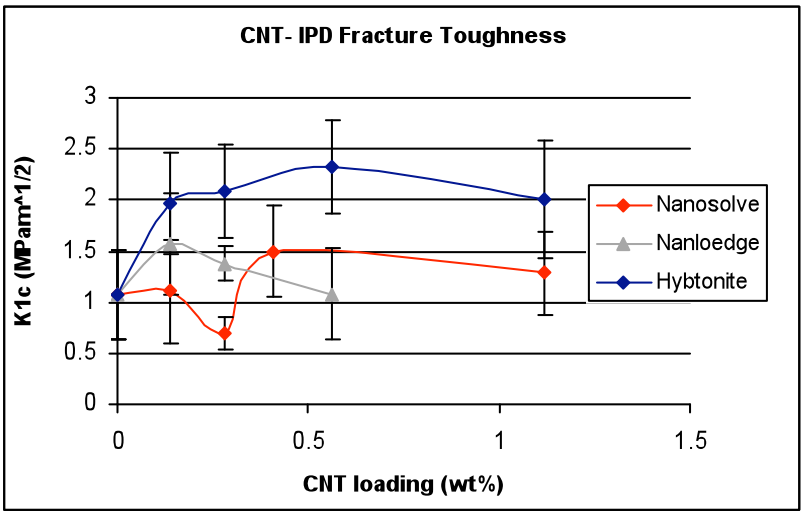

Figure 6-20 K_{1c} Fracture toughness of IPD cured resin systems epoxy systems

The graph in Figure 6-20 shows that the IPD epoxy system exhibits inherently low fracture toughness, relative to the D230 system, with a pristine resin fracture toughness of $1.1MPa^{1/2}$. In contrast to the D230 results all three CNT systems show an increase in fracture toughness to some degree, Hybtonite showing the greatest increase. The Nanosolve sample also has a result that shows a decrease in fracture toughness at 0.26wt%. This appears to be dissimilar to the trend shown by the Hybtonite and Nanoledge systems yet the standard deviation is the lowest in the series. Both Hybtonite and Nanoledge materials show a maximum performance at around 0.5wt% CNT and the average K_{1C} value is not degraded significantly

at higher CNT content as seen with some property trends. This is not the case with Nanosolve , showing a greatest performance at 0.13wt% and the average value decreasing with greater CNT content .

As shown previously in Figure 6-5 the *Tg* value of the IPD is greater than that of the D230 having a greater cross-link density. This result confirms that it behaves in a more brittle material manner. The addition of CNT had decreased the *Tg* in some cases therefore the toughness would be expected to increase. The results for D230 cured resin fracture toughness do not agree entirely with the *Tg* results. They show that the Nanosolve resin reduces performance with increasing CNT content. The Nanoledge resin corresponds more accurately with the *Tg* data, showing very little change. The Hybtonite resin initially drops to a 34% decrease then increases to an 11% improvement at 0.52wt% CNT loading. This increase, however, is at the same level as the standard deviation. The initial drop in fracture toughness may have been caused by a curing fault batch or entrapped air; however, a corresponding increase in the standard deviation would also be expected. The following three data points for the Hybtonite CNT resin cured with D230 repeat the trend seen before with the bulk properties, which demonstrates that an increase in property value is followed by a reduction at higher CNT content.

6.6.4 Charpy impact toughness

Charpy impact toughness was measured using the method described in ISO 179/ eA. Ten coupons were cut from each batch sample (prepared as in section 6.2) of dimensions 80x10mm. A bespoke Charpy notch saw in the shape of a chamfered V was used to make a notch half way along the sample. A Zwick pendulum impact test machine with a 7.5J strike hammer was used. Before the testing took place the pendulum was swung without a test coupon to measure the friction in the system. The coupon was then placed into the test apparatus with the notch facing away from the strike hammer. The pendulum was released from its trigger and the energy used in breaking the sample was displayed digitally. The friction energy was then subtracted and from this the Charpy impact toughness for the notched specimen was then calculated using equation 6-3.

$$a_{cN} = \frac{W_B}{hb_N} \times 10^3$$ **Equation 6-3**

WB= the energy at break (J)

h = is the thickness of the specimen (mm)

bN = the width remaining at the base of the the notch specimen(mm)

N denotes the type of notch

6.6.5 Carbon nanotube Charpy impact toughness results

The results in Table 6-7 and Figure 6-21 and Figure 6-22 show the average charpy impact toughness energy for the D230 and IPD cured CNT systems. The error bars indicate the standard deviation of the average results and the values give in Table 6-7.

D230	Charpy Fracture Toughness			IPD	Charpy Fracture Toughness		
CNT wt%	Average kJ / m²	% change	Standard deviation	CNT wt%	Average kJ / m²	% change	Standard deviation
Nanoledge							
0%	10.50		1.441	**0%**	3.10		0.395
0.13%	8.25	-21.5%	2.221	**0.14%**	4.15	33.7%	1.054
0.26%	8.22	-21.8%	2.781	**0.28%**	5.11	64.9%	0.914
0.52%	10.06	-4.2%	0.960	**0.56%**	4.30	38.6%	0.889
				1.14%	3.17	2.3%	1.039
Hybtonite							
0%	10.50		1.444	**0%**	3.10		0.395
0.13%	7.70	-26.7%	1.759	**0.14%**	2.46	-20.8%	0.639
0.26%	9.09	-13.5%	0.373	**0.28%**	2.92	-6.0%	1.444
0.52%	6.38	-39.3%	1.483	**0.56%**	2.26	-27.2%	0.346
1.05%	5.78	-74.1%	0.611	**1.12%**	2.76	-15.2%	0.933

Table 6-7 Charpy impact results for D230 and IPD CNT systems.

Table 6-7 gives the data and the percentage change of CNT loaded specimens relative to the pristine resin value. It shows that at the D230 system has not exhibited an improvement with addition of CNT. At the 1.05wt% CNT the Hybtonite system has significantly reduced by 74%. The IPD system shows the greatest reduction is 27% with Hybtonite. The Nanoledge shows a distinct difference in behaviour with all loadings material showing evidence of an improvement in the Charpy impact toughness.

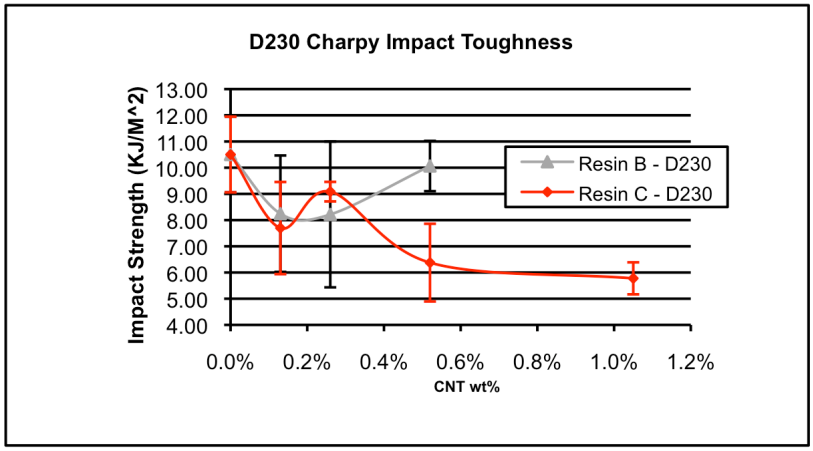

Figure 6-21 Charpy impact toughness of CNT D230 resin systems.

The results in Figure 6-21 of the D230 impact toughness show no improvement with addition of nanotubes as shown by the resin. The trend shows decreasing toughness with

the addition of carbon nanotubes. The 0.52wt% Nanoledge sample, however, goes against this trend. This sample also has a relatively lower standard deviation (9%), however, it is unclear with the large standard deviation observed (26%) whether there is a true return in the toughness behaviour at higher CNT loadings.

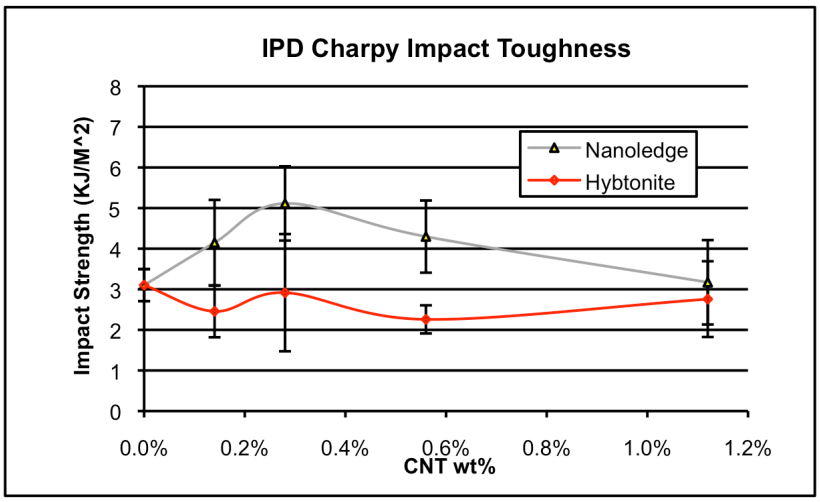

Figure 6-22 Charpy Impact Toughness of IPD CNT resin systems.

The IPD CNT impact toughness results are given in Figure 6-22. These results show that, unlike the D230 system, the impact toughness shows an increase of up to 65% at 0.28wt% loading of the Nanoledge material. Even with the large standard deviation found in the results the Nanoledge material displays significantly improved results over the Hybtonite material.

6.6.6 Discussion and analysis of the Fracture toughness

The results from both the fracture toughness and the Charpy impact toughness both show that CNTs appear to give greater enhancement to the brittle IPD cured epoxy CNT. In the quasi-static fracture conditions this enhancement is greatest in the covalently bonded, Hybtonite, resin. However, at higher impact speeds in the Charpy tests the covalently bonded CNT show no improvement in toughness.

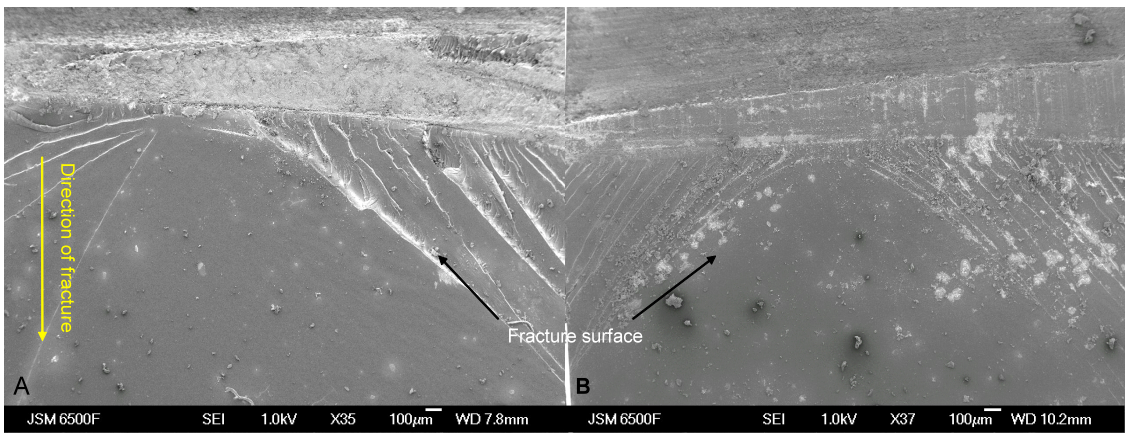

Figure 6-23 SEM of the SENB fracture surface of Hybtonite A) 0.26wt% and B) 1.05wt% D230 cured epoxy system.

Figure 6-23 shows the site of fracture surface morphology in the Hybtonite D230 sample. It is a good example of ridge formation on the fracture surface. Both images show similar striation formation at approximately 45° angle from a point near the centre of the span, along the notch face, where the fracture is understood to have initiated. The increase in CNT content, Figure 6-23B, gives a greater frequency striation ridges, indicating a higher resistance to fracture, and also give less relief than in Figure 6-23A, indicating a lower intensity of the ridge (Ganguli et al., 2006).

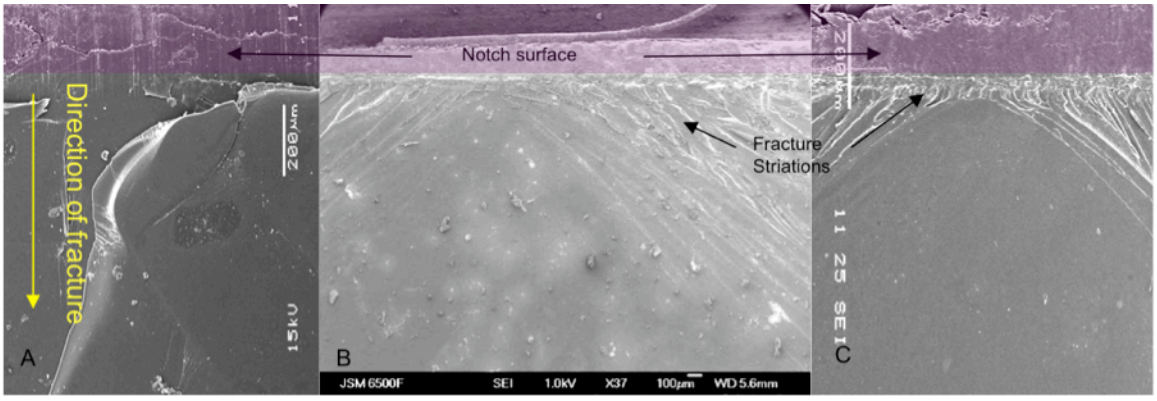

Figure 6-24 SEM of fracture surface A) pristine Epikote 828 IPD cured epoxy B) Hybtonite 0.14wt% IPD cured epoxy system and C) Hybtonite 1.12wt% IPD cured epoxy system.

Figure 6-24 represents the difference between the fracture surfaces of pristine epoxy and CNT enhanced epoxy cured with IPD. Figure 6-24A shows the pristine epoxy specimen the clean, fracture surface characteristic of a brittle material (Zhou et al., 2008b). When CNTs are added the topography of the fracture surface begins to change. Fracture striation ridges are formed, in a similar fashion to the D230 resin fracture surface, which indicates a resistance to fracture as shown with Figures 6-24B and 6-24C. Ganguli et al., (2005) claim that an increased number of features on the surface corresponds to greater area for the absorption of the fracture energy.

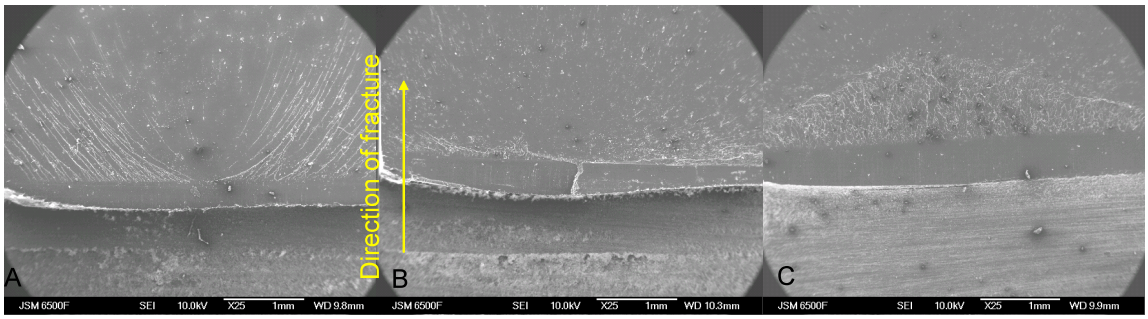

Figure 6-25 SEM micrograph of the Nanosolve D230 cured nanocomposite with the crack head at the bottom and the direction of fracture going up the page. A) 0.26wt%, B) 0.52wt% and 1.05wt%.

In Figure 6-25 different behaviour is observed on the topography of the Nanosolve epoxy system. The striations are visible in the lowest loading of CNT (Figure 6-25A) but are not present in the 0.52wt% (Figure 6-25B). In Figure 6-25C the 1.05wt% CNT loaded sample shows a triangular formation of a mottled rough surface with no clear ridge formation. This effect does not correspond to an increase in fracture toughness in the results and may have been caused by crazing in the epoxy due to low interfacial bonding or an excess of entrapped air. At this resolution of the fracture surface there is no evidence of the CNT and how they are dispersed. Even at higher resolution the CNT were not visible limiting any dispersion analysis made via SEM.

In almost all images, at the point immediately after the notch tip, the material is torn up and there can be many fibrils bridging the crack opening surfaces. These bridging fibrils divert the stresses away from the crack tip as does the micro-cracking around the crack tip. All these fracture processes vary in degree and relate to the inherent fracture toughness properties of the material (Dear, 1999).

Lowering the material *Tg* inherently gives the matrix natural fracture toughness due to effectively increasing the plastic yield region, r_y, around a crack tip. This is related to the cross-link density of an epoxy, which is important in crack propagation and described Irwins relationship of yield stress to the size of the process zone under plain strain conditions as described in equation 6-4.

$$r_y = \frac{1}{2\pi}\left(\frac{K_{1C}}{\sigma_y}\right)^2$$

Equation 6-4

Materials with a high yield stress, σ_y, such as many structural epoxies, rarely produce a large r_y as well as absorbing the energy in the crack. The size of the plastic zone of brittle epoxy resins is relatively small. This is the reason that most epoxy formulations require a toughening agent or filler. For a resin is filled with nano-particles, a significant number of particles occur in the plastic zone, compared with micro fillers used for fracture enhancement. Nanotubes, which possess extremely high aspect ratios, influence the growth of the process zone in front of the crack tip. This is also important due to the stress/strain interaction between nanoparticles and matrix (Fiedler et al., 2006). This has been seen shown before with increased toughness is observed by dispersed DWCNT-NH_2, which are expected to decrease the stress concentration in the process zone ahead of the crack tip by the induction of secondary cracks and crack-bridging (Gojny et al., 2005).

The properties of the two epoxies are very similar in modulus but the D230 cured epoxy has a much lower *Tg*. This would give it greater inherent fracture toughness as shown

experimentally with both the SENB test and the Charpy impact test. The covalently bonded nanotubes manage to keep approximately the same *Tg* value but increase the fracture toughness by 117% in the IPD and only 11% in the inherently tougher D230. However, only the non-covalently bonded CNT managed to improve the impact toughness in the brittle IPD cured resin. It is suggested that the lower binding energy of the Van der Waals bonding, taking the π-electrons of carbon nanotubes utilized to promote adsorption on the CNT surface via π- π stacking interactions (Vaisman et al., 2006,Wise et al., 2004) allowed more impact energy to be absorbed during the fracture than the stronger covalent bonding. There are similarities in the fibre reinforcement impact behaviour (Bader et al., 1973) where untreated fibres with low interfacial properties recorded higher impact energies than the treated fibre specimens. There has been no previous work comparing the different CNT bonding mechanisms and this is the first time this relation between quasi static and impact behaviour of these different mechanisms has been highlighted.

Where CNTs have improved the modulus and strength of flexible epoxies improvements on the fracture toughness have not been reported. In contrast, in a brittle matrix, Li et al. (2008) showed an increase in fracture toughness of 57% and a 15% – 20% increase in flexural modulus but very little improvement in flexural strength. This is in agreement with Ci and Bai (2006) who attributed this to better dispersion due to the reduced viscosity of the lower modulus epoxy in the mixing stage. Vasconcelos et al., (2005) also showed how the addition of nano-fillers can improve the Charpy impact fracture toughness of a brittle epoxy but was significantly detrimental to the toughness of lower *Tg*, rubbery epoxy. Lui and Wagner(2005) looked at two systems and found that tensile property values were increased significantly with MWNTs, functionalised by carboxylic groups, over the control resin and unmodified CNT resin in a rubbery epoxy, and much more so than in a glassy, brittle epoxy. The impact toughness showed the reverse; due to the high toughness of the rubbery epoxy, an increase was only seen in the glassy epoxy.

6.7 Concluding Remarks

Chapter 6 looks at the remaining key factors highlighted in Chapter 3. The type of nanoparticles was changed to look at the properties of carbon nanotubes (CNT) which have greater specific strength properties than the nanoclay. The study also looks at the effects of the bonding mechanism of the nanocomposite and how different interface mechanisms affect the mechanical properties of the material. Analysis of the dispersion and mechanical properties according to Figure 3-2 compared the two bonding methods and looked at the behaviour over a range of nanotube loadings. Figure 6-26 highlights the key factors as described.

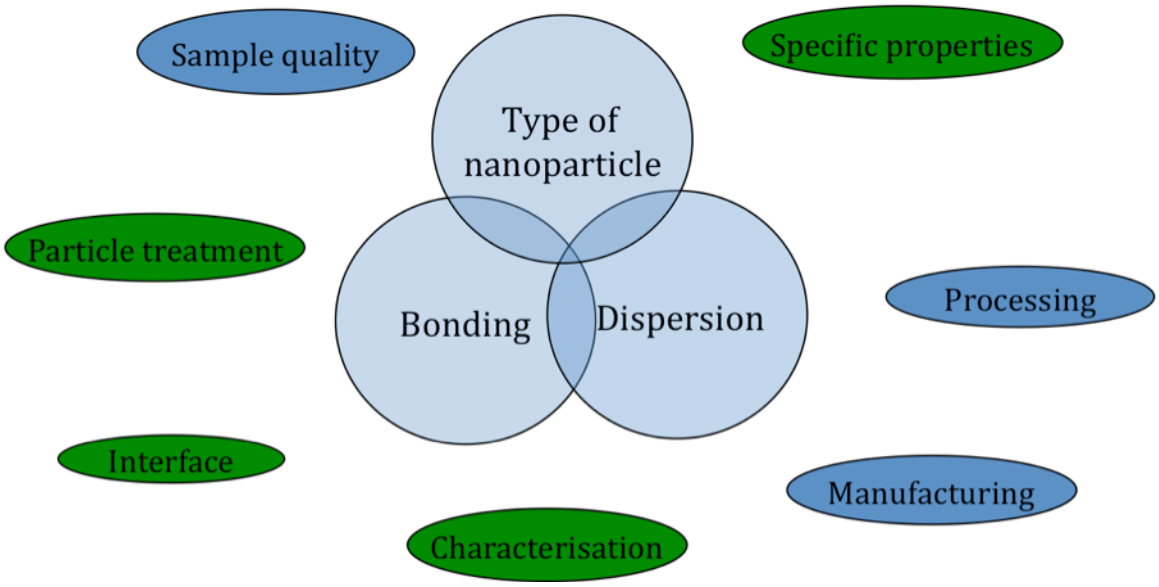

Figure 6-26 The key issues regarding structural nanocomposites with areas that have been investigated in Chapter 6 highlighted in green.

Mechanical properties of two different CNT bonding mechanisms in epoxy CNT resins have been tested and compared. Each test assessed the behaviour with increasing the load of CNT of commercially available nanotube –epoxy dispersions. This behaviour was analysed in two different cured systems to compare the effects in the different characteristic brittle or flexible systems. These systems represent two of the most commonly used basic amines used in the formulation of hardeners used in structural epoxies.

Measurement of *Tg* and rheology showed a difference in behaviour between covalently bonded nanotubes and adhered nanotubes. This contributed to the understanding of the behaviour between the two types of interface as well as highlighting some changes with the type of particle treatment.

TEM, SEM and microscopic analysis observed some agglomeration in the samples. This may explain why, in some cases, the property value appears lower than expected. The effect may also have been heightened by the dilution of master-batches. The most significant contribution, however, to a reduction in property value and an increase in standard deviation is concerned with the entrapment of air within the sample.

Despite this, mechanical improvements were observed in resin casts cured with IPD , a high strength, brittle system with a relative high crosslink density and Jeffamine D230 curing agents a more flexible, tougher D230 system. The only outstanding contrast to this was the tensile strength in the IPD system which was not improved. This possibly was because the CNTs hinder cross-linking affecting the strong structural make-up. Changing the ratio of the resin to IPD may provide better structural behaviour of the nanocomposite as results in Appendix C suggest.

All other bulk mechanical properties tested showed an increase in value by one or more of the materials. The biggest increase is generally found with the covalent bonded CNT sample with a loading of 0.28wt% in the IPD system and 0.26wt% in the D230 system. The data also indicates that the D230 system will hold on to an increase in performance as the loading goes beyond that, where as the IPD in tensile strength, strain to failure, flexural strength and fracture toughness show a drop in performance at higher CNT content. This may be due to the failure mechanism due to a difference in cross-linking of the polymers. The increase in cross-linking can heighten the effect of stress concentration caused by agglomerated CNT.

Two different fracture properties, K_{1C} and Charpy impact toughness, of the D230 and IPD systems show significant difference in the CNT enhancement. They show that the more brittle system can be toughened by the addition of CNTs. The less brittle system is not affected so dramatically and shows a decrease in fracture toughness in some cases. The most significant analysis regards the fracture behaviour applied by the two interfaces. The Van der Waals bonding is weaker than the covalent bonding methods. From this testing it has been shown that the two bonding mechanism exhibit similar trends to the interface strengths of carbon fibre under impact loading. Previous work has not tested this distinction and this contrast in behaviour has only been seen before in the work carried out in macro-scale fibre reinforcement. Further work would verify these findings and analyse the mechanisms at the interface between nanotube and matrix which will shed further light on how these differences occur and aid the modelling and understanding of these materials.

The next stage is to combine these property enhancements into fibre reinforced composites and to process the nano-material within formulated resins that make up the composite matrix.

7 Fibre reinforced nanocomposites

This chapter represents the work taken forward from the epoxy resin work to fibre reinforced laminate testing and in doing so follows the flow diagram in Figure 3-2, Chapter 3, to its completion in terms of the structural assessment of nanocomposites. This has concentrated on the addition of CNTS to the composite as it has the potential to be more beneficial in a carbon fibre system and the most likely material used in structural application. The assessment is also a test for the routes to manufacture the nano-enhanced composites. These include vacuum assisted resin transfer moulding VARTM of laminates and the formulation of pre-preg resins. Each method encountered obstacles involved with applying CNT enhanced resin to the manufacturing processes. Each CNT enhanced composite process is compared in mechanical performance with the equivalent control material. The mechanical testing has been chosen to assess the properties that have high resin property dominance such as the interlaminar shear strength (ILSS) and the compressive properties.

7.1 Nanocomposite fibre work

Increased mechanical performance of epoxy resin does not necessarily mean an increased performance of fibre-reinforced composites. Several methods and different materials for nano-enhanced laminate were used in an exploration of enhancement of the structural properties. Initially some work with nanoclay was used to test the speed of infusing a laminate. This was unsuccessful due to the high viscosity of the epoxy-nanoclay mixture slowing the rate of infusion. This meant that the basic amine hardeners cause the matrix to cure before it was fully infused. This outcome meant that no mechanical analysis could carried out. There have been examples where a fibre reinforced laminate has been successfully infused with an epoxy nanoclay resin matrix. Siddiqui et al., (2007) found that most CFRP property improvement showed similar trends to that of nanoclay/epoxy matrix trends. They claim that there is a strong correlation between fracture toughness (critcal strain energy release rate), G^{m}_{IC}, of the nanoclay modified epoxy matrix and G^{c}_{IC}, fracture toughness of the CFRP composite. This implies that an improved static toughness of the epoxy matrix may be directly related to the improved composite interlaminar fracture toughness. This assumption is validated by similar data found when comparing other enhanced epoxies such as liquid rubber, alumina particles and short fibres.

The next stage of the investigation concentrated attention to CNT enhanced epoxies. These require a much lower weight fraction and the resin viscosity was found not to increase so drastically. Glass laminates were infused with various levels of CNT loaded Hybtonite resin

and tested in short beam interlaminar shear testing and compression strength testing. The addition of CNTs to epoxy was also tested in their effectiveness in a range of formulated pre-preg materials. Initial testing was conducted by taking the enhanced bisphenol A epoxy and combining it with proprietary pre-preg formulation on carbon fibre laminates. Another pre-preg enhancement method was the addition of CNT to the proprietary formulation in semi-solid form by the manufactures of the CNT enhanced liquid bisphenol A. Testing was carried out on the resin and on lab made carbon laminates. The CNT enhanced resins were compared with the original formulated product in compression and ILSS.

7.2 *Infusion of Hybtonite resins*

Taking the same formulations of the Hybtonite CNT enhanced resins used and tested in Chapter 5 glass fibre reinforced laminates were manufactured for testing in Interlaminate shear strength (ILSS) and compressive strength. Vacuum assisted RTM manufactured laminates were produced using 4 plies of WRE600 E-glass fabric. Laminates were sandwiched between 2 layers of peel ply to help the resin in the transfer process and placed on a pre-released flat glass plate. Resin distribution mesh fabric was placed at the point the resin pipe entered the vacuum bag and the vacuum pump left to help the resin travel across the whole width of the laminate evenly and also keep the vacuum from being blocked which also helped the removal of trapped air. The vacuum bag was then placed over the laminate with sealed breach point inserted for the resin and vacuum pipes before being sealed with sealant tape. Figure 7-1 shows a schematic of a typical layup of an infusion. Once the laminate was infuse the samples were left to cure under vacuum at room temperature for 12 hours then placed in the oven with a vacuum still applied for 1hour at 120°C.

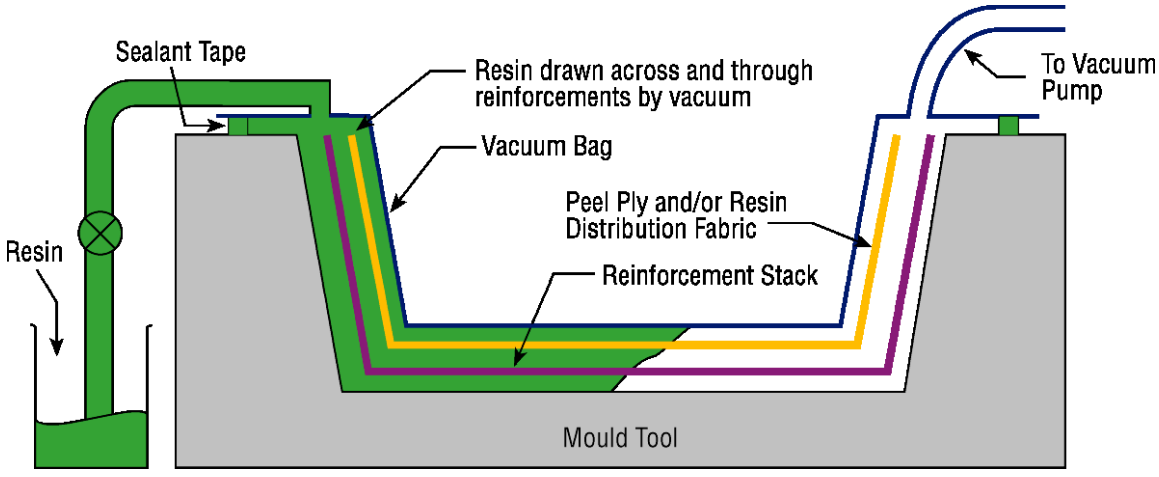

Figure 7-1 Schematic diagram of infusion in a mould tool, courtesy of Gurit.

Initial attempts had found that, especially at higher CNT levels, the CNT resin needed to be heated to reduce viscosity enough to allow infusion. Glass plates acted as a heat sink

reducing the temperature and the speed of infusion. To aid the infusion the glass mould tool was heated prior to infusion to lower the viscosity of the infusion resin.

7.2.1 Hybtonite - infused laminates results

After curing the samples were cut for testing. The interlaminar shear strength of the samples was tested on Zwick mechanical test equipment to test standard ASTM D2344 using a short-beam shear test. A section of the laminate was cut 10mm in width and tested in 3-point bending with a support span of 9.50mm. A test speed of 1.3mm/min was used. The compression strength samples were tested on Zwick mechanical test equipment, with a load cell of 250kN. The test procedure followed was BS EN ISO 14126, using the ASTM D695 modified testing jig. The samples were cut to 80mm in length by 13.5mm width, with tri-axial glass laminate tabbing bonded to the ends of the samples to protect the laminate and prevent bowing of the laminate. At least five specimens for each sample were tested and the average data is shown in Table 7-1.

	IPD				**D230**					
	Control	0.28wt%	0.56wt%	1.12wt%	Control	0.26wt%	0.26wt% heated glass	0.52wt%	0.52wt% heated glass	1.05wt%
ILSS /MPa	34.6	30.51	30.48	29.39	39.31	28.97	30.72	31.67	34.78	26.33
Compression /MPa	264.11	234.77	227.36	199.05	292.92	241.43	267.85		222.72	205.46

Table 7-1 ILSS and Compression strength for different loading of Hybtonite used in IPD and D230 cured glass laminate composite systems

Figure 7-2 and 7-3 compare the average results in graphical form of the ILSS and compression strength for the various CNT weight fraction and curing agent with the data also given in Table 7-1. The heated glass process method is indicated against its equivalent standard processing result.

The ILSS shows that all forms of the CNT enhanced glass laminate did not perform better than the control Epikote 828. However, the technique of heating the glass to allow better infusion of the 0.52wt% D230 cured system did show an improvement over the initial infusion method.

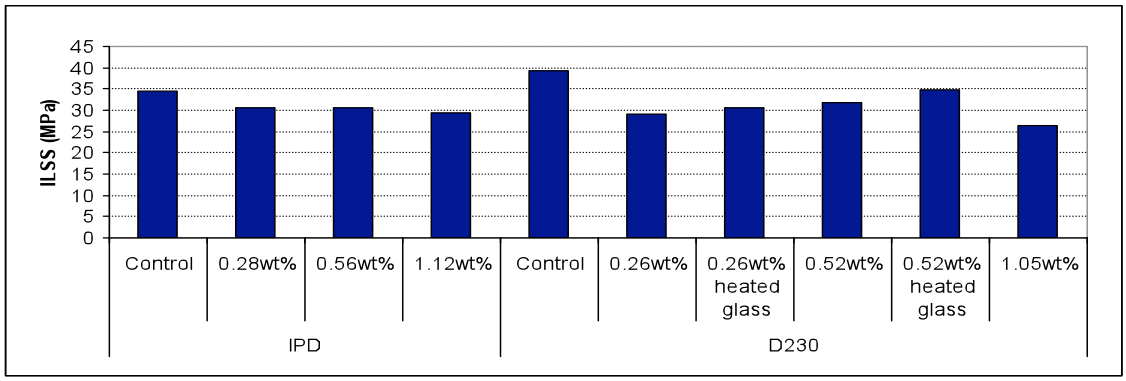

Figure 7-2 ILSS of IPD and D230 cured infused glass laminate.

Compression strength is not enhanced with the use of Hybtonite CNT resin. As the CNT content increases the compressive strength decreases further. The use of the heated glass again shows an improvement over the initial method; however, the improvement is not enough to increase the pristine resin laminate.

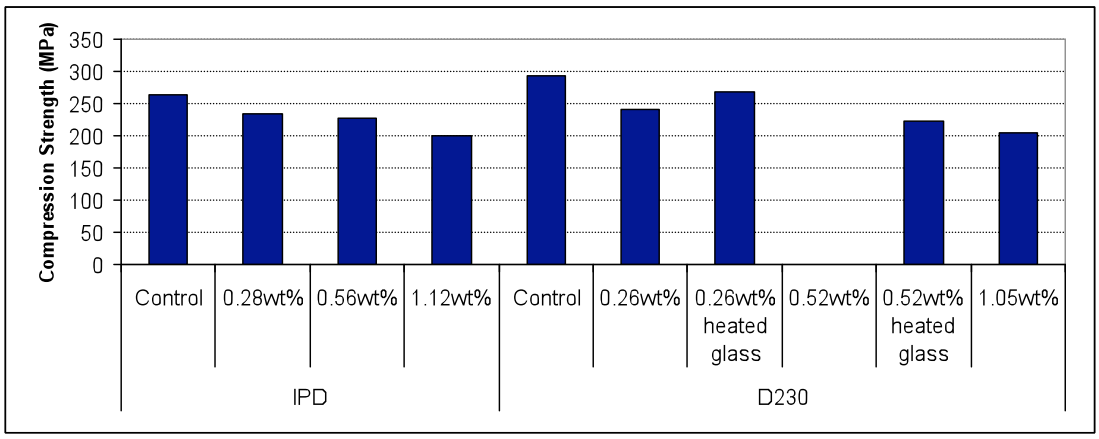

Figure 7-3 Compression strength of the IPD and D230 cured glass laminate.

Figure 7-4A to 7-4D shows a degree of voiding and dry fibre in the different concentrations of Hybtonite laminates. Figure 7-4B shows matrix cracking where the 0.52wt% CNT enhanced matrix has come away from the glass fibre. This is indicates poor fibre wet-out. Voiding is worse in the 0.52wt% laminate than the 0.26wt% laminate and this is probably because of the increased viscosity trapping more air. Figure 7-4C shows a greater number of voids occurring in the 1.05wt% CNT system. There is also evidence of cracking with the sample where the fibres are dry. These could have occurred again due to poor wet-out of the fibre and debonding occurring during the action of removing the peel ply from the laminate which could apply some stress and it seems that most cracking occurs on the top and bottom surface of the laminate. Figure 7-4D shows the control Epikote 828 laminate. Although there are a number of voids also occurring in the control system these are much smaller than in the CNT enhanced laminates.

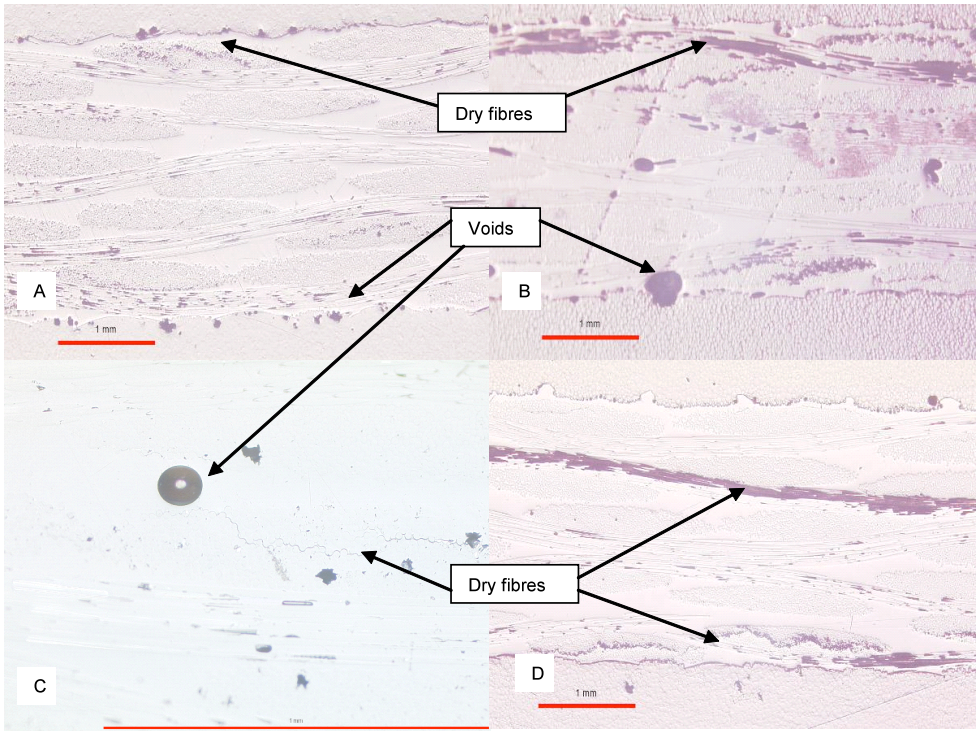

Figure 7-4 Micrographs of a polished cross section of the Hybtonite infused laminate A) 0.26wt% CNT laminate B) 0.52wt% CNT laminate C) 1.05wt% CNT laminate and D) Pristine Epikote 828 laminate.

7.2.2 Discussion of CNT enhanced Infusion laminates

The properties enhancements that have been seen in the resin cast in Chapter 5 have not been translated into laminate composites made by vacuum infusion methods. Analysis of the ILSS and compressive strength data showed that the properties decrease when the resin system incorporated CNT. Further microscopic analysis of the laminate showed this was most likely a result of poor wetting of the glass fibres. This problem is thought to be a caused by the high viscosity of the infused resin. Normally infusion resins are formulated to be a blend of very low viscosity resins and often air removal agents are added to help the release of entrapped air. This would account for the relatively poor quality of all the laminates including the control sample. To counter the high viscosity of the CNT enhanced resins the glass plates were heated as well as the resins to keep the viscosity lower for a longer time period. Unfortunately the IPD curing agent started to exotherm when heated and therefore was not tested. When the 1.05wt% resin was heated the infusion still took a long time and the glass had cooled before it had finished. However, with the 0.26wt% and 0.52wt% specimens the average ILSS and compressive strength increased when the glass-heated method was implemented.

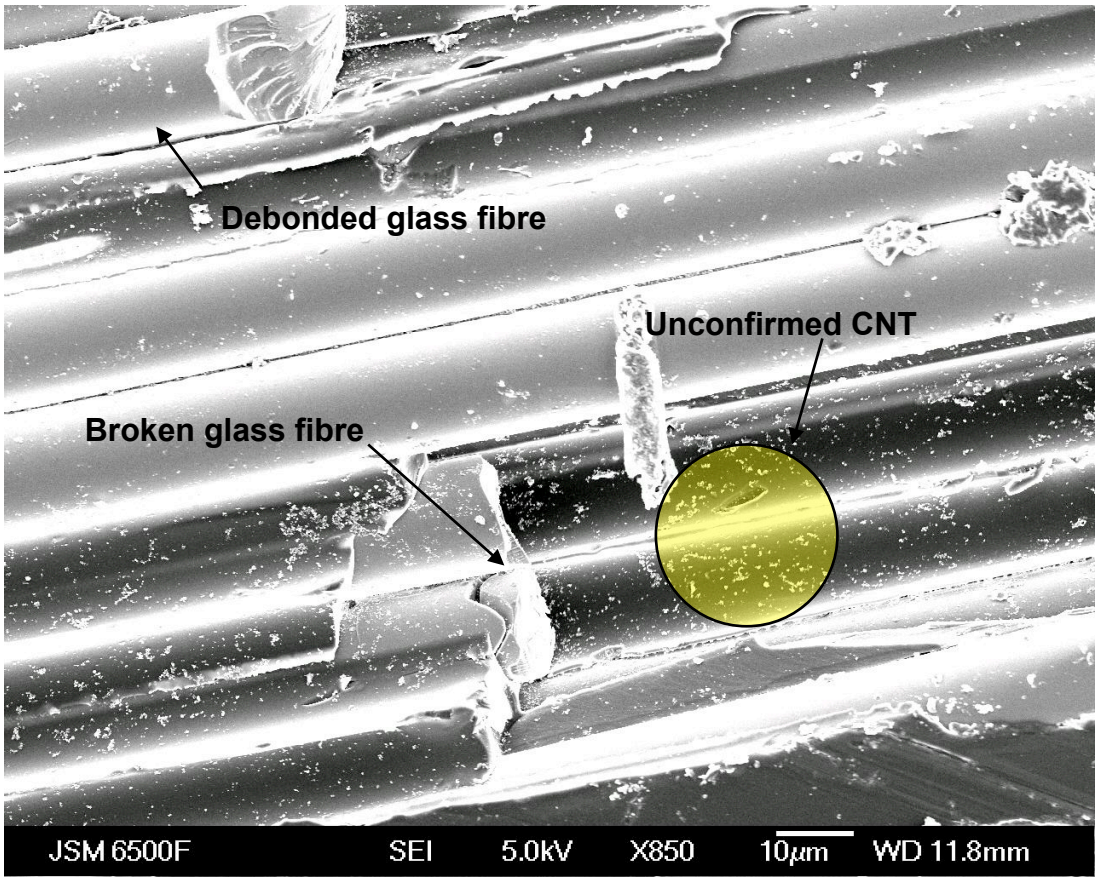

Figure 7-5 SEM micrograph of the Hybtonite CNT enhanced resin matrix and glass fibre.

Figure 7-5 shows an SEM micrograph of a delaminated specimen of infused glass fibre with CNT, the scale bar shows a magnification of 10μm. The image shows the debonded and broken glass fibres and surrounding matrix. The debonding is due to the poor wetting of the fibres in the infusion process. The small agglomerations of material in the highlighted area are thought to be CNT. If this is so then further dispersion of the CNT may help increase the properties. The use of carbon fibre may lead to a better fibre interface due to greater fibre surface area and the use of pre-preg technology may aid the issue wetting of the fibre due to the process that are involved in layup and curing which allows an even dispersion of the semi-solid resin throughout the laminate.

7.3 Zyvex Nanosolve - carbon nanotube enhanced prepreg - SE84

Currently SE84LV is Gurit's highest performing resin matrix in terms of compressive strength properties. Application of CNT would be highly desirable if they are developed in a resin matrix such as this and further increases the laminate properties. Work with Carbon nanotube (CNT) composites has shown improvements in base resin property values, including compressive strength and modulus. In a partnership between Gurit and Zyvex the semi solid CNT enhanced SE84 formulation was processed by Zyvex using their Kentera

technology and tested for resin and fibre reinforced mechanical properties. The resin bulk properties were tested at two loadings and compared with the original formulation. Films of the semi-solid resin were then pressed and applied to 300g woven roving twill carbon to produce a carbon laminate for testing in ILSS and compressive modulus.

7.3.1 Formulation of SE84LV (control) – SPX 8642

The Gurit formulated SE84LV semi solid resin is made up of two parts; the resin - SPX8642 which is made up of a formulation of Epikote 893, GT6099B, ECN 9699CH and Epikote 05370; and the catalyst paste – SPX6951 which is made up of a formulation of Epikote 893, CG1200 and UR 2T. The mix ratio of the two parts is 100:29.4, SPX8642 : SPX 6951.

The SPX8642 formulation was enhanced by Zyvex to include 1.5wt % multi-walled carbon nanotubes. This gave an overall loading of 1.16wt% in the cured sample. A 0.75wt% SPX 8642 formulation was made by mixing a 50:50 blend of the Zyvex nano-enhanced and control resins. This gave an overall loading of 0.58wt% CNT in the cured composite.

7.3.2 Experimental

Two CNT enhanced semi –solid pre-preg systems and the control SE84LV were mixed by a DAC centrifugal mixing machine and weighed out onto backing paper while in liquid form to be pressed into semi-solid films. Six films were made up from the chosen systems were laminated with 12 plies of RC200T woven carbon fibre material. 7g of catalyzed resin pressed into a roughly circular film of about 20cm diameter would to give a resin content of 37% by volume. 2 plies of RC200T were carefully applied to either side of one resin film, making sure the fibres stayed as straight as possible and were aligned. These sheets of carbon and rein film were then cut to a template of 12 x 12cm and placed into a recessed press jig shown in Figure 7-6 with flash tape around the edges and peel ply either side of the laminate. A pressure was applied to the press of 6bar and the laminate was cured for 1 hour at 120°C.

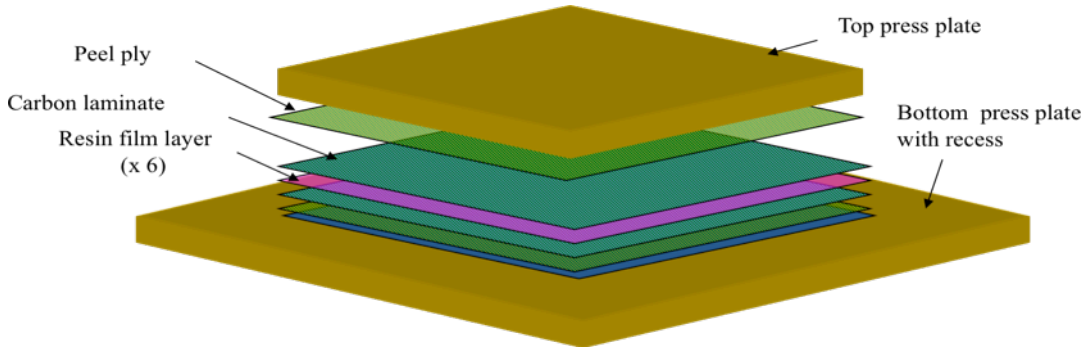

Figure 7-6 lay-up of the pre-preg sample in the press jig. The laminate is made up of 6 resin films and 12 carbon laminates and peel ply applied top and bottom.

A control SE84LV laminate was made in the lab batch method, in the same way as the Zyvex CNT sample batch. A production RC200T pre-preg control SE84LV material, taken from the online pre-preg machine at Gurit was also cut and cured in the same way for comparison. The alignment of the production material is expected to be much better than the lab made laminates and this should show in the properties. The problems arise when cutting the dry fibre and applying the prepreg film which allows the fibres to bend and warp. This makes it very difficult to align the fibres when fitting in the press jig.

A second pre-preg labratory manufacturing method was devised to compare properties with the first method. This involved diluting the resin and catalyst paste mixture with a solvent and mixing with a cowel dissolver for up to an hour to reduce the viscosity of the semi-solid resin. The resin became liquid allowing it to be impregnated onto the woven carbon fibre material by rolling it straight on to the carbon fabric. To keep the alignment the fabric fastened and tension with flash tape to a large piece of flat plywood with backing paper attached.

7.4 Resin casts results and discussion

For a comparison with wet resin the semi-solid pre-preg resin was made into resin cast for testing as described in Chapters 5 and 6. The technique to make resin cast from a semi-solid resin is not easy due to the semi-solid nature of the resin entrapping air. The amount of air entrapped significantly affects the average outcome and standard deviation in strength and modulus values. The technique with the SE84 resin was to heat the resin, once the two parts had been mixed, enough so that it became a liquid but not so much that it started curing. SE84LV could be heated to 50°C then a combination of centrifugal mixing and vacuum degassing helped to remove the air. The technique of creating the resin cast was to heat the glass plates and leave the resin to drain into the cast though a funnel. If the resin became too cool it would regain its semi-solid properties and in this case the resin was reheated or the funnel and glass plate cast was placed in an oven and left to drain. The draining of the high viscosity resin into the glass plates often entraps large pockets of air which collect together rendering large parts of the cast unusable.

7.4.1 Rheology

The SPX8642 and nano enhanced 1.5wt%CNT SPX8642 samples were studied before adding the catalyst paste. A TA Instruments AR2000 rheometer fitted with the Peltier cooling system and 20mm rotating steel disc was used to give coarse shear rate sweeps between $0.001s^{-1}$ and $1500s^{-1}$ at 35°C, 40°C, 45°C, 50°C and 70°C. The resin film gap setting used was 1000μm.

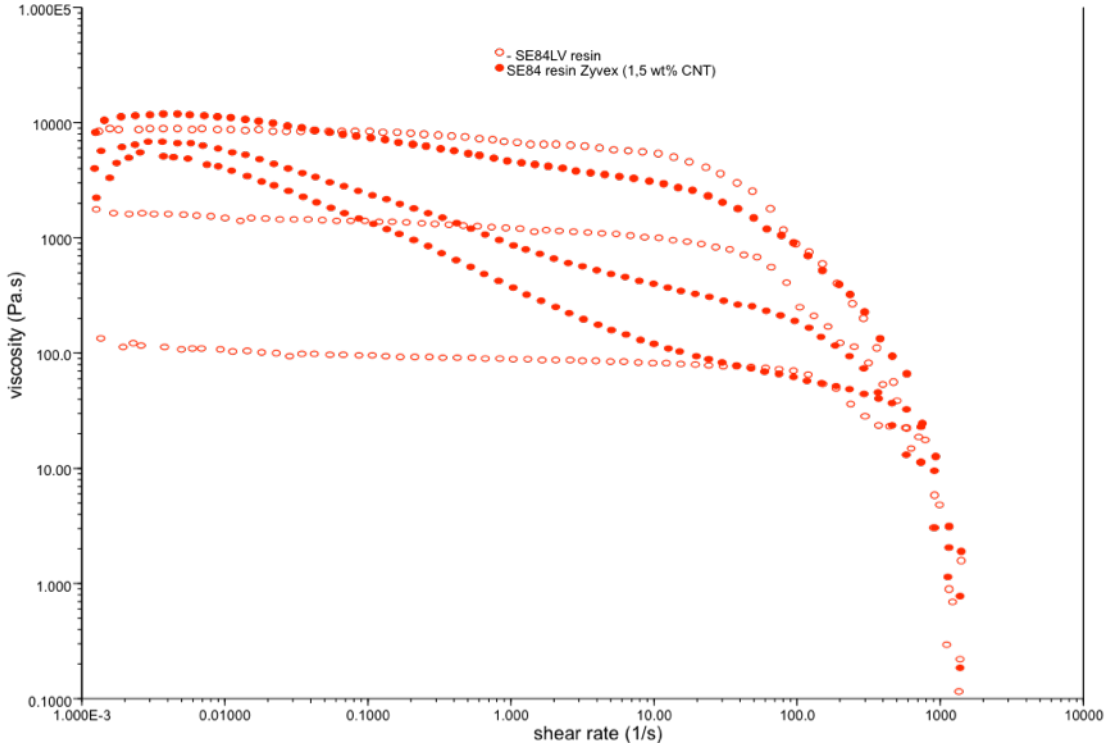

Figure 7-7 Viscosity – shear profile of SPX8642 and 1.5wt% CNT SPX 8642 at 40°C, 50°C and 70°C.

At room temperature both resins are semi solid and could not be tested in the rheometer. A temperature of 35°C was the lowest at which it was found both resins could be run through the shear sweep program and at low shear rates they both exhibited a viscosity of 11000Pa.s. As the shear rate increases the CNT resin begins to shear thin where the control stays at the same viscosity. As the temperature increases the initial viscosity of the control resins reduces, becoming less than the CNT resin. Figure 7-7 shows the viscosity - shear profiles of both the nano-enhanced and original pre-preg resin at various temperatures. It shows the difference in shear behaviour between the two resins. The CNT resin behaviour corresponds with the previous analysis of non-covalently bonded CNT liquid resins. This confirms the presence of non-covalently bonded nanotubes in the formulation. It also shows the gradual reduction in viscosity and change in shear behaviour as the temperature is increased. At 40°C both resins have a similar starting viscosity and the CNT resin has a slightly greater shear thinning gradient. Increasing the temperature decreases the viscosity. The starting viscosity of the CNT resin changes relatively little and the shear gradient increases with temperature. At 70°C the initial viscosity of the control resin is approximately the same as the reduced viscosity of the CNT resin being 100Pa.s at a shear rate of 100 1/s.

7.4.2 Compressive testing of resin casts

The compression strength samples were tested on Zwick mechanical test equipment, with a load cell of 250kN. The test procedure followed was BS EN ISO 14126, using the ASTM D695 modified testing jig. The samples were cut to 10mm in length by 10mm width. The compression modulus samples were tested on Zwick mechanical test equipment, with a load cell of 250kN at a compression rate of 1mm/min.

System	Compressive strength (MPa)	% Standard deviation	Compressive Modulus (GPa)	% Standard deviation
SPX 8642/6951 SE84LV	176.7	5.36	1.47*	0.02
0.58wt% CNT SE84	171.0	3.76	1.97*	0.04
1.16wt% CNT SE84	173.3	5.76	2.09*	0.03

Table 7-2 Compressive strength and modulus for the CNT enhanced SE84 resin. *Data from compressive strength samples, only for comparative purposes.

Compressive results, given in Table 7-2 show very little significant difference in strength. The relatively small size of the compressive strength test specimens meant that the samples could be chosen with the least defect and voids and hence may account for the relatively low standard deviation compared to the tensile and flexural results. The modulus are measured from the compressive strength graphs and not measured according to the standard technique that is tested from coupons of a different dimension. However, when comparing the modulus from the compressive strength data the CNT enhanced resin had improved the modulus by 42%.

7.4.3 Tensile testing of pre-preg resin casts

Systems were cured as neat resin casts and cut into tensile coupons using the CNC router. The samples were tested on Zwick mechanical test equipment, with a load cell of 5kN. The test procedure followed was ISO 527 – 2:1996, using 30kN wedge grips at an actuator speed of 1mm/min.

System/CNTwt%	Tensile strength (MPa)	% Standard deviation	Young's Modulus (GPa)	% Standard deviation	% Elongation to break
SPX 8642/6951 SE84LV	84.8	7.66	3.7	0.093	2.93
0.58wt% CNT SE84	43.3	16.87	3.5	0.117	1.19
1.16wt% CNT SE84	67.8	10.39	3.9	0.123	2.02

Table 7-3 - Tensile Strength and Young's modulus of SE84LV resin casts with different CNT loadings.

The tensile strength data, shown in Table 7-3, shows a significant reduction in strength and increased variance with the addition of carbon nanotubes. This may be partly due to the difficulty in producing void free casts with the high viscosity pre-preg CNT resin. There is no data trend in the change in value for Young's modulus with the 1.16wt% CNT sample increasing modulus by 5% and the 0.58wt % CNT sample reducing by 5%, relative to the control resin and both with a similar standard deviation of 3%. Elongation to break does not show any increase in variation.

7.4.4 Flexural testing of pre-preg resin casts

The flexural strength and modulus was tested according to ISO 178. The resin cast was cut into coupons of 100x10mm and tested on a 3-point test bed, with an 80mm span on Zwick test machine. The test was carried out at a speed of 3mm/min and data measured using a 5KN load cell.

Material Description	Average modulus (GPa)	Standard Deviation Modulus (Gpa)	Average strength (MPa)	Standard Deviation strength(MPa)
SPX8642/SPX6591 SE84LV	3.52	0.061	141.4	5.10
0.58wt% CNT SE84	2.46	0.148	122.2	2.04
1.16wt% CNT SE84	3.38	0.039	117.4	10.45

Table 7-4 Flexural strength and modulus results of SE84LV resin casts with different CNT loadings

Table 7-4 gives the flexural modulus and strength data for the cured Nanosolve SE84 resin. It shows that both strength decreases significantly with the addition of CNTs. The modulus does not show a trend with the level of CNT. It first drops at the O.58wt% loading then increases again.

7.4.5 DMA analysis of the resin

The *Tg* of the cured SE84 resin was measured using a single cantilever bend test in a TA Q100 DMA 25°C to 300°C at 3°C/min, at a frequency of 1Hz as described in chapter 5.

Material Description	Tg °C	Peak Delta tan °C
SPX8642/SPX6591 SE84LV	101.7	122.9
0.58wt% CNT SE84	98.9	126. 1
1.16wt% CNT SE84	97.00	120.9

Table 7-5 *Tg* result by DMA of SE84 resin casts at different CNT loadings

Table 7-5 gives the *Tg* and the peak delta Tan values for the CNT enhanced SE84 resin. The data shows a slight reduction in *Tg* value with the addition of CNTs. The peak delta tan value shows a small increase at 0.58wt% CNT and at higher CNT levels it decreases again.

7.4.6 Charpy impact toughness

The Charpy impact toughness of the pre-preg resins was tested according to ISO 179 / eA as described in section 6.5.5. Testing was done using a Zwick pendulum impact test machine with a 0.5J hammer.

	Charpy impact strength kJ / m²	Standard deviation kJ / m²
SPX 8642 / 6591 (SE84LV)	1.48	0.139
1.5%wt CNT Nano SE84	1.46	0.151

Table 7-6 Charpy impact toughness of the SE84 resin.

The average Charpy impact toughness results, given in Table 7-6, show very little change with the addition of CNT. Both samples give lower values of toughness compared to the basic DEGBA resin values shown in section 6.5.5. However, the standard deviation value, approximately 10% of the mean toughness value, is also relatively low when considering the values observed in section 6.5.5. This suggests greater confidence in the results showing less sensitivity to imperfections.

7.5 Laminate testing results and discussion

7.5.1 ILSS

The interlaminar shear strength of the samples was tested on Zwick mechanical test equipment to test standard ASTM D2344. A strip of the laminate was cut 10mm in width and tested in 3 point bending with a support span of 9.50mm. A test speed of 1.3mm/min was used. Tests were made at five points along the laminate strip.

		Production		Laboratory			
spx8642% wt CNT		**0**	**0**	**0.75**	**1.5**	**0**	**1.5**
se84% wt CNT		**0**	**0**	**0.58**	**1.16**	**solvented 0**	**solvented 1.16**
ILSS	**N/mm²**	67.23	57.38	68.45	66.75	76.63	85.6
Standard deviation	**N/mm²**	1.3	2.33	3.19	6.2	4.69	1.13
max shear	**N/mm²**	68.88	60.12	71.17	77.43	81.69	87.52
% change	**%**	-	-	19.29%	16.33%	-	11.71%

Table 7-7 ILSS of the CNT - enhanced SE84 RC200T laminate.

Table 7-7 gives the ILSS average value as well as the standard deviation for the test as well as the maximum shear force measured for a sample and the percentage change of the mean average value. This is given for the control and CNT enhanced SE84 incorporating the initial laboratory method and the solvented method as well as the control production material. The average data is shown below in the graph and the standard deviation given in the error bars. This shows the solvented production method giving higher values than the production material. With the original production method the 0.58wt% CNT sample has

greater average performance than the 1.16wt% CNT sample. The 1.16wt% CNT sample shows wide variabilty, perhaps due to void content or misalignment of the fibres. Taking into account the maximum ILSS values the 1.16wt% CNT sample has the greater maximum value, even more so than the production laminate, with 77MPa.

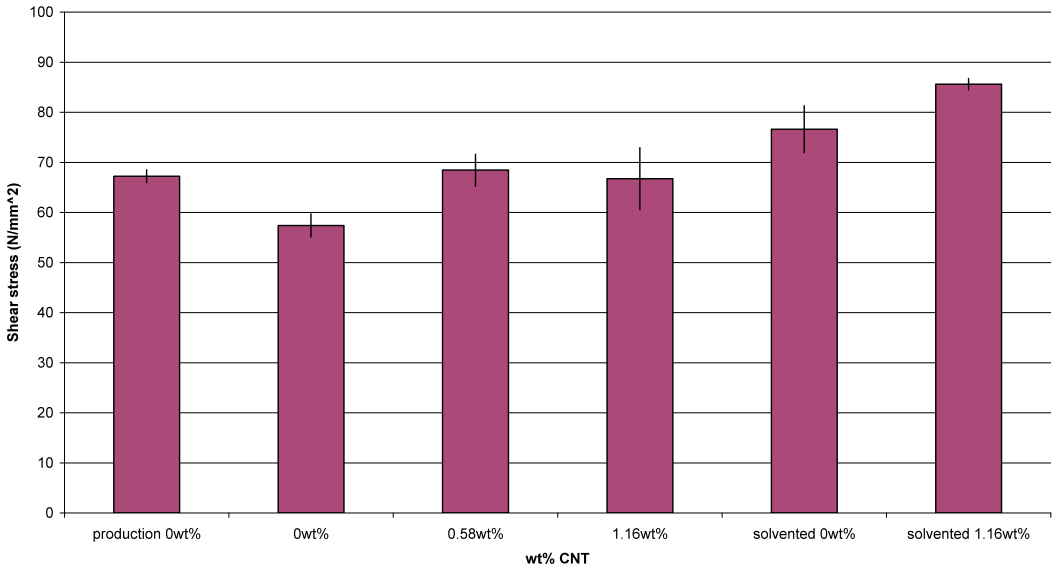

Figure 7-8 ILSS of CNT enhanced SE84LV RC200T laminates.

With both manufacturing methods given in Figure 7-8 the ILSS shows increased performance with the addition of CNT compared to their relative laboratory made control. The solvent method control sample gives a good indication of how much the shear strength can improve with good production technique. The solvented control has a higher ILSS value than the production made control material, although a greater degree of variation is observed in the solvent method. The standard deviation is relatively low with the 1.16wt% CNT enhanced solvented laminate increasing the confidence in the improved result.

7.5.2 Compressive strength and modulus

The compression strength samples were tested on Zwick mechanical test equipment, with a load cell of 250kN. The test procedure followed was BS EN ISO 14126, using the ASTM D695 modified testing jig and the ISO 14126 : 1999 procedure for the compressive modulus. The samples were cut to 80mm in length by 13mm width, with triaxial glass laminate tabbing bonded to the ends of the compressive strength samples, which were cured in a press at 0.5bar for 1 hour at 120°C. The results are shown in Table 7-8 and in graphical form in Figure 7-9 giving the average values and the maximum values in the error bar.

The compressive modulus results of the RC200T laminates found that stiffness was increased by the introduction of CNT to the pre-preg resin. The original production method shows an increasing trend with increasing CNT content, the 1.16wt% increasing the

modulus by 9%. The solvented method also shows an increase in the laminate stiffness when CNT is added to the matrix. The 1.16wt% CNT solvented laminate increased the compressive modulus by 14% over the solvented control and has 6% improvement on the production SE84LV laminate.

		Production		Laboratory			
spx8642 % wt CNT		**0**	**0**	**0.75**	**1.5**		**1.5**
se84 % wt CNT		**0**	**0**	**0.58**	**1.16**	**solvented 0**	**solvented 1.16**
Compressive Stress	**MPa**	794.3	570.9	626.0	638.2	731.5	773.0
Standard deviation	**MPa**	27.83	41.75	37.67	37.2	49.02	31.46
max stress	**MPa**	822.64	610.35	688.35	672.54	813.94	804.83
% change	**%**	-	-	9.7%	11.8%	-	5.7%
Compressive modulus	**GPa**	61.08	54.51	57.11	59.56	56.93	64.75
Standard deviation		0.53	1.03	1.91	1.54	2.162	1.72

Table 7-8 Compressive strength and modulus of CNT SE84LV RC200T.

The compressive strength in the RC200T SE84LV laminate is improved by introduction of CNTs to the pre-preg resin for their relative production methods. There is an average increase of 10% and 12% over the lab control batch. The production control batch has greater compressive strength mean values than the CNT enhanced laminate. This highlights the effect of the fibre alignment and straightness on compressive strength. The production material is straighter than that of the laboratory made samples due to tension applied to the fibre as well as having a lower void content, which was visibly greater in the lab batches. The problem is addressed with the use of the solvented manufacture method that allows the pre-preg resin to be applied to the fibres whilst under strain and fastened to a flat board. This improves the performance by 28% for the control laminate, giving a maximum stress that is almost the same as the production material. The CNT enhanced laminate also show improvement, increasing by 21%, with the solvented method.

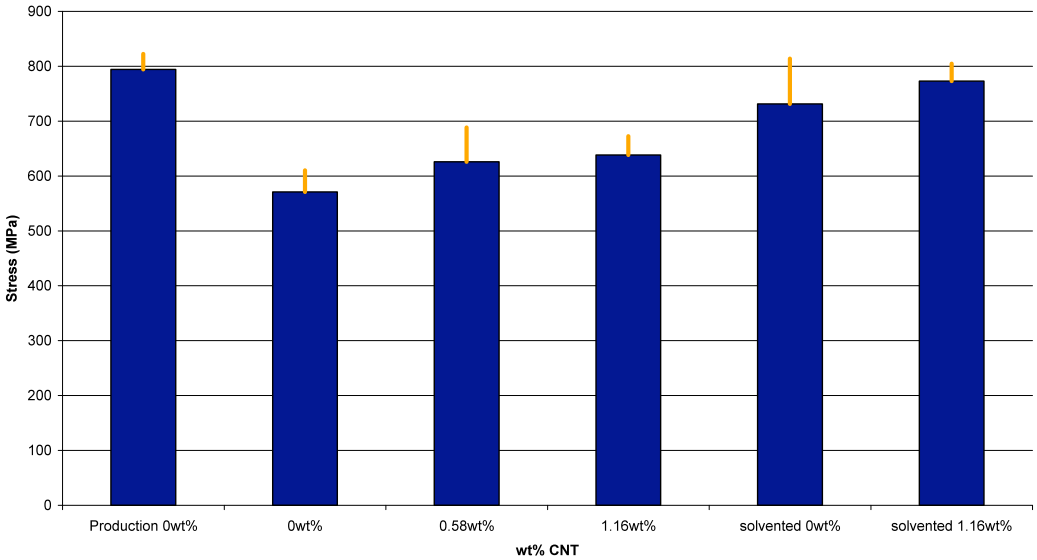

Figure 7-9 Compressive strength of CNT enhanced SE84LV/RC200T.

7.5.3 DMA of the laminate

Samples were evaluated by DMA (TA Instruments Q800) using an operating program of 25°C to 300°C at 3°C/min, at a frequency of 1Hz in double cantilever bending mode.

Sample	Tg_1(°C)	Peak tan δ
SE84 CNT 1.16wt%	97	118
SE84 CNT 0.58%	122	153
SE84 Control	140	149

Table 7-9 *Tg* of CNT enhanced SE84RC200T laminates

Table 7-9 shows the DMA results for the two CNT enhanced laminates and control SE84 laminate. A significant drop in *Tg* is observed with addition of CNT. The CNT filler may, due to the decreased cross-linking, induce this. Peak tan delta is not affected at 0.58wt% CNT but drops at the 1.16wt% loading.

7.6 Discussion

The rheology results showed similarity between the basic Bisphenol A wet resin CNT systems and CNT SE84 resin. Both Nanosolve systems show shear thinning behaviour and this effect can be used to confirm the presence of non-covalently bonded CNT. The CNT resin does not respond to a thermal reduction in viscosity to the extent of the control SE84LV at low shear rates but the change in viscosity affects the shear-thinning gradient instead.

Resin properties of the SE84LV CNT resins do not stand out with any significant improvement and often show a decrease with addition of nanotubes. It is difficult to get an accurate value due to the high variance often seen due to the large void content and possible dispersion issues caused by the nature of the semi-solid resin. Compressive modulus, which is calculated from the compressive strength test data, shows an increase. The Charpy impact toughness results did not show any change with addition of CNT. The indication that the pre-preg resin is a brittle, high modulus resin like the IPD cured bisphenol A resin, yet none of the fracture toughness or bulk property enhancements seen in the that system appear to be present in the semi-solid system.

In contrast to the lack of improvement in the resin cast data the RC200T laminate system showed some property increase with CNT. Interlaminar shear strength was improved with CNT addition even with the lower quality laminates. The compressive modulus data shows

an increase with addition of CNT. This is observed with both production methods and in this case agrees with the resin cast modulus data trend. The laminate compressive strength properties of all the laboratory made batched have lower mean strengths than the equivalent online production pre-preg laminates due to the fibre straightness and void content discussed. However with both laboratory production methods improvement with addition of CNT to the resin relative to each production method indicates some potential enhancement of the nanocomposite.

The laminate data highlight the difficulty in attempting to produce high quality pre-preg from labrotary made resin films. Alignment of the fibres is an unknown factor that evidently plays a greater role in the compressive properties than the resin enhancement. Revising the pre-preg laminating method to account for the alignment issue by using the solvented pre-preg method reduces the variability this causes. This increased the ILSS value of the CNT enhanced laminate so it was greater than that of the production material. It also significantly increased the compressive strength and modulus. No detailed void analysis has been made to check the difference between the solvented and initial laboratory process methods, however, Thomason (1995) shows evidence that ILSS of unidirectional reinforced glass fibre/epoxy decreases 2-10MPa per 1% voiding. The solventing process would have reduced the entrapped air in the mixing process and by applying the liquid form of the resin directly to the carbon material.

Other work, such as Zhou et al (2007b), has looked at the effect of commercially available nanoclay and carbon nanofibres on an epoxy pre-preg laminate systems. With good quality infused laminates the performance in matrix driven properties such as ILSS and G_{IIC} was improved significantly; however, there was no increase in tensile or compressive strengths. The G_{IIC} was improved by over 100% due to the high aspect ratio of the nano additive constraining the growth of micro-cracks.

Zhu et al (2007) also increased the ILSS of glass fibre/ vinyl ester composite laminates with the addition of SWNT. Tests of the bulk matrix also showed a reduction in Young's modulus and *Tg*, which was caused by the SWNT, is claimed to reduce the cross-linking of the polymer. This induces a toughening effect on the resin and this, combined with fibre bridging providing cohesion between the interlayers and adjoining composite laminates, can improve the ILSS. It is also argued that the nano-sized tubes can reduce the stress concentration between fibre and matrix. However, initially this work found that the presence of CNT in the composite produced lower shear strength due to retarding of the matrix polymerization in the immediate nanotube interface area. It is thought that nanotubes trap free radicals in a room temperature cure, reducing the crosslink density at the nanotube

surface. This is based on work showing retardation of polymerization in the presence of fullerene C60. The *Tg* is also reduced by up to 20°C with the addition of nanotubes. Specimens with a 'high temperature initiator' coating on the nanotube, promoted cross-linking on the nanotube surface, show a 20-45% improvement in shear strength with 0.2% ratio to fibre weight.

The SE84LV laminate also decreased in *Tg* value when the CNT were added. This is a parallel behaviour to that of the non-covalently bonded CNT liquid bisphenol A resin described in Chapter 6.3.2. As described in that section this is a function of the cross-linking due to the CNT bonding mechanism and also any unknown parts in the proprietary dispersant formulation. In contrast Cho and Daniel (2008) claimed the *Tg* increase with the addition of nanotubes. This is caused by the confinement of the polymer molecules by nanoparticles. Poor nanoparticle dispersion may actually decrease *Tg* by generating a greater amount of free volume in the matrix causing the *Tg* to drop.

7.7 Concluding remarks

The fibre reinforced work is the culmination of the resin processing work and material testing with the aim of translating the property enhancements to the application of structural fibre composites as originally instructed in Chapter 3. This work is the first comparison of an enhanced formulated epoxy system and shows a snap shot of the possibilities and properties in a high performance epoxy composite system. However, it has left doubt as to whether formulation of a CNT enhanced infusion resin will allow any increase or, in fact, if it is commercially viable.

The mechanical data from the resin cast highlights the difficulty in working with a semi-solid resin for the purposes of resin properties. The tensile and flexural data especially highlight the large standard deviation due to the nature of their sensitivity to defects in the resin. The purpose of the resin work was to asses how the CNTs performed in a formulated resin and check how the addition of other substances to the resin affect the property enhancement shown in the basic epoxy resin work in Chapter 6. From this work it is not possible to conclude if the properties are indeed improves and it would require further work on formulated systems to generate enough data to assess its performance. However, an increase in the resin-influenced properties such as ILSS has seen a dramatic increase and compressive strength and modulus values have also shown increased performance over the original formulated pre-preg with improved production methods.

8 Discussion

The aim of this thesis was to investigate the key factors that affect the enhancement of structural properties of the composites when nanoparticles are applied. The key areas and the main influences associated with them are introduced in Chapter 3 and highlighted again here in Figure 8-1. In this chapter the summary of findings are discussed in reference to the key factors that have been tested.

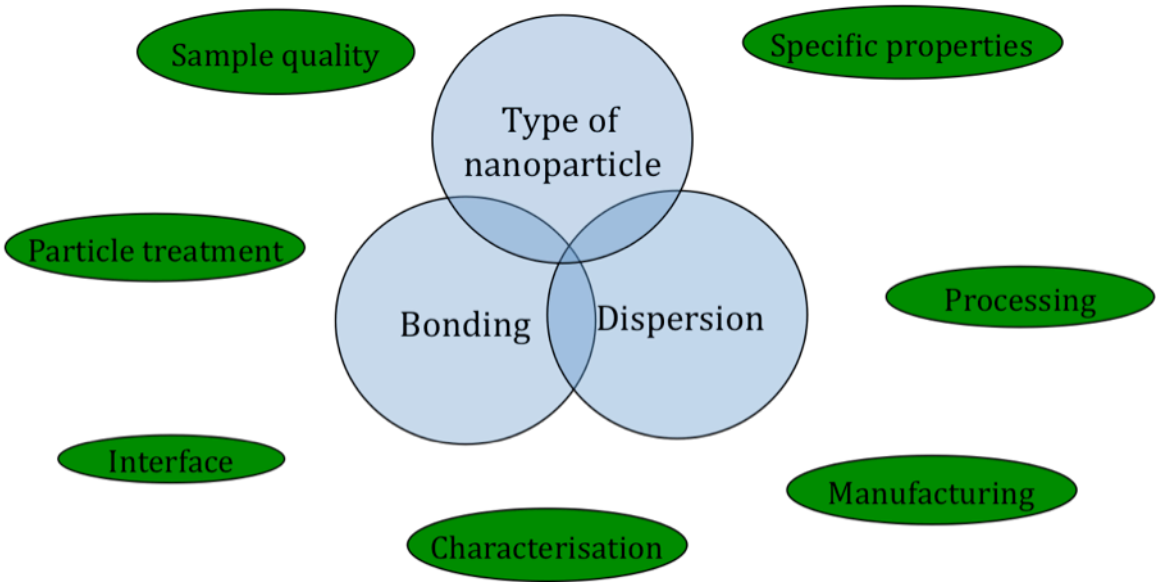

Figure 8-1 The influencing factors on the performance of nanocomposites.

Following this further discussion looks at the implications of the matrix cross-linking properties in terms of to structural application. The influence of nanocomposites on the development on structural fibre reinforced composites is also discussed and the future direction of nanocomposite development.

8.1 Dispersion

Dispersion is generally affected by the treatment / surface modification of the nanoparticles, the shearing process and in some cases by the method of manufacturing. These are all designed with the aim of achieving a homogeneous dispersion of the nanoparticles throughout the matrix. This ensures that the particles are not agglomerated and act as inclusions or allow resin rich areas, reducing the effectiveness of the nano-filler and acting as possible paths of least resistance to the propagation of cracks. This would reduce the breaking stress and the potential enhancement to structural properties. Surface modification is the treatment of the pristine nanoparticles by the attachment of surfactants or polarised ions that affect the way they interact with other particles and the matrix by. This stage of the processing is well researched and many patents have been used in the development of

the commercial “nano additives”. Therefore with all nano-materials tested in this work the modification has been proprietary to the supplier.

To disperse particles on the nanoscale the high shearing techniques are required to break apart the nano bundles or agglomerates. The shearing process also blends the nano-phase with the polymer matrix physically dispersing the particle. Experimental work on the two shearing methods investigated show that a high shear bead mill is more effective in dispersion than the same amount of process time with a high shear cowel dissolver. This is shown by microscopic analysis to break up the bundles of nanoparticles. The bead mill acts by the application of shear force to the entire capacity of the equipment bead mixing chamber through impact between beads, while the cowel dissolver relies on the shear flow in the mixture induced by the toothed disc. Increasing the processing time also showed a greater homogeneity of the nanoclay dispersion but also allows increased entrapment of air into the liquid epoxy system. This was removed through vacuum stirring of the liquid mixture. The use of vacuum shearing equipment would be useful for this kind of processing.

The type of particle changes the many aspects of the processing of the composite. With nanoclay the process of exfoliation has been identified as important to the structural properties of a composite. This involves the separation of the individual clay lamella that makes up the nanoclay. To measure the lamella separation X-ray diffraction technique was employed using Braggs law to calculate the *d* spacing and TEM analysis was used to make visual analysis of the clay morphology. This analysis showed that both shearing processes increased the *d* spacing of the nanoclay. The type of material used to disperse in changed the exfoliation of the nanoclay to a significant extent as well. The results give a bigger separation for the tri-functional epoxy, Araldite DY-T. One explanation is that it is a more flexible epoxy molecule can migrate into the interlayer of the nanoclay and on curing can further separate the lamella. The literature, however, speculates that further exfoliation can be obtained with a bisphenol A epoxy resin. To attempt further exfoliation, shear blending the nanoclay in ethanol or in the amine curing agent was thought to allow the smaller molecule to migrate into the clay interlamella space and also aid the migration of the epoxy molecule with it. The XRD analysis was not able to determine the of the effect of the amine processing and this may have been caused by a large variance in the *d*-spacing or due to the separation of the clay lamellae being greater than the limitations of the equipment. Images from the TEM show that this processing gave some good intercalation.

A straight comparison between ethanol shear processing and amine shear processing showed that the processing in solvent with the resin allowed a greater separation than

processing in amine. When comparing the material properties of these two processes the solvent slurry method again showed greater flexural strength and modulus. This method, when progressed to the bead mill shearing, gave even greater properties due to the dispersion.

The importance dispersion was also apparent with the CNT composites. The effect of diluting the pre-dispersed master-batches may be a causing a change in material properties. It has been observed that the "as supplied" master-batch, when diluted, correspond with a decreased in value for some the material properties. This was consistently seen in the Hybtonite material batches at the lowest loading for tensile and flexural strength; however, in compressive strength this was not the case. The added value of being able to use master-batches of pre-dispersed carbon nanotubes means that specialised dispersion techniques and equipment are not required. The use of master-batches also allows tighter control of CNT for health and safety as CNTs are transported and handled in wet form without the need to engage with them while in more hazardous dry form. From an economic point of view it means that a high percent master-batch requires less material to be transported and stored. The dispersion of master-batches may rely on the type of surface modification or bonding.

8.2 Type of Nano Particle

The varying amounts the material properties are improved or reduced, as reviewed in Chapter 2, highlights the difficulty in improving structural properties with nanoparticles. The silicate clay layers are high in aspect ratio, being plate-like, which should be beneficial for enhancing fracture resistance. The draw back is that the nanoclay plates are difficult to disperse, as exfoliation of the nanoclay is also a factor, and also the process of removing air becomes harder, with clay platelets acting as a barrier to the entrapped air.

The chemical structure of the CNT gives them greater specific properties than clay nanoparticles that are desirable in the pursuit of improvement in the composite structural performance. The dimension of the nanotubes also mean there is a much larger specific surface area. This means the amount of CNT applied to the epoxy matrix is less in terms of weight fraction compared to the nanoclay.

The difference between the types of nanoparticles is demonstrated in the changes in mechanical properties. It emerges that there is a significant increase in the performance of CNT-epoxy nanocomposites. This is observed in tensile, flexural and compressive strengths and moduli. The nanoclay/epoxy material testing did not show a significant tensile strength improvement and a reduction in impact toughness while the tensile modulus and the flexural properties were found to show some improvement. The difference between the effect of nanotubes and nanoclay inclusions in the epoxy matrices suggests that the CNTs enhance

properties with greater improvements. However, the nanoclay testing showed an increase of up to 14% over the pristine resin in modulus and 5% in flexural strength in a bisphenol A, D230 cured epoxy system. The CNTs increased the flexural modulus by up to 13% and 11% in strength.

The CNTs differed significantly in the ideal weight fraction, demonstrating the greatest performance at a lower weight fraction than the nanoclay. This obviously has overall weight as well as cost implication and also affects the processing ability. These improvements in properties values indicate the best performance at varying weight fractions but predominantly this is seen below 1wt% for CNT enhanced epoxy. The strength property values for CNT composites show a trend to decrease at higher loadings. The maximum performance for the nanoclay is argued to be at approximately 2wt%. . This trend is not necessarily true for the modulus values where, in some cases the increase in stiffness is greatest at the highest nanoparticles content, over 1wt% for CNT and 4wt% for nanoclay.

8.3 Bonding

The bonding mechanism is affected by the type of surface treatment and indicative treatment processing method for the dispersion of nanoparticles in the polymer matrix. The desired outcome is a particle that is dispersed and can create a homogenous network as well as provide good interaction to the matrix. This can be achieved with CNTs using a surfactant, which acts as a link between the epoxy and nanotube using Van der Waals forces to bond to its surface. Another method is to covalently bond epoxy molecules to defects in the carbon lattice make up of the CNT and the exposed nanotube ends. This can be achieved through reacting oxygen with a free carbon atom in the nanotube lattice and applying energy to bond directly to the epoxy ring, a process called hybridization.

Certain different characteristic traits were found in with each bonding mechanism. When rheological properties were tested the non-covalent bonded CNT-epoxy resins displayed shear thinning behaviour whilst the covalently bonded CNT-epoxy resin showed Newtonian behaviour. This is most likely to be explained with the analogy of a gel network structure formed by dimethyl-coated silica. The break down of the mechanical entanglement of methyl-extended silicone polymer chains is expected to be a similar process to the surfactant-extended CNT polymer chains. When glass transition temperatures were investigated the non-covalently bonded CNT-epoxy samples showed a greater reduction in *Tg* than the covalently bonded CNT-epoxy composites. The reduction may be caused by the surfactant-induced plasticisation of the epoxy.

The two bonding methods were compared for performance in bulk properties and fracture properties over a range of CNT weight fractions. The results showed that the covalently bonded CNT epoxy demonstrated the greatest increase for strength property values in tensile, flexural, and compressive test data. Strength increases were also observed for the non-covalently bonded CNT resins.

Modulus values have also increased to a greater extent with the addition of covalently bonded nanotubes. The non-covalent bonded CNT did not consistently show an increase in stiffness. There are, similar to the strength testing, some discrepancies with the flexural testing of the IPD cured samples. In this case the non-covalent bonded CNTs increased the modulus to a greater extent. The sensitivity of the IPD cured samples once again caused a greater a variance in these tests.

The covalent bonding, being a stronger bond than Van der Waals, would be expected to increase the strength of the resin to a greater extent when the high strength of the CNT is captured effectively. The cause of the greater improvement on the modulus values is argued to be related to the observation that Van der Waals bonded CNT composites decrease in *Tg* values to a greater extent than the covalent bonded samples indicating a lower cross-link density. It can also be associated with the high stiffness of the CNTs being directly bonded into the epoxy polymer network.

The examination of the CNT bonding effect on K_{1c} fracture toughness continues the same performance trend. Covalent bonds improve the K_{1c} value more than the Van der Waals method. In contrast when Charpy impact toughness was tested the Van der Waals bonded CNT showed an improvement over the covalently bonded. As discussed the implications give rise to comparisons with treated carbon fibre under impact conditions. This agrees with some research where Izod impact toughness has reduced with fluorinated MWNT (Miyagawa and Drzal, 2004b), however, certain studies have seen improvements with impact fracture toughness with amino functionalised MWNTs (Wang et al., 2006a).

8.4 Effect of epoxy curing agent cross-linking and CNT

The CNT's were tested in an epoxy resin and their effectiveness compared with different curing agents. The significant difference was the change in cross-linking in the cured epoxy as shown by the *Tg* of the material. This effectively meant that one system is a strong but brittle material and the other is a tougher, slightly more flexible or ductile material with a greater strain to break but lower breaking stress.

The CNTs have improved the modulus and strength of flexible D230 epoxies by up to 17%. Improvements on the fracture toughness have not been reported. This was due to D230

cured epoxy having a lower *Tg* giving it greater inherent fracture toughness as shown experimentally with both the SENB fracture test and the Charpy impact test. Nanotubes are able to increase the fracture toughness by up to 117% in the brittle IPD formulation and only an increase up to 11% in the inherently tougher D230.

In a brittle IPD matrix the modulus and strengths were increased by up to 16%, though on average a lower increase is seen in the bulk properties than the flexible, tough matrix. In tensile strength testing the strength was not increased significantly and showed a greater variance in results. This is thought to be caused by the IPD's sensitivity to the cure ratio. Testing the off ratio properties, as described in Appendix C, confirmed that better material property values were observed at +2 part of the stoichiometric curing ratio.

Li et al. (2008) showed an increase in fracture toughness of 57% and a 15% – 20% increase in flexural modulus but very little improvement in flexural strength for a brittle resin matrix. This is in agreement with Ci and Bai (2006) who attributed this to better dispersion due to the reduced viscosity of the lower modulus epoxy in the mixing stage. Vasconcelos et al., (2005) also showed how the addition of nano-fillers can improve the Charpy impact fracture toughness of a brittle epoxy but was significantly detrimental to the toughness of a rubbery epoxy with a lower *Tg*.

8.5 Influence on the structural nanocomposite development

As a structural material nanocomposites have, at times, been promoted as the next revolution in material technology. With nanocomposite development its potential can be assessed in terms of the "market now" composite application and in terms of the future market of new applications. For example the development may allow the evolution of new manufacturing techniques and designs. It is widely understood that confidence in the new material is needed and for safety tolerances to be accepted. The novel material development is also dependent on cost/performance ratio. With structural nano-materials the application is most likely to be with high-cost, high-tech applications. This is due to the cost of CNT material and cost of development. The cost of CNT is decreasing and should continue decreasing, along with the development costs, over the coming years (Zhu and Kissel, 2007). This means that structural benefits of CNTs need to be achieved with high performance carbon fibre pre-preg material for use in high performance applications. However, there may be some applications where the nanocomposites can reduce the overall life cycle costs by significant increased in fatigue failure time.

This does not take into account the environmental cost of structural polymers and nanocomposites. Recently, with the increase in oil prices and environmentally sensitive issues, more naturally produced structural composites are reaching the market. As shown in

this study a weaker matrix shows greater improvement in strength with CNT compared to a stronger one and it also indicated a brittle resin is given a greater percentage increase in toughness over an inherently tough resin. The performance of most natural or semi-natural composites is relatively low compared to properties of formulated epoxy composites and this is perhaps where some benefit will be seen with the use of nanocomposites (Haq et al., 2008).

For structural composites thermosetting resins are the predominant choice due to their stiffness, thermal properties and their relatively easy application with fibre reinforcement. With epoxy polymer nanocomposites, the nano-material can be added to already formulated, toughened epoxy for further mechanical advantage with the addition of certain other properties to the matrix material or it could be used to replace additives in the formulation, perhaps to give the same performance at reduced cost or weight or for other benefits such as fire retardancy. However, an important objective in epoxy resin chemistry is to improve the material properties balance without sacrificing any handling properties and the rheological properties that are designed t make it processible.

Added costs of manufacture can be contributed by further processing steps, increased processing and fabrication temperatures and pressures as well as the increase in timescale of epoxy processing and structure fabrication. The processing of nanocomposites has been difficult and the addition of solvent (as seen in some processes) adds extra cost as well as environmental consideration on the large scale. The quality of the material also has to be considered. The characterisation testing undertaken for nanocomposites is expensive and time consuming. This study has demonstrated, however, that in some cases rheology testing can be a check for the presence of CNT.

The improvement in nanocomposite performance in bulk properties is modest in comparison to some of the performance enhancements shown in previous work or by the claims of the material suppliers. Never the less there is still an improvement seen in the resin properties and some significant ones seen in the fracture toughness performance of the brittle matrix in this study. When considering purely structural performance the data shows greatest increase with the covalently bonded CNT. However, the shear thinning properties displayed by the non-covalently bonded resin may prove to be advantageous in some steps of CNT processing. Increased performance is of no benefit to structural application unless these improvements can be achieved with the fibre reinforced composite properties. That does not imply that work on resin is not useful. It is essential for the development and understanding of the material and provides the basis of the motivation behind further investigation. Translation into fibre reinforcement has shown that nanocomposites can

potentially be useful in composite design and that there are no significant decreases in properties within a formulated high performance pre-preg.

The focus on other properties such as the long-term life and properties after damage may be the key nanotube influence on the structural enhancement. Zhang et al. (2007) found increased fatigue performance with increased weight percentage of MWNT. The enhanced performance is most improved at lower stresses and decreases but is still greater than the control material, as stress intensity increases. Increasing the aspect ratio of MWNT also gave the greatest enhancement.

8.6 Future development of the nanocomposites

The work on fibre-reinforced hybrid CNT recognised the problems with of making laboratory batch pre-preg laminates. The next development is to apply the nano-enhanced pre-preg to the scaled up batch with online production. This would require a large batch of pre-preg resin to be enhanced by CNT and attention to the resin viscosity for use with the machinery. The production of CNT laminate through this method would provide a clear indication of property performance with the improved alignment of fibres and reduction of voiding. The work presented here has also not taken into account the volume fraction of the carbon fibre. A study with a testing different fibre volume fraction and different CNT weight fraction would identify the most desired processing parameters of the hybrid composite and also highlight any significant behaviour traits of the CNT. This could show whether CNT composites have a better performance at higher fibre volume fractions and thus reducing the overall composite weight. Cho and Daniel (2008) demonstrated that the compressive modulus reduced in value with increasing CNT loading. This is attributed to the reduced effective fibre volume ratio caused by swelling of the matrix phase. This swelling is related to agglomeration of the nanoparticles as agglomerates occupy a larger volume than the same amount of dispersed particles.

It is suggested that a lower loading of SWCNT or DWCNT compared to MWCNT is possible due to their relative specific surface area. SWNT have a specific surface area (SSA) of up to $1300m^2/g$, compared to $600 – 800m^2/g$ for double walled carbon nanotubes (DWNT) and $200 – 600m^2/g$ for MWNT (Peigney et al., 2001), depending on the diameter. There is trade off between the good stress transfer via the increased interface area and the increased difficulty in dispersion, with re-agglomeration occurring with more ease due to the greater specific surface area. At 0.3wt%, however, the nanotubes improve ILSS by 20% attributed to a strengthened interface between the glass fibre and the DWCNT which is caused by the tendency of nanotubes to aggregate around the fibre (Gojny et al., 2005). Zhu et al., (2007) also increased the ILSS of glass fibre/ vinyl ester composite laminates with

the addition of SWNT. Tests of the bulk matrix also showed a reduction in Young's modulus and *Tg*, which was caused by the SWNT, is claimed to reduce the cross-linking of the polymer. This induces a toughening effect on the resin and combined with fibre bridging, provides cohesion between the interlayer's and adjoining composite laminates that can improve the ILSS. The shear strength was improved by up to 45% with just 0.015wt% nanotubes coated in just the mid ply of the laminate. At the moment these grades of nanotube are more expensive than the multi-walled grades but more important is the question of the quality and quantity that can be produced at the moment.

Some of the latest techniques take a different approach to integrating nano-materials in a structural composite. Such examples apply the nanoparticles directly to the fibres by spraying or growing directly to the fibres (Kepple et al., 2008,Mathur et al., 2008). Other methods weave fibres from nanotubes show promising results (Mora et al., 2008). These techniques have their own individual processing issues, which will have to be overcome when scaling up for manufacturing but offer many solutions to the drawbacks with traditional nanoparticle dispersion techniques.

9 Novel aspects and overall conclusion

9.1 Novel aspects of the investigation

Work with nanoclays looked at the key area of dispersion represented by work on the resin processing and testing of structural resin properties. The research highlighted the materials and processing routes previously investigated, taking the combined findings to design processing, characterisation and material testing for use with structural polymer application. This work has suggested that solvent processing with a bead mill gave the best structural improvements and this agrees with previously published data. This gave tangible evidence of the link between processing and clay morphology.

CNT bonding methods have been compared. Individually these have been tested but never previously studied side by side. The comparison here examines commercially supplied material in a standard structural epoxy. Covalent and Van der Waals bonded CNT epoxy resins display subtle differences in behaviour. Van der Waals bonding shows shear thinning rheology behaviour whilst the covalent bond CNT displays Newtonian behaviour. From this a newly formed analogy of CNT to the silica thixotropic mechanism is made. The difference in the various bonding mechanisms continues with the *Tg* decreasing with the addition of non-covalently bonded CNT. Bulk property testing in covalent bonded CNTs also shows greater average increase than the non-covalent bonding mechanisms. This is also the case in quasi-static fracture toughness and for the first time the impact toughness gives contrasting results. This indicates that the lower energy of the Van der Waals CNT bonding could be absorbing more energy in the impact in a similar way that untreated carbon fibre shows better impact absorbance than well bonded treated carbon fibre.

The research has been taken a stage further by looking at the performance of CNT with fibre reinforcement. This incorporated initial testing of CNT performance in a high strength semi-solid pre-preg carbon material. This is a unique experiment looking at the process of manufacture and comparing CNT technology with an example of one of the best performing high strength pre-preg material available with current technology.

9.2 Overall conclusion

This investigation has been based on the three factors; type of material, dispersion and bonding, identified as the main criteria for the success of nanocomposites in structural application. In studying them the work has looked at the main influences of these factors in a systematic method that aimed to characterise the properties of the nanocomposites. This

brought together studies of both nanoclay and CNT types of nanoparticles, looking at both the characterisation of the dispersion and material properties in epoxy.

The processing factors that effect the dispersion of nanoparticles were characterised using a range of techniques to compare them. The use of a bead-mill to disperse nanoclay was identified as the most effective method.

Measuring the property performance of the nanocomposite material compared the processing methods. The use of solvents to enhance the dispersion proved to increase the material flexural properties

CNT – epoxy composites were also tested and the bonding methods of the nanocomposites were analysed by measuring the material property performance. This showed an improvement in tensile, flexural and compressive properties as well as fracture toughness by covalently bonded nanotubes.

CNT composites properties were also analysed in different cured matrices, creating both a brittle and flexible polymer. Improved structural properties over the basic pristine resin have been observed with good dispersion technique. Differences in the behaviour of the material between the two bonding mechanisms used were observed. A semi-solid matrix used in fibre pre-preg manufacture was tested for changes in material properties with addition of CNT. Work with fibre reinforcement indicates that there is potential for increased performance with existing pre-preg formulations.

10 References

AGAG, T., KOGA, T. & TAKEICHI, T. (2001) Studies on thermal and mechanical properties of polyimide-clay nanocomposites. *Polymer,* 42**,** 3399-3408.

ALEXANDRE, M. & DUBOIS, P. (2000) Polymer-layered silicate nanocomposites: preparation, properties and uses of a new class of materials. *Materials Science and Engineering: R: Reports,* 28**,** 1-63.

ALLAOUI, A., BAI, S., CHENG, H.M. & BAI, J.B. (2002) Mechanical and electrical properties of a MWNT/epoxy composite. *Composites Science and Technology,* 62**,** 1993-1998.

ANDERSON, T.L. (2004) *Fracture Mechanics: Fundamentals and Applications*, CRC.

AVELLA, M., BONDIOLI, F., CANNILLO, V., PACE, E.D., ERRICO, M.E., FERRARI, A.M., FOCHER, B. & MALINCONICO, M. (2006) Poly([epsilon]-caprolactone)-based nanocomposites: Influence of compatibilization on properties of poly([epsilon]-caprolactone)-silica nanocomposites. *Composites Science and Technology,* 66**,** 886-894.

BADER, M.G., J.E. BAILEY & BELL, I. (1973) The effect of fibre matrix Interface strength on the impact and fracture toughness of carbon-fibre-reinforced epoxy composites *J. Phys. D: Appl. Phys,* 6.

BECKER, O., VARLEY, R.J. & SIMON, G.P. (2004) Thermal stability and water uptake of high performance epoxy layered silicate nanocomposites. *European Polymer Journal,* 40**,** 187-195.

BEKYAROVA, E., THOSTENSON, E.T., YU, A., KIM, H., GAO, J., TANG, J., HAHN, H.T., CHOU, T.W., ITKIS, M.E. & HADDON, R.C. (2007) Multiscale carbon nanotube-carbon fiber reinforcement for advanced epoxy composites. *Langmuir,* 23**,** 3970-3974.

BELLENGER, V., MOREL, E. & VERDU, J. (1988) Structure-properties relationships for densely crosslinked epoxide-amine systems based on epoxide or amine mixtures. *Journal of Materials Science,* 23**,** 4244-4250.

BERKETIS, K. & HOGG, P.J. (2007) Impact response of composites after long-term water immersion. *Journal of Materials Science,* 42**,** 6642-6650.

BRETON, Y., DESARMOT, G., SALVETAT, J.P., DELPEUX, S., SINTUREL, C., BEGUIN, F. & BONNAMY, S. (2004) Mechanical properties of multiwall carbon nanotubes/epoxy composites: influence of network morphology. *Carbon,* 42**,** 1027-1030.

CABOT Cab-O-Sil TS-720 - Treated fumed silica Technical data. Cabot

CAMINO, G., TARTAGLIONE, G., FRACHE, A., MANFERTI, C. & COSTA, G. (2005) Thermal and combustion behaviour of layered silicate-epoxy nanocomposites. *Polymer Degradation and Stability,* 90**,** 354-362.

CHEN, B. & EVANS, J.R.G. (2006) Elastic moduli of clay platelets. *Scripta Materialia,* 54**,** 1581-1585.

CHEN, B., LIU, J., CHEN, H. & WU, J. (2004) Synthesis of Disordered and Highly Exfoliated Epoxy/Clay Nanocomposites using Organoclay with Catalytic Function via Acetone-Clay Slurry Method. *Chemistry of Materials,* 16**,** 4864-4866.

CHEN, C. & CURLISS, D. (2003a) Preparation, characterization, and nanostructural evolution of epoxy nanocomposites. *Journal of Applied Polymer Science,* 90**,** 2276-2287.

CHEN, C.G. & CURLISS, D. (2003b) Preparation and exfoliation mechanism of the epoxy nanocomposite. *Abstracts of Papers of the American Chemical Society,* 225**,** 53-PMSE.

CHEN, C.G., KHOBAIB, M. & CURLISS, D. (2003) Epoxy layered-silicate nanocomposites. *Progress in Organic Coatings,* 47**,** 376-383.

CHEN, C.G. & TOLLE, T.B. (2004) Fully exfoliated layered silicate epoxy nanocomposites. *Journal of Polymer Science Part B: Polymer Physics,* 42**,** 3981-3986.

CHEN, J.H.S., POLIKS, M.D., OBER, C.K., ZHANG, Y., WIESNER, U. & GIANNELIS, E. (2002) Study of the interlayer expansion mechanism and thermal-mechanical properties of surface[hyphen]initiated epoxy nanocomposites. *Polymer,* 43**,** 4895-4904.

CHO, J. & DANIEL, I.M. (2008) Reinforcement of carbon/epoxy composites with multi-wall carbon nanotubes and dispersion enhancing block copolymers. *Scripta Materialia,* 58**,** 533-536.

CI, L. & BAI, J. (2006) The reinforcement role of carbon nanotubes in epoxy composites with different matrix stiffness. *Composites Science and Technology,* 66**,** 599-603.

COLEMAN, J.N., KHAN, U., BLAU, W.J. & GUN'KO, Y.K. (2006) Small but strong: A review of the mechanical properties of carbon nanotube-polymer composites. *Carbon,* 44**,** 1624-1652.

CUI, S., CANET, R., DERRE, A., COUZI, M. & DELHAES, P. (2003) Characterization of multiwall carbon nanotubes and influence of surfactant in the nanocomposite processing. *Carbon,* 41**,** 797-809.

DEAR, J.P. (1999) A study of polymer fracture surface features and their relationship to toughness. *Journal of Material Science,* 34**,** 4897 - 4907.

DONG, Y., BHATTACHARYYA, D. & HUNTER, P.J. (2008) Experimental characterisation and object-oriented finite element modelling of polypropylene/organoclay nanocomposites. *Composites Science and Technology,* 68**,** 2864-2875.

EPOXY.DOW.COM/.http://epoxy.dow.com/epoxy/products/prod/liquid.htm#A Accessed 23 August 2006.

FIEDLER, B., GOJNY, F.H., WICHMANN, M.H.G., NOLTE, M.C.M. & SCHULTE, K. (2006) Fundamental aspects of nano-reinforced composites. *Composites Science and Technology,* 66**,** 3115-3125.

FOSTER-MILLER.http://www.foster-miller.com/projectexamples/t_am_polymers/nanotube_composite_structures.htm Accessed 22 August 2006.

FRANKLAND, S.J.V., CAGLAR, A., BRENNER, D.W., GRIEBEL, M. (2002) Molecular simulation of the influence of chemical cross-links on the shear strength of carbon nanotube-polymer interfaces. *Journal of Physical Chemistry B* 106**,** 3046-3048

FRANKLAND, S.J.V. & HARIK, V.M. (2003) Analysis of carbon nanotube pull-out from a polymer matrix. *Surface Science,* 525**,** L103-L108.

GANGULI, S., AGLAN, H. & DEAN, D. (2005) Microstructural Origin of Strength and Toughness of Epoxy Nanocomposites.

GANGULI, S., AGLAN, H., DENNIG, P. & IRVIN, G. (2006) Effect of Loading and Surface Modification of MWCNTs on the Fracture Behavior of Epoxy Nanocomposites.

GOJNY, F.H., WICHMANN, M.H.G., FIEDLER, B., BAUHOFER, W. & SCHULTE, K. (2005) Influence of nano-modification on the mechanical and electrical properties of conventional fibre-reinforced composites. *Composites Part A: Applied Science and Manufacturing,* 36**,** 1525-1535.

GORDON, N. (2003) Disruptive Technologies Part II. IN ROCKY RAWSTERN (Ed.) *Nanotechnology Now*

GU, A. & LIANG, G. (2003) Thermal degradation behaviour and kinetic analysis of epoxy/montmorillonite nanocomposites. *Polymer Degradation and Stability,* 80**,** 383-391.

GUO, B., JIA, D. & CAI, C. (2004) Effects of organo-montmorillonite dispersion on thermal stability of epoxy resin nanocomposites. *European Polymer Journal,* 40**,** 1743-1748.

HACKMAN, I. & HOLLAWAY, L. (2006) Epoxy-layered silicate nanocomposites in civil engineering. *Composites Part A: Applied Science and Manufacturing,* 37**,** 1161-1170.

HAQ, M., BURGUEÑO, R., MOHANTY, A.K. & MISRA, M. (2008) Hybrid bio-based composites from blends of unsaturated polyester and soybean oil reinforced with nanoclay and natural fibers. *Composites Science and Technology,* 68**,** 3344-3351.

HAQUE, A., SHAMSUZZOHA, M., HUSSAIN, F. & DEAN, D. (2003) S2-glass/epoxy polymer nanocomposites: Manufacturing, structures, thermal and mechanical properties. *Journal of Composite Materials,* 37**,** 1821-1838.

HATA, K., FUTABA, D.N., MIZUNO, K., NAMAI, T., YUMURA, M. & IIJIMA, S. (2004) Water-Assisted Highly Efficient Synthesis of Impurity-Free Single-Walled Carbon Nanotubes. *Science,* 306**,** 1362-1364.

HULL, D. (1981) *An introduction to composite materials,* Cambridge, Cambridge University Press.

IIJIMA, S. (1991) Helical microtubules of graphitic carbon. *Nature* 354**,** 56−58

ISIK, I., YILMAZER, U. & BAYRAM, G. (2003) Impact modified epoxy/montmorillonite nanocomposites: synthesis and characterization. *Polymer,* 44**,** 6371-6377.

JAWAHAR, P., GNANAMOORTHY, R. & BALASUBRAMANIAN, M. (2006) Tribological behaviour of clay - thermoset polyester nanocomposites. *Wear,* 261**,** 835-840.

KEPPLE, K.L., SANBORN, G.P., LACASSE, P.A., GRUENBERG, K.M. & READY, W.J. (2008) Improved fracture toughness of carbon fiber composite functionalized with multi walled carbon nanotubes. *Carbon,* 46**,** 2026-2033.

KIM, H.G., LEE, D.H., SEO, K.H., KIM, W.S., PARK, S.Y. & MIN, K.E. (2003) Effect of organic modifiers and mixing times on the properties of unsaturated polyester/montmorillonite nanocomposite. *Polymer-Korea,* 27**,** 589-595.

KIM, H.G., OH, D.H., LEE, H.B. & MIN, K.E. (2004) Effect of reactive diluents on properties of unsaturated polyester/montmorillonite nanocomposites. *Journal of Applied Polymer Science,* 92**,** 238-242.

KIM, J.-K., HU, C., WOO, R.S.C. & SHAM, M.-L. (2005) Moisture barrier characteristics of organoclay-epoxy nanocomposites. *Composites Science and Technology,* 65**,** 805-813.

KNOL, W.H.C. (2004) Nanotechnoology and business opportunaties: scenarios as awarness instrument. *12th International Conference 'High Technology Small Firms'.* Enschede, Netherlands, Qeam.

KORNMANN, X., LINDBERG, H. & BERGLUND, L.A. (2001a) Synthesis of epoxy-clay nanocomposites. Influence of the nature of the curing agent on structure. *Polymer,* 42**,** 4493-4499.

KORNMANN, X., LINDBERG, H. & BERGLUND, L.A. (2001b) Synthesis of epoxy-clay nanocomposites: influence of the nature of the clay on structure. *Polymer,* 42**,** 1303-1310.

KORNMANN, X., REES, M., THOMANN, Y., NECOLA, A., BARBEZAT, M. & THOMANN, R. (2005) Epoxy-layered silicate nanocomposites as matrix in glass fibre-reinforced composites. *Composites Science and Technology,* 65**,** 2259-2268.

KOVACS, J.Z., ANDRESEN, K., PAULS, J.R., GARCIA, C.P., SCHOSSIG, M., SCHULTE, K. & BAUHOFER, W. (2007) Analyzing the quality of carbon nanotube dispersions in polymers using scanning electron microscopy. *Carbon,* 45**,** 1279-1288.

LAM, C.-K., LAU, K.-T., CHEUNG, H.-Y. & LING, H.-Y. (2005) Effect of ultrasound sonication in nanoclay clusters of nanoclay/epoxy composites. *Materials Letters,* 59**,** 1369-1372.

LAN, T. & PINNAVAIA, T.J. (1994) Clay-Reinforced Epoxy Nanocomposites. *Chem. Mater.,* 6**,** 2216 - 2219.

LI, J., WONG, P.-S. & KIM, J.-K. (2008) Hybrid nanocomposites containing carbon nanotubes and graphite nanoplatelets. *Materials Science and Engineering: A,* 483 - 484**,** 660 - 663.

LILLEHEI, P.T., KIM, J.W., PARK, C., CROOKS, R.E., SIOCHI, E.J.Optical, electron and probe microscopy characterization of carbon nanotube composites. NIST practice guide: measurement issues in single wall carbon nanotubes. http://www.msel.nist.gov/Nanotube2/Practice%20Guide_Section5_Microscopy.pdf Accessed 17/05/2008.

LIU, L. & WAGNER, H.D. (2005) Rubbery and glassy epoxy resins reinforced with carbon nanotubes. *Composites Science and Technology,* 65**,** 1861-1868.

LIU, W., HOA, S.V. & PUGH, M. (2005a) Fracture toughness and water uptake of high-performance epoxy/nanoclay nanocomposites. *Composites Science and Technology,* 65**,** 2364-2373.

LIU, W., HOA, S.V. & PUGH, M. (2005b) Organoclay-modified high performance epoxy nanocomposites. *Composites Science and Technology,* 65**,** 307-316.

LOURIE, O., COX, D.M. & WAGNER, H.D. (1998) Buckling and Collapse of Embedded Carbon Nanotubes. *Physical Review Letters,* 81**,** 1639 -1641.

LU, H.-J., LIANG, G.-Z., MA, X.-Y., ZHANG, B.-Y. & CHEN, X.-B. (2004) Epoxy/clay nanocomposites: Further exfoliation of newly modified clay induced by shearing force of ball milling. *Polymer International,* 53**,** 1545-1553.

MA, P.C., KIM, J.-K. & TANG, B.Z. (2007) Effects of silane functionalization on the properties of carbon nanotube/epoxy nanocomposites. *Composites Science and Technology,* 67**,** 2965-2972.

MANEVITCH, O.L. & RUTLEDGE, G.C. Elastic properties of a single lamella of montmorillonite by molecular dynamics simulation. *Journal of Physical Chemistry B,* 108**,** 1428-1435.

MASSAM, J. & PINNAVAIA, T.J. (1998) Clay nanolayer reinforcement of a glassy epoxy polymer. *Mater. Res. Soc. Symp. Proc.,* 520**,** 223-232.

MATHUR, R.B., CHATTERJEE, S. & SINGH, B.P. (2008) Growth of carbon nanotubes on carbon fibre substrates to produce hybrid/phenolic composites with improved mechanical properties. *Composites Science and Technology,* 68**,** 1608-1615.

MESSERSMITH, P.B. & GIANNELIS, E.P. (1994) Synthesis and Characterisation of Layered Silicate - Epoxy Nanocomposites. *Chem. Mater.,* 6**,** 1719 - 1725.

MIYAGAWA, H. & DRZAL, L.T. (2004a) The effect of chemical modification on the fracture toughness of montmorillonite clay/epoxy nanocomposites. *Journal of Adhesion Science and Technology,* 18**,** 1571-1588.

MIYAGAWA, H. & DRZAL, L.T. (2004b) Thermo-physical and impact properties of epoxy nanocomposites reinforced by single-wall carbon nanotubes. *Polymer,* 45**,** 5163-5170.

MIYAGAWA, H., RICH, M.J. & DRZAL, L.T. (2004) Amine-cured epoxy/clay nanocomposites. II. The effect of the nanoclay aspect ratio. *Journal of Polymer Science Part B: Polymer Physics,* 42**,** 4391-4400.

MNYUSIWALLA, A., DAAR, A.S. & SINGER, P.A. (2003) Mind the gap: science and ethics in nanotechnology. *Nanotechnology,* 14**,** 9-113.

MOHAN, T.P., KUMAR, M.R. & VELMURUGAN, R. (2005) Rheology and curing characteristics of epoxy-clay nanocomposites. *Polymer International,* 54**,** 1653-1659.

MORA, R.J., VILATELA, J.J. & WINDLE, A.H. (2008) Properties of composites of carbon nanotube fibres. *Composites Science and Technology,* In Press, Accepted Manuscript.

N.R.C.G (2006) NANOTECHNOLOGY RESEARCH SPECIFICATIONS: . IN ADVISORY COMMITTEE ON HAZARDOUS SUBSTANCES (Ed.) *Consideration of Task Force Research Project Specifications.* DEFRA

NANOFORUM.ORG. 4th Nanoforum Report: Benefits, Risks, Ethical, Legal and Social Aspects of NANOTECHNOLOGY Part 3: Potential Risks of Nanotechnologies. http://www.nanoforum.org/dateien/temp/ELSIPart%203.pdf?29062006163048. Accessed 15 July.2006.

Nanoscience and nanotechnologies: opportunities and uncertainties. (2004) IN THE ROYAL SOCIETY & THE ROYAL ACADEMY OF ENGINEERS (Ed.) London.

NORMAN, D.A. & ROBERTSON, R.E. (2003) Rigid-particle toughening of glassy polymers. *Polymer,* 44**,** 2351-2362.

PANDEY, J.K., RAGHUNATHA REDDY, K., PRATHEEP KUMAR, A. & SINGH, R.P. (2005) An overview on the degradability of polymer nanocomposites. *Polymer Degradation and Stability,* 88**,** 234 - 250.

PARK, S.-J., JEONG, H.-J. & NAH, C. (2004) A study of oxyfluorination of multi-walled carbon nanotubes on mechanical interfacial properties of epoxy matrix nanocomposites. *Materials Science and Engineering A,* 385**,** 13-16.

PAVLIDOU, S. & PAPASPYRIDES, C.D. (2008) A review on polymer-layered silicate nanocomposites. *Progress in Polymer Science,* 33**,** 1119-1198.

PEIGNEY, A., LAURENT, C., FLAHAUT, E., BACSA, R.R. & ROUSSET, A. (2001) Specific surface area of carbon nanotubes and bundles of carbon nanotubes. *Carbon,* 39**,** 507-514.

PETRIE, E.M. Nanomaterials in Adhesives and Sealants. http://www.specialchem4adhesives.com/resources/articles/article.aspx?id=525 Accessed 13 August.2006.

PINNAVAIA, T.J., TRIANTAFILLIDIS, C.S. & LEBARON, P.C. (2002) Homostructured Mixed Inorganic-Organic Ion Clays: A new approach to Epoxy-polymer-exfoliated Clay Nanocomposites with a reduced Organic modifier content. . *CHEMISTRY OF MATERIALS,* 14**,** 4088-4095

POTSCHKE, P., ABDEL-GOAD, M., ALIG, I., DUDKIN, S. & LELLINGER, D. (2004) Rheological and dielectrical characterization of melt mixed polycarbonate-multiwalled carbon nanotube composites. *Polymer,* 45**,** 8863-8870.

Q. M. JIA, M.Z.C.Z.X.H.X.C. (2006) The mechanical properties and tribological behavior of epoxy resin composites modified by different shape nanofillers. *Polymers for Advanced Technologies,* 17**,** 168-173.

QIAN, D., DICKEY, E.C., ANDREWS, R. & RANTELL, T. (2000) Load transfer and deformation mechanisms in carbon nanotube-polystyrene composites. *Applied Physics Letters,* 76**,** 2868-2870.

QUARESIMIN, M. & VARLEY, R.J. (2008) Understanding the effect of nano-modifier addition upon the properties of fibre reinforced laminates. *Composites Science and Technology,* 68**,** 718-26.

RAHATEKAR, S.S., KOZIOL, K.K.K., BUTLER, S.A., ELLIOTT, J.A., SHAFFER, M.S.P., MACKLEY, M.R. & WINDLE, A.H. (2006) Optical microstructure and viscosity enhancement for an epoxy resin matrix containing multiwall carbon nanotubes. *Journal of Rheology,* 50**,** 599-610.

REN, Y., LI, F., CHENG, H.M. & LIAO, K. (2003) Fatigue behaviour of unidirectional single-walled carbon nanotube reinforced epoxy composite under tensile load. *Advanced Composites Letters,* 12**,** 19-24.

RYAN, J. Nanotechnology: separating fact, fiction, hype and hope. http://nanotechweb.org/cws/article/indepth/19979. Accessed 2006.

RYU, J.G., PARK, S.W., KIM, H. & LEE, J.W. (2004) Power ultrasound effects for in situ compatibilization of polymer-clay nanocomposites. *Materials Science and Engineering: C,* 24**,** 285-288.

SALAHUDDIN, N.A. (2004) Layered silicate/epoxy nanocomposites: synthesis, characterization and properties. *Polymers for Advanced Technologies,* 15**,** 251-259.

SCHADLER, L.S., GIANNARIS, S.C. & AJAYAN, P.M. (1998) Load transfer in carbon nanotube epoxy composites. *Applied Physics Letters,* 73**,** 3842-4.

SCPROD.COM. http://www.scprod.com/news/hummer.asp. Accessed 12/01/2008.

SEYHAN, A.T., GOJNY, F.H., TANOGLU, M. & SCHULTE, K. (2007) Critical aspects related to processing of carbon nanotube/unsaturated thermoset polyester nanocomposites. *European Polymer Journal,* 43**,** 374-379.

SHAH, D., FYTAS, G., VLASSAPOULOS, D., DI, J., SOGAH, D. & GIANNELIS*, E.P. (2004) Structure and Dynamics of Polymer-Grafted Clay Suspensions.

SIDDIQUI, N.A., WOO, R.S.C., KIM, J.-K., LEUNG, C.C.K. & MUNIR, A. (2007) Mode I interlaminar fracture behavior and mechanical properties of CFRPs with nanoclay-filled epoxy matrix. *Composites Part A: Applied Science and Manufacturing,* 38**,** 449-460.

SINHA RAY, S. & OKAMOTO, M. (2003) Polymer/layered silicate nanocomposites: a review from preparation to processing. *Progress in Polymer Science,* 28**,** 1539-1641.

SONG, Y.S. & YOUN, J.R. (2005) Influence of dispersion states of carbon nanotubes on physical properties of epoxy nanocomposites. *Carbon,* 43**,** 1378-1385.

SUBRAMANIYAN, A., BING, Q., NAKAIMA, D. & SUN, C.T. (2003) Effect of nanoclay on compressive strength of glass fibre composites. *American Society for Composites 18th Technical Conference* Gainesville, FL.

SUHR, J. & KORATKAR, N.A. (2008) Energy dissipation in carbon nanotube composites: A review. *Journal of Materials Science,* 43**,** 4370-4382.

SUN, C.T. Nanoclay-Enhanced Fiber Composites. *Marine Composites and Sandwich Structures.* School of Aeronautics and Astronautics, Purdue University, West Lafayette, Indiana. .

SUN, L., WARREN, G.L., O'REILLY, J.Y., EVERETT, W.N., LEE, S.M., DAVIS, D., LAGOUDAS, D. & SUE, H.J. (2008) Mechanical properties of surface-functionalized SWCNT/epoxy composites. *Carbon,* 46**,** 320-328.

THOMASON, J.L. (1995) The Interface region in glass fibre-reinforced epoxy composites: 1. Sample preparation, void content and interfacial strength. *Composites,* 26**,** 467-475.

TIBBETTS, G.G. & BEETZ, C.P. (1987) Mechanical-properties of vapor-grown carbon-fibers. *J Phys D-Appl Phys* 20**,** 292-297.

TIMMERMAN, J.F., HAYES, B.S. & SEFERIS, J.C. (2002) Nanoclay reinforcement effects on the cryogenic microcracking of carbon fiber/epoxy composites. *Composites Science and Technology,* 62**,** 1249-1258.

VAISMAN, L., WAGNER, H.D. & MAROM, G. (2006) The role of surfactants in dispersion of carbon nanotubes. *Advances in Colloid and Interface Science,* 128-130**,** 37-46.

VANORIO, T., PRASAD, M. & NUR, A. (2003) Elastic properties of dry clay mineral aggregates, suspensions and sandstones. *Geophysical Journal International,* 155**,** 319-326.

VASCONCELOS, P.V., LINO, F.J., MAGALHAES, A. & NETO, R.J.L. (2005) Impact fracture study of epoxy-based composites with aluminium particles and milled fibres. *Journal of Materials Processing Technology,* 170**,** 277-283.

VEEDU, V.P., ANYUAN, C., XUESONG, L., KOUGEN, M., SOLDANO, C., KAR, S., AJAYAN, P.M. & GHASEMI-NEJHAD, M.N. (2006) Multifunctional composites using reinforced laminae with carbon-nanotube forests. *Nature Materials,* 5**,** 457-62.

WANG, J., FANG, Z., GU, A., XU, L. & LIU, F. (2006a) Effect of amino-functionalization of multi-walled carbon nanotubes on the dispersion with epoxy resin matrix. *Journal of Applied Polymer Science,* 100**,** 97-104.

WANG, K., WANG, L., WU, J., CHEN, L. & HE, C. (2005) Preparation of Highly Exfoliated Epoxy/Clay Nanocomposites by "Slurry Compounding": Process and Mechanisms. *Langmuir,* 21**,** 3613 -3618.

WANG, S., LIANG, Z., LIU, T., WANG, B. & ZHANG, C. (2006b) Effective amino-functionalization of carbon nanotubes for reinforcing epoxy polymer composites. *Nanotechnology,* 17**,** 1551-1557.

WANG, Z.Z., WANG, H. & CATES, M.E. (2001) Effective elastic properties of solid clays. *Geophysics,* 66**,** 428-440.

WISE, K.E., PARK, C., SIOCHI, E.J. & HARRISON, J.S. (2004) Stable dispersion of single wall carbon nanotubes in polyimide: the role of noncovalent interactions. *Chemical Physics Letters,* 391**,** 207-211.

WONG, E.W., SHEEHAN, P.E. & LIEBER, C.M. (1997) Nanobeam Mechanics: Elasticity, Strength, and Toughness of Nanorods and Nanotubes. *Science,* 277**,** 1971-1975.

WWW.ANTARIA.COM. http://www.antaria.com/index.php?page=nanoz. Accessed 19/07/06.2006.

WWW.FLAMERETARDANTS-ONLINE.COM.http://www.flameretardants-online.com/fsm/frame_fsm_neben.htm Accessed 22 August 2006.

WWW.HUNTSMAN.COM.http://ww1.huntsmanservice.com/AM/ui/PSDetailProductList.do?pInfoSBUId=9&PCId=4200 Accessed 24 August 2006.

WWW.ITACTRADE.ORG.http://www.itactrade.org/WebSiteTemp/en/01-4.asp?page=2&v_id=43860633 Accessed 23 July 2003.

WWW.NANOCLAY.COM.http://www.nanoclay.com/faqs.asp Accessed 17 March 2005.

WWW.NETZSCH-FEINMAHLTECHNIK.DE.http://www.netzsch-feinmahltechnik.de/technologie/e-nass_zeta.html Accessed 17 March 2005.

XING, X.S. & LI, R.K.Y. (2004) Wear behavior of epoxy matrix composites filled with uniform sized sub-micron spherical silica particles. *Wear,* 256**,** 21-26.

YANG, Z., CHEN, X., CHEN, C., LI, W., ZHANG, H., XU, L. & YI, B. (2007) Noncovalent-wrapped sidewall functionalization of multiwalled carbon nanotubes with polyimide.

YASMIN, A., ABOT, J.L. & DANIEL, I.M. (2003) Processing of clay/epoxy nanocomposites by shear mixing. *Scripta Materialia,* 49**,** 81-86.

YASMIN, A., LUO, J.J., ABOT, J.L. & DANIEL, I.M. (2006) Mechanical and thermal behavior of clay/epoxy nanocomposites. *Composites Science and Technology,* 66**,** 2415-2422.

YU, M.-F., LOURIE, O., DYER, M.J., MOLONI, K., KELLY, T.F. & RUOFF, R.S. (2000) Strength and Breaking Mechanism of Multiwalled Carbon Nanotubes Under Tensile Load. *Science,* 287**,** 637-640.

ZHANG, L.C., ZARUDI, I. & XIAO, K.Q. (2006) Novel behaviour of friction and wear of epoxy composites reinforced by carbon nanotubes. *Wear,* 261**,** 806-811.

ZHANG, W., PICU, R.C. & KORATKAR, N. (2007) Suppression of fatigue crack growth in carbon nanotube composites. *Applied Physics Letters,* 91**,** 193109-3.

ZHOU, Y., PERVIN, F., JEELANI, S. & MALLICK, P.K. (2008a) Improvement in mechanical properties of carbon fabric-epoxy composite using carbon nanofibers. *Journal of Materials Processing Technology,* 198**,** 445-453.

ZHOU, Y., PERVIN, F., LEWIS, L. & JEELANI, S. (2007a) Experimental study on the thermal and mechanical properties of multi-walled carbon nanotube-reinforced epoxy. *Materials Science and Engineering A,* 452-453**,** 657-664.

ZHOU, Y., PERVIN, F. & MALLICK, P.K. (2007b) Influence of multi-walled carbon nanotubes on the thermal and mechanical behaviour of carbon/epoxy composites. *SAMPE 2007.* Baltimore, SAMPE.

ZHOU, Y.X., WU, P.X., CHENG, Z.-Y., INGRAM, J. & JEELANI, S. (2008b) Improvements in electrical, thermal, and mechanical properties of epoxy by filling carbon nanotube. *Express Polymer Letters,* 2**,** 40 - 48.

ZHU, J., IMAM, A., CRANE, R., LOZANO, K., KHABASHESKU, V.N. & BARRERA, E.V. (2007) Processing a glass fiber reinforced vinyl ester composite with nanotube

enhancement of interlaminar shear strength. *Composites Science and Technology,* 67**,** 1509-1517.

ZHU, J., KIM, J., PENG, H., MARGRAVE, J.L., KHABASHESKU, V.N. & BARRERA, E.V. (2003) Improving the Dispersion and Integration of Single-Walled Carbon Nanotubes in Epoxy Composites through Functionalization.

ZHU, J. & KISSEL, K. (2007) Nanocomposites Technology SAMPE tutorial. *SAMPE 07.* Baltimore Maryland, SAMPE.

ZHU, J., PENG, H., RODRIGUEZ-MACIAS, F., MARGRAVE, J.L., KHABASHESKU, V.N., IMAM, A.M., LOZANO, K. & BARRERA, E.V. (2004) Reinforcing epoxy polymer composites through covalent integration of functionalized nanotubes. *Advanced Functional Materials,* 14**,** 643-648.

ZILG, C., THOMANN, R., FINTER, J. & MULHAUPT, R. (2000) The influence of silicate modification and compatibilizers on mechanical properties and morphology of anhydride-cured epoxy nanocomposites. *Macromolecular Materials and Engineering,* 280**,** 41-46.

ZUNJARRAO, S.C. & SINGH, R.P. (2006) Characterization of the fracture behavior of epoxy reinforced with nanometer and micrometer sized aluminum particles. *Composites Science and Technology,* 66**,** 2296-2305.

Appendix A

A.1 Citation references for the summary tables in Chapter 2

These numbered references refer to the reviewed literature in Table 2-6 to Table 2-8. These tables use the numbered references to show the current knowledge of the nanoclay dispersion techniques.

1. Kim, J.-K., et al., *Moisture barrier characteristics of organoclay-epoxy nanocomposites.* Composites Science and Technology, 2005. **65**(5): p. 805-813.
2. Frohlich, J., et al., High-performance epoxy hybrid nanocomposites containing organophilic layered silicates and compatibilized liquid rubber. Journal of Applied Polymer Science, 2004. **92**(5): p. 3088-3096.
3. Chen, J.h.S., et al., Study of the interlayer expansion mechanism and thermal-mechanical properties of surface[hyphen]initiated epoxy nanocomposites. Polymer, 2002. **43**(18): p. 4895-4904.
4. Isik, I., U. Yilmazer, and G. Bayram, Impact modified epoxy/montmorillonite nanocomposites: synthesis and characterization. Polymer, 2003. **44**(20): p. 6371-6377.
5. Pinnavaia, T.J., T. Lan, and P.D. Kaviratna, *Epoxy self-polymerization in smectite clays.* Journal of Physics and Chemistry of Solids, 1995. **57**(6-8): p. 1005-1010.
6. Ke Wang, L.W., Jingshen Wu, Ling Chen, and Chaobin He* Preparation of Highly Exfoliated Epoxy/Clay Nanocomposites by "Slurry Compounding": Process and Mechanisms. Langmuir, 2005. **21**(8): p. 3613 -3618.
7. Yasmin, A., J.L. Abot, and I.M. Daniel, *Processing of clay/epoxy nanocomposites by shear mixing.* Scripta Materialia, 2003. **49**(1): p. 81-86.
8. Miyagawa, H. and L.T. Drzal, The effect of chemical modification on the fracture toughness of montmorillonite clay/epoxy nanocomposites. Journal of Adhesion Science and Technology, 2004. **18**(13): p. 1571-1588.
9. Messersmith, P.B. and E.P. Giannelis*, *Synthesis and Characterisation of Layered Silicate - Epoxy Nanocomposites.* Chem. Mater., 1994. **6**: p. 1719 - 1725.
10. Haque, A., et al., S2-glass/epoxy polymer nanocomposites: Manufacturing, structures, thermal and mechanical properties. Journal of Composite Materials, 2003. **37**(20): p. 1821-1838.
11. Timmerman, J.F., B.S. Hayes, and J.C. Seferis, *Nanoclay reinforcement effects on the cryogenic microcracking of carbon fiber/epoxy composites.* Composites Science and Technology, 2002. **62**(9): p. 1249-1258.
12. Becker, O., R.J. Varley, and G.P. Simon, *Thermal stability and water uptake of high performance epoxy layered silicate nanocomposites.* European Polymer Journal, 2004. **40**(1): p. 187-195.
13. Aktas, L., Y.K. Hamidi, and M.C. Altan, *Characterisation of nanoclay dispersion in resin transfer moulded glass/nanoclay/epoxy composites.* Plastics, Rubber and Composites, 2004. **33**: p. 267-272.

14. Hackman, I. and L. Hollaway, *Epoxy-layered silicate nanocomposites in civil engineering.* Composites Part A: Applied Science and Manufacturing, 2006. **37**(8): p. 1161-1170.
15. Chen, K.H. and S.M. Yang, *Synthesis of epoxy-montmorillonite nanocomposite.* Journal of Applied Polymer Science, 2002. **86**(2): p. 414-421.
16. Zilg, C., et al., The influence of silicate modification and compatibilizers on mechanical properties and morphology of anhydride-cured epoxy nanocomposites. Macromolecular Materials and Engineering, 2000. **280**(7-8): p. 41-46.
17. Chen, C.G., M. Khobaib, and D. Curliss, *Epoxy layered-silicate nanocomposites.* Progress in Organic Coatings, 2003. **47**(3-4): p. 376-383.
18. Chen, C. and D. Curliss, *Preparation, characterization, and nanostructural evolution of epoxy nanocomposites.* Journal of Applied Polymer Science, 2003. **90**(8): p. 2276-2287.
19. Brunner, A.J., et al., *The influence of silicate-based nano-filler on the fracture toughness of epoxy resin.* Engineering Fracture Mechanics, 2006. **73**(16): p. 2336-2345.
20. Kornmann, X., et al., *Epoxy-layered silicate nanocomposites as matrix in glass fibre-reinforced composites.* Composites Science and Technology, 2005. **65**(14): p. 2259-2268.
21. Siddiqui, N.A., et al., *Mode I interlaminar fracture behavior and mechanical properties of CFRPs with nanoclay-filled epoxy matrix.* Composites Part A: Applied Science and Manufacturing, 2007. **38**(2): p. 449-460.
22. Chen, C.G. and T.B. Tolle, *Fully exfoliated layered silicate epoxy nanocomposites.* Journal of Polymer Science Part B: Polymer Physics, 2004. **42**(21): p. 3981-3986.
23. Liu, W., S.V. Hoa, and M. Pugh, *Fracture toughness and water uptake of high-performance epoxy/nanoclay nanocomposites.* Composites Science and Technology, 2005. **65**(15-16): p. 2364-2373.
24. Salahuddin, N.A., *Layered silicate/epoxy nanocomposites: synthesis, characterization and properties.* Polymers for Advanced Technologies, 2004. **15**(5): p. 251-259.
25. Potschke, P., et al., Rheological and dielectrical characterization of melt mixed polycarbonate-multiwalled carbon nanotube composites. Polymer, 2004. **45**(26): p. 8863-8870.
26. Lu, H.-J., et al., Epoxy/clay nanocomposites: Further exfoliation of newly modified clay induced by shearing force of ball milling. Polymer International, 2004. **53**(10): p. 1545-1553.
27. Chen, B., et al., Synthesis of Disordered and Highly Exfoliated Epoxy/Clay Nanocomposites using Organoclay with Catalytic Function via Acetone-Clay Slurry Method. Chemistry of Materials, 2004. **16**(24): p. 4864-4866.
28. Guo, B., D. Jia, and C. Cai, Effects of organo-montmorillonite dispersion on thermal stability of epoxy resin nanocomposites. European Polymer Journal, 2004. **40**(8): p. 1743-1748.
29. Lam, C.-K., et al., Effect of ultrasound sonication in nanoclay clusters of nanoclay/epoxy composites. Materials Letters, 2005. **59**(11): p. 1369-1372.

Appendix B

B.1 Table of CNT tensile resin properties

D230	wt%	Tensile strength Mpa	% change	Standard deviation	Young's modulus E GPa	% change	Standard deviation	Strain at break Strain	% change	Standard deviation
Nanosolve										
	0%	62.94		0.38	2.99		0.06	9.39		2.67
	0.13%	61.12	-2.9%	0.4	3.06	2.3%	0.11	9.85	4.9%	1.97
	0.26%	64.2	2.0%	0.16	2.91	-2.7%	0.08	9.71	3.4%	2.06
	0.38%	60.11	-4.5%	0.5	3.08	3.0%	0.07	9.07	-3.4%	1.69
	1.05%	50.97	-19.0%	0.72	2.96	-1.0%	0.02	10.6	12.9%	2.21
Nanoledge										
	0%	62.94		0.38	2.99		0.06	9.39		2.67
	0.13%	63.46	0.8%	0.29	3.09	3.3%	0.11	7.33	-22.0%	0.82
	0.26%	63.82	1.4%	0.3	2.7	-9.7%	0.04	12.24	30.3%	2.06
	0.52%	64.62	2.7%	0.16	2.8	-6.4%	0.08	9.31	-0.9%	2.59
Hybtonite										
	0%	62.94		1.03	2.99		0.05	9.39		2.09
	0.13%	62.77	-0.3%	0.41	3.09	3.4%	0.05	9.42	0.3%	1.25
	0.26%	69.68	10.7%	1.1	3.24	8.5%	0.1	10.09	7.4%	2.3
	0.52%	69.97	11.2%	0.18	3.23	8.1%	0.15	8.9	-5.2%	0.97
	1.05%	71.9	14.2%	0.45	3.12	4.4%	0.06	8.62	-8.2%	1.18

Table B-1 D230 cured CNT epoxy system tensile results refers to the results in Figures 6-7, 6-8 and 6-9.

IPD	wt% CNT	Tensile strength MPa	% change	Standard deviation	Young's modulus GPa	% change	Standard deviation	Strain at break Strain	% change	Standard deviation
Nanosolve										
	0%	79.66		5.31	2.89		0.092	4.639		1.23
	0.14%	83.09	4.3%	1.11	2.94	1.9%	0.06	6.75	45.5%	0.8
	0.28%	85.38	7.2%	0.32	3	3.9%	0.11	7.42	60.0%	1.42
	0.41%	84	5.4%	1.8	3.16	9.5%	0.07	5.79	24.8%	1.14
	1.12%	64.18	-19.4%	5.31	2.85	-1.3%	0.04	4.00	-13.8%	0.98
Nanoledge										
	0%	79.66		5.31	2.89		0.092	4.639		1.23
	0.14%	85.71	7.6%	10.75	3.393	17.6%	0.21	5.2	12.1%	0.49
	0.26%	84.68	6.3%	0.49	3.08	6.7%	0.1	6.42	38.4%	0.95
	0.58%	81.82	2.7%	20.45	2.95	2.2%	0.14	3.72	-19.8%	1.98
Hybtonite										
	0%	79.66		5.309	2.89		0.092	4.639		1.23
	0.14%	82.28	3.3%	6.51	3.11	7.8%	0.1	6.24	34.5%	2.19
	0.28%	64.96	-18.5%	14.58	3.2	10.9%	0.12	2.55	-45.0%	0.76
	0.56%	57.99	-27.2%	17.08	3.19	10.5%	0.12	2.22	-52.1%	0.86
	1.12%	42.18	-47.1%	10.11	3.21	11.2%	0.04	1.44	-69.0%	0.38

Table B-2 IPD cured CNT epoxy system tensile results refers to the results in Figures 6-7, 6-8 and 6-9.

B.2 Table of CNT flexural properties

D230	CNT wt%	Flexural strength Fmax (MPa) (MPa)	%change	Standard deviation	Flexural modulus (GPa) (GPa)	%change	Standard deviation
Nanosolve							
	0%	97.21		0.59	2.94		0.06
	0.13%	100.14	3.0%	0.95	2.64	-10.2%	0.1
	0.26%	96.74	-0.5%	0.66	2.98	1.5%	0.05
	0.38%	96.62	-0.6%	0.74	2.95	0.3%	0.03
	1.05%	87.12	-10.4%	1.88	2.78	-5.4%	0.1
Nanoledge							
	0%	97.21		0.59	2.94		0.06
	0.13%	97.38	0.2%	0.72	2.8	-4.8%	0.29
	0.26%	96.84	-0.4%	0.45	2.82	-4.1%	0.11
	0.52%	98.45	1.3%	0.27	2.99	1.7%	0.02
Hybtonite							
	0%	97.21		0.59	2.94		0.06
	0.13%	98.35	1.2%	0.80	2.89	-1.7%	0.03
	0.26%	108.27	11.4%	0.78	3.26	10.9%	0.08
	0.52%	109.05	12.2%	0.33	3.2	8.8%	0.15
	1.05%	109.89	13.0%	0.91	3.11	5.8%	0.05

Table B-3 Flexural results for D230 cured CNT epoxy systems refers to the results in Figure 6-10 and Figure 6-11.

IPD	CNT wt%	Flexural strength Fmax (MPa) (MPa)	%change	Standard deviation	Flexural modulus (GPa) (GPa)	%change	Standard deviation
Nanosolve							
	0%	120.21		0.36	2.96		0.06
	0.14%	120.40	0.2%	1.6	2.65	-10%	0.07
	0.28%	122.22	1.7%	0.93	3.04	3%	0.03
	0.41%	126.5	5.1%	0.79	3.17	7%	0.07
	1.12%	103.65	-13.1%	2.08	2.57	-12%	0.1
Nanoledge							
	0	120.21	0.0%	0.36	2.96	0%	0.06
	0.14%	132.97	10.6%	1	2.78	-6%	0.05
	0.28%	122.45	1.9%	7.14	2.79	-6%	0.11
	0.56%	119.78	-0.4%	2.78	2.78	-6%	0.11
Hybtonite							
	0%	120.21		0.36	2.96		0.06
	0.14%	129.43	7.7%	0.58	3.05	3%	0.01
	0.28%	129.34	7.6%	15.79	3.13	6%	0.13
	0.56%	113.16	-5.9%	17.25	3.21	8%	0.10
	1.12%	86.17	-28.3%	10.19	3.03	2%	0.05

Table B-4 Flexural results for IPD cured CNT epoxy systems refers to the results in Figure 6-10 and Figure 6-11.

B.3 Table of CNT compressive properties

D230	CNT	Compressive Strength Fmax			Compressive modulus		
	Wt%	(MPa)	% change	Standard deviation	(GPa)	% change	Standard deviation
Nanosolve							
	0%	99.14		1	3.21		0.05
	0.13%	106.00	6.9%	0.65	3.11	-3.1%	0.02
	0.26%	108.83	9.8%	1.01	3.13	-2.5%	0.03
	0.38%	111.07	12.0%	0.99	3.33	3.7%	0.07
	1.05%	95.12	-4.1%	0.85	3.21	0.0%	0.07
	2.27%	76.10	-23.2%	2.34	2.94	-8.4%	0.04
Nanoledge							
	0%	99.14		1	3.21		0.05
	0.13%	101.53	2.4%	1.09	3.14	-2.2%	0.03
	0.26%	106.06	7.0%	1.5	3.14	-2.2%	0.08
	0.52%	104.49	5.4%	1.13	3.11	-3.1%	0.03
Hybtonite							
	0.00%	99.14		1	3.20		0.05
	0.13%	112.16	13.1%	1.24	3.74	16.6%	0.11
	0.26%	113.87	14.9%	0.56	3.65	13.7%	0.05
	0.52%	116.15	17.2%	1.21	3.55	10.8%	0.04
	1.05%	115.36	16.4%	3.48	3.54	10.3%	0.07

Table B-5 Compressive properties of D230 cured CNT epoxy systems refers to the results in Figure 6-12 and Figure 6-13.

IPD	CNT	Compressive Strength			Compressive Modulus		
	Wt%	(MPa)	% change	Standard deviation	(GPa)	% change	Standard deviation
Nanosolve							
	0%	134.15		1.04	3.1		0.07
	0.14%	141.4	5.4%	0.85	3.02	5.4%	0.09
	0.28%	143.68	6.7%	0.96	3.28	6.7%	0.08
	0.41%	147.84	10.2%	2.78	3.45	10.2%	0.07
	1.12%	133.93	-0.2%	4.06	2.99	-0.2%	0.04
Nanoledge							
	0%	134.15		1.04	3.1		0.04
	0.14%	143.08	6.7%	1.57	3.11	0.3%	0.07
	0.28%	146.32	8.5%	1.25	3.09	-0.3%	0.07
	0.56%	141.11	4.9%	1.44	3.1	0.0%	0.07
Hybtonite							
	0%	134.15		1.04	3.1		0.04
	0.14%	146.43	9.2%	2.28	3.85	24.2%	0.06
	0.28%	148.94	11.0%	1.47	3.54	14.9%	0.16
	0.56%	150.16	11.9%	0.75	3.51	16.1%	0.08
	1.12%	147.81	10.2%	0.85	3.49	13.8%	0.06

Table B-6 Compressive properties of IPD cured CNT epoxy systems refers to the results in Figure 6-12 and Figure 6-1.

Appendix C

C.1 CNT IPD off-ratio curing properties

Due to speculation from the tensile results of the IPD cured Hybtonite resins, as discussed in Chapter 6, a series of tests were conducted on changing the curing ratio. The ratios were altered changing the parts per hundred from -2 parts to +4 parts over the stoichiametric ration. The samples were then cured at room temperature for 12 hours and then at 120°C for 1hr. The samples were then tested in deflection and tensile strengths and moduli as well as *Tg* and ultimate *Tg*. The values are presented here in Table C-1 and C-2 with stnadard deviation values in brackets

Epikote 828 part	**-2**	**-1**	**0**	**1**	**2**	**3**	**4**
Ratio	**100:20.7**	**100:21.7**	**100:22.7**	**100:23.7**	**100:24.7**	**100:25.7**	**100:26.7**
Flexural strength / MPa	125.00	125.64	120.21	120.09	122.59	116.86 (0.532)	116.46 (0.806)
Flexural Modulus /GPa	3	3.08	2.93	3.07	3.02	2.85 (0.054)	2.83 (0.037)
Elongation at break/% (flex)	7.52	8.8	7.74	7.79	8.24	10.07	9.06
Tensile strength	84.91 (3.487)	74.73 (19.174)	79.66 (0.920)	84.62 (0.320)	87.05 (4.603)	82.59 (0.351)	81.66 (0.529)
Tensile modulus / GPa	3.03 (0.094)	2.99 (0.049)	2.89 (0.094)	2.96 (0.076)	3 (0.197)	2.84 (0.075)	2.83 (0.075)
Elongation at break/% (tensile)	5.77	4.46	4.64	6.21	6.73 (0.799)	7.64 (0.860)	7.53 (0.890)
***Tg*2 / °C**	130.82	130.6	134	131.2	127.28	126.4	125.5
Ult imate *Tg*°C	148.94	155.16	165	164.01	162.87	148.1	153.2

Table C-1 Off-ratio tensile and flexural mechanical property data for Epikote 828.

The results of the pristine Epikote 828 cure ratio study shows that the maximum *Tg* and ultimate *Tg* show maximum results at the stoichiametric ratio. However it does not nesacerily mean the best mechnical preoperties. Increaing the ratio appears to increase the tensile properties while decressing the IPD parts it gains better flexural properties. The standrd deviation increases for the tensile strength in bothe directions.

Hybtonite G4.E – IPD part	-2	-1	0	1	2	3	4
ratio	100:20.7	100:21.7	100:22.7	100:23.7	100:24.7	100:25.7	100:26.7
(G4E) Flexure strength / MPa	133.73	126.92	129.34	129.45	130.24	126.3 (0.547)	122.69 (1.380)
(G4E)Flexural modulus /GPa	3.26	3.27	3.13	3.16	2.61	3.12 (0.051)	3.07 (0.022)
(G4E) Elongation at break/% (flex)	7.69	5.56	6.57	8.05	7.87	4.45	11.05
(G4E) Tensile strength / MPa	66.06 (11.280)	53.16 (15.886)	64.69 (15.785)	73.75 (10.821)	87.75 (3.385)	85.19 (9.94)	85.48
(G4E) Tensile modulus /GPa	3.31 (0.052)	3.31 (0.228)	3.2 (0.135)	3.13 (0.082)	3.08 (0.050)	3.15 (0.093)	3.23
(G4E) Elongation at break/% (tensile)	2.63 (1.066)	1.96 (0.284)	2.55	3.52 (2.197)	5.62 (1.755)	4.19	6.46
G4.E *Tg*2 / °C	127.27	126.7	127	131.85	131.73	125.9	129.6
G4.E Ult imate *Tg* / °C	141.48	143.57	151	149.01	155.4	149.9	146.1

Table C-2 ratio tensile and flexural mechanical property data for Hybtonite G4.E.

The Hybtonite off-ratio data shows that *Tg* and ultimate *Tg* give maximum values at +2part, increaseing by almost 5°C over the stoichiametric ratio. At this cure ratio the tensile strength is improved by up over 20MPa on the stoichiametric ratio. In doing so the standard deviation is redeuced significantly and the tensile strenght becomes a greater value than the stoichiametric ratio of Epikote 828. However, the +2 part ratio of the pristine Epikote 828 also shows a similar increase in tensile strength but a reduction in flexural strengtth. The *Tg* at +2 part ratio of the prisitne Epikote 828 is also reduced but the ultimate *Tg* is increased by over 7°C on the Hybtonite value.